TRANSLATIONAL STUDIES ON THE VASCULAR TARGETING AGENT COMBRETASTATIN A4 PHOSPHATE

by

Susan Mary Galbraith

A thesis submitted for the degree of

Doctor of Philosophy

University of London
Faculty of Oncology

2001

Department of Medical Oncology, Mount Vernon Hospital
and
The Gray Laboratory Cancer Research Trust
Northwood, Middlesex, UK

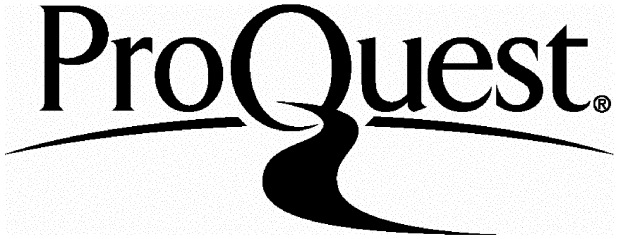

Abstract

This thesis describes *in vitro* experiments with the novel vascular targeting agent Combretastatin A4 Phosphate (CA4P) and non-invasive magnetic resonance imaging (MRI) measurements in patients treated with CA4P to derive parameters which reflect tumour and normal tissue blood flow and permeability.

Shape changes induced following tubulin depolymerisation by CA4P are quantified in human umbilical vein endothelial cells (HUVECs) and are measurable after only 10 minutes exposure. The effect is more marked in proliferating than confluent HUVECs, and begins at doses that have no anti-proliferative activity. In contrast, human smooth muscle cells show no shape change after treatment. The similar time course of HUVEC shape changes *in vitro* and tumour vascular shutdown *in vivo* suggest that this might be an early event involved in vascular shutdown. The effects and recovery rates of several other tubulin-binding agents are compared with CA4P. Colchicine and vinblastine also induce changes in HUVEC shape but unlike CA4P, HUVECs do not recover after drug removal. For these drugs, shape change and antiproliferative effects occur at similar doses. ZD6126, which like CA4P also has vascular targeting activity at well tolerated doses, induces recoverable changes in HUVEC shape at doses with no anti-proliferative activity. The difference in recovery rates with different tubulin-binding agents might therefore be related to their therapeutic window.

The reproducibility of dynamic contrast enhanced MRI is measured in 21 patients who had 2 pre treatment scans within a week. Comparing the technique in rats with an established method for measuring absolute blood flow provides verification that the kinetic parameters derived from this technique reflect blood flow changes. Significant reductions in these parameters in patients' tumours are seen 4 and 24 hours after treatment at well tolerated doses of CA4P at 52mg/m^2 to 68 mg/m^2. No significant mean changes are seen in kidney, liver, spleen or skeletal muscle, although a small proportion of patients have significant reductions which are generally not maintained, and not associated with clinical consequences.

ACKNOWLEDGMENTS

Completion of the work described in this thesis would not have been possible without the contribution of many people in the Gray Laboratory and Mount Vernon Hospital. I would like to thank my supervisors Dr Dai Chaplin and Prof Gordon Rustin for the opportunity to contribute to this project, and for their enthusiasm, support and help throughout its completion.

The Tumour Microcirculation Group has been a very friendly and welcoming place in which to work. I am grateful to Angela Holder and Margaret Watts, who taught me about endothelial cell culture when I first started, to Francesca Lee, who worked with me on many of the *in vitro* experiments and particularly to Gill Tozer for her great help and advice in the writing up phase. The Group would not be the same without Davina Honess, who has been a good friend and source of advice. I would also like to thank Sally Hill, for letting me share her office for the last 3 years, listening to my witterings, and always managing to find the relevant reference within 2 minutes of asking!

I am grateful to Mike Stratford, who did the clinical pharmacokinetc studies for CA4P and DMXAA, and who has performed HPLC analysis for CA4P hydrolysis *in vitro*, and Boris Vojnovic and Ros Locke of the Advanced Technology Group who developed the program for image acquisition and cell shape analysis.

I am indebted to several people in the Paul Stickland scanner centre. Jane Taylor, who wrote the MR sequences used in this project, provided gradual enlightenment about the physics of MRI and with whom I spent endless hours drawing regions of interest and had many valuable discussions. James Stirling and Linda Culver, MRI radiographers who did the scanning. Martin Lodge, who wrote and developed the program to derive pharmacokinetic parameters from the dynamic series of scans. Anwar Padhani, who helped enormously in developing the pharamcokinetic data, and whose comments during the writing up phase have been invaluable. Ross Maxwell, who runs the animal MRI in the Gray Lab, and who performed the rat MR experiments. As a team we have had many helpful discussions which have gradually refined the MRI technique and its analysis.

I am very grateful to the research nurses, Julie, Kath, Fiona and especially to Jane Boxall, for her excellent organisation, care of our patients, and support for me. I owe a special debt to the patients and their relatives who have taken part in the phase I trials of DMXAA and CA4P, without whom progress would not have been made. They have shown patience and considerable courage, as well as humour in the face of their illness.

I have been supported financially by a grant from the National Lotttery Charities Board, and the Cancer Research Campaign funded the Phase I trial of DMXAA and organised the Phase I trial of CA4P, which was funded by OXiGENE Inc. Several people in the CRC Drug Development Office have had regular useful input regarding the trials, particularly Luiza Sena and Adele Robbins.

Finally, I could not have seen this through without the support of my husband Ian. Our two children, Jennifer and Alexander have been born and grown during this project – the amount they have learned in that time puts it into perspective!

TABLE OF CONTENTS

LIST OF FIGURES

Chapter 1

Chapter 2

Chapter 3

Chapter 4

Chapter 5

Chapter 6

Chapter 7

LIST OF TABLES

Chapter 1

Chapter 5

Chapter 6

Chapter 7

CHAPTER 1 INTRODUCTION

This chapter discusses the development of tumour vasculature, the abnormalities in its morphology and function and the consequences of these abnormalities in terms of blood flow, oxygenation and energy status as well as the implications for chemotherapy drug delivery and resistance to radiotherapy. Methods of measuring tumour blood flow are described and compared. The potential exploitation of the differences between normal tissue and tumour vasculature in order to derive a therapeutic benefit is explored. The structure and function of the cytoskeleton is examined, and hypotheses explaining why disruption of the microtubular network might cause tumour vascular shutdown are discussed. Finally, the discovery of a novel tubulin-binding agent, Combretastatin A4 is described together with the pre-clinical studies published prior to the beginning of this project.

1.1 Tumour vasculature

1.1.1 Introduction

In the development of a malignant tumour, normal cells accumulate a number of genetic abnormalities, which favour proliferation, or remove controls on growth, leading to the transformation into a malignant cell (Mitchell, 1992; Parodi, 1992; Vogelstein & Kinzler, 1993; Roth, 1995; Compagni & Christofori, 2000). Proliferation of the progeny of this malignant cell produces a small tumour nidus. Evidence from the 1960s and 70s demonstrated that in order for a tumour to grow above 1-2mm^3 or when it contains 10^5-10^6 cells, new blood vessel formation or 'angiogenesis' is required (Folkman *et al.*, 1963; Folkman, 1971). Such tumours may remain dormant in this pre-vascular phase until the process of angiogenesis is 'switched' on (Folkman & Hanahan, 1991; Hanahan & Folkman, 1996).

Other tumours may develop neovasculature very early in their growth – a recent study has demonstrated functional new blood vessels in a tumour mass of 100-300 cells (Li *et al.*, 2000a) (see Figure 1.1). In addition, malignant tumour cells have been shown to migrate through tissues towards existing host vessels (Li *et al.*, 2000a), and may use these existing vessels to provide oxygen and nutrients (Holash *et al.*, 1999), growing around the mature host vasculature for some time before generating new vessel formation (Skinner *et al.*, 1990). Some malignant tumours develop from pre-existing benign tumours, which have an increased proliferative rate, but lack the invasive properties of malignant cells. Such benign

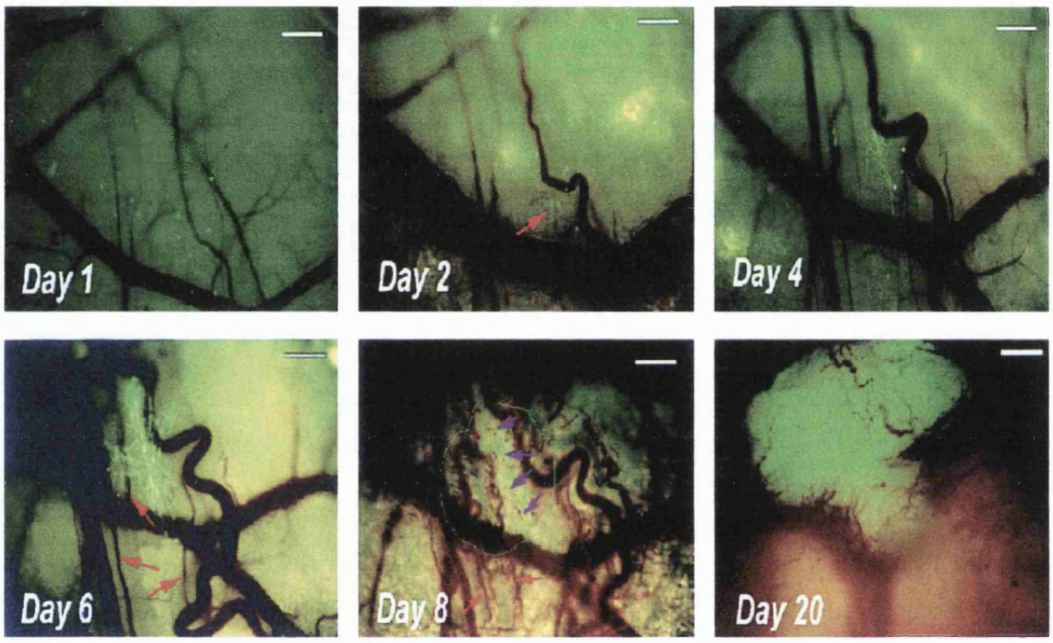

Figure 1.1 Growth of a tumour from 20 green fluorescent protein expressing cells implanted into a mouse window chamber. *Red arrow* in day 2 panel indicates an elongated cell migrating towards host vessels. *Red arrows* in day 6 panel indicate dilated host vessels compared with day 4. Day 8 panel – new microvessels – *pink arrows* – tumour (outlined) associated – *red arrows* – tumour induced vasculature outside tumour. Size bars day1-8 = 200μm.
Day 20 – 2.5mm diameter tumour with associated abnormal tumour vasculature. Size bar = 0.5mm

From Li *et al*, 2000a

tumours may already have an increased vascular density in comparison to the surrounding normal tissue (Skinner *et al.*, 1995).

1.1.2 Angiogenesis

Embryonic blood vessel formation involves differentiation of angioblasts to endothelial cells that assemble into a primary vascular plexus. This process is known as vasculogenesis (Risau, 1997). Further new blood vessel formation mainly occurs by angiogenesis in which new capillaries are formed from pre-existing post-capillary venules (Carmeliet, 2000) (see Figure 1.2). Angiogenesis may begin with vasodilatation mediated by nitric oxide (Gallo *et al.*, 1998). There is an increase in vascular permeability, and extravasation of plasma proteins, which form a scaffold for migrating and proliferating endothelial cells. These endothelial cells may form sprouts from the dilated venules, or the venules may be divided by pillars of periendothelial cells (intussusception), or by the formation of transendothelial cell bridges, which then divide into individual capillaries (Carmeliet, 2000). The primary vascular plexus is remodelled by a combination of pruning and further angiogenesis into a mature network.

Angiogenesis is therefore not specific to tumours, but is also present in normal growth, in physiological conditions such as the placenta and endometrium, and in other pathological conditions such as inflammation, wound healing and diabetic retinopathy (Folkman, 1995). Frequently angiogenesis is preceded by tissue hypoxia (Pe'er *et al.*, 1995; Ozaki *et al.*, 1999; Lee *et al.*, 2000; Marti *et al.*, 2000), which produces increased levels of hypoxia inducible transcription factors (Beck *et al.*, 1991; Wang & Semenza, 1993). These in turn increase production of angiogenic factors such as vascular endothelial growth factor (VEGF) (Levy *et al.*, 1995; Brogi *et al.*, 1996; Forsythe *et al.*, 1996; Maxwell *et al.*, 1997; Hartmann *et al.*, 1999). There is an increasing family of angiogenic factors, anti-angiogenic factors and their receptors responsible for the stimulation, inhibition and control of angiogenesis and vascular remodelling (Risau, 1997; Carmeliet, 2000), and there are differences in the factors present in pathological angiogenesis compared with those in the embryo (Konerding *et al.*, 1998).

In normal adult tissues (except placenta and endometrium), endothelial cells become quiescent and survive for years once they are assembled in new vessels, (Hobson & Denekamp, 1984). In tumours, the continued high level of expression of angiogenic factors (Fox *et al.*, 1993; Carmeliet *et al.*, 1998; Grunstein *et al.*, 1999) leads to endothelial cell proliferation at a rate 20-2000 times that seen in normal tissues (Denekamp & Hobson, 1982).

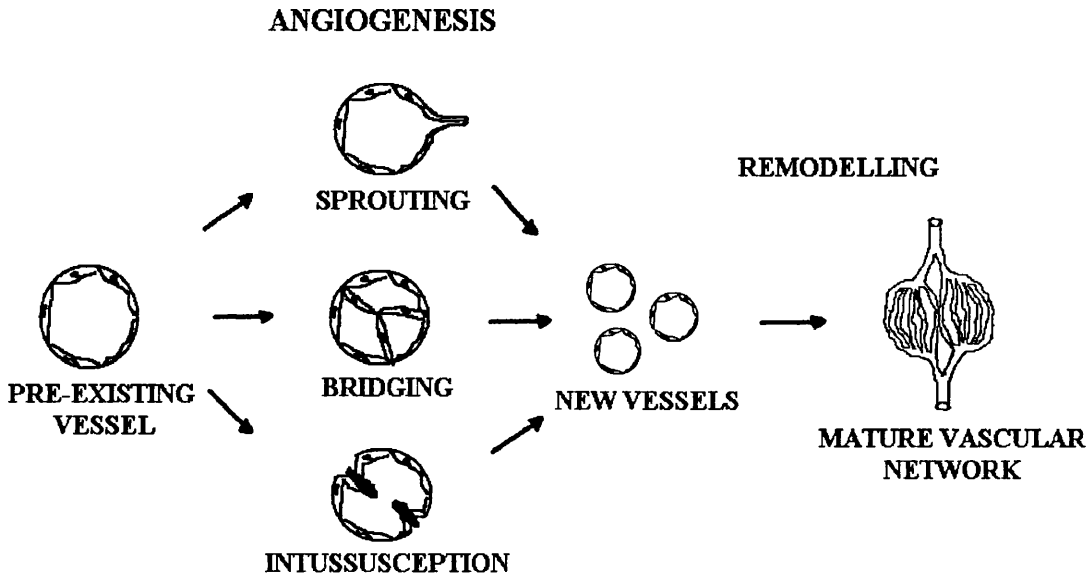

Figure 1.2 Process of angiogenesis in adult vasculature

Adapted from Carmeliet et al 2000

1.1.3 Morphology of tumour vasculature

The newly formed blood vessels in solid tumours do not have the usual morphology and hierarchy seen in normal tissues. They have a range of structural and functional abnormalities. Microvascular corrosion casts demonstrate the chaotic organisation of the vasculature in a colonic tumour and the contrasting ordered and hierarchical structure in a normal colonic mucosal plexus (Figure 1.3) (Konerding *et al.*, 1998). Tumour vessels are often dilated, tortuous, elongated and saccular. There are arterio-venous shunts, abnormal branching patterns, and blind endings. In addition, there is extreme heterogeneity of vascular density (Wesseling *et al.*, 1994). Abrupt changes in diameter and extravasations due to abnormally leaky vessels are common (Skinner *et al.*, 1995). Some tumour vessels lack a complete endothelial lining, or there may be fenestrations along the vessel wall (Warren, 1979).

Although there may be continuous remodelling of the newly formed vessels in tumours (Miodonski *et al.*, 1980; Bugajski *et al.*, 1989) this is disordered, and does not result in the mature vascular network seen after angiogenesis in wound healing (Phillips *et al.*, 1991; Konerding *et al.*, 1998;) or hypertrophy of an adult tissue (Hansen-Smith *et al.*, 1996). There is a disproportionate number of immature vessels in tumours which lack surrounding basement membrane, pericytes or smooth muscle (Benjamin *et al.*, 1999; Kakolyris *et al.*, 1999; Kakolyris *et al.*, 2000), and are therefore unable to respond to vasodilating or constricting substances (Abramovitch *et al.*, 1999). The supplying arteries and arterioles may nevertheless be able to respond and alter the tumour blood flow.

There is evidence that individual tumour-types express individual microvascular architecture (Katoh *et al.*, 1999; Konerding *et al.*, 1999). The lack of organisation and control of vascular development is a result of the multiple genetic abnormalities in the tumour cells, which alter the balance of angiogenic and anti-angiogenic factors and the timing and sequence of control signals for vessels to divide, regress or mature (Rastinejad *et al.*, 1989; Millauer *et al.*, 1994; Mukhopadhyay *et al.*, 1995; Rak *et al.*, 1995; Sato *et al.*, 1995; Mazure *et al.*, 1996; Stratmann *et al.*, 1997). As different tumour types have a different spectrum of such abnormalities, it is not surprising that they differ in their vascular morphology. Tumours of the same type in different sites also differ in morphology, and this reflects the importance of the interaction between tumour cells and their environment (Fukumura *et al.*, 1997; Konerding *et al.*, 1998; Schmidt *et al.*, 2000).

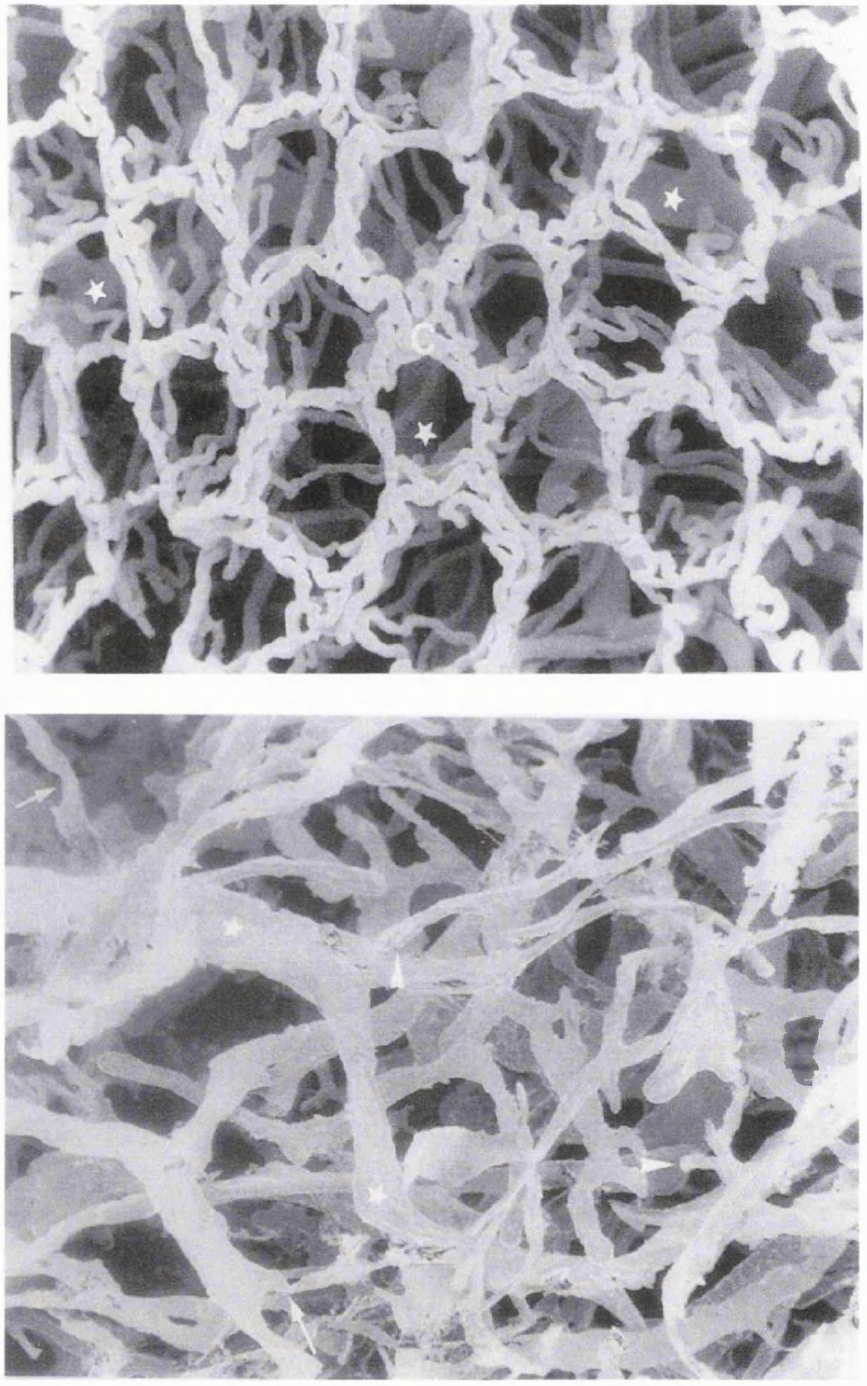

Figure 1.3 Microvascular corrosion cast of a human colon.

Top – Normal colonic mucosal capillary plexus C is arranged in a regular honeycomb pattern.
***Stars* - underlying submucosal vessels**
Bottom – Colonic carcinoma vasculature (from same patient).
***Arrowheads* -blind ends, *stars* - flattened vessels, *arrows* - variations in diameter**

Reproduced from Konerding et al 1998

The volume of the tumour occupied by the vasculature (vascular volume) can be measured in a variety of ways, and has been found to vary between 1% and 25-30% (Jain, 1988; Smith *et al.*, 1988; Dewhirst *et al.*, 1989; Meyer *et al.*, 1993; Skinner *et al.*, 1995). Some of this variation may be due to differences in measurement technique. Studies using the fluorescent Hoechst dye 33342, which measures functional vascular volume, are at the lower end of this range, whilst those that use morphometric methods using corrosion casts or window chambers have higher estimates. Evidence for the change in vascular volume as tumours grow is mixed, with some reporting an increase in vascular volume in the early stages of growth (Su *et al.*, 2000), then no further change (Jain, 1988). Others have found a decrease in vascular volume with increasing tumour size (Vaupel, 1977; Meyer *et al.*, 1993;), or no change (Hilmas & Gillette, 1974; Su *et al.*, 1999). Despite the variation in changes in vascular volume, frequently the intercapillary distance and necrotic fraction do increase with increasing tumour size as the heterogeneity in vascular density across the tumour increases (Vogel, 1965; Tannock & Steel, 1969; Hilmas & Gillette, 1974; Vaupel, 1977).

1.1.4 Tumour blood flow

The abnormalities of tumour vasculature described above have direct effects on the blood flow through tumours. Blood flow rate, Q, in any tissue, normal or malignant is given by

$$Q = \frac{\Delta p}{\eta . Z} \qquad (1)$$

where Δp, is the pressure difference between the arterial and venous ends of the tissue circulation (perfusion pressure). η is the blood viscosity and Z is the geometric resistance to flow (Jain, 1988).

For flow through a single, rigid, cylindrical vessel, Z is proportional to the vessel length and inversely proportional to the fourth power of the vessel diameter (Poiseuille's Law). For a network of vessels Z is a more complex function of the vascular morphology, dependent on vessel numbers, branching pattern, diameter and length. In normal tissues Z is independent of perfusion pressure (Zweifach & Lipowsky, 1984). In solid tumours however, Z increases dramatically at low perfusion pressures (Sevick & Jain, 1989a; Sensky *et al.*, 1993) of 40mmHg and below. This is because at low microvessel pressures, vessels begin to collapse or occlude. Several investigators have shown that the interstitial pressure in the centre of both experimental and human tumours is abnormally raised (Boucher & Jain, 1992; Tufto *et al.*,

1996; Milosevic *et al.*, 1998; Griffon-Etienne *et al.*, 1999). This has been attributed to the increased leakiness of tumour vasculature and to the absence of functioning lymphatic vessels in the centre of tumours (Gullino, 1975). In a study of primary cutaneous melanoma, there was no lymphangiogenesis despite increased angiogenesis, and lymph vessels inside tumours were infrequent. However, at the edge of tumours, subepidermal lymphatic vessels were invaded by tumour cells, thus explaining why lymphatic spread is a frequent occurrence in cancer despite the absence of lymphangiogenesis (de Waal *et al.*, 1997). Proliferation of cancer cells in areas, which are relatively confined, will also increase pressure on vessels (Griffon-Etienne *et al.*, 1999). If the hydrostatic pressure within the vessel drops below this combination of interstitial and cellular pressure, the vessel will collapse. Comparison of histological stains for blood vessels, and a vascular space marker demonstrate that the perfused fraction of tumour vessels can vary from 20-85% (Bernsen *et al.*, 1995). Even at high perfusion pressures Sevick et al measured the geometric resistance in a rat adenocarcinoma as being 1-2 orders of magnitude higher than that in several normal tissues (Sevick & Jain, 1989a), and found that it increased with increasing tumour size.

The perfusion pressure depends on the pressure in the feeding artery or arteriole and draining vein of a tissue and is less than the systemic arteriovenous difference, so tumours may have a perfusion pressure less than 40mmHg, at which geometric resistance is increased. For example in a rat subcutaneous tumour, the pressure in the feeding vessels to the tumour increased from 30-85mmHg with increasing tumour size, although mean systemic arterial pressure was 107mmHg (Hori *et al.*, 1993). Venous pressure is around 10-15mmHg. In this case the tumour perfusion pressure ranged from 20-70mmHg. Peters et al, found that in tumours the arterial and arteriolar pressures were similar to those in subcutaneous tissue, but the venous pressures were 5mmHg lower, thus increasing the perfusion pressure a little (Peters *et al.*, 1980).

The other factor affecting blood flow, blood viscosity, is also abnormally raised in tumours (Sevick & Jain, 1989b). The viscosity of blood is determined mainly by haematocrit and shear rate (velocity gradient in the fluid), but also depends to some degree on cell deformability, aggregation, and plasma viscosity (Jain, 1988). Cancer patients frequently have raised plasma viscosity and red cell aggregation (Dintenfass, 1981; Miller & Heilmann, 1988; von Tempelhoff *et al.*, 1998). Red cell deformability may also be reduced by low pH levels found in tumours (Jain, 1988). The systemic haematocrit is, however often lower in cancer patients (Krantz, 1994; Strum *et al.*, 1997; Lee *et al.*, 1998; Sadahiro *et al.*, 1998; Del *et al.*, 1999;

Groopman & Itri, 1999). As blood flows through a vessel, cells migrate to the centre of the vessel, leaving a cell free margin at the periphery. Since the red cells in the centre of the vessel travel faster than the cell free layer at the edge, the haematocrit in small vessels (<500μm) is lowered (Fahraeus effect), thus lowering blood viscosity (Fahraeus-Lindqvist effect). Both these effects are less marked in tumours compared with normal tissues (Sevick & Jain, 1989b) due to the increased vessel diameter, tortuosity and abnormal branching patterns, which tend to mix the red cells and the cell free layer. In addition, the increased leakiness of tumour vessels leads to increased plasma losses, and therefore an increase in intravascular haematocrit. (Butler *et al.*, 1975) The larger vessel diameter and sluggish flow reduces the shear rate in tumour vessels, further increasing blood viscosity.

All of the factors described above therefore tend to produce abnormalities in tumour blood flow. The overall level of blood flow in a tumour will depend on the relative contribution of these factors, the individual vascular structure and the tumour site. Vaupel has collated results from various techniques for measuring human tumour blood flow (Figure 1.4) (Vaupel *et al.*, 1989; Vaupel, 1998). This illustrates that there is great inter-tumour heterogeneity in overall blood flow with a range of 100 fold, even within similar tumour types, and that blood flow in a tumour can be higher or lower than blood flow in the surrounding normal tissue (Beaney *et al.*, 1984; Rowell *et al.*, 1989; Inaba, 1992; Hill *et al.*, 1994; Mineura *et al.*, 1995; Namba *et al.*, 1996; Toglia *et al.*, 1996; Mineura *et al.*, 1999). Some tumours have blood flow rates similar to those measured in liver, heart or brain. There is evidence that blood flow tends to decrease with increasing tumour size in experimental (Jirtle *et al.*, 1978; Lyng *et al.*, 1992; Sundqvist *et al.*, 1978), and human tumours (Rowell *et al.*, 1993; Hering *et al.*, 1995; Holm *et al.*, 1995), but Mantyla found no correlation with size (Mantyla, 1979).

In addition to the variability in blood flow between different tumours, the disordered vascular architecture and variations in intercapillary distances in tumours leads to large intratumour heterogeneity in flow. Intermittent collapse of vessels, or plugging by tumour or white cells, also leads to marked temporal fluctuations in flow within microregions of a tumour. This phenomenon has been noted in both experimental and human tumours (Chaplin & Hill, 1995; Pigott *et al.*, 1996). The overall tumour blood flow may also vary with time, although there is no evidence about the extent of this in humans. In a rat subcutaneous model there was a circadian rhythm in tumour blood flow with flow at night twice as high as during the day (Hori *et al.*, 1992; Hori *et al.*, 1995).

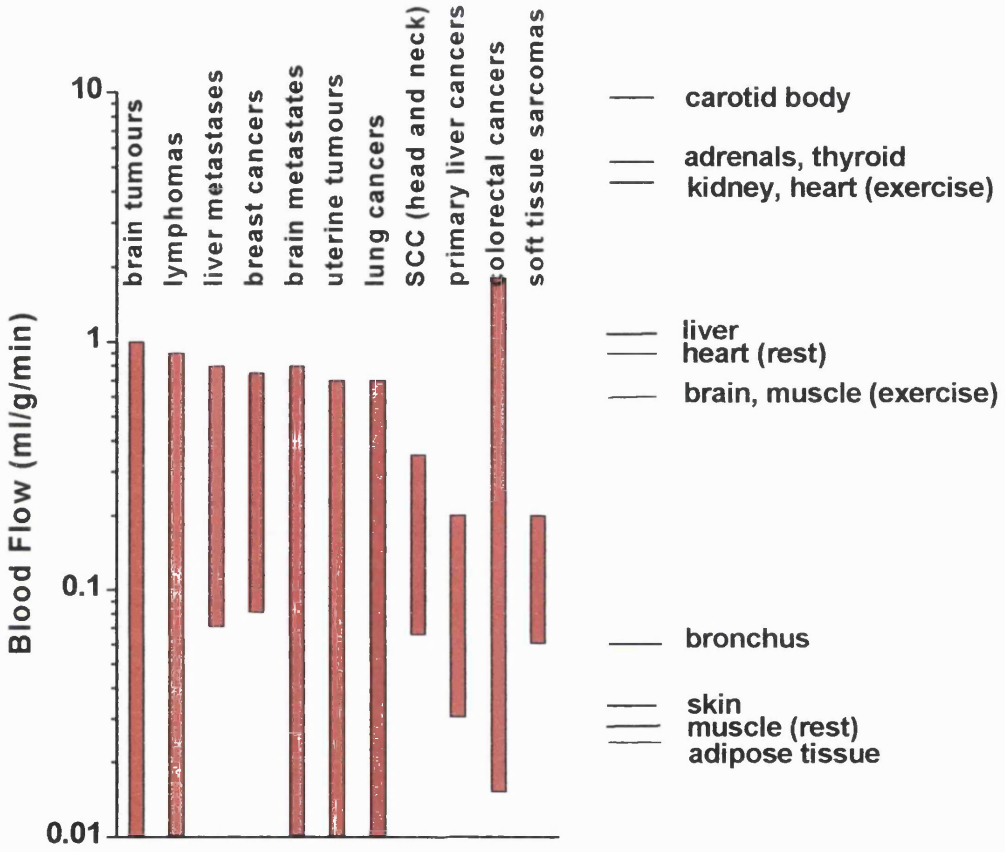

Figure 1.4 Variability of blood flow in human tumours and mean flow values of normal tissues.
SCC = squamous cell carcinoma

Reproduced from Vaupel 1998

1.2 Methods of measuring tumour blood flow rate

1.2.1 Introduction

There are several methods for measuring blood flow rate in a tissue. These include direct measurements, for example by insertion of electromagnetic flowmeters into or around a vessel, and a variety of indirect methods, some of which are invasive, and some which require only intravenous injection. There are three general principles underlying the indirect methods: those that use a measurement of the mean transit time of a tracer through a tissue, those that model the uptake of a tracer into a tissue, or clearance from it, and those that measure the fractional distribution of cardiac output. In addition there are methods such as laser Doppler flowmetry and colour Doppler ultrasound which do not measure tissue blood flow rate itself, but microregional red cell flux, and flow velocities within the larger vessels in a tissue respectively.

1.2.2 Central Volume Theorem

The first method is based on Stewart's Central Volume Theorem (Stewart, 1894). This states that the tissue blood flow rate F is determined by

$$F = \frac{V}{MTT} \qquad (2)$$

where V is the volume of distribution of the agent within the tissue, and MTT is the mean transit time, or the average time it takes for a tracer to pass through the tissue.

There are several reasons why this apparently simple equation may be difficult to solve. First, the volume of distribution of the tracer may be biologically multicompartmental, with transfer of the tracer between different tissue volumes occurring at different rates. The passage of the tracer through tissue compartments must therefore be modelled. Secondly, even for single-compartment models such as pure intravascular markers, the theorem assumes an instantaneous bolus injection, which is not achievable *in vivo*, and measurement of the MTT requires an adequate temporal sampling rate. The actual measured tissue-concentration time curve, Tissue (t) is the convolution of the arterial input function Art (t) and the residue function RF (t)

$$\text{Tissue (t)} = \text{Art (t)} \otimes RF(t) \qquad (3)$$

Therefore, to measure RF (t), and the associated MTT, the Art (t) is required. This can be measured directly with arterial blood sampling, or indirectly if a non-invasive method exists with sufficient temporal resolution. For pure intravascular markers the volume of distribution is the blood volume and is determined by,

$$V = \frac{\int Tissue(t)}{\int Art(t)} \qquad (4)$$

This principle has been used for calculation of cerebral blood volume (Rosen *et al.*, 1990), and cerebral blood flow rate by MRI, after intravenous injection of gadopentetate dimeglumine (Gd-DTPA) (Ostergaard *et al.*, 1996a; Ostergaard *et al.*, 1996b), which behaves as an intravascular tracer in brain, due to the blood brain barrier. The advent of higher molecular weight MRI contrast agents, which remain in the vascular compartment enables this principle to be used in other tissues (Furman-Haran *et al.*, 1998; Su *et al.*, 1998). It has also been used with ultrasound techniques, using microbubbles injected intravenously as contrast agents (Albrecht *et al.*, 1999).

1.2.3 Kety model

In 1948 Kety described a model of tissue uptake of a freely diffusible, inert tracer, based upon the Fick principle, that was originally used for the determination of cerebral blood flow rate using nitrous oxide (Kety & Schmidt, 1948), and adapted for determining regional blood flow rate by measuring the local clearance of a radioactive tracer (Kety, 1949). The model was further developed to allow quantitative regional blood flow rate determination using an intravenous bolus of an inert, freely diffusible tracer, iodoantipyrine (Kety, 1960a; Kety, 1960b). The Fick principle in turn is based on the theory of mass conservation. That is, for a substance distributed to a tissue in the blood within a time Δt, the quantity brought in Q_a is equal to the quantity accumulated in the tissue Q_t metabolised Q_m or removed from the tissue Q_e:

$$\frac{Q_a}{\Delta t} = \frac{\Delta Q_t}{\Delta t} + \frac{Q_m}{\Delta t} + \frac{Q_e}{\Delta t} \qquad (5)$$

A freely diffusible substance injected as a rapid intravenous bolus, will accumulate in the tissue until its tissue concentration C_t is equivalent to that in the arterial blood C_a. If the substance is inert $Q_m=0$, and as Q_a is the product of blood flow F and C_a, then:

$$\frac{dQ_t}{dt} = F(C_a - C_v) \qquad (6)$$

After a sufficient period of time (T), there will be equilibration between the concentration of the substance in the tissue and the venous blood, so:

$$C_t = \frac{Q_{t(T)}}{V} = C_{v(T)}\lambda \qquad (7)$$

where λ is the tissue-blood partition coefficient of the substance, and V is the volume of the tissue. Integrating (6) and substituting (7) yields:

$$\frac{F}{V} = \frac{C_{v(T)}\lambda}{\int_0^T (C_a - C_v)dt} \qquad (8)$$

which requires knowledge of the arterial and venous concentrations in order to determine blood flow rate. This has been used to determine cerebral blood flow rate using nitrous oxide. If the substance is not freely diffusible then equation (6) needs to be modified to include the extraction fraction E (fractional loss from blood to tissue in a single passage). Also, in other organs, determination of C_v may not be practical:

$$\frac{dQ_t}{Vdt} = \frac{dC_t}{dt} = \frac{EF}{\lambda V}(\lambda C_a - C_t) \qquad (9)$$

Integrating and solving this equation when C_a is negligible, as for interstitial injection of an inert radioactive tracer,

$$C_t(T) = C_t(0)e^{-(\frac{EF}{\lambda V})t} \qquad (10)$$

This equation has been used to calculate blood flow rate in superficial tumours after local injection of xenon-133, argon-41 and krypton-85 (Mantyla *et al.*, 1988). This method is obviously invasive, only gives information about a region of a tumour, and is not suitable for large or deep-seated tumours.

When C_a is variable, but 0 at time 0, and where F is blood flow rate per unit mass of tissue rather than total blood flow rate then:

$$C_t(T) = EF \int_0^T C_a e^{\frac{-EF}{\lambda}(T-t)} dt \qquad (11)$$

This equation, known as the Kety equation, has been used to derive blood flow rate using radiolabelled iodoantipyrine (IAP) as a tracer, for which E=1 (Kety, 1960b; Tozer *et al.*, 1994). It requires knowledge of the arterial input function $\int_0^T C_a dt$, which can be obtained by direct arterial sampling and the partition coefficient for the tracer in the tissue of interest. This method is widely established for measurement of blood flow rate in experimental tumours, but has not been used clinically.

The same principle is used in Positron Emission Tomography (PET) studies using the positron emitting isotope ^{15}O in water, $H_2{}^{15}O$ (Beaney *et al.*, 1984; Lammertsma & Jones, 1992). This tracer, like IAP is freely diffusible, but has the disadvantage that its half life is only 2.5 minutes, thus requiring a cyclotron to generate the isotope on the same site as the experiment. Dynamic contrast enhanced magnetic resonance imaging (DCE-MRI) also uses models based on the Kety equation (Tofts *et al.*, 1999), although the tracer used, gadopentetate dimeglumine (Gd-DTPA) is neither freely diffusible, nor a pure intravascular marker. This means that the values derived from the analysis will not give a pure measure of blood flow rate, but will also be affected by the permeability of the tissue's vessels and the vascular surface area. Non-invasive measurement of the arterial input function is also problematic, making it difficult to obtain fully quantitative measurements. It has advantages over PET however, as it does not use ionising radiation, has much better spatial resolution, and is more widely applicable due to the greater number of MRI machines in clinical centres. Xenon-enhanced computed tomography (CT) is another method that utilises the Kety equation for calculation of cerebral blood flow, using end-tidal xenon concentrations as a measure of arterial input. However, there can be errors introduced when the breathing pattern, or pulmonary function is altered (Sase, 1996; von Oettingen *et al.*, 2000).

1.2.4 Fraction of cardiac output or 'first pass' methods

Methods employing the uptake of an agent as a fraction of cardiac output include microspheres and $^{86}RbCl$. Radiolabelled microspheres are injected into the left ventricle or atrium where mixing occurs, and are then distributed according to the cardiac output to different organs. Sphere size is chosen so they are trapped in the arterioles and capillaries of the first vascular bed they encounter (Jirtle *et al.*, 1978), which requires some knowledge of the microvessel diameter in the vascular bed of interest (Endrich *et al.*, 1981). This can be

problematic in tumours, as the size of the microvessels is variable, and there are numerous arteriovenous shunts. Absolute measures of flow rate can be obtained by cannulating an artery, and collecting a reference sample at a constant volume rate in a calibrated syringe.

The ^{86}RbCl technique does not involve trapping of the tracer in the tissues. However, because it has a reasonably high extraction fraction, E (the fractional loss from blood to tissue in a single passage), its concentration in tissues remains relatively constant over the first 90 seconds after intravenous injection and dependent on the fractional distribution of cardiac output (Sapirstein, 1958). This method assumes that E is the same for all tissues (except brain), and that it is not taken up significantly by lung. These assumptions should be tested for each model system used. It requires sacrifice of the animal 90 seconds after injection, so serial measurements are impossible. It does not measure flow in arterial-venous shunts, so measures functional rather than total blood flow. Absolute measurements of flow can be obtained by determination of cardiac output from the arterial concentration time curve, by direct arterial sampling.

Both techniques are obviously invasive, the need for intraventricular injection of microspheres makes it suitable for clinical use only during a procedure such as cardiac catheterisation, which is being performed for diagnostic or therapeutic reasons. ^{86}RbCl is not suitable for clinical use. There are methods used clinically, which are based on the same principle, however. These include technetium-99m labelled hexamethyl-propyleneamine oxime, ^{99}Tc^{m}HMPAO, which is mainly used as a tracer for cerebral blood flow rate, measured by SPECT (single photon emission computed tomography). This compound is unstable and converts rapidly from the lipophilic form, which passes the blood brain barrier, to the hydrophilic form which is then trapped in the brain, and levels remain stable for 24 hours (Andersen, 1989). It has also been used to measure tumour blood flow rate in sites other than brain (Hammersley *et al.*, 1987), when it was shown to correlate well with ^{86}RbCl uptake. Rowell et al used this technique to measure blood flow in human lung tumours (Rowell *et al.*, 1993). Its main disadvantage is poor spatial resolution, and cardiac output measurement is required for absolute flow calculation. Dynamic CT measurements made in the first 30-40 seconds after intravenous bolus injection of contrast agent (during the 'first pass' of the agent through the vascular bed) also provide quantitative blood flow measurements, based on the principle of delivery in relation to cardiac output (Blomley *et al.*, 1993; Hermans *et al.*, 1999). This technique provides good spatial and temporal resolution, although the ionising radiation dose received has disadvantages when several serial measurements are required in each

patient. In addition only a single slice through the tumour can be obtained, and there are artefacts produced from sites that move with arterial pulsation or respiration.

1.2.5 Laser Doppler flowmetry

The principle described by Doppler underlying this method is that the frequency of light reflected from an object moving relative to an observer is shifted. The velocity of red blood cells is calculated from this frequency shift, using several microprobes inserted into the tissue of interest. Laser light is emitted from optical fibres in the probes, and the frequency of reflected light is detected by photodetectors. The blood volume can also be derived from the signal obtained. The product of the red cell velocity and volume gives the red cell flux. Each probe samples a microregion of the tissue of $0.01mm^3$ (Chaplin & Hill, 1995). This technique has been used to demonstrate temporal and spatial fluctuations in flow in human tumours (Acker *et al.*, 1990; Pigott *et al.*, 1996). It is invasive, suitable for superficial tumours only, and because it samples microregions rather than the whole tumour, cannot be used for serial measurements, as repositioning of the probe in the same microregions for repeated assessments would be impossible. As the technique is difficult to quantitate, results from a second probe insertion cannot be compared to those of the first.

1.2.6 Colour Doppler ultrasonography

The Doppler frequency shift is also used in this ultrasound technique to give a measure of flow velocities in tissue blood vessels. The resolution of ultrasound, and the reduced blood velocity in smaller arterioles and capillaries means that flow in these vessels is not measured by this technique. In addition bulk tissue movements produce artefacts, which can be a problem in some organs (Eriksson *et al.*, 1991). Parameters obtained include vascularity index, peak flow velocity and flow resistance index. Although these parameters have been used to improve discrimination between benign and malignant tumours (Lee *et al.*, 1995; Kurjak *et al.*, 2000; Strobel *et al.*, 2000), to give prognostic information (Sohn *et al.*, 1997) and to monitor the changes in tumour vascularity after treatment (Kedar *et al.*, 1994; Pirhonen *et al.*, 1995; van der Woude *et al.*, 1995), it has not been possible to directly relate them to other measures of angiogenesis such as microvessel density (Peters-Engl *et al.*, 1998). The technique has been improved by the use of Power Doppler, which also encodes the power in the Doppler signal, therefore giving a measure of blood volume as well as velocity (Martinoli *et al.*, 1998), and also improving the sensitivity.

1.2.7 Thermal clearance

The theory behind this method for measuring blood flow rate is based on the theory of conservation of energy. This invasive technique has been used most commonly in conjunction with hyperthermia treatments. It can be used when a tissue has reached a steady state temperature, or after the heating is stopped, by measuring the thermal clearance (Roemer *et al.*, 1985; Feldmann *et al.*, 1992). A fundamental problem with this technique is that thermal clearance is not just affected by tissue blood flow, but also by the tissue's thermal conductivity (Roemer, 1990) In addition, raising the temperature of a tissue will have effects on its blood flow.

1.2.8 Summary

Table 1.1 summarises the different techniques for measuring blood flow rate. Several different methods are suitable for clinical use, but differ in their potential for giving fully quantitative results, spatial resolution, and repeatability. As many of the models used to describe the uptake of contrast agents into tissues were initially developed for the cerebral circulation, it is important that clinical techniques are also validated for the measurement of blood flow rate in extracranial sites. No systematic comparisons of the different methods in human tumours have been performed. However, Feldmann et al have compared thermal washout techniques, dynamic CT and dynamic MRI in pelvic tumours, with good correlations (Feldmann *et al.*, 1993). Dynamic MRI and CT both provide excellent spatial resolution, and dynamic MRI has the advantage of no ionising radiation dose. However, the extracellular MR contrast agents used introduce an additional level of complexity in analysis due to their size, being neither freely diffusible nor purely intravascular, and because the increase in signal intensity they produce is not necessarily linearly related to concentration. This method was the one chosen for assessment of tumour blood flow rate in patients at Mount Vernon Hospital, due to its availability and it is discussed more fully in Chapter 4.

1.3 Tumour microenvironment

1.3.1 Tumour oxygenation

The microenvironment of tumour cells is abnormal and heterogeneous in comparison to the carefully controlled environment in normal tissues, because the alterations in blood flow described above affect the delivery of oxygen and nutrients, and the removal of waste products from the tumour tissue. Thomlinson and Gray in 1955 (Thomlinson & Gray, 1955) described the diffusion distance of oxygen in human lung carcinomas (150μm), and the occurrence of hypoxic regions of tumour and necrotic areas where the intercapillary distance

Principle	*Methods*	*Invasive*	*Quantitative*	*Serial Measurements*	*Used Clinically*	*Whole tumour*	*Resolution*
Bolus tracking (Stewart theorum)	MRI –DCE or T2*	No	Yes	Yes	Yes	Yes	Excellent
	Ultrasound with microbubble contrast	No	Yes	Yes	Yes	Yes	Good
Tracer uptake / clearance (Kety model)	^{133}Xe, ^{85}Kr, ^{41}Ar clearance	Yes	Yes	Yes (radiation dose)	Yes	No	Region
	Radiolabelled iodoantipyrine	Yes	Yes	No	No	Yes	Good
	^{15}O PET	Arterial Line	Yes	Yes (radiation dose)	Yes	Yes	Moderate
	DCE-MRI	No	Possible	Yes	Yes	Yes	Excellent
	^{133}Xe enhanced CT	No	Yes	Yes (radiation dose)	Yes	Yes	Good
Cardiac output fraction (first pass)	Microspheres	Cardiac Catheter	Yes	Limited	Yes	Yes	Poor
	RbCl	Yes	Yes	No	No	Yes	Whole tissue
	HMPAO	No	Yes	Yes (radiation dose)	Yes	Yes	Poor
	Dynamic CT	No	Yes	Yes (radiation dose)	Yes	Yes	Good
Conservation of energy	Thermal clearance	Yes	Yes	Yes	Yes	Yes	Whole tissue

Table 1.1 Indirect methods of measuring blood flow

exceeded this distance. Intratumoural pO_2 measurements using the Eppendorf polarographic electrode have demonstrated that both experimental (Figure 1.5) and human tumours frequently contain areas with very low pO_2 levels (<7.5mmHg), whereas regions with this level of pO_2 are rare in normal tissues, which usually have pO2 levels around 30-40mmHg (Vaupel & Hockel, 1998). Median pO_2 levels are also reduced in tumours. The temporal fluctuations in tumour blood flow are also reflected in temporal changes in pO_2 (Kimura *et al.*, 1996). Thus some areas of the tumour are chronically hypoxic because of the distance from the nearest capillary, and others are intermittently acutely hypoxic due to collapse or inadequate perfusion of their supplying vessel.

1.3.2 Tumour pH and energy status

Tissue pH can be measured by microelectrodes, which measure extracellular pH (pH_e) and non-invasively by magnetic resonance spectroscopy (MRS), which measures intracellular pH (pH_i). These methods have shown that tumours frequently have areas of low pH_e (Wike-Hooley *et al.*, 1985), associated with high lactate content and a shift to the glycolytic pathway for the release of energy. pH_i is however, maintained at normal levels (Griffiths, 1991). This means that the pH gradient across the plasma membrane of tumours ($pH_i > pH_e$) is the reverse of normal tissues ($pH_e > pH_i$) (Stubbs *et al.*, 1995). Other pathways that contribute to the lowering of pH_e include the production of lactate from the breakdown of glutamine, and CO_2 accumulation from cellular respiration (Newell *et al.*, 1993).

MRS has been used to measure the energy status of tumours, using the ratio of nucleotide triphosphates or phosphocreatinine to inorganic phosphate. ATP concentrations can also be measured by bioluminescence on rapidly frozen tissues. Such studies have demonstrated that the bioenergetic status in many tumours is lower than in normal tissues (Stubbs *et al.*, 1995).

The exact spatial heterogeneities in these factors do not necessarily directly overlap the local variation in pO_2 levels (Helmlinger *et al.*, 1997), although mean pH and pO_2 levels correlate well. Combination studies using bioluminescence imaging of ATP and autoradiographic measurement of local blood flow rate in a subcutaneous hamster tumour indicated that above flow rates of 0.3-0.4 ml/min/g, ATP levels are independent of flow, but below this rate, ATP levels drop rapidly (Walenta *et al.*, 1992). Overall, increasing hypoxic cell fractions in tumours correlate inversely with bioenergetic status (Koutcher *et al.*, 1990).

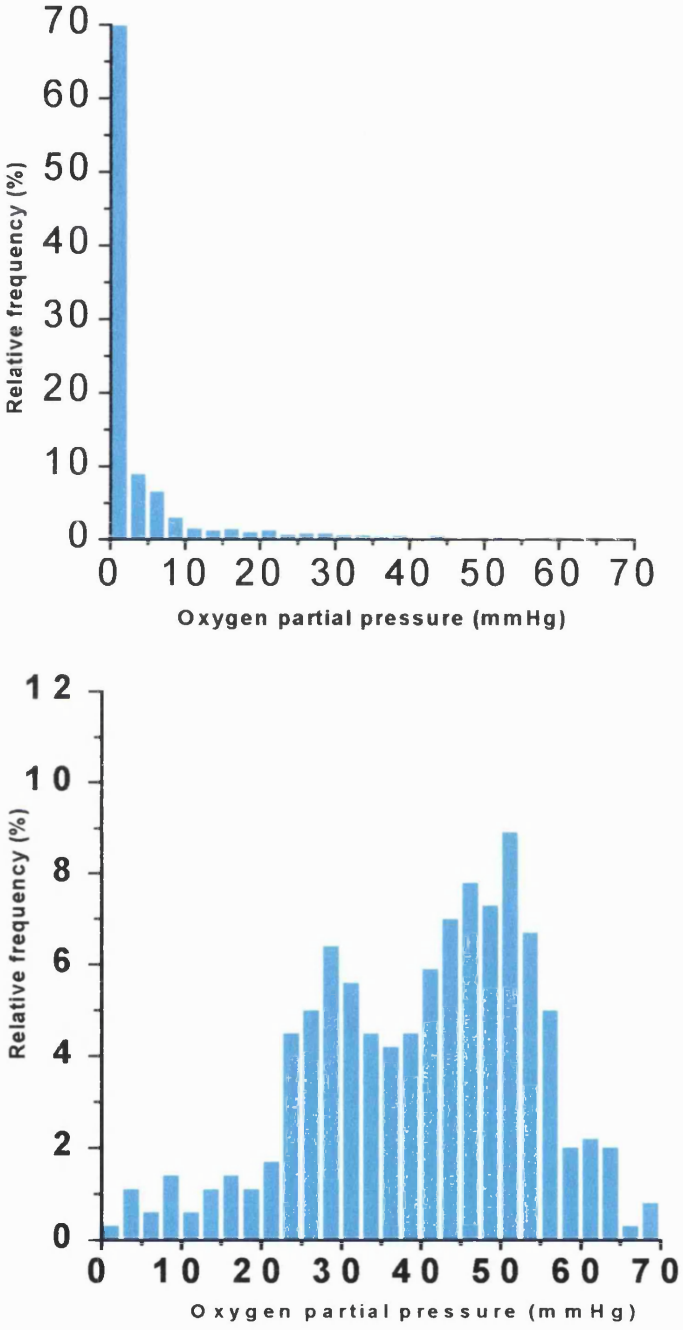

Figure 1.5 pO_2 Histograms in SaF tumour (top) and subcutis (bottom) in mice

Collingridge, Hill and Chaplin, unpublished data

1.3.3 Fluid and solute transport in tumours

Solutes in blood are delivered over long distances in the body by convection, along with bulk flow of the solvent. When they reach the exchange vessels in the capillary bed they can pass into the interstitial space by diffusion, convection or transcytosis (Jain, 1991).

Diffusion is proportional to the capillary surface area, and the concentration gradient of the solute between the vascular and interstitial compartments. It also depends on the diffusion medium, the molecular weight of the solute, and temperature. The permeability of a vessel (P) is the constant relating diffusive flux to the concentration gradients. In normal tissues, transport of low molecular weight substances occurs mainly by diffusion, with increasing convection at higher molecular weights. In tumours, however, the high permeability of the capillaries will increase diffusion, but the reduction in vascular surface area will decrease diffusion. This latter effect becomes more marked with increasing tumour size (Baxter & Jain, 1990).

Convection is proportional to the rate of fluid leakage from the vessel, which is dependent on vessel surface area, and the vascular to interstitial hydrostatic pressure gradient minus the vascular to interstitial osmotic pressure gradient. The hydraulic conductivity (L_p) of a vessel is the constant relating fluid leakage to these pressure gradients. Although the incomplete endothelial linings in tumour vessels increase L_p, the high interstitial fluid pressures in the centre of tumours reduce fluid and solute extravasation, and this is exacerbated by higher oncotic pressure in tumour interstitial space (Baxter & Jain, 1989; Stohrer *et al.*, 2000). The high interstitial pressure in the centre of tumours drops precipitously to normal at the tumour periphery (Boucher *et al.*, 1990), although vessels here may still be abnormally leaky.

In the interstitial space, solute transport occurs by diffusion and convection. Again diffusion is proportional to concentration gradients, whilst convection is proportional to interstitial fluid velocity, and the structure and composition of the interstitial compartment determine the rates of these processes. The levels of hyaluronate and proteoglycan are lower in tumour interstitial space (Gullino, 1975), which has a higher volume of free fluid than normal tissues. This tends to increase the diffusion coefficient in tumours, especially for macromolecules (Gerlowski & Jain, 1986). However the diffusion distances are increased, due to large intercapillary distances, so the time taken for macromolecules to reach the centre of tumours is dramatically increased (Jain, 1991). Convective transport in tumours is significantly increased in tumours, also due to the changes in its composition. In normal tissues

convective currents form <1% of plasma flow, whereas in tumours they can reach 14% (Vaupel & Kallinowski, 1987). The high central and low peripheral interstitial pressure lead to fluid flowing from the centre to the edge of tumours, contributing to the formation of peritumoural oedema (Butler *et al.*, 1975).

1.4 Implications for cancer treatment

1.4.1 Angiogenesis and hypoxia as prognostic markers

Many groups have used microvessel density (MVD), assessed on histological sections, as a measure of tumour angiogenesis, and found that increased MVD is associated with an adverse prognosis in a wide range of different cancer types (Horak *et al.*, 1992; Weidner *et al.*, 1992; Bochner *et al.*, 1995; Bremer *et al.*, 1996; Tanigawa *et al.*, 1996; Roychowdhury *et al.*, 1996; Crew *et al.*, 1997; Tanigawa *et al.*, 1997; Abdulrauf *et al.*, 1998). The method of measuring MVD varies, but is usually assessed in 1 or more areas of high vascular density or 'hot-spots' using immunohistochemical staining with antibodies to Factor VIII antigen, CD31 or CD34 (Weidner, 1995). Thus it is not a measure of a tumour's overall vascularity, nor of the heterogeneity of vascularity, but of the vascular density in the best vascularised parts of the tumour. In particular increased MVD or increased expression of VEGF has been associated with an increased risk of metastasis (Weidner *et al.*, 1991; Fox *et al.*, 1997; Tanigawa *et al.*, 1997; Seo *et al.*, 2000).

The presence of hypoxia has also been found to be an adverse prognostic factor in head and neck cancers, cervical cancer and soft tissue sarcomas (Brizel *et al.*, 1996; Brizel *et al.*, 1997; Hockel *et al.*, 1996). This may not just be related to the well-recognised increased radioresistance of hypoxic cells. There is evidence that in the presence of hypoxia, there is an increase in point mutations, deletions and gene amplifications, as well as induction of genomic instability (Rofstad, 2000). Furthermore, hypoxia induces apoptosis via mechanisms involving p53, but in tumours with increased genetic instability this may cause a selective pressure for clones with mutated p53 that are resistant to apoptosis (Graeber *et al.*, 1996; Hockel *et al.*, 1999). The presence of hypoxia also produces increased expression of VEGF and other angiogenic factors (Maxwell *et al.*, 1997; Dachs & Chaplin, 1998) as well as genes important in the metastatic process (Sutherland, 1998; Beavon, 1999).

The apparent paradox of both increased microvessel density and hypoxia being adverse prognostic factors is explained as the induction of angiogenesis is very much related to the presence of hypoxia, and associated with a range of genetic abnormalities which also

promote increased tumour growth and metastasis. In a study of 109 breast cancers, the presence of necrosis was closely associated with high microvessel density (Leek *et al.*, 1999). The factors that promote increased angiogenesis, because they are present in a disordered temporal and spatial array, also promote the disordered heterogeneous vascular structure, which is associated with hypoxia and necrosis (Gillies *et al.*, 1999).

1.4.2 Hypoxia and acidity - effects on radiotherapy and chemotherapy

The increased resistance of cells to radiation at pO_2 levels less than 10mmHg has been well established for nearly 50 years (Gray *et al.*, 1953). This is because oxygen affects the initial chemical products of the interaction of radiation with tissues, producing superoxide, and other oxygen related free radicals, which then increase the DNA damage produced (Lavelle *et al.*, 1973; Oberley *et al.*, 1976). There is evidence from animal tumours that such radiobiologically hypoxic cells are clonogenic (Rojas *et al.*, 1992) and as discussed above, such hypoxic areas affect prognosis in human tumours treated with radiotherapy.

Cells distant from their supplying blood vessel have a lower proliferation rate than those adjacent to the vessel (Tannock, 1968). As many chemotherapy drugs have increased activity against rapidly dividing cells, this will tend to make them more resistant to treatment. In addition the more distant cells will also be more hypoxic, and hypoxia will reduce the efficacy of several chemotherapeutic drugs (Teicher *et al.*, 1981), although others such as mitomycin-C have increased cytotoxicity in hypoxic cells. The increased extracellular acidity which occurs in tumours also has significant effects on chemotherapy agents. It increases the cell uptake and cytotoxicity of weak acids such as chlorambucil, but decreases the uptake and toxicity of weak bases such as vinblastine (Gerweck & Seetharaman, 1996). pH may also affect a drug's stability, active transport processes, or interaction with its target molecule.

1.4.3 Heterogeneous tumour fluid and solute transport

There are many molecular mechanisms of tumour cell resistance to chemotherapy. As tumours grow there is an increased likelihood that the genetic abnormalities present in different tumour clones will produce resistant cells. However, even if all the malignant cells in a tumour were sensitive to a drug's action, the drug would still need to be delivered in adequate concentrations to all clonogenic cells in order to effect a cure. The above description of the heterogeneous distribution of solutes within tumours illustrates that drug delivery, especially to the less well perfused central regions of tumours, forms a significant barrier to drug treatment of solid tumours (Jain, 1991; Krol *et al.*, 1999). This also applies to

more recently developed modes of therapy such as monoclonal antibodies, liposomal drug delivery, activated immune cells and gene therapy.

1.5 Vascular targeting

The chaotic organisation of tumour vasculature and its effects on tumour microenvironment leads to the problems outlined above in treating tumours with conventional anti-cancer agents. However, the differences between normal tissue and tumour vessels and microenvironment also provide an opportunity for specific targeting of tumours. This approach has received less attention in the past than attempts to exploit cellular and molecular differences between normal and malignant cells.

One rapidly expanding field is in the development of anti-angiogenic agents, which oppose the action of the angiogenic agents released by tumour cells. Table 1.2 lists the drugs and their targets currently in clinical development as anti-angiogenic agents. Many of them target the VEGF pathway, by neutralising these powerful angiogenic factors, or blocking their receptors. Some are naturally occurring anti-angiogenic agents, while the metalloproteinase inhibitors aim to block the interaction of growing vessels with the surrounding tissues. The attraction of these agents is that they may well have a different spectrum of toxicities from traditional cancer treatments, and in pre-clinical models some agents have had significant anti-tumour activity with little or no toxicity (O'Reilly *et al.*, 1997; Zhu & Witte, 1999; Laird *et al.*, 2000). However, it may well be necessary to maintain treatment with these drugs over much longer periods than traditional treatments, requiring long-term tolerability and raising issues of affordability. It is also possible that some of these drugs may stabilise disease rather than inducing tumour shrinkage, and therefore clinical development needs modification from the traditional clinical response assessment to include measures of biological activity in the early clinical trials.

Vascular targeting is a different approach, because the aim is not prevention of the growth of a tumour's vessels, but rather the rapid and selective destruction of the abnormal vasculature already established in the tumour. The suggestion that the differences in tumour vasculature might lend themselves to therapeutic attack was first suggested by Denekamp in 1982 (Denekamp, 1982). The potential therapeutic benefit of this approach was confirmed by artificially inducing ischaemia in a tumour by clamping off its feeding vessel, resulting in tumour growth delay and, after prolonged ischaemia, cures (Denekamp *et al.*, 1983).

Drugs that block matrix breakdown:			
Drug	**Sponsor**	**Trial**	**Mechanism**
Marimastat	British Biotech	Phase III non-small cell lung, small cell lung, breast cancers.	Synthetic inhibitor of matrix metalloproteinases (MMPs)
AG3340	Agouron;	Phase II glioblastoma multiforme.	Synthetic MMP inhibitor
COL-3	Collagenex;	Phase I/II brain.	Synthetic MMP inihibitor. Tetracycline® derivative
Neovastat	Aeterna;	Phase III renal cell (kidney) cancer, Phase III non-small cell lung cancer.	Naturally occurring MMP inhibitor
BMS-275291	Bristol-Myers Squibb;	Phase II/III Advanced or Metastatic Non-Small Cell Lung.	Synthetic MMP inhibitor

Drugs that inhibit endothelial cells directly:			
Drug	**Sponsor**	**Trial**	**Mechanism**
Thalidomide	Celgene	Phase I/II Melanoma, Phase II head and neck cancer, ovarian, metastatic prostate, and Kaposi's sarcoma; Phase II with chemotherapy against solid tumors; adjuvant recurrent or metastatic colorectal cancer; Phase II Graft vs Host Disease; Phase II gynecologic sarcomas, liver cancer; multiple myeloma; CLL, Recurrent or Progressive Brain, Phase III non-small cell lung, nonmetastatic prostate, refractory multiple myeloma, renal cancer.	Unknown
Squalamine	Magainin Pharmaceuticals	Phase II non small cell lung cancer; Phase II Ovarian; Phase I	Extract from dogfish shark liver; inhibits sodium-hydrogen exchanger, NHE3
Endostatin	EntreMed;	Phase I.	Inhibition of endothelial cells

Drugs that block activators of angiogenesis:			
Drug	**Sponsor**	**Trial**	**Mechanism**
SU5416	Sugen	Phase I; Phase I with chemotherapy against solid tumors; Phase I/II AML; Phase I/II glioma, advanced malignancies, advanced colorectal, Phase II von-Hippel Lindau disease, advanced soft tissue; Phase II prostate cancer, colorectal cancer, metastatic melanoma, multiple myeloma, malignant mesothelioma: metastatic renal, advanced or recurrent head and neck, Phase III metastatic colorectal cancer.	Blocks VEGF receptor signaling
SU6668	Sugen	Phase I advanced tumors.	Blocks VEGF, FGF, and PDGF receptor signaling
Interferon-alpha	Commercially available	Phase II/III	Inhibition of bFGF and VEGF production
Anti-VEGF Antibody	National Cancer Institute, Genentech	Phase I refractory solid tumors. Phase II metastatic renal cell cancer.	Monoclonal antibody to vascular endothelial growth factor (VEGF)

Drugs that inhibit endothelial-specific integrin/survival signaling:			
Drug	**Sponsor**	**Trial**	**Mechanism**
EMD121974	Merck	Phase I advanced or metastatic cancer, Phase I HIV related Kaposi's Sarcoma, Phase I/II Anaplastic Glioma	Small molecule blocker of integrin present on endothelial cell surface

Drugs with non-specific mechanism of action:			
Drug	**Sponsor**	**Trial**	**Mechanism**
CAI	National Cancer Institute	Phase I combination solid tumors; Phase II ovarian cancer; advanced renal cell cancer, metastatic renal cell cancer, Phase III non-small cell lung cancer.	Inhibitor of calcium influx
Interleukin-12	Genetics Institute	Phase I/II Kaposi's sarcoma; Phase I/II Interleukin-12 gene therapy.	Up-regulation of interferon gamma and IP-10
IM862	Cytran	Phase I recurrent ovarian cancer; Phase II metastatic colorectal cancers; Phase III Kaposi's sarcoma.	Unknown mechanism

Table 1.2 Listing of anti-angiogenic drugs in clinical trial on National Cancer Institute website Nov 2000 VEGF = vascular endothelial growth factor, FGF = fibroblast growth factor, PDGF = platelet derived growth factor

There are several advantages to targeting tumour vasculature rather than the malignant cells themselves either using anti-angiogenic or vascular targeting agents (Chaplin & Dougherty, 1999). Each vessel supplies many thousands of tumour cells, so damage to a small section of the vessel, which causes occlusion, is amplified to produce large-scale tumour cell death. The delivery problems of conventional chemotherapy to tumour cells, which were outlined above, are dramatically reduced as the target is the endothelial cell within the vessel, and delivery to every endothelial cell is not required. Furthermore, the target endothelial cells are not malignant, and do not have the high mutation rate of tumour cells, so drug resistant clones are much less likely to occur.

Many different ways of achieving vascular targeting are being developed.

1.5.1 Photodynamic therapy and hyperthermia

The use of moderate hyperthermia in experimental tumours has been shown to produce vascular damage and ischaemic tumour cell death (Reinhold & Endrich, 1986), and although the mechanism of the anti-tumour effect in hyperthermia is multifactorial, there is evidence that proliferating endothelium is more sensitive to heat (Fajardo *et al.*, 1985). After hyperthermia there is endothelial cell swelling and disintegration, as well as haemorrhage, red blood cell and platelet aggregation (Eddy, 1980). Despite this, the response of human tumours to hyperthermia has been less dramatic than the results from experimental tumours, and this technique is practically limited to superficial tumours, which usually require invasive methods of heating.

Photodynamic therapy (PDT) involves the systemic administration of a photosensitiser, which is locally activated by treatment with light. Like hyperthermia, some of the anti-tumour action of PDT has been attributed to vascular damage, with induction of haemorrhagic necrosis in tumours (Star *et al.*, 1986), although there is also an element of direct tumour cell killing by production of reactive oxygen species. Observations in a window chamber indicated that vascular stasis occurred in tumour vessels when light treatment was given at a time when the photosensitiser concentration was maximal in the tumour vessels, but did not occur if light treatment was given 3 hours later. Greater tumour regression occurred in the tumours that had vascular stasis (Fingar *et al.*, 1999). Some of the endothelial damage may result from local production of TNF-α from tumour associated macrophages (Pass, 1993). Due to the limited tissue penetration of the light used in PDT however, this treatment

modality is also restricted to superficially situated tumours, and is not applicable to bulky tumour masses.

1.5.2 Antibody targeting

Several groups are developing methods for antibody directed targeting of tumour vasculature. Huang et al demonstrated the validity of this approach using an experimental murine tumour model transfected with interferon-γ. This induced local expression of MHC class II molecules on tumour endothelium, which are normally absent from murine vasculature. Antibodies against MHC class II were conjugated to a human coagulation inducing protein - tissue factor, and 38% of treated mice had complete tumour regressions (Huang *et al.*, 1997). More recently they have extended this to targeting a naturally occurring marker – vascular cell adhesion molecule 1 (VCAM –1), which is present on tumour endothelium in a number of human tumours, and only expressed in a few normal tissues (Ran *et al.*, 1998). Treatment caused selective tumour vessel thrombosis and growth retardation. Hu et al used an immunoconjugate consisting of altered factor VII, a component of the clotting cascade that binds with high specificity to tissue factor, combined with an effector domain that induces cell killing. Tissue factor is expressed in tumour endothelium but not normal endothelium, and this immunoconjugate caused tumour regression in a human melanoma xenograft in mice (Hu *et al.*, 1999). Another group has used immunotoxin conjugates with antibodies targeted to endoglin, a proliferation associated antigen on endothelial cells, (Seon *et al.*, 1997; Matsuno *et al.*, 1999), with complete tumour growth inhibition, even though these were anti-human endoglin antibodies with limited cross reactivity with mouse endothelial cells. Integrin αVβ3 is also preferentially expressed on proliferating endothelium and monoclonal antibodies against this integrin promote tumour regression by causing apoptosis of proliferating endothelial cells (Brooks *et al.*, 1994) A humanised form of this antibody has proved safe in Phase I trials, and recruitment into Phase II trials is on-going (Gutheil, 1998). Others have generated monoclonal antibodies against rat tumour endothelial cells and used these unconjugated, which produced growth suppression and intravascular thrombosis in tumours (Ohizumi *et al.*, 1999), and conjugated with neocarzinostatin, an antitumour polypeptide, which produced tumour haemorrhagic necrosis (Makimoto *et al.*, 1999).

The above studies demonstrate the potential therapeutic benefit of this method of vascular targeting, but for clinical development a truly specific target for human tumour endothelium is required. The use of phage libraries has enabled selection of antibodies and peptides with improved specificity for tumour endothelium (Arap *et al.*, 1998; Pasqualini, 1999; Cooke *et al.*,

2000), and this work provides hope that antibody or peptide targeting of human tumour vasculature will become a useful clinical tool. At present, however it remains largely in the pre-clinical phase of development.

1.5.3 Gene therapy

In theory, gene therapy directed at tumour vasculature has greater potential for tumour selectivity than other methods of vascular targeting, as this could be controlled at several stages in the process. Gene delivery may be less of a problem in this context than in many other areas of gene therapy, as the target cell is next to the blood stream. Also even the low transfection rates currently achievable *in vivo* might be sufficient to cause enough vascular damage to slow tumour growth. Selectivity of gene delivery to tumour vessels might be achieved by genetically engineering retroviral or adenoviral vectors to include single chain Fv proteins, bispecific antibodies, or peptide sequences which have specificity to tumour endothelium (Chaplin & Dougherty, 1999). A further level of selectivity could be added by the use of regulatory elements that limit gene expression to tumours. For example, incorporation of a hypoxia responsive element (HRE) in the vector would restrict gene expression to the hypoxic regions of tumours (Dachs *et al.*, 1997). Use of a prodrug system, which is only activated into a toxic species by the successfully transfected and expressed gene product, should further enhance specificity of activity (Vile & Hart, 1993).

Although there is increasing interest in the development of this therapeutic strategy, clinical trials of vascular targeted gene therapy remain some way off.

1.5.4 Cytokines

The cytokines TNFα, interferon, IL-2 and IL-12 have all been shown to have some anti-vascular actions, which might contribute to their overall anti-tumour effect. Interferons α and β caused rapid onset endothelial cell damage and coagulative necrosis in experimental tumours (Dvorak & Gresser, 1989). IL-12 has several direct cellular and humoral anti-tumour effects, but in addition promotes the destruction of tumour vasculature and inhibition of angiogenesis (Boggio *et al.*, 1998). Lymphokine activated killer cells, used in combination with high dose IL-2 also have endothelial cytotoxicity, and this action may be responsible for the capillary leak syndrome associated with this treatment (Kotasek *et al.*, 1988). Of all these cytokines, TNF-α is the one whose activity has been most clearly attributed to its anti-vascular effects.

TNFα is a soluble factor isolated from the blood of mice infected with bacille Calmette-Guerin (BCG) and challenged with endotoxin (Carswell *et al.*, 1975). It caused marked tumour necrosis when transferred into tumour bearing mice. It is likely that the tumour responses seen after spontaneous or induced bacterial infection (Coley's toxin) were probably due to endotoxin induced production of TNF-α (Wiemann & Starnes, 1994). TNF-α can induce direct tumour cell kill and stimulate other immune responses, but its main effect in tumours is due to damage to the vasculature (Kallinowski *et al.*, 1989). However, when recombinant TNF-α was used systemically it had a very low maximum tolerated dose (MTD), much less than the effective dose in animals, and only rare tumour responses were seen, with severe side effects (Lejeune *et al.*, 1998). Despite this, it has found a role as a regional treatment for patients with melanoma with *in transit* metastases or in limb sarcomas, using isolated limb perfusion (ILP). Much higher concentrations of the cytokine can be achieved locally, whilst limiting the systemic dose. Generally it is used in combination with a chemotherapy agent such as melphalan. Response rates of 81% with 28% complete responses were seen with this regimen in advanced soft tissue sarcomas (Eggermont *et al.*, 1997). In patients with melanoma in a multicentre randomised phase II trial, overall response rates of 91% were seen and addition of interferon-γ (IFN-γ) did not make a significant difference to the response rate (Lienard *et al.*, 1999). Other groups have confirmed the high response rates of this technique (Gutman *et al.*, 1997; Lev-Chelouche *et al.*, 1999). Histological and angiographic studies have established that ILP with TNF-α causes disruption of the tumour vasculature, with evidence of early infiltration into the tumour of lymphocytes and macrophages (Lejeune *et al.*, 1998). More recently the mechanism of this disruption has been elucidated - Ruegg et al have shown that treatment of human endothelial cells with TNF-α and interferon-γ leads to deactivation of integrin αVβ3, loss of adhesion and death by apoptosis. In melanoma patients treated with ILP with melphalan alone, apoptosis of tumour cells only occurred. However, after treatment with ILP with TNF-a, IFN-γ and melphalan in combination, apoptosis and detachment of endothelial cells occurred (Ruegg *et al.*, 1998) with subsequent tumour haemorrhagic necrosis.

These studies illustrate the high response rates achievable with a combination of vascular targeting and a cytotoxic drug, but the systemic toxicity of TNF-α limits its use to the relatively uncommon situation of locally advanced cancer in a limb.

1.5.5 Drug therapy

Although several chemotherapy drugs in current use have vascular toxicities associated with them (Doll *et al.*, 1986), there are only two groups of drugs that have been shown to have significant tumour vascular targeting activity. These are flavone acetic acid (FAA) and its derivatives, and tubulin-binding agents. This is in contrast to the many drugs being developed with anti-angiogenic activity. The relative lack of drug development in this area is partly due to the absence of relevant *in vitro* assays for vascular targeting activity. This activity has only been identified after drugs have been tested *in vivo*, in solid tumour models, when increased anti-tumour activity has been seen in comparison to *in vitro* tumour cytotoxicity.

5,6-dimethyl xanthenone acetic acid (DMXAA) is a more potent derivative of FAA (Rewcastle *et al.*, 1991). DMXAA and FAA have been shown to induce vascular collapse and haemorrhagic necrosis in subcutaneous transplanted tumours (Smith *et al.*, 1987; Rewcastle *et al.*, 1991; Zwi *et al.*, 1994; Laws *et al.*, 1995). Both drugs have little direct cytotoxicity in vitro, but have activity against a range of transplantable murine tumours with an established vasculature (Plowman *et al.*, 1986; Bibby *et al.*, 1988; Hill *et al.*, 1989; Rewcastle *et al.*, 1991). They also stimulate immune responses and cytokine release (Ching & Baguley, 1987; Mace *et al.*, 1990; Ching *et al.*, 1992; Baguley *et al.*, 1997). The early vascular effects appear to be related to production of TNF-α, as antibodies to TNF-α prevent vascular shutdown with FAA (Mahadevan *et al.*, 1990). The anti-tumour effect of DMXAA correlates well with TNF-α production across a series of DMXAA analogues (Philpott *et al.*, 1995). However, it is intratumoural levels of TNF-α rather than serum levels which are important in determining both vascular shutdown and anti-tumour activity (Ching *et al.*, 1995; Ching *et al.*, 1998; Cao *et al.*, 1999).

FAA failed to show any anti-tumour activity in humans in Phase I and II trials (Kerr *et al.*, 1987; Kerr *et al.*, 1989; Kaye *et al.*, 1990; Thatcher *et al.*, 1990; Havlin *et al.*, 1991; O Reilly *et al.*, 1993). This was thought to be due to a species specific difference in the ability to induce TNF-α, as FAA is much less effective in inducing TNF-α in human rather than mouse cell lines (Ching *et al.*, 1994). DMXAA however induces TNF-α in cell lines from both species. A phase I trial, organised by the Cancer Research Campaign in the UK at Mount Vernon Hospital, Bradford Royal Infirmary and in New Zealand has just been completed.

The vascular effects of tubulin-binding agents have been noted for many years. Ludford described the effects of colchicine on tumours in the 1940s, including the induction of haemorrhagic necrosis, and damage to growing tumour blood vessels (Ludford, 1945). In 1954, another tubulin-binding agent, podophyllotoxin was shown to cause tumour blood flow reduction and subsequent necrosis (Algire *et al.*, 1954). However, both these drugs had severe systemic toxicity at doses required to produce anti-vascular effects. Following the development of cytotoxic agents at this time attention was diverted to the anti-proliferative effects of tubulin-binding agents, which were shown to produce mitotic arrest in tumour cells and cell death (Wilson, 1975). More recently, the anti-vascular activity of the vinca alkaloids and colchicine has been clearly documented (Baguley *et al.*, 1991; Hill *et al.*, 1993; Hill *et al.*, 1995; Nihei *et al.*, 1999). Once again, this anti-vascular action was only seen at doses very close to the MTD, much higher than the equivalent clinical doses used in man, although there was some degree of tumour selectivity (Hill *et al.*, 1993). 6 hours post treatment with vincristine there was >70% reduction in tumour blood flow, but 20-30% reduction in kidney, liver skin and muscle. All normal tissues had recovered by 24 hours, but tumour blood flow remained 40% below pre-treatment levels. Vinblastine at its MTD produced 90% reduction in tumour blood flow at 6 hours, with little recovery at 24 hours. Changes in normal tissues were similar to vincristine, although kidney blood flow was not reduced. The typical histological changes indicating vascular damage were seen, with areas of haemorrhagic necrosis in the centre of tumours, and a surviving rim of viable tumour cells. The vascular targeting effects were not related to production of TNF-α (Hill *et al.*, 1995). Although the extensive haemorrhagic necrosis produced looks impressive, it only represents 1-2 logs of cell kill, and the surviving rim of cells rapidly repopulate the tumour, leading to only brief tumour growth delay (Denekamp, 1991).

1.5.6 Summary

It is possible to exploit the abnormalities of the tumour vasculature and microenvironment to produce selective tumour vascular targeting. Some of the methods of achieving this are limited to localised or superficial tumours (PDT and hyperthermia), others are limited by systemic toxicity (TNF-α, colchicine and vinca alkaloids), or require further pre-clinical development (gene therapy and antibody/ peptide targeted therapy). A few have made it into early clinical development (anti-integrin αVβ3, DMXAA). All produce typical rapid histological changes in tumours, and tend to spare the rim of cells around the edge of tumours. This may be because the raised interstitial pressure in the centre of tumours

contributes to the reduction in tumour blood flow there. Close to the edge of tumours however, the pressure drops rapidly to normal so that the vascular damage caused by any of the above agents does not cause cessation of blood flow in this region. The sparing of some areas of tumour allows rapid repopulation by the remaining viable tumour cells. The place of vascular targeting in cancer therapy is therefore likely to be in combination with conventional agents, which are less limited by the problems of drug delivery, low pO2 and low pH in the comparatively well perfused rim of tumours. Indeed this approach has been shown to produce improved anti-tumour efficacy by the combination of DMXAA with chemotherapy (Cliffe *et al.*, 1994; Pruijn *et al.*, 1997; Lash *et al.*, 1998), radiotherapy (Wilson *et al.*, 1998) and radioimmunotherapy (Pedley *et al.*, 1996)

1.6 Cytoskeleton structure and function

1.6.1 Introduction

In order to understand why tubulin-binding agents might share vascular targeting activity it is necessary to understand the structure and function of tubulin. Most eukaryotic cells contain three types of filaments that make up the cytoskeleton, and which integrate cytoplasmic activities; microfilaments, intermediate filaments and microtubules. These three types of filament interact with each other, and with organelles, other proteins and the cell membrane to co-ordinate and control cell shape, movement and division, as well as the spatial organisation and movement of organelles. (Bershadsky & Vasiliev, 1988; Amos & Amos, 1991). Figure 1.6 illustrates the different localisation of the 3 types of filament within the cell.

Microfilaments are two-stranded helical polymers of the globular protein actin, with a diameter of 5-9 nm, and are typically organised into linear bundles or networks, often concentrated just beneath the plasma membrane. Intermediate filaments are rope-like fibres with a diameter of around 10 nm. They are a heterogeneous family, with many proteins specific to cell types (Fuchs & Weber, 1994). For example, epithelial cells contain a diverse family of keratins, and neurones contain neurofilaments. Intermediate filaments are able to withstand higher stresses and stretching forces than microfilaments or microtubules, and have a universal property of mechanical reinforcement. Microtubules, the largest components of the cytoskeleton, are formed from polymerisation of heterodimers of α and β tubulin. Actin and tubulin are highly conserved throughout eukaryotes.

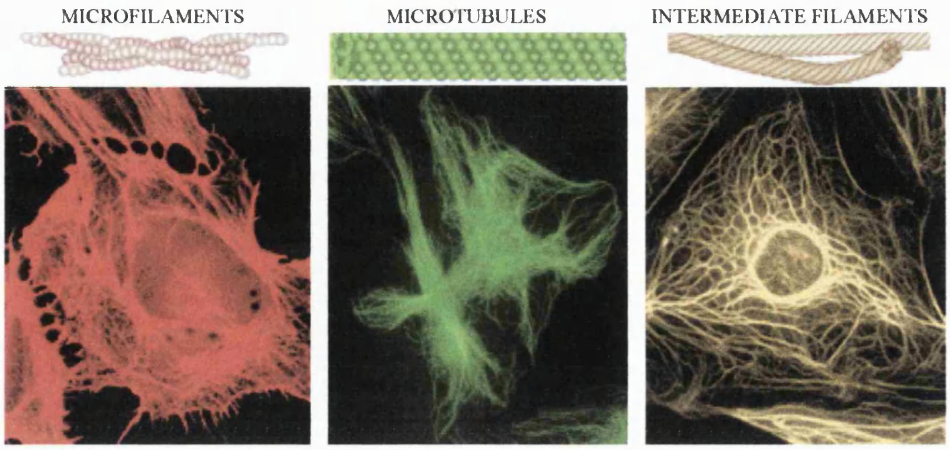

Figure 1.6 The components of the cytoskeleton. Cells stained with fluorescent antibodies to actin (left), tubulin (middle) and intermediate filaments (right)

Adapted from Ingber Scientific American January 1998
http://www.sciam.com/1998/0198issue/0198ingber.html

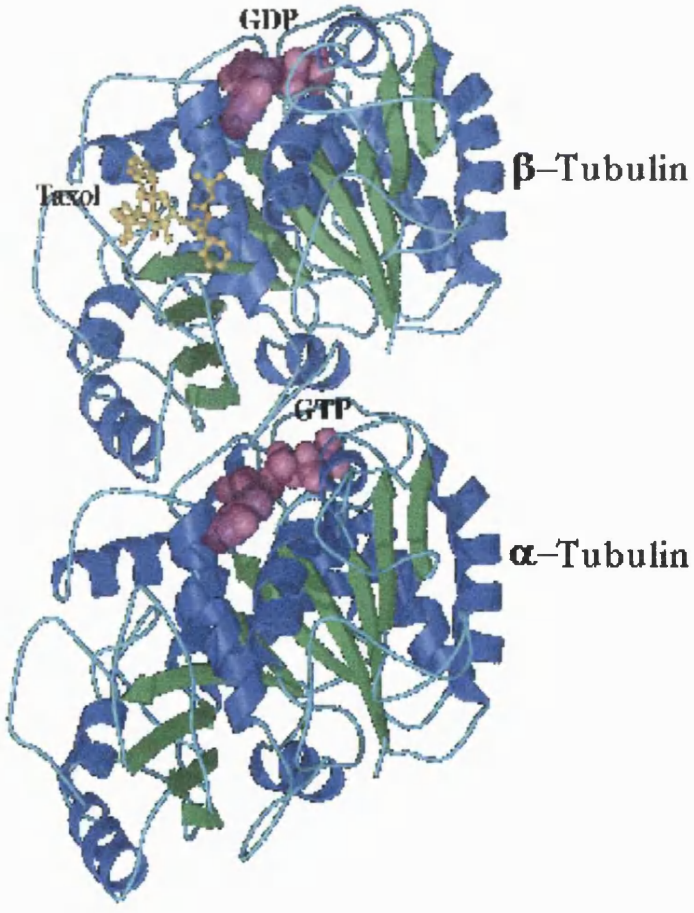

Figure 1.7 Ribbon diagram of the tubulin dimer. β tubulin with bound GDP is at the top, α tubulin with bound GTP is at the bottom.

From Nogales E et al. Nature 1998

1.6.2 Tubulin structure

α and β tubulin each contain around 450 amino acids, with a molecular weight of 50,000. The amino acid sequence of each subunit is very similar, and each contains a GTP binding site, which is non-exchangeable in α tubulin, but exchangeable in β tubulin. Both α and β tubulin have several isotypes and undergo post-translational modifications such as phosphorylation, acetylation, detyrosination and glutamylation. The 3D structure of α and β tubulin is also similar; each monomer is formed by a core of two beta-sheets surrounded by alpha helices (Nogales *et al.*, 1998). The 3D structure is illustrated in Figure 1.7. Heterodimers of α and β tubulin self assemble into protofilaments as shown in Figure 1.8. GTP at the exchangeable site is required for assembly into protofilaments, and is hydrolysed to GDP following addition of a dimer.

1.6.3 Microtubule structure and dynamic instability

Microtubules are formed by the lateral association of protofilaments to form hollow cylinders 25 nm in diameter, with 8 nm spacing between dimers. *In vivo* there are generally 13 protofilaments in each microtubule arranged in the form of a B lattice as shown in Figure 1.9 (Wade & Hyman, 1997). Microtubules have been shown to grow by elongation of open sheets of this B lattice formation that later close into a cylinder (Chretien *et al.*, 1995). In a B lattice, the nearest lateral neighbour of each α or β tubulin monomer is identical, but slightly offset. In an A lattice organisation, the lateral neighbours alternate. As the lattice closes to form a cylinder, the rows of identical monomers form helices, with each complete turn bringing the transverse helices to a point 3 monomers above the position in the first protofilament. This means that where the first and last protofilament meet there is a discontinuity, known as a seam (Wade & Hyman, 1997).

After the addition of a dimer to the end of a protofilament, and the exchange of GTP for GDP, the 'straight' conformation of tubulin-GDP becomes 'curved' as seen in Figure 1.8. Within the lattice however, the lateral subunit contacts maintain the 'straight' conformation, but on depolymerisation, when the lateral constraints are lost, the protofilaments curve away from the microtubule.

An individual microtubule has a half-life of only 10 minutes, whereas the half-life of the tubulin molecule is more than 20 hours. This illustrates the dynamic state of microtubules, which have three stages in their life, nucleation, assembly and disassembly (Mitchison &

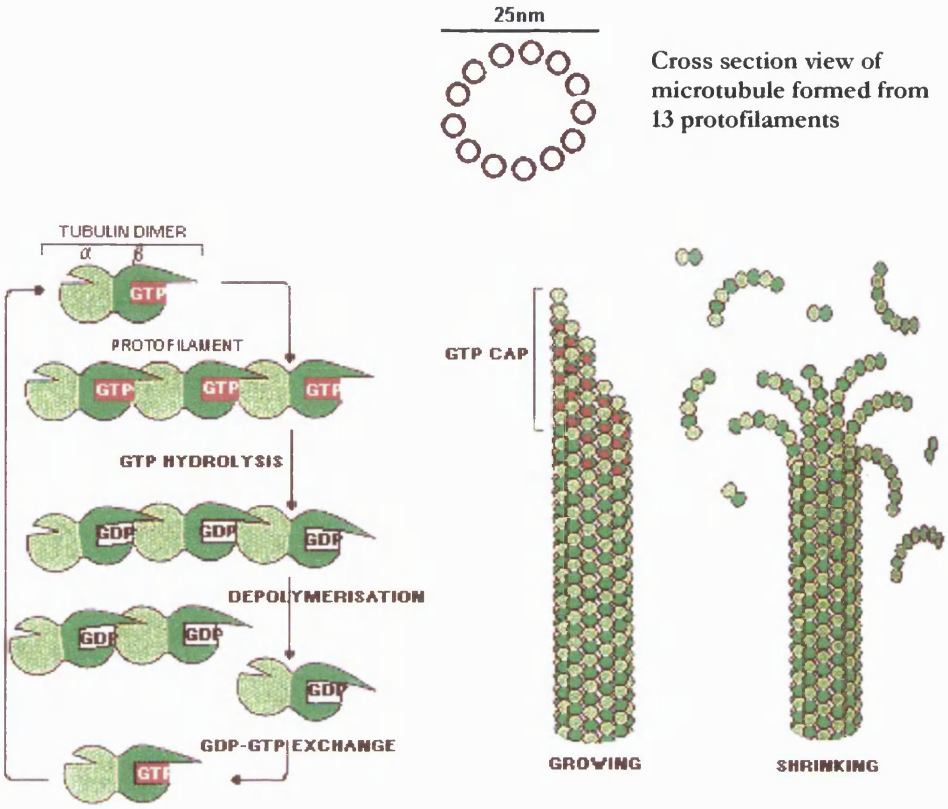

Figure 1.8 Microtubule Structure. Heterodimers of α and β tubulin self assemble into protofilaments with the β subunit at the more rapidly growing plus end. GTP is bound at the exchangeable site on β tubulin. Protofilaments make lateral contacts with each other to form a hollow tube 25nm in diameter– the microtubule. The growing microtubule has a GTP cap at the plus end, which protects it from depolymerisation. Loss of the GTP cap leads to rapid depolymerisation.

Adapted from Alberts et al 1994

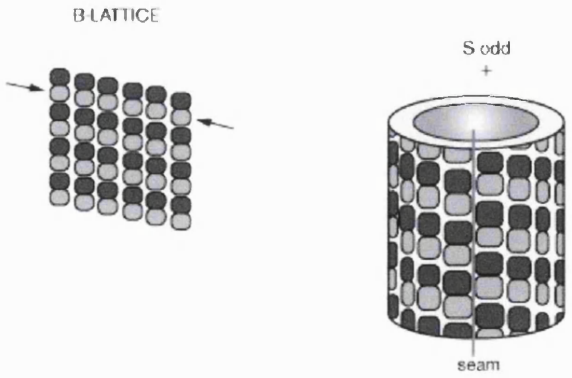

Figure 1.9 Microtubule surface lattice shown as a flat sheet (left) and as a tube (right). In a B lattice organisation, the nearest lateral neighbour of each monomer is identical. In the tube, one complete turn brings the transverse helices to a position S monomers above the start along the first protofilament. *In vivo* microtubules generally have 13 protofilaments and 3 starts. In this case there is a discontinuity in the helices, referred to as a seam.

Adapted from Wade and Hyman, 1997

Kirschner, 1984). *In vitro,* microtubules self-nucleate and grow from both ends, but one end – the 'plus' end - grows at three times the rate of the other – the 'minus' end. This is due to the structural polarity of the microtubule discussed above. The β tubulin subunit is aligned towards the plus end (Mitchison, 1993). *In vivo,* microtubules nucleate within the centrosome, which contains γ tubulin (Joshi *et al.*, 1992), and other centrosome specific proteins important for nucleation (Zheng *et al.*, 1995). The minus end is embedded in the centrosome, protecting it from depolymerisation. The centrosome is located in the perinuclear area of the cell, and the microtubules grow out from this area towards the plasma membrane. Microtubules depolymerise 100 times faster from an end containing GDP tubulin than from one containing GTP tubulin. The GTP cap at the 'plus' end therefore favours growth as shown in Figure 1.8. If the cap is lost, then rapid depolymerisation occurs – an event known as 'catastrophe'. Individual microtubules therefore alternate between periods of slow growth and rapid disassembly, a phenomenon called 'dynamic instability' (Mitchison & Kirschner, 1984). A switch from shortening to elongation may also happen abruptly and is termed 'rescue'.

Not all microtubules within a cell are so labile. There is a sub-population of 10-20% of microtubules, which are more stable, with increased resistance to depolymerisation. These microtubules usually accumulate some of the post-translationally modified forms of tubulin (Schulze *et al.*, 1987), and may also be stabilised by binding to microtubule associated proteins (MAPs) (Cassimeris, 1999), by interaction with intermediate filaments and microfilaments, and by association with organelles (Gelfand & Bershadsky, 1991). In contrast to the short half-life of dynamic microtubules, they have a half-life of the order of hours, and they accumulate in more differentiated cells (Bulinski & Gundersen, 1991)

1.6.4 Microtubule Isotypes and Microtubule Associated Proteins

The dynamic nature of microtubules and their polar orientation are essential features that enable them to perform their functions. These include formation of the mitotic spindle and chromosome separation, providing a structure for the intracellular transport of organelles, involvement in cell motility, and maintenance of cell shape and polarity (Avila, 1992).

In order to perform these functions microtubules interact with three main classes of proteins (Mandelkow & Mandelkow, 1995). The microtubule associated proteins or MAPs bind to, stabilise and promote the assembly of microtubules, and can be co-purified with microtubules through cycles of assembly and disassembly. Examples include MAP1, MAP2,

MAP4 families and tau protein. Some of these proteins only occur in certain cell types, and they are located in different regions of the cell, associated with different functions. For example, tau protein is abundant in brain and neuronal tissue, where it predominates in the axon, stabilising the microtubules and promoting the formation of parallel bundles. MAP2 is also found in neurones, but predominates in dendrites. MAP4 in contrast, is ubiquitous. The motor proteins form a second class, and generate movement along microtubules, hydrolysing ATP to provide energy for the process. Kinesin moves towards the plus end of microtubules, and dynein moves towards the minus end, and is also involved in movement of cilia and flagella. These motor proteins are essential for the movement of organelles through the cytoplasm. The third class consists of a range of proteins that may associate closely, but sometimes transiently with microtubules such as glycolytic enzymes, kinases, biosynthetic proteins, proteins linking to membrane receptors, and ribonucleoproteins. These may be important in signal transduction to and from membrane receptors and integrins to produce appropriate changes in cell shape, movement, organelle transport or cell division (Gundersen & Cook, 1999).

Microtubules in different cell types not only differ in the MAPs associated with them, but also in the spectrum of tubulin isotypes from which they are constructed. There are at least seven isotypes of α and β tubulin, which are expressed in a tissue-specific pattern (Ludueña, 1993), and γ tubulin which is involved in nucleation of microtubules from the centrioles (Zheng *et al.*, 1995). For example β_{III} is found in brain and dorsal root ganglia, and expression increases during axonal outgrowth (Joshi & Cleveland, 1989), whereas β_{VI} is only found in haemopoetic tissues (Wang *et al.*, 1986). Tubulin isotypes differ mainly in their terminal carboxy portion (Sullivan, 1988). Despite the tissue specific expression, some have argued that isotypes may be functionally interchangeable (Bond *et al.*, 1986). However, there is evidence that this is not always true. For example, Falconer et al demonstrated preferential incorporation of β_{II} and β_{III} isotypes in labile and stable microtubules respectively in neuronal cells (Falconer *et al.*, 1992). Experiments with genetic substitution of isotype genes or mutations of these genes have resulted in functional abnormalities in the mutants (Ludueña, 1993). Differences in the isotype spectrum present in tubulin result in different microtubule assembly kinetics (Luduena *et al.*, 1985), and different binding kinetics to drugs (Banerjee & Luduena, 1992).

1.6.5 Cell cycle changes

The dynamic instability of microtubules is not constant through the cell cycle. As the cell enters mitosis, the radial array of long interphase microtubules is disassembled and a bipolar spindle of much shorter microtubules is formed. This reorganisation is associated with around a 10-fold increase in the rate of microtubule turnover (Cassimeris, 1999) (Figure 1.10). Dumontet et al showed that cells undergoing mitosis contained larger amounts of total tubulin, a larger fraction of polymerised tubulin, and a selectively increased content of β_{IV} isotype compared with quiescent cells. Microtubule dynamics are also modified by cellular differentiation – as cells become more highly differentiated they have a higher proportion of stable microtubules (Black *et al.*, 1986; Gundersen *et al.*, 1989) accompanied by a change in the proportion of different tubulin isotypes incorporated into microtubules (Falconer *et al.*, 1992). Selective stabilisation of microtubules determines cell polarity, by establishing predominant directions of intracellular transport and expansion of cell processes (Gelfand & Bershadsky, 1991).

1.6.6 Interaction with microfilaments and intermediate filaments

As mentioned above, actin microfilaments have a different spatial organisation within the cell than the microtubule array, but there are many structural interactions between them (Schliwa & van Blerkom, 1981), and they co-operate functionally during a variety of cellular processes. These include nuclear positioning, orienting the mitotic spindle in relation to the axis of cell division, and transferring vesicles and organelles between microtubule and microfilament transport systems (Fuchs & Yang, 1999). Actin filaments are organised into three types of array. In *parallel bundles* the filaments are oriented with the same polarity and are closely spaced. In *contractile bundles* as in stress fibres, they are arranged with opposite polarities, more loosely spaced and contain the motor protein myosin. In the *gel-like networks* of the cell cortex they are arranged in a loose open array with many orthogonal interconnections. Interactions between microfilaments intermediate filaments and microtubules are mediated by a variety of MAPs, plakins and actin binding proteins. For example, cortical actin foci are formed at points where the cell membrane adheres to the extracellular matrix. The growing ends of microtubules are targeted to and captured at these cortical foci, and then may be stabilised by binding to the actin binding protein coronin (Kaverina *et al.*, 1998).

The maintenance of cell shape and polarity is another example of interaction between the different cytoskeletal components. Ingber describes the cell in terms of a tensegrity structure (Ingber, 1997). In such a structure, all the structural members are under stress. Some bear

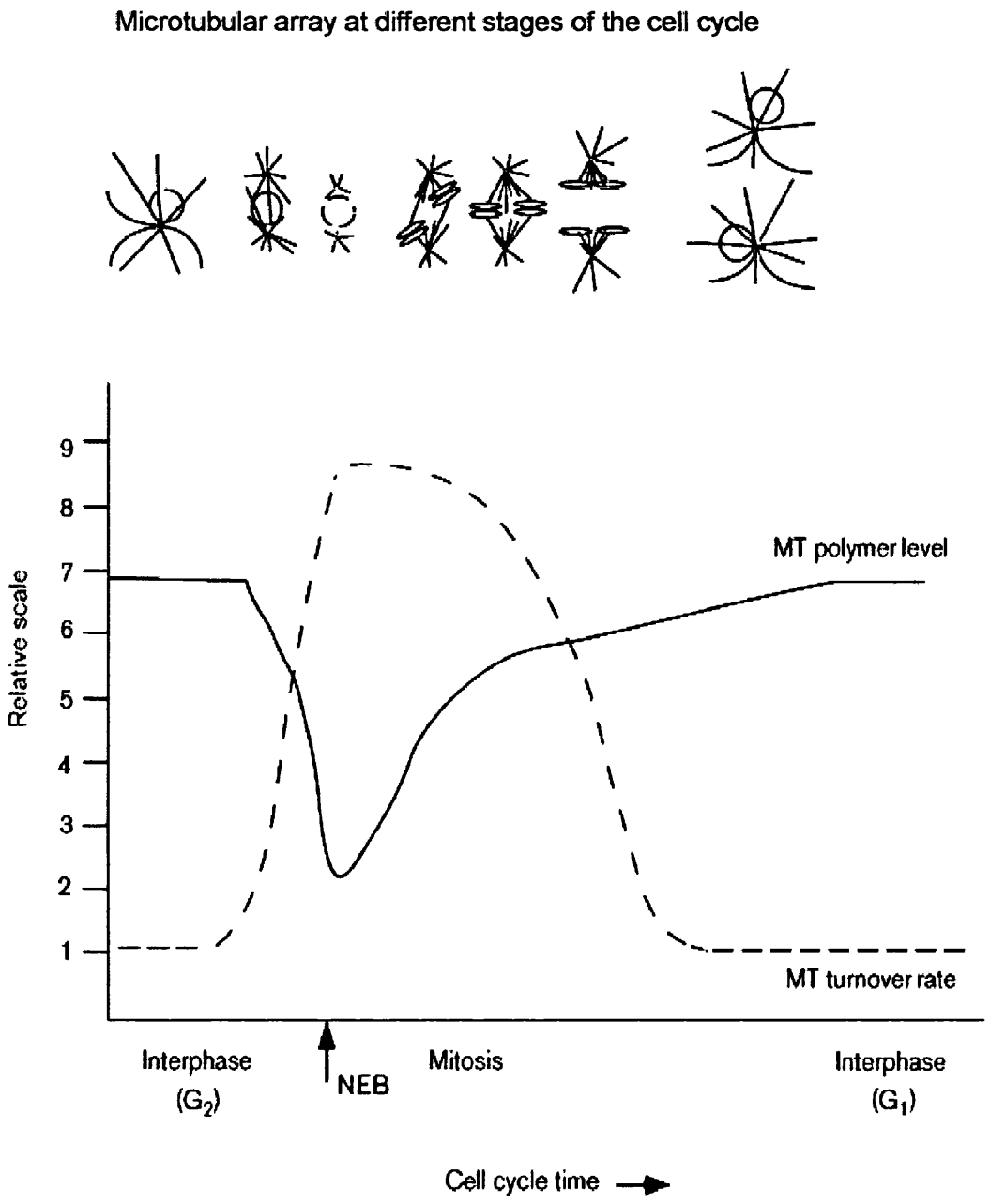

Figure 1.10 Relative changes in microtubule (MT) polymer levels (solid line) and turnover rate (dashed line) through the cell cycle

Top – Microtubular array at corresponding stages of the cell cycle

From Cassimeris, 1999

tensional stress, others are under compressive stress. These counteracting forces equilibrate across the structure, enabling it to stabilise itself. Applying this theory to the cytoskeleton, Ingber proposes that the network of contractile microfilaments, which extends throughout the cell, exerts tension and pulls the cell membrane and cytoplasm towards the nucleus. Opposing this inward pull are two main types of compressive elements, one of which is outside the cell and the other inside. The component outside the cell is the extracellular matrix to which the cell is bound by cell adhesion molecules called integrins. The compressive "struts" inside the cell can be either microtubules or large parallel bundles of cross-linked microfilaments. The third component of the cytoskeleton, the intermediate filaments, integrate these compressive and tensile forces, connecting microtubules and contractile microfilaments to one another as well as to the surface membrane and the cell's nucleus.

If the cell does have a tensegrity structure rather than just a fluid-like cytoplasm and surrounding elastic membrane, then pulling on receptors at the cell surface should produce immediate structural changes at distant sites inside the cell. This has been tested by applying forces to endothelial cell membranes via integrin bound beads, and observing deformation of the nucleus and cytoplasm, associated with reorientation of actin microfilaments (Maniotis *et al.*, 1997). By selective disruption of the three cytoskeletal components, it was demonstrated that both microfilaments and intermediate filaments transferred tensile force to the nucleus, whereas microtubules stabilised the nucleus against lateral compression. In addition, Pourati et al have shown that the actin cytoskeleton is under tensile stress, by detaching endothelial cells from their basal surface and observing rapid retraction, which was abolished by disruption of the actin microfilaments (Pourati *et al.*, 1998). Similar results have been seen in fibroblasts, where microfilament disruption abolished contractile forces, whereas microtubule disruption produced a further increase in contraction (Brown *et al.*, 1996).

An alternative theory is that the mechanical consequences of microtubule disruption are mediated through activation of cytoplasmic myosin motor activity, and Kolodney et al have demonstrated increased phosphorylation of the myosin regulatory light chain after treatment with nocodazole, a microtubule depolymerising agent (Kolodney & Elson, 1995).

1.6.7 Drug interactions

A large number of chemically diverse compounds, many of which are derived from natural products, bind to tubulin or microtubules. They can be divided into three main classes,

depending on their binding site on tubulin, and examples of drugs in each class are listed in Table 1.3. The majority of these drugs inhibit microtubule polymerisation, whereas the taxanes stabilise microtubules and increase microtubule polymer mass. Recently several depolymerising agents such as colchicine and the vinca alkaloids have also been show to stabilise microtubule dynamics at doses below those that cause depolymerisation (Jordan & Wilson, 1998). All these drugs interfere with the formation of the mitotic spindle, and therefore treated cells accumulate at the G2/M interface. Mitotic block persists for varying time, depending on cell type, and most cells then exit mitosis and undergo apoptosis by a process involving phosphorylation of the apoptotic regulator bcl2 (Blagosklonny *et al.*, 1997; Haldar *et al.*, 1997; Poruchynsky *et al.*, 1998).

From the above discussion of the multiple roles of microtubules throughout the cell cycle, suppression of microtubule dynamics during interphase would be expected to have many other effects. These are manifest in the toxicities of tubulin-binding agents, many of which cause neurological damage due to axonal degeneration. The relative affinity for and kinetics of binding to tubulin has some influence on the relative tumour cell cytotoxicity and normal tissue toxicity, but does not explain all of the differences seen. Cellular retention and pharmacokinetics of drugs, which relate partly to relative lipophilicity, may also influence efficacy and toxicity (Donoso *et al.*, 1977; Ferguson & Cass, 1985). For example vincristine has the longest terminal half life and slowest clearance, and is also the most neurotoxic of the vinca alkaloids (Nelson, 1982)

Colchicine is derived from the seeds and corms of *Colchicum autumnale*. This plant has been used for medicinal purposes for many centuries, mainly in the treatment of gout (Wallace, 1973). It has also long been used in the investigation of the cytoskeleton, and tubulin used to be known as the 'colchicine binding protein' (Borisy & Taylor, 1967; Weisenberg *et al.*, 1968). Colchicine has a 3 ring structure (Figure 1.11), and has been shown to bind to the tubulin heterodimer on the β tubulin subunit, orientated so that the C ring binds to the β subunit while the A ring is adjacent to the α-β interface (Shearwin & Timasheff, 1994). The B ring serves to maintain the orientation of the A and C rings and does not contribute to binding. Other agents that bind at this site share the same bicyclic angular structure of colchicine (McGown & Fox, 1989). It has pseudoirreversible kinetics of binding to tubulin, inducing a conformational change in the protein (Andreu & Timasheff, 1982; Hastie, 1991). Like the vinca alkaloids, it has a very large volume of distribution, and long terminal half-life. Its toxicities include gastrointestinal effects, of nausea and diarrhoea, when given orally but not

Binding Site on Tubulin	*Drugs*
Vinca	Vincristine Vinblastine Vindesine Vinorelbine Spongistatin Rhizoxin Dolastatins Maytansine
Colchicine	Colchicine Nocodazole Combretastatins Amphetinile Chalcones Indanocine Aromatic Carbamates Podophyllotoxin
Taxane	Paclitaxel Docetaxel Epothilones
Other	Estramustine

Table 1.3 Examples of different classes of tubulin binding agents

intravenously, leucopaenia and impairment of renal function (Wallace, 1974). After chronic use in patients with renal impairment, it caused proximal myopathy and neuropathy. The neuropathy was due to axonal degeneration, but the myopathy appeared to be due to affects of microtubule disruption on muscle lysosomal function (Kuncl *et al.*, 1987). When given in excess, orally or intravenously it leads to multisystem failure, disseminated intravascular coagulation and bone marrow suppression, usually fatal (Putterman *et al.*, 1991).

The vinca alkaloids are naturally occurring or semisynthetic compounds that are found in minute quantities in the periwinkle plant *Catharanthus roseus*. The early medicinal uses of this plant led to the screening of these compounds for their hypoglycaemic activity, which turned out to be of little importance compared to their cytotoxic effects. The vinca binding site is also thought to be located on β tubulin (Hamel, 1992; Sackett, 1995), close to but not overlapping the colchicine site, although there may be other sites on microtubules that also bind vinca alkaloids with different affinity (Jordan *et al.*, 1986). As mentioned above, vinca alkaloids, in particular vincristine cause peripheral and autonomic neuropathy, but for the other vinca alkaloids the dose limiting toxicity is myelosuppression (Bayssas *et al.*, 1980; Budman, 1997).

The taxanes were initially discovered in 1963, when an extract from the bark of *Taxus brevifolia* was found to have broad antitumour activity in the National Cancer Institute screening program. Paclitaxel was later identified as the active compound in this extract (Wani *et al.*, 1971). Taxanes also bind to β tubulin, but on the surface which forms the inside of protofilaments. They may exert some of their stabilising effects through the lateral contacts within the protofilament (Nogales *et al.*, 1999). Taxane-treated microtubules are stable even after treatment with calcium or low temperatures which usually produce disassembly and induce microtubule bundling throughout the cell cycle (Rowinsky *et al.*, 1988), although cytotoxicity is related to interference with formation of the mitotic spindle. Like colchicine and the vinca alkaloids, taxanes have a very large volume of distribution, and a prolonged terminal half-life (Walle *et al.*, 1995). Their dose limiting toxicity is myelosuppression; other toxicities include hypersensitivity related to the drug vehicle, peripheral and autonomic neuropathy and a fluid retention syndrome with docetaxel (Verweij *et al.*, 1994).

Estramustine was originally synthesised as a combination of a nitrogen mustard and oestradiol, which might be preferentially taken up in prostate and breast cancer cells.

However it was subsequently shown to exert its effects via interactions with microtubules (Tew *et al.*, 1992). It does not bind directly to tubulin, but to MAPs, thus interfering with their ability to stabilise microtubules, and causing depolymerisation (Stearns & Tew, 1988). An alteration in the proportion of different tubulin isotypes in cells can confer resistance to estramustine (Ranganathan *et al.*, 1996), to taxol (Ranganathan *et al.*, 1998a) and to vinblastine (Ranganathan *et al.*, 1998b).

1.6.8 Summary

Microtubules form an important part of an integrated and dynamic cellular cytoskeleton. Disruption of the microtubular network by tubulin-binding drugs will have important effects on the arrangement of the other cytoskeletal components, and will also have functional and morphological consequences for the cell. These consequences will vary depending on cell type, proliferation status and its relationship to other cells and to the extracellular matrix

1.7 Combretastatin A4 Phosphate

Following the studies on colchicine and the vinca alkaloids which demonstrated vascular targeting activity in these different tubulin-binding agents despite their different binding sites on tubulin, further experiments on novel tubulin-binding agents were performed (Chaplin *et al.*, 1996). These included compounds isolated from the root bark of the South African Bush Willow, *Combretum Caffrum*, which were named combretastatins (Pettit *et al.*, 1982). They have a similar structure to colchicine (Figure 1.11), and bind to the colchicine-binding site on tubulin (Hamel & Lin, 1983). Combretastatin A4 is one of the most potent of these compounds (Pettit *et al.*, 1989), and its disodium phosphate (CA4P) is a more water-soluble pro-drug (Pettit *et al.*, 1995), which is converted by non-specific endogenous phosphatases present in plasma and on endothelial cells into combretastatin A4.

The initial in vivo studies demonstrated that combretastatin A4 reduced tumour blood flow rate 24 hours after injection of 50mg/kg in mice by >60% (Chaplin *et al.*, 1996). Its selective tumour vascular targeting action has been confirmed by further *in vivo* studies using CaNT tumours in mice, where a single dose of 100 mg/kg caused >95% reduction in tumour vascular volume and extensive haemorrhagic necrosis (Dark *et al.*, 1997). As with other vascular targeting agents however, a rim of viable tumour cells remained, and these cells were sufficient to rapidly repopulate the tumour, so that a single dose of 100 mg/kg produced minimal tumour growth delay (Chaplin *et al.*, 1999). In addition necrosis was only seen in vascularised tumours after treatment with CA4P, but not in orthotopically transplanted

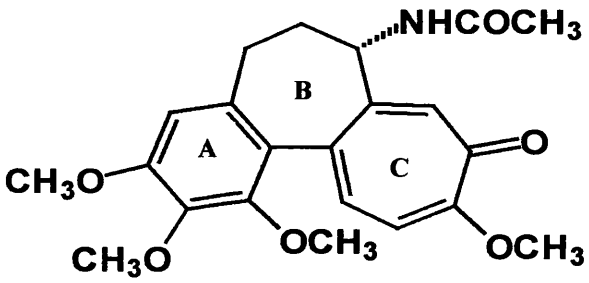

Colchicine

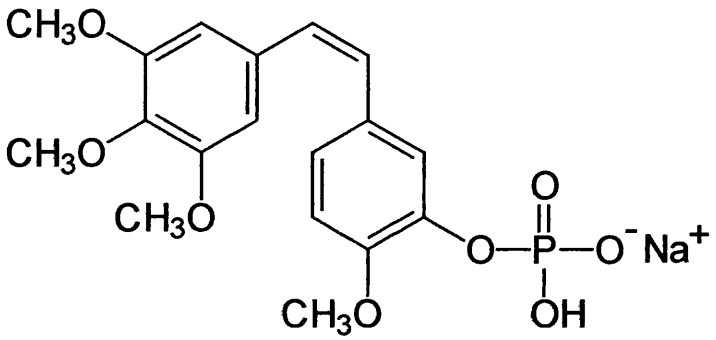

cis-combretastatin A-4 3-O-phosphate

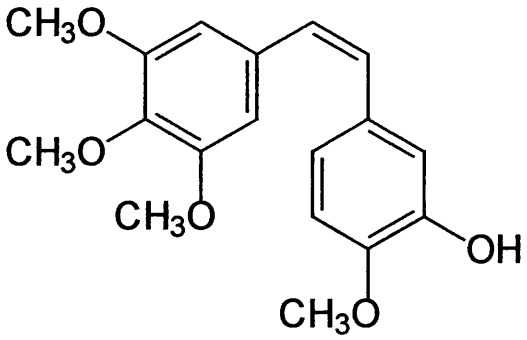

cis-combretastatin A-4

Figure 1.11 Chemical structure of Colchicine, Combretastatin A4 Phosphate and Combretastatin A4

avascular tumours (Grosios *et al.*, 1999). Unlike colchicine and the other tubulin-binding agents, the doses at which vascular targeting activity was seen were well below the maximum tolerated dose of 1000mg/kg in mice. This was therefore the first tubulin-binding agent that appeared to have a wide enough therapeutic window to achieve tumour vascular targeting effects at tolerable doses.

In an *ex vivo* isolated tumour perfusion system, CA4P caused a more than three-fold increase in tumour vascular resistance within 20 minutes of the onset of the drug infusion, but no change in vascular resistance in a similarly isolated limb perfusion (Dark *et al.*, 1997; Tozer *et al.*, 1999). As an increase in tumour vascular resistance was seen even when using a cell-free perfusate, haemodynamic changes, intravascular coagulation and neutrophil adhesion cannot fully account for this effect. In P22 carcinosarcomas in rats, a rapid reduction in tumour blood flow rate occurred within an hour. A 100-fold decrease in tumour blood flow rate was seen at 6 hours, with a much smaller reduction to blood flow rate in spleen, skin, skeletal muscle and brain. No significant reduction was observed in heart, kidney and small intestine (Tozer *et al.*, 1999). MRI studies of the changes produced in murine tumours by CA4P demonstrated a reduction in the initial rate of uptake of Gd-DTPA within treated tumours, particularly in the centre of tumours, and a corresponding decrease in the energy status and pH measured using MRS (Beauregard *et al.*, 1998). A decrease in tumour oxygenation, maximal between 1 and 6 hours, has also been observed using the Eppendorf electrode in a variety of spontaneous murine tumours (Horsman *et al.*, 1998).

In vitro studies have shown a concentration dependent action with much greater cytotoxic/anti-proliferative activity against proliferating human endothelial cells compared with quiescent endothelial cells or human breast carcinoma cells (Dark *et al.*, 1997). Disruption of endothelial cellular networks in a collagen layer was seen after treatment with CA4 or the phosphate (Grosios *et al.*, 1999) CA4P also produced a rapid increase in permeability of endothelial cell monolayers, which was enhanced in the presence of tumour conditioned medium (Watts *et al.*, 1997). This was associated with a disruption of the actin and tubulin cytoskeleton, and a marked change in endothelial cell shape.

Although an anti-proliferative action on tumour endothelium would be expected to reduce angiogenesis, the time course of this action is too slow to explain the rapid reduction in tumour blood flow rate seen with both the *ex vivo* and *in vivo* studies. This raised the hypothesis that it is the effect on endothelial cell shape that is the initiating factor in causing

vascular shutdown. Since the vinca alkaloids, colchicine and CA4P all produce tubulin depolymerisation, they would be expected to share the ability to affect cell shape. There might be some differences however, in their relative abilities to cause cytotoxicity and cell shape change, which might explain the difference in therapeutic window.

1.8 Aims

The aims of this project were:

1. to further explore the mechanisms of action of CA4P in vitro by developing a method for quantitating the endothelial cell shape change produced and to establish the dose and time response of this change

2. to compare the effects of CA4P and other tubulin-binding agents on endothelial cell shape change and anti-proliferative activity

3. to examine whether the time course of endothelial cell shape change and comparison with other tubulin-binding agents could support the hypothesis that this shape change is a key factor in the vascular targeting activity and therapeutic window of this agent

4. to use and refine the DCE-MRI technique to measure tumour and normal tissue blood flow rate in cancer patients

5. to establish the validity and reproducibility of this technique

6. to measure the changes in tumour and normal tissue blood flow rate following treatment with CA4P in the Phase I clinical trial of this agent

CHAPTER 2 - EFFECT OF CA4P ON ENDOTHELIAL CELL SHAPE AND PROLIFERATION

2.1 Introduction

This chapter contains details of the quantitative assay developed to measure cell shape, and the shape change produced by CA4P in proliferating and quiescent human endothelial cells. The time course and dose response of these effects are described, and compared with the antiproliferative effects. Comparison is made with the effects on human fibroblasts and human smooth muscle cells.

2.2 Methods and Materials

2.2.1 Cell Culture

Human umbilical vein endothelial cells (HUVECs), which had been isolated as primary explants according to the method of Jaffe (Jaffe *et al.*, 1973), characterised and frozen in liquid nitrogen at passage 2 were used for all experiments. After rapid defrosting, they were maintained in medium M199 (Sigma Chemical Co.) supplemented with 1.5% HEPES buffer, 0.15% NaHCO3, 0.01% glutamine, 20% foetal calf serum (FCS), 20 μg/ml endothelial cell growth supplement (First Link (UK)) and 15 units/ml heparin (Sigma). All culture flasks, plates and slides used for culturing HUVECs were coated with 0.2% gelatin (Sigma) and incubated at 37°C for at least 4 hours prior to plating. Individual experiments used cells from the same umbilical cord at the same passage, and cells were not used after passage 6. Cells were incubated in a low oxygen incubator set to 1% O2, to mimic the tumour endothelial cell microenvironment.

Human smooth muscle cells and fibroblasts (TCS Biologicals Ltd, UK) were grown in Dulbecco's modified essential medium (DMEM) (Sigma) supplemented with 10% FCS. These cells were also incubated in a low oxygen incubator as for the HUVECs. No gelatin was used for these cell lines.

2.2.2 Drug preparation

Cis-combretastatin A4 phosphate (CA4P) was supplied by Oxigene. The trans isomer of CA4P was a gift from Dr G.R. Pettit, Arizona State University. Both drugs were dissolved in PBS to a concentration of 10 mM then diluted in HUVEC medium to the desired concentration.

2.2.3 *Measurement of conversion of CA4P to CA4*

5 ml HUVEC medium pre-warmed to 37°C was placed in 6 cm round petri dishes containing either confluent cultures of HUVECs or no cells. 50 µl of stock 10 mM CA4P was added and mixed thoroughly. The dishes were then placed in the 1% O_2 incubator. 200 µl samples were withdrawn at 5 minute intervals for 30 minutes and placed on ice. High performance liquid chromotography (HPLC) was kindly performed by Dr M.R.L. Stratford to determine the concentration of CA4P and CA4 in each sample (Stratford & Dennis, 1999).

2.2.4 *Neutral Red Assay*

HUVECs were plated onto 96 well plates coated with 0.25% gelatin at 4 x 10^3 cells/well. They were exposed to either cis or trans-CA4P 24 hrs later for 10 to 120 minutes, washed twice with PBS and incubated in fresh medium as above for 5 days, until the untreated control wells had become confluent. The trans isomer of CA4P does not cause microtubule depolymerisation (Woods *et al.*, 1995), and was used as a control. Neutral red solution (Sigma) was diluted in medium to 39.6 µg/ml, spun down (5 minutes at 1100 x g) and filtered. The medium was removed from the cells, replaced with the prepared neutral red solution and incubated at 37°C for three hours to allow for cellular uptake of the dye. The neutral red was then removed and the cells fixed with 0.5% formalin/1% $CaCl_2$, then solubilised with 1% acetic acid/50% ethanol for 5 minutes with gentle agitation. The absorbance was then measured at 540 nm on a Labsystems Multiskan MCC/340 microplate reader. Each assay was repeated 3 times, with 6 wells used per drug concentration. The absorbance of wells containing medium only with no cells was subtracted from the results for control and treated wells, and results plotted as the fraction of the absorbance of control wells.

2.2.5 *Cell Shape Change Assay*

22 x 32 mm glass coverslips were sterilised in 70% ethanol then flamed, and placed in 6cm petri dishes. 0.2% gelatin was added, and incubated at 37°C for at least 4 hrs. HUVECs were plated at 1 x 10^5 cells and 7.5 x 10^5 cells per dish in 5 ml HUVEC medium for proliferating and confluent cultures respectively. Human smooth muscle cells were plated at 1 x 10^4 cells, and human fibroblasts at 1 x 10^5 cells per dish. Fresh medium was added the following day, and proliferating cells treated 24 hrs later. Gelatin coating was not used for these cell types. Confluent cell cultures were generally confluent by 24 hrs after plating and were maintained at confluence for at least 48 hrs before treating.

The coverslips were removed from the original dish and placed in a dish with the appropriate drug concentration or medium at 37°C and incubated for 10 minutes to 2 hours. The medium was then removed and the coverslips washed twice in PBS at 37°C, and fixed for 10 minutes with freshly made microtubule stabilising fixative at 37°C (4% ACS grade formaldehyde and 0.1% Triton X-100 in PHEM buffer – 60mM Pipes, 25mM Hepes, 10mM EGTA, 3mM $MgCl_2$ adjusted to pH 6.1 (all from Sigma)). They were then washed twice in PBS and 10% FCS added for 15 minutes. For the recovery experiments, incubation of proliferating cells with the drug was performed as described above, then the coverslips were washed 4 times with serum free medium, and medium replaced for 24 hours prior to fixation as above.

Fresh 6 cm petri dishes were used for staining. 120 µl of primary mouse monoclonal anti-β tubulin antibody (Sigma) was placed in each dish at 1 in 500 or 1 in 1000 dilution for confluent or proliferating cells respectively. The coverslips were then carefully inverted onto the antibody solution, and incubated at 37°C for 1 hr. 2 ml 10% FCS was added to each dish and the coverslips carefully re-inverted and replaced in their original dishes. After two further washes in 10% FCS, the staining procedure was repeated for the secondary antibody, FITC-linked anti-mouse antibody (Sigma) at 1 in 25 and 1 in 50 dilution for confluent and proliferating cells respectively, and incubated for 30 minutes. The coverslips were then re-inverted into their original dishes, washed twice in PBS and mounted onto glass slides using anti-fade fluorescent mounting medium. Experiments were repeated 3 times with HUVECs from different cords.

The tubulin stained cells were visualised under blue excitation light and photographs taken using an Olympus BH2 fluorescence microscope and Kodak ASA 200 film. For quantitation of cell shape, images were acquired and stored on computer using a Nikon Optiphot fluorescence microscope, camera and in-house image acquisition software. Images were acquired from randomly selected areas of slides, and then analysed using Visilog v4 software (Noesis, France), adapted in-house. On each image, a light pen was used to draw around each cell outline, using the zoom feature to increase magnification to x 850. The perimeter and cell area (in pixels) contained by the outline were calculated. 1 pixel measured 0.71 x 0.71 µm. At least 80 cells were outlined in this way for each slide. Cells incompletely imaged at the edge of the field were excluded as shown in Figure 2.1 The form factor was calculated using the formula ($1 - 4\pi \times \text{area} \times \text{perimeter}^2$) as described by Verschueren *et al.* (Verschueren *et al.*,

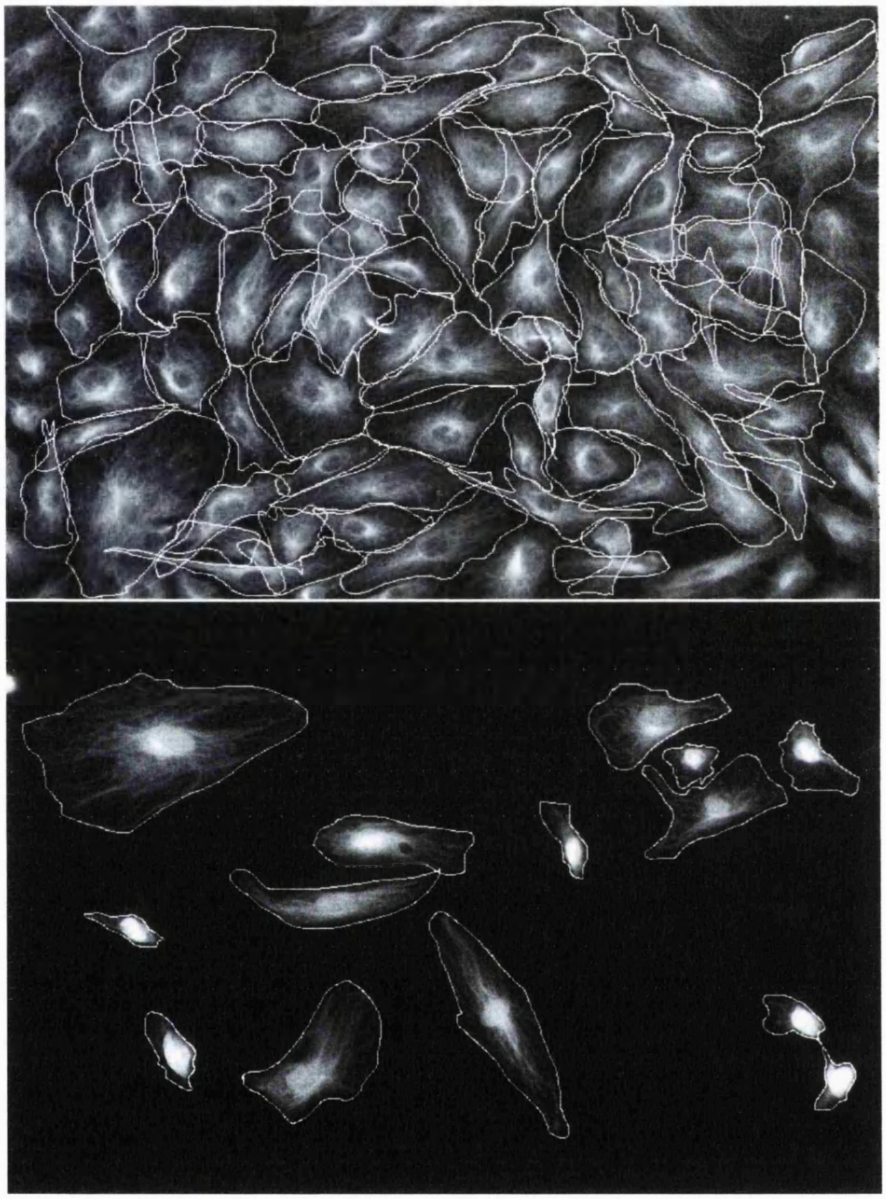

Figure 2.1 Outlined cells – Top- confluent, Bottom- proliferating HUVEC cultures fixed and stained for tubulin. Cells outlined on images acquired and stored on computer using Visilog software (Noesis, France).

1993). It is zero for a circle, and increases as the shape elongates thereby increasing its perimeter. A form factor of 1 would thus represent an infinitely elongated ellipse.

2.2.6 Dual Staining Technique

For dual staining of tubulin and actin, cells were plated, treated and fixed as described above. Texas Red-phallotoxin (Molecular Probes Europe BV) was obtained as lyophilised solids in a 300-unit vial. Stock solution was made by dissolving the solids in 1.5 ml methanol to yield a final concentration of 200 units/ml. The normal tubulin staining procedure was followed but at the secondary antibody stage 5 µl of stock solution per slide to be stained was added to the secondary antibody solution and mixed. 125 µl of the combined solution was placed on each slide, and incubated as above. Actin staining was observed under green excitation light. Dual colour photographs were obtained by exposure using blue excitation light to obtain an image of tubulin, followed by a second exposure under green light to obtain an image of actin. The microscope stage was not moved between exposures.

2.2.7 Statistics

The distributions of cell area were skewed, and therefore the data was analysed using JMP software to obtain Spearman's rho correlation coefficients relating cell area to drug concentration at the different time points and for confluent and proliferating cells. The coefficients thus obtained were then tested for a significant difference. The form factor was normally distributed, and means at 10^{-8}M and 10^{-5}M compared with control means using the z test. Comparison of cell area after treatment and recovery with control cells was done using the Wilcoxon rank sum test

2.3 Results

2.3.1 Conversion of CA4P to CA4

The increase of CA4 concentration with time is illustrated in Figure 2.2. There was no effect of the presence of confluent HUVEC cultures on the hydrolysis of CA4P to CA4. After 30 minutes incubation with medium containing 100 µM CA4P, with or without cells, the concentration of CA4 was 20 µM.

2.3.2 Anti-Proliferative Effect of CA4P on HUVECs

The results of the neutral red assay for cytotoxic/ anti-proliferative effect are shown in Figure 2.3 with increasing doses of cis and trans CA4P after 10, 30 and 120 minutes drug exposure. HUVEC growth was unaffected at doses below 0.5 µM of cis-CA4P, with a 50% growth

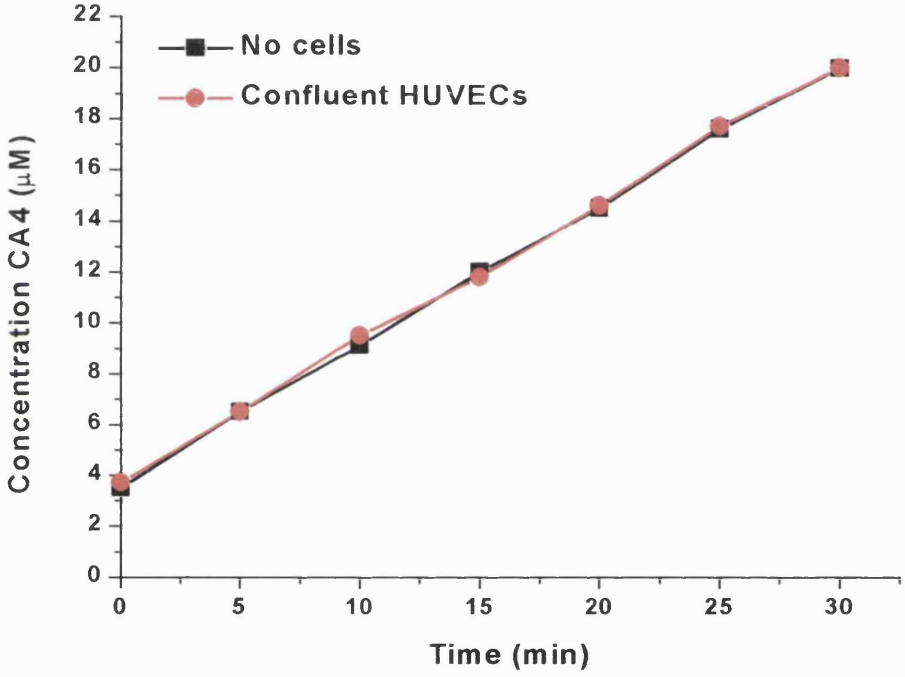

Figure 2.2 Effect of HUVECs on dephosphorylation rate of CA4P to CA4. Concentration of CA4 with time in HUVEC medium at 37°C in cell free culture or with confluent HUVECs. Initial CA4P concentration 100 μM at time 0.

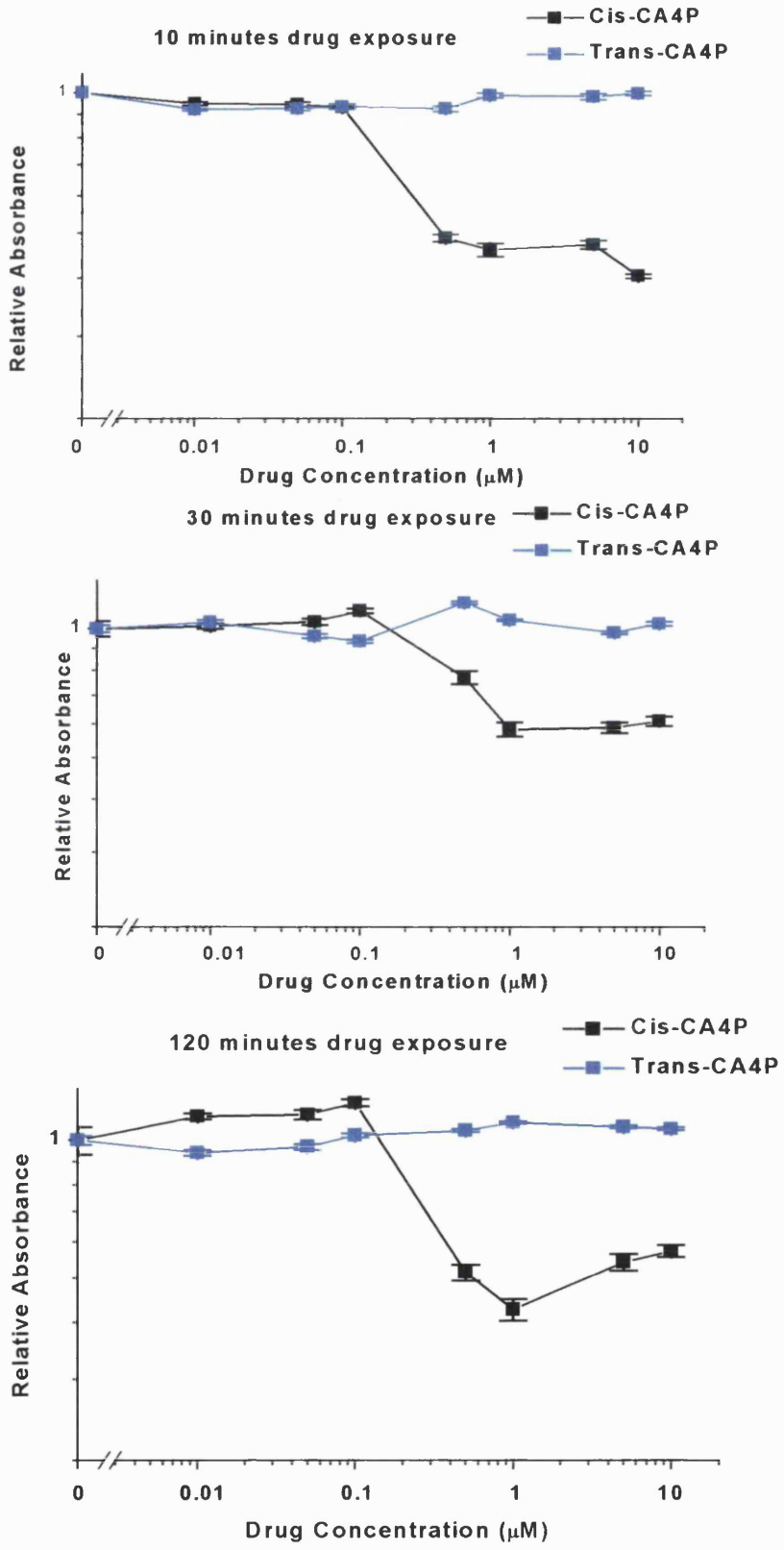

Figure 2.3 Neutral red assay. Relative absorbance of HUVECs stained with neutral red plotted against concentration of cis-combretastatin A4phosphate (CA4P) and the inactive trans isomer. HUVECs were exposed to drug for 10 minutes (top), 30 minutes (middle) and 120minutes (bottom), then washed x3 and fresh medium replaced. Assay performed once control wells reached confluence. Results plotted as mean +/- SE for 6 replicate wells.

inhibition at dose of 1 μM and above. There was no difference in anti-proliferative effects with the different exposure times tested. Trans-CA4P had no significant antiproliferative effect at any time.

2.3.3 Effect of CA4P on HUVEC Shape - Time Course and Dose Response

Figure 2.4 to 2.6 illustrate the appearance of microtubules in control and treated proliferating and confluent HUVECs after 30 minutes exposure to increasing doses of CA4P. In proliferating cells, the microtubules begin to depolymerise at 1 nM, shortening from the distal ends at the cell periphery (Figure 2.4 and 2.5). At this dose there is no change in the appearance of confluent cells (Figure 2.6) and equivalent changes become noticeable at 10 nM. At 10 nM in proliferating cells the microtubules have a tangled appearance and the cytoplasm becomes more uniformly stained as the depolymerised tubulin molecules disperse (Figure 2.4 and 2.5). Again these changes also occur in confluent cells but at a higher dose (100 nM, Figure 2.6). At 100 nM in proliferating cells there has been a marked reduction in cell area and at 1 μM many cells exhibit blebbing of the plasma membrane (Figure 2.4 and 2.5). At 1 μM in confluent cells there is near complete depolymerisation of the microtubules, and while some cells demonstrate rounding up and membrane blebbing, the majority have much less reduction in area than proliferating cells at the same dose. These changes commence at doses well below those that cause antiproliferative effects (see Figure 2.3 for comparison).

The quantitative data for cell area is illustrated in Figure 2.7. Proliferating control cells are larger than confluent control cells. There is a significant decrease ($p < 0.01$) in cell area with increasing concentration for proliferating cells at all time points and for confluent cells at 20 minutes and above. After 10 minutes, proliferating cell area has decreased to 53% of controls, with a further decrease to 33% of control cell area by 60 minutes. At 60 minutes, confluent cell area has decreased to 63% of controls. The strength of the correlation between cell area and drug concentration is greater for proliferating cells. There is a significant difference ($p < 0.05$) between the Spearman's rho correlation coefficients for proliferating and confluent cells at all time points after 10 minutes. In addition, Figure 2.7 illustrates that the decrease in cell area occurs at much lower doses for proliferating than for confluent cells.

Figure 2.8 shows the changes in form factor with increasing concentration for the same proliferating and confluent cells. Control proliferating cells are more elongated, with a

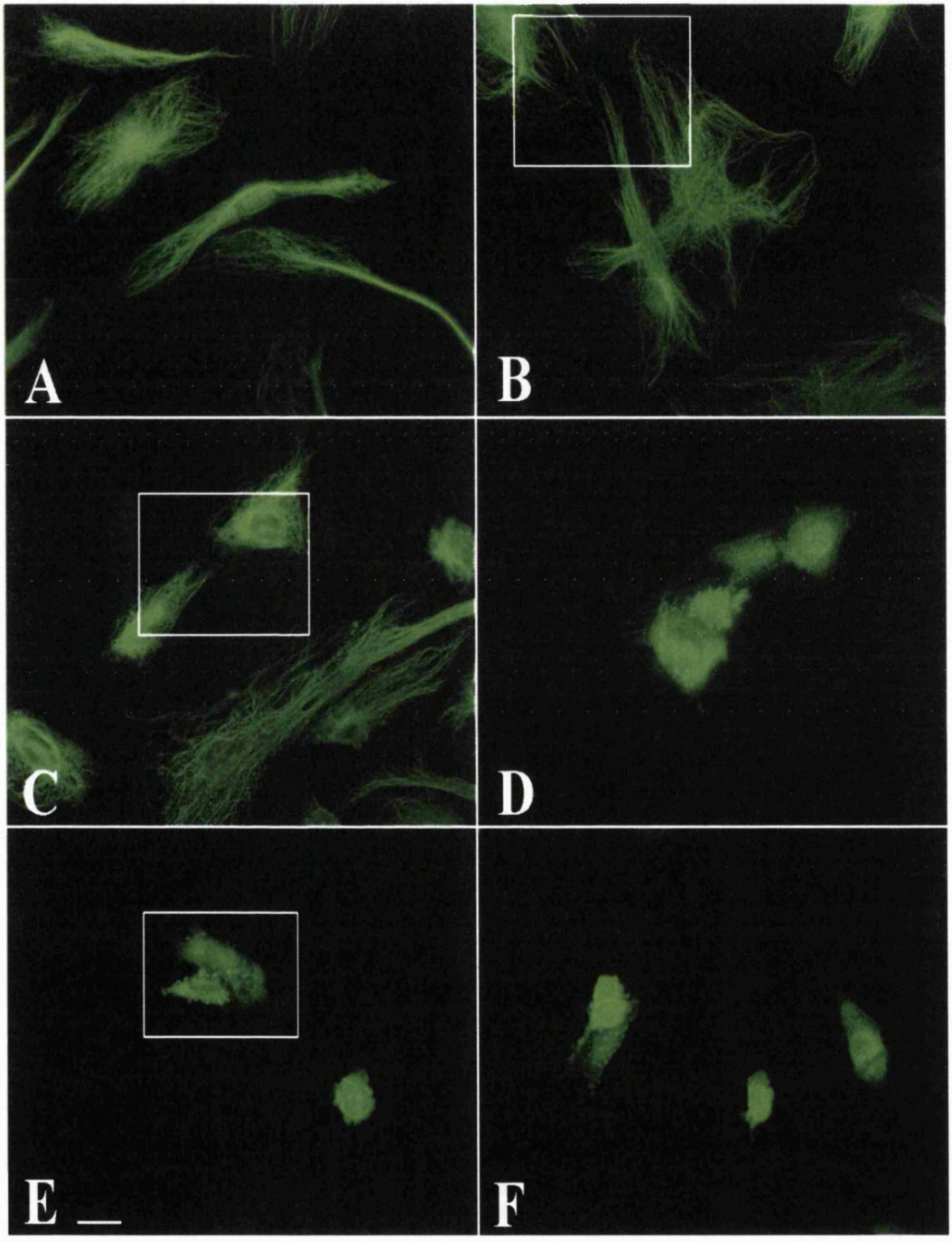

Figure 2.4. Proliferating HUVECs fixed after 30 minutes treatment with CA4P and stained with primary mouse monoclonal anti-β tubulin antibody and secondary FITC-linked anti-mouse antibody.
A=Control, B=1 nM, C=10 nM, D=100nM, E=1μM, F=10μM. Bar =50 μm

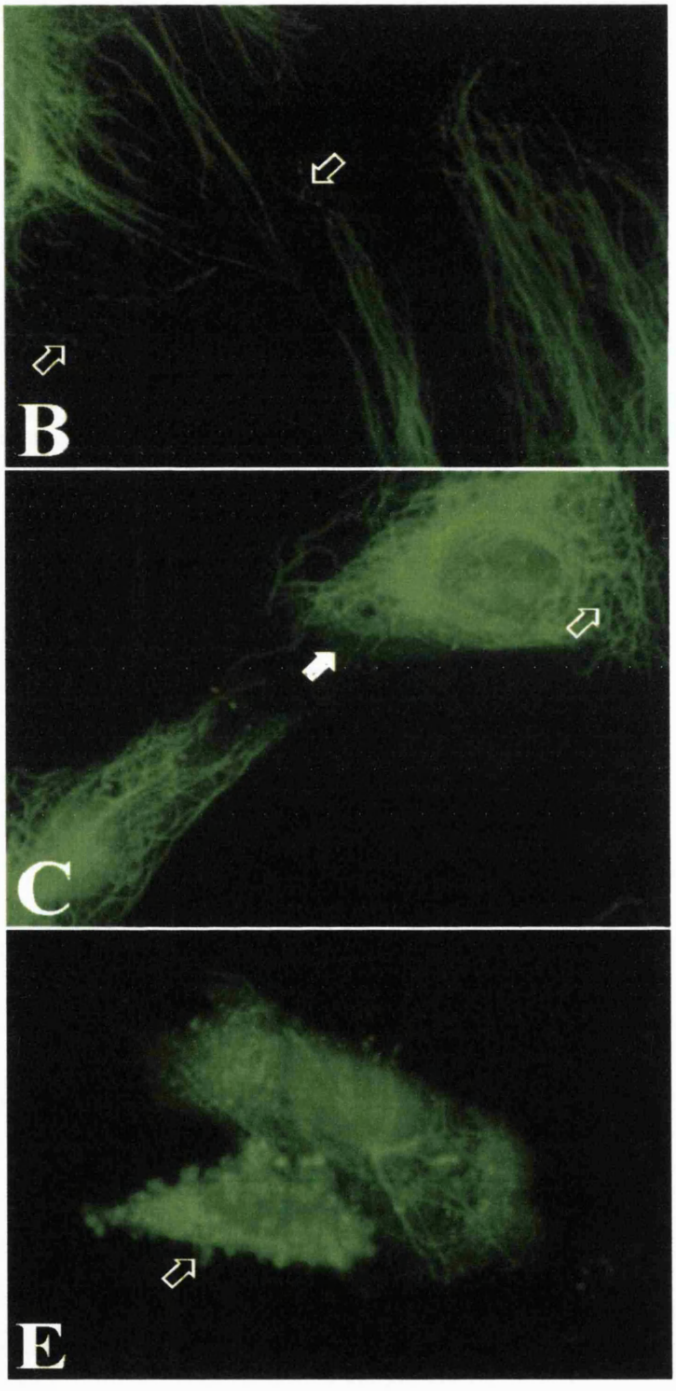

Figure 2.5. Proliferating HUVECs fixed after 30 minutes treatment with CA4P and stained with primary mouse monoclonal anti-β tubulin antibody and secondary FITC-linked anti-mouse antibody. Increased magnification view of boxed areas in Figure 2.4.
B=1 nM, open arrows indicate depolymerisation at ends of microtubules, C=10 nM, open arrow indicates tangled appearance of microtubules, closed arrow indicates diffuse staining due to depolymerised tubulin, E=1μM, open arrow indicates blebbing of cell membrane.

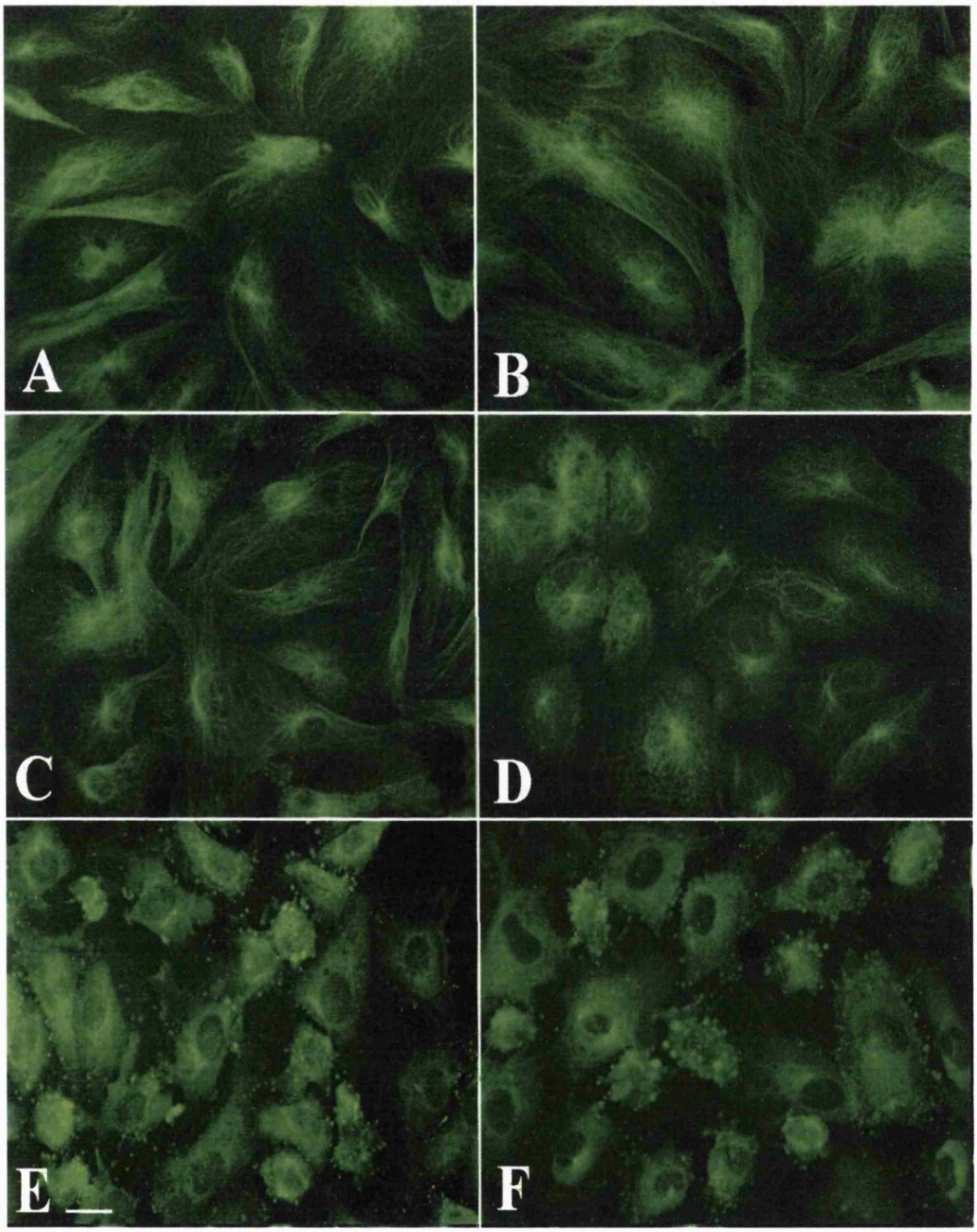

Figure 2.6. Confluent HUVECs fixed after 30 minutes treatment with CA4P and stained with primary mouse monoclonal anti-β tubulin antibody and secondary FITC-linked anti-mouse antibody.
A= controls, B=1 nM, C=10 nM, D=100 nM, E=1 μM, F=10 μM. Bar=50 μm

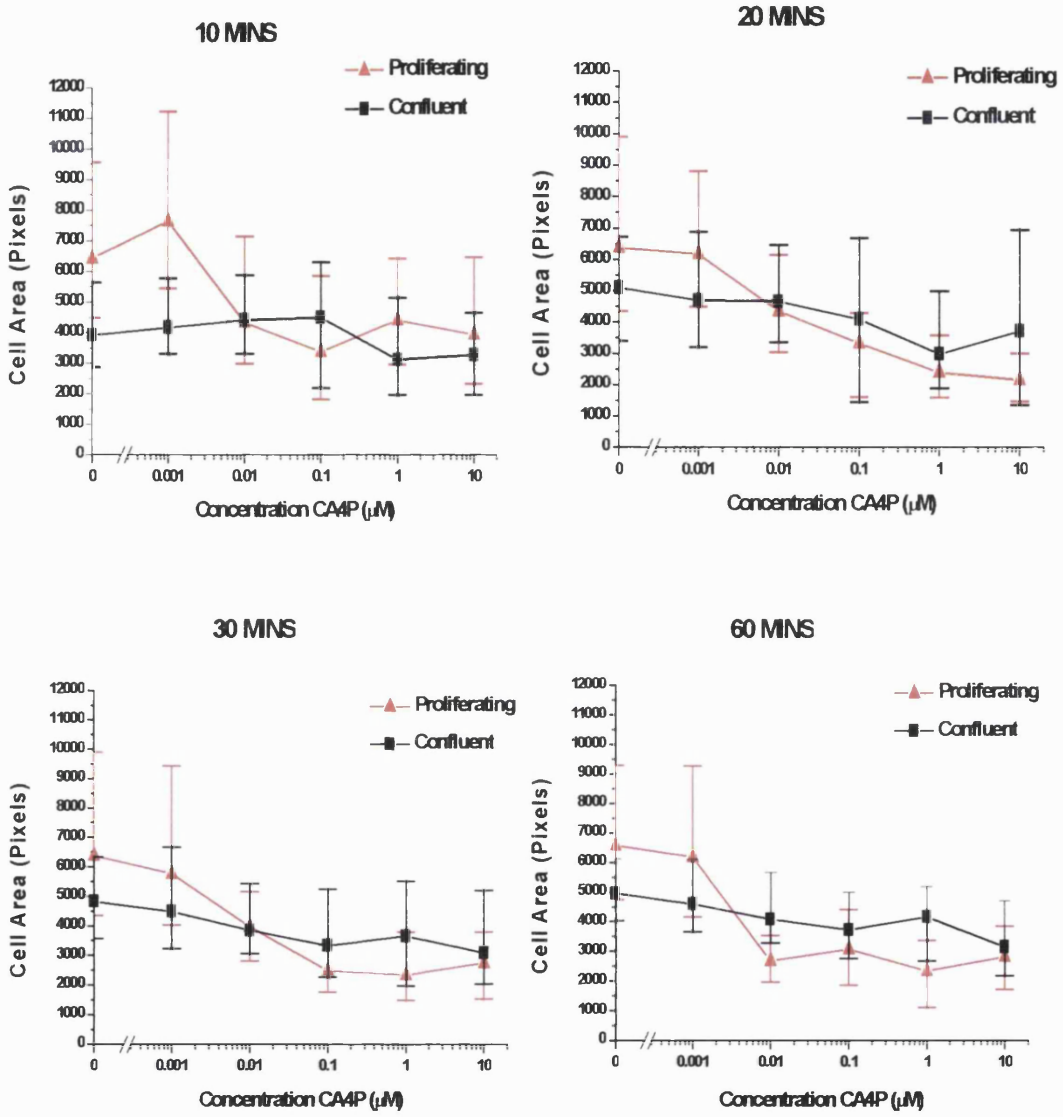

Figure 2.7 Change in cell area with concentration of combretastatin A4 phosphate (CA4P) after 10, 20, 30 and 60 minutes drug exposure for proliferating and HUVEC cultures. Values are plotted as median and interquartile ranges, as distributions of cell area are skewed

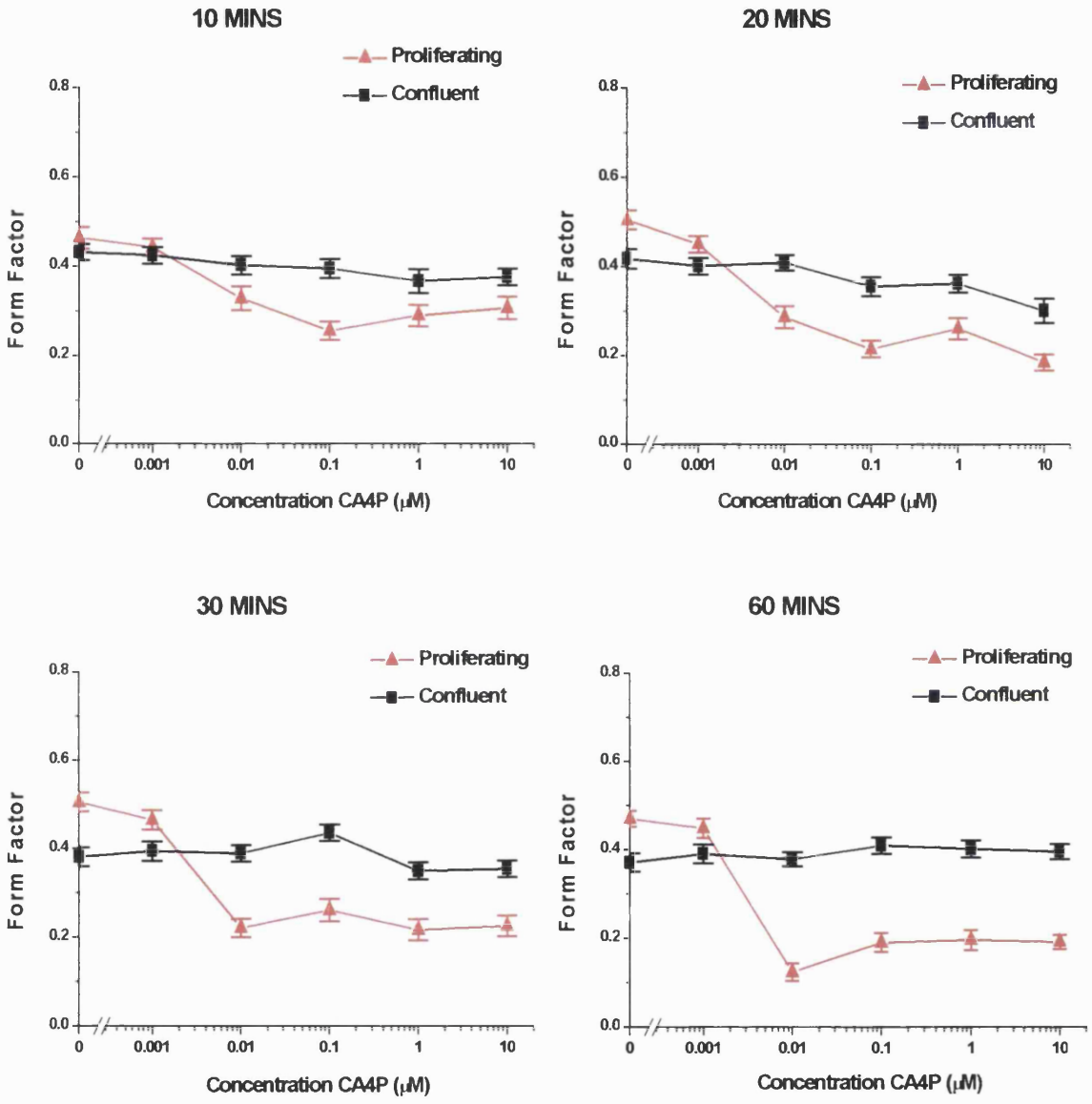

Figure 2.8 Change in form factor with concentration of CA4P after 10, 20, 30 and 60 minutes drug exposure for proliferating and confluent HUVEC cultures. Data refer to the same cells as shown in Figure 2.6. Results are plotted as means +/- SE

correspondingly higher form factor than confluent cells. After 10 minutes exposure to CA4P proliferating cells have a significant decrease in form factor for concentrations of 10 nM (0.01 μM) and above to 56% of controls, but there is no significant decrease for confluent cells. The form factor decreases further at later time points for proliferating cells (to 40% of controls at 60 minutes), but there is only a significant decrease for confluent cells at 10 μM treated for 20 minutes. The form factor is not reduced even when reductions in cell area are seen for confluent cells, because the increase in ruffling of the cell membrane visible in Figures 2.5 and 2.6 compensates for the smaller reduction in cell elongation that occurs in confluent cells.

2.3.4 Recovery of HUVEC Shape

Figure 2.9 illustrates the recovery of proliferating HUVECs' area and form factor after 30-minute exposure to cis-CA4P, washing and replacement of medium for 24 hours. The cells undergoing immediate fixation have the same dose response for changes in cell area and form factor as described above. After 24 hours recovery period, HUVECs treated at 0.01 μM have an increased cell area compared with controls ($p < 0.05$, Wilcoxon rank sum), although the form factor is unchanged ($p > 0.05$, z test). Both form factor and cell area have significant recovery after 24 hours compared with immediately fixed cells. At 10 μM there is no significant difference in cell area after 24 hours recovery compared with controls. However, the form factor remains reduced at 10 μM compared with controls, but is significantly greater than for immediately fixed cells.

Histograms of the population of cell areas in controls and cells treated at 10 μM with and without recovery are shown in Figure 2.10. Both control populations have a similar distribution. The histogram for cells immediately fixed after treatment with 10 μM CA4P is shifted to the left, and 55% of cells have an area <4000 pixels. After 24 hours recovery only 28% of treated cells have an area <4000 pixels. However, there was also some loss of cells in the treated group – the mean (+/- SE) number of cells per field imaged was 3.7 (+/- 0.4) in treated cells after recovery, 6.8 (+/- 0.4) in control groups and 8.9 (+/- 0.9) in treated cells with no recovery. This suggests that those cells with most marked cell rounding may become detached from the slide during the recovery period, and this could explain the increase in cell area seen at 0.01 μM. Any loss of small rounded cells would tend to overestimate the extent of cell shape recovery measured in this way. Cell loss and failure of recovery of cell shape

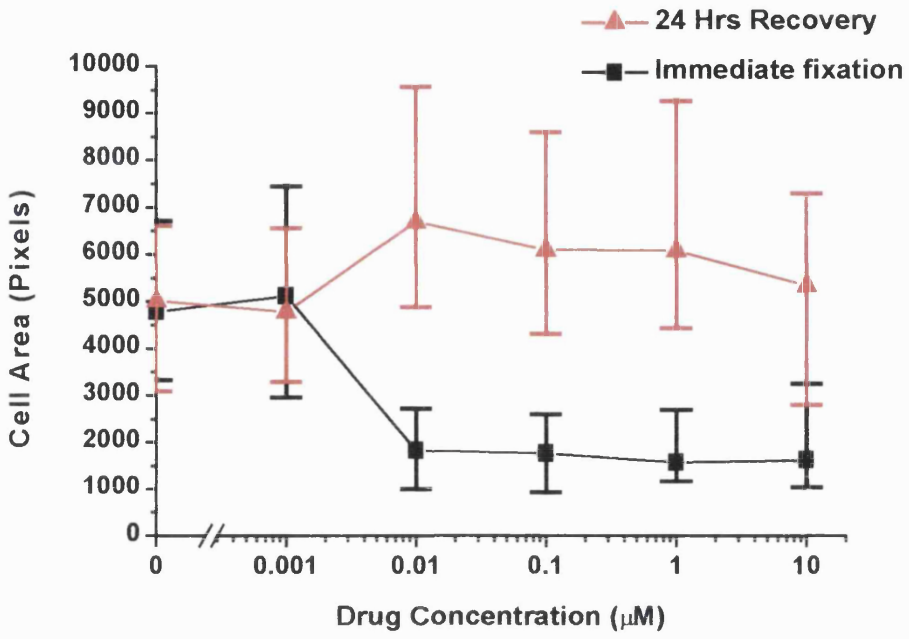

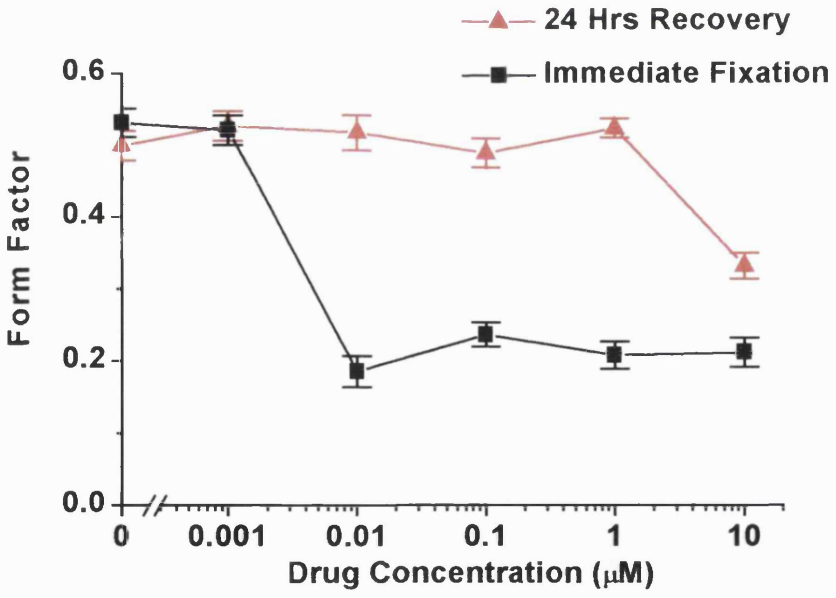

Figure 2.9 Recovery of HUVEC area (top) and form factor (bottom) after 30 minute exposure to CA4P , washing x 4 in serum free medium and either immediate fixation (■) or replacement of fresh medium for 24 hours prior to fixation (▲)

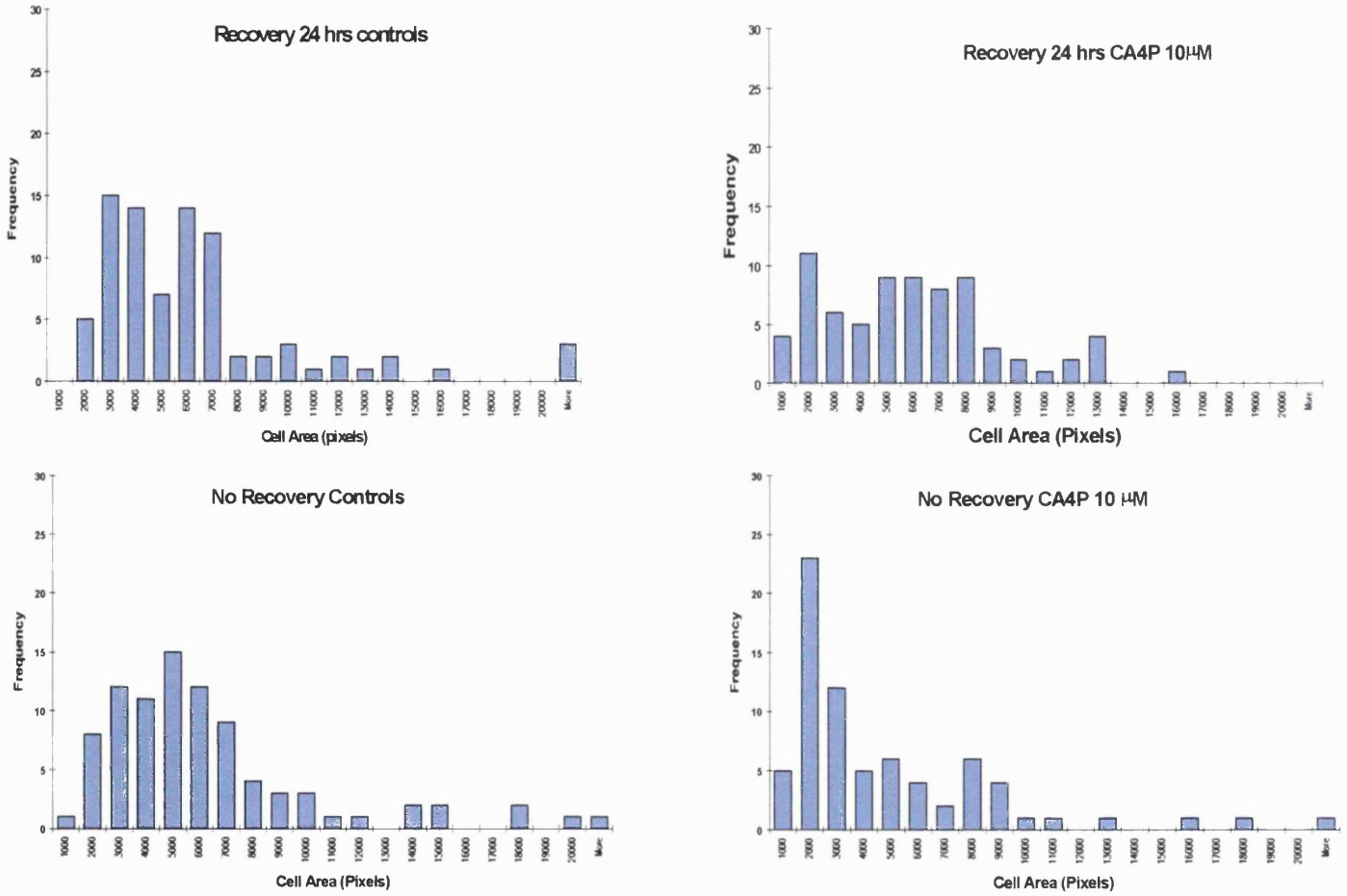

Figure 2.10 Distributions of cell area. Top Left – Control cells exposed to medium only for 30 minutes, washed x4 and fresh medium replaced for 24 hours prior to fixation. Bottom Left – Control cells exposed to medium only and fixed immediately. Top Right – Cells treated with 10 μM CA4P for 30 minutes, washed x4 and fresh medium replaced for 24 hours prior to fixation. Bottom Right – Cells treated with 10 μM CA4P for 30 minutes and fixed immediately.

would both contribute to the effects measured in the neutral red assay, where anti-proliferative/cytotoxic effects are seen at doses above 0.5 μM.

The typical appearance of HUVECs after recovery from CA4P treatment is shown in Figure 2.11. In comparison with Figure 2.4, where the microtubule network is nearly completely depolymerised at 0.1 μM, after 24 hours recovery the microtubular network is reformed for doses ≤ 1 μM. However, at 10 μM the microtubular network remains largely depolymerised, and there is only partial recovery of cell shape.

The time course of form factor recovery at 1 μM is illustrated in Figure 2.12, with corresponding images in Figure 2.13. There is no significant change in form factor 1 hour after washing and medium replacement, and the microtubular network remains largely depolymerised, although microtubular organising centres (MTOCs) are visible. By 4 hours the form factor has recovered to baseline, and the microtubular network is reformed.

2.3.5 Comparison with Effects on Human Smooth Muscle Cells and Fibroblasts

CA4P had no effect on human smooth muscle cell (HMSC) area or form factor at doses of ≤ 100 μM, as shown in Figure 2.14 for form factor. Even at 100 μM figure 2.15 illustrates that the microtubule network was not completely depolymerised. The same cell stained for actin and dual stained is also shown in Figure 2.15. The actin cytoskeleton is well developed in HSMCs, and there is a reaction to the action of CA4P with increased numbers of actin stress fibres visible in the periphery of the cell, in those regions where more of the microtubules are depolymerised. In comparison with Figure 2.16, which illustrates actin staining in confluent and proliferating HUVECs, the actin cytoskeleton is better developed in HSMCs than in the proliferating HUVECs. Confluent HUVECs however, form a dense peripheral band of actin fibres. Following treatment with CA4P these confluent cells also demonstrate increased stress fibre production, as well as condensation of the dense peripheral band. This is particularly noticeable in those cells that have the membrane blebbing phenotype. In treated proliferating HUVECs, the actin cytoskeleton also becomes condensed around the cell periphery.

Human fibroblasts do undergo some shape change after treatment with CA4P at 10 μM for 30 minutes, but to a lesser extent than HUVECs, as demonstrated in Figures 2.17 and 2.18. Tubulin depolymerisation is seen at this dose (Figure 2.18), but not at lower doses.

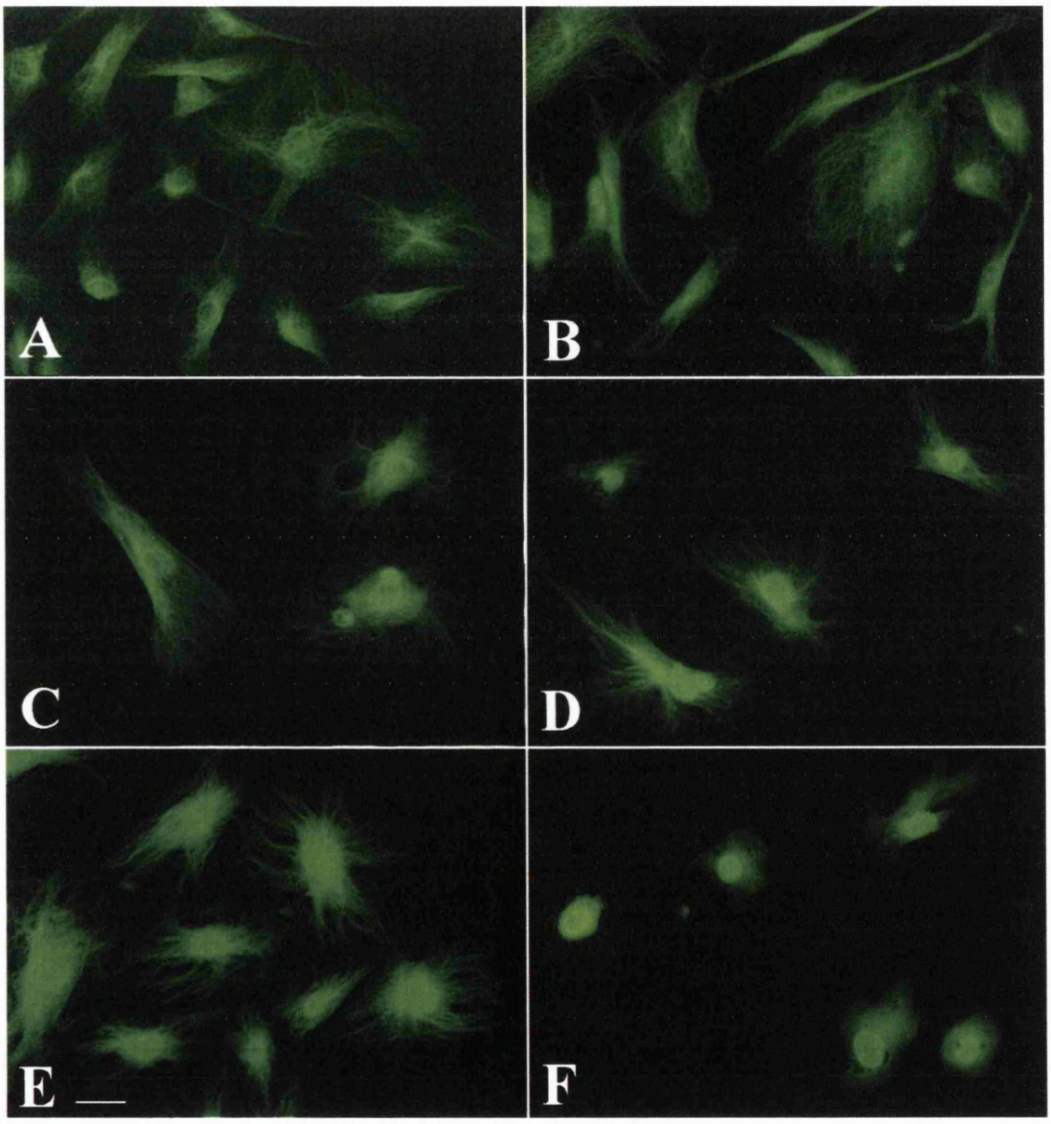

Figure 2.11 Recovery of HUVEC shape and microtubule network after CA4P. Proliferating HUVECs treated with CA4P for 30 minutes, washed x 4, and normal medium replaced for 24 hours prior to fixation and immunofluorescent staining with primary mouse monoclonal anti-β tubulin antibody and secondary FITC-linked anti-mouse antibody.
A= controls, B=1 nM, C=10 nM, D=100 nM, E=1 μM, F=10 μM. Bar = 50 μm.

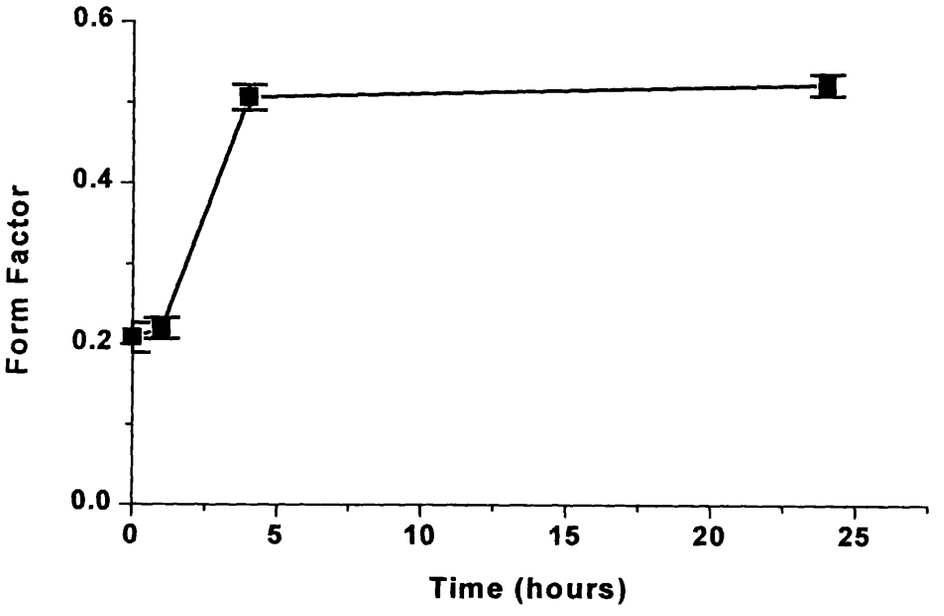

Figure 2.12 Time course for recovery of form factor in HUVECs treated with 1 μM CA4P for 30 minutes, washed x 4 and normal medium replaced prior to fixation and staining.

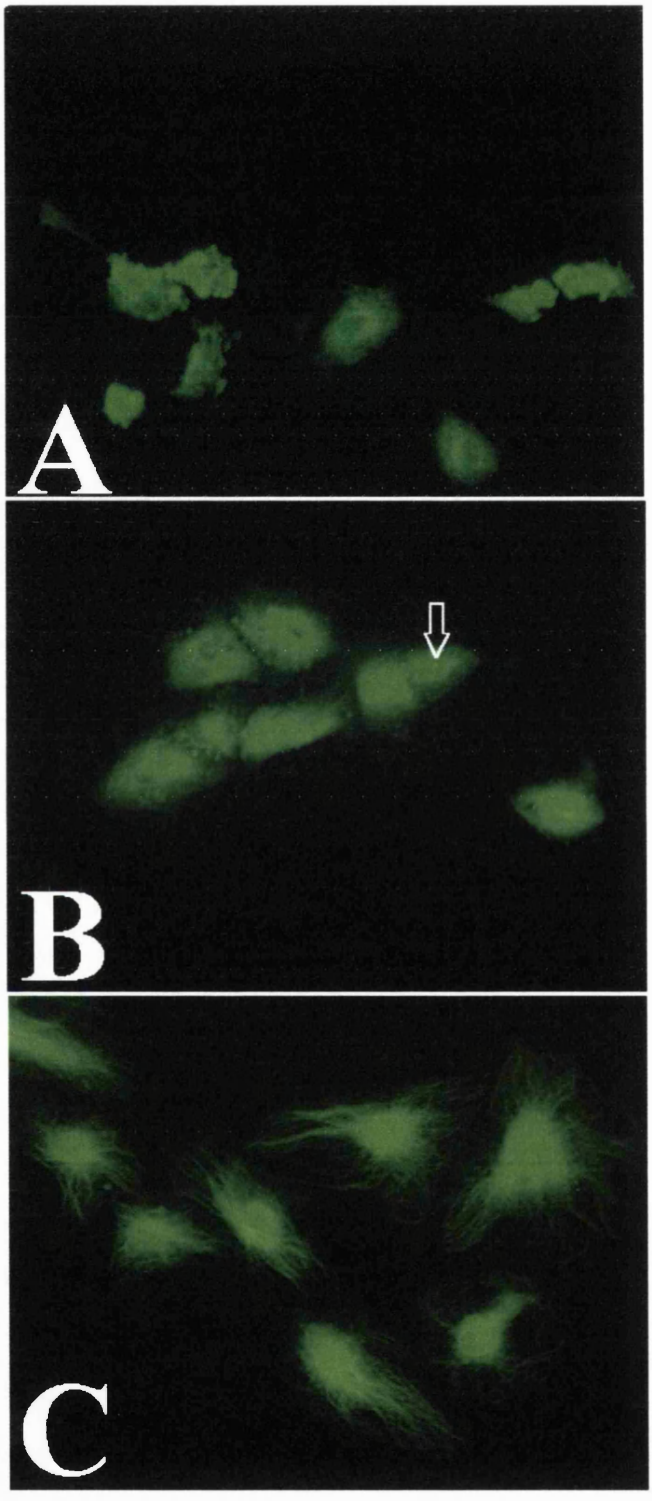

Figure 2.13 Time course of recovery from CA4P – images of proliferating HUVECs treated with 1μM CA4P for 30 minutes
A = Immediate fixation, B = 1 hr recovery prior to fixation. Arrow indicates microtubule organising centre, C = 4 hrs recovery prior to fixation
Fixed cells underwent immunofluorescent staining with primary mouse monoclonal anti-β tubulin antibody and secondary FITC-linked anti-mouse

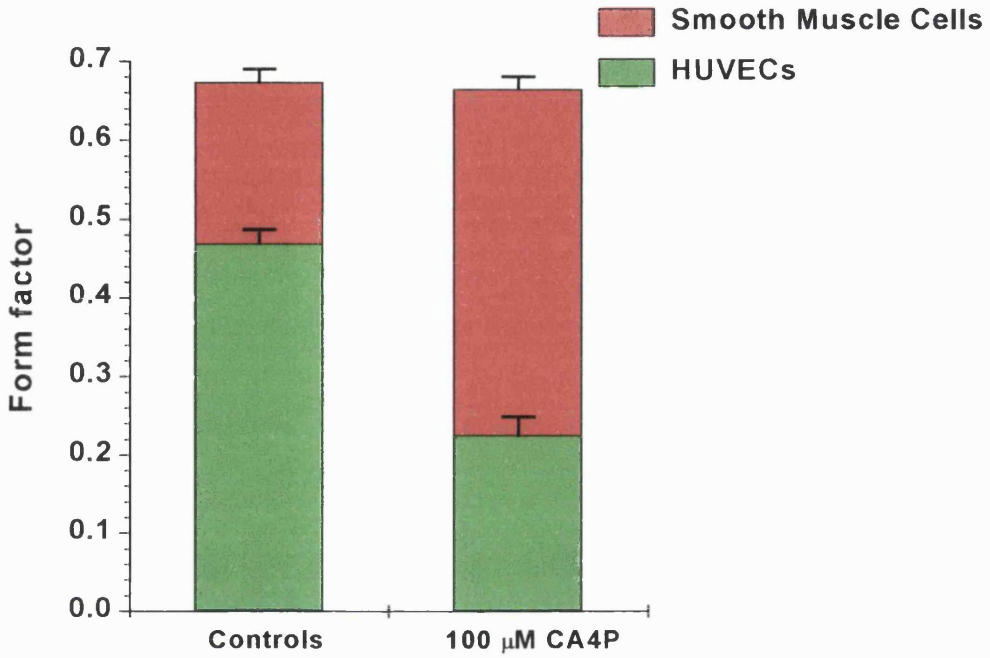

Figure 2.14 Effect of 30 minutes treatment with 100 μM CA4P on form factor in human smooth muscle cells and HUVECs. Plotted as mean and SE

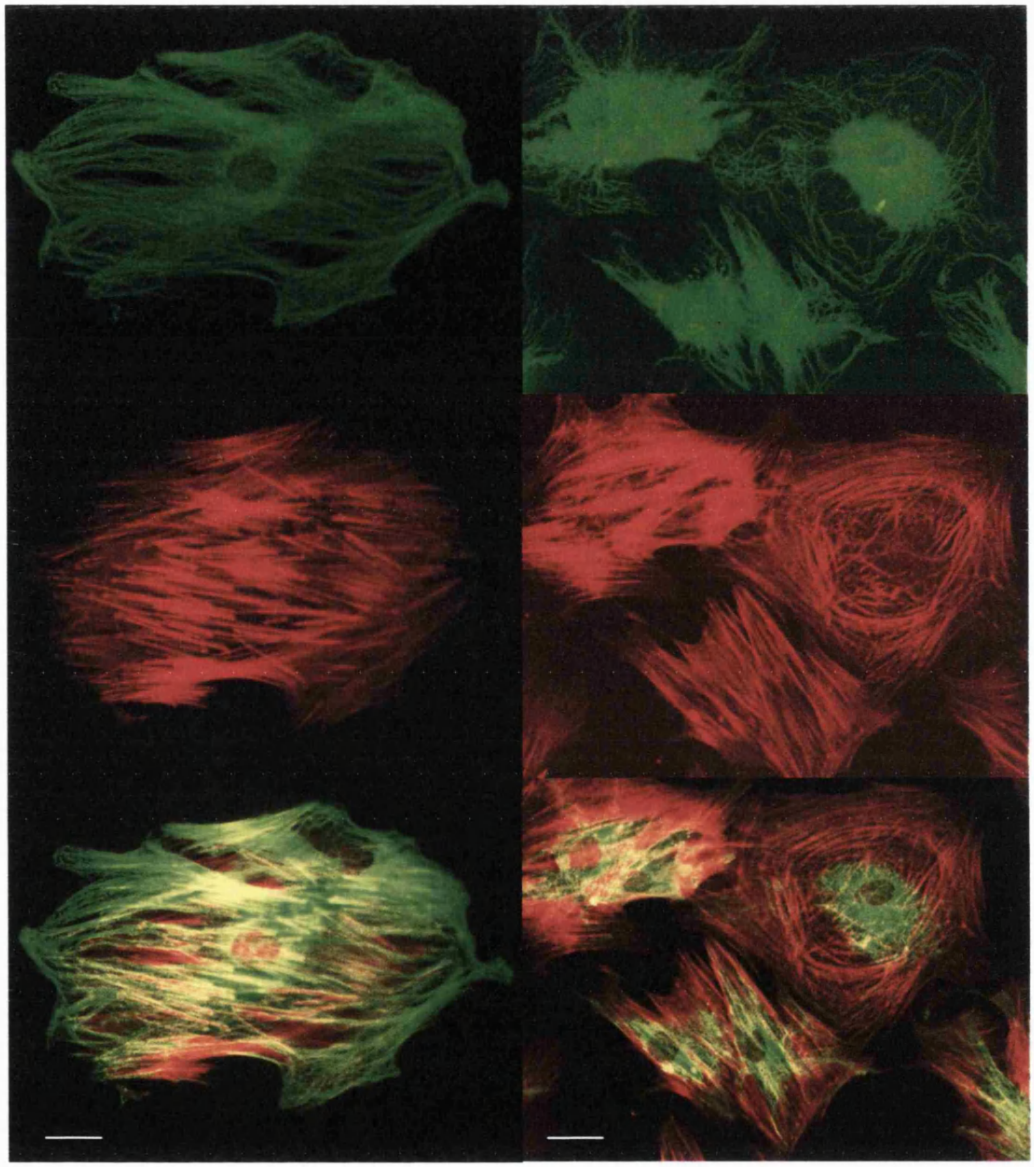

Figure 2.15 Effect of CA4P on human smooth muscle actin and tubulin cytoskeleton.
Human smooth muscle cells fixed and stained with dual antibody technique, using mouse primary anti-β tubulin antibody and secondary FITC-linked anti-mouse antibody for tubulin staining (top), and Texas red-phalloidin for actin staining (middle). Dual stained cells were visualised under blue excitation light to obtain tubulin images (top) and green excitation light to obtain actin images (middle). A double exposure was used to obtain dual staining images (bottom). Left – untreated control cell. Right – cells treated with CA4P 100 μM Bar = 50 μm

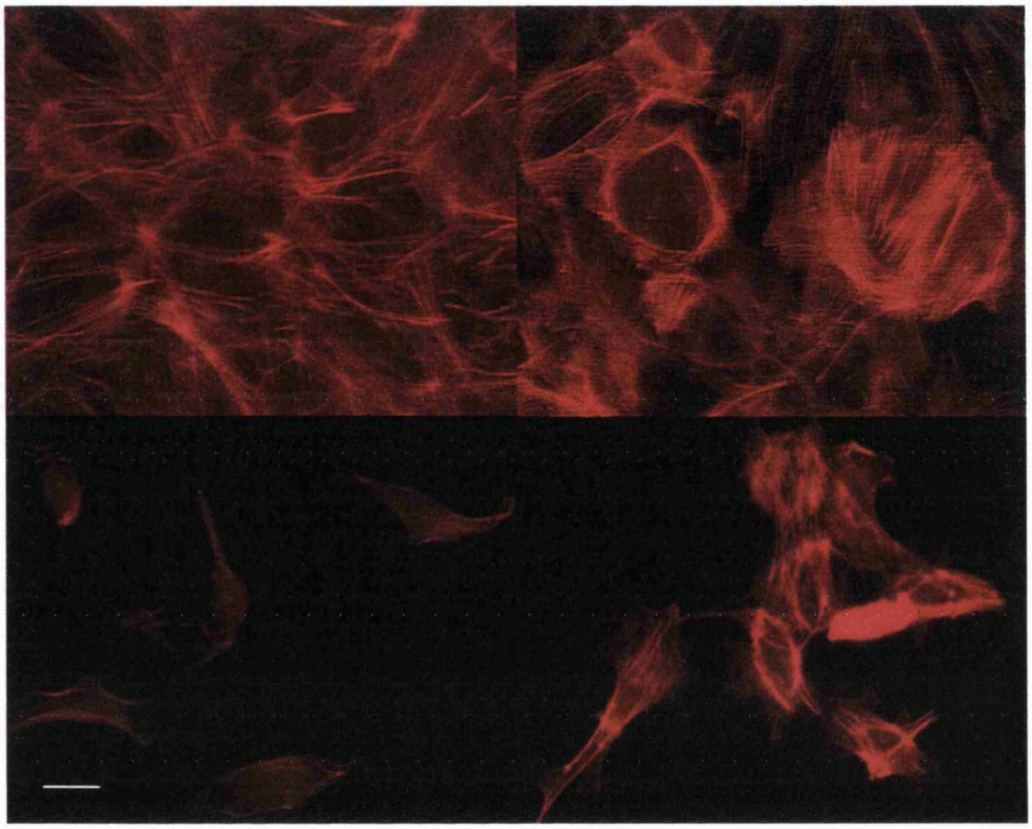

Figure 2.16 Effect of CA4P on actin cytoskeleton in HUVECs .
HUVECs fixed and stained with Texas red-phalloidin. Top – confluent cell cultures. Bottom – proliferating cell cultures. Left – untreated controls. Right – Treated with CA4P 10 μM for 30 minutes.
Increased actin stress fibres are seen in treated cells, with some condensation of actin microfilaments around the cell periphery. Bar = 50μm

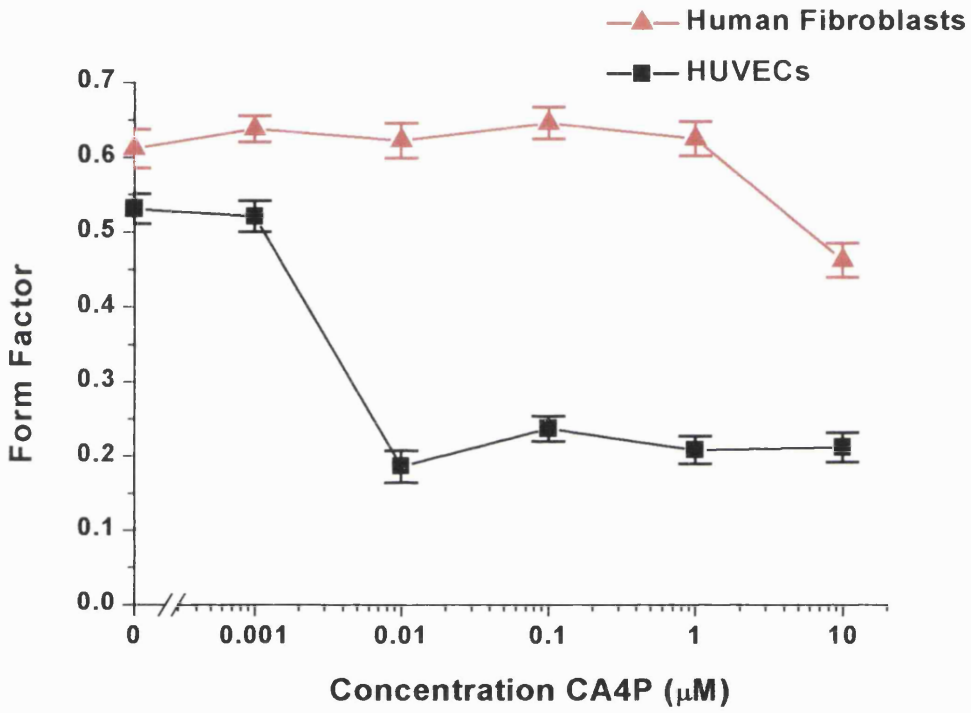

Figure 2.17 Effect of 30 minutes treatment with CA4P on form factor in human fibroblasts and HUVECs. Plotted as mean and SE

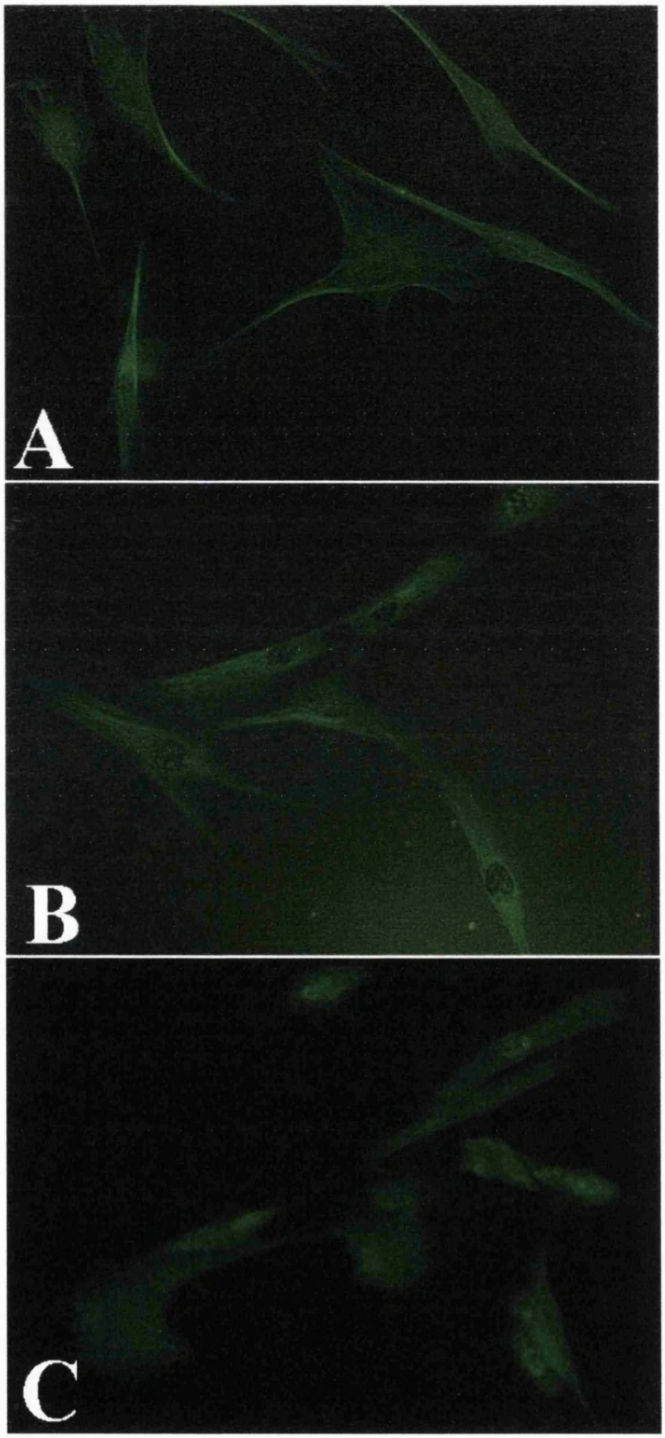

Figure 2.18 Human fibroblasts fixed after 30 minutes treatment with CA4P and stained with primary mouse monoclonal anti-β tubulin antibody and secondary FITC-linked anti-mouse antibody.
A=Control, B=1 μM, C = 10 μM

2.4 Discussion

The assay of cell area described here is similar to that used by Ingber *et al* (Ingber *et al.*, 1987), but the use of a tubulin stain allows for assessment of the degree of tubulin depolymerisation at the same time as the cell area. Kieler *et al* (Kieler *et al.*, 1989) have used Fourier analysis to describe cell shape but this is far more labour intensive. Versheuren *et al* (Verschueren *et al.*, 1993) used the same form factor as used here and Fourier analysis to quantitate the shape of lymphocytes. Both methods discriminated well between different cell populations, although Fourier analysis gave more information about the number of cell projections. The degree of information obtainable from Fourier analysis is not required for the assessment of the effect of combretastatin, and therefore the combination of cell area and form factor was chosen for this project.

CA4P is rapidly dephosphorylated by endogenous alkaline phosphatases present in plasma and on the endothelial cell surface to release the active drug CA4. The half-life for the dephosphorylation of CA4P to CA4 in mice bearing CaNT tumours was 11 minutes after 100 mg/kg intraperitoneal injection (Dr MRL Stratford, personal communication). CA4 had biphasic elimination, with initial half-life of 18.5 minutes, and terminal half-life of 1 hour in this study. This dose produces more than 90% tumour functional vascular shutdown (Chaplin *et al.*, 1999), and peak plasma levels of 300 μM CA4P and 40 μM CA4. However, CA4P is highly protein bound (68% in mouse plasma, Dr M.R.L. Stratford, personal communication), and plasma contains a higher concentration of proteins than the HUVEC medium, which contains 20% serum. After 2 hours the plasma concentration of CA4P and CA4 was < 1 μM and 1.5 μM respectively. The upper end of the range of CA4P concentrations used for these *in vitro* studies is therefore compatible with the peak plasma concentrations seen after a biologically active dose *in vivo*. The 10 to 120 minute drug exposure times chosen are also a reasonable representation of the likely exposure of endothelial cells *in vivo* for CA4.

The time course of endothelial cell shape change induced by CA4P is very rapid, with reduction in cell area and form factor measurable by 10 minutes for proliferating cells. This is consistent with the rapid increase in vascular resistance observed for solid tumours perfused *ex vivo* with CA4P (Dark *et al.*, 1997; Tozer *et al.*, 1999), and for reduction of red cell velocity in tumours treated *in vivo* (Galbraith *et al.*, 2001). The *in vivo* events leading to vascular shutdown are probably complex, and such a marked change in endothelial cell shape will have multiple functional consequences such as growth regulation (Folkman & Moscona,

1978; Barbee, 1995; Ingber *et al.*, 1995), control of cell death (Chen *et al.*, 1997a) and endothelin-1 gene expression (Malek *et al.*, 1997). However, the similarity in the time course of events seen *in vitro* and *in vivo* suggest that a change in endothelial cell shape may be involved early in the events leading to tumour vascular shutdown. Further studies to examine whether such shape changes can be detected *in vivo* will be needed to confirm this hypothesis.

Once the endothelial cells begin to round up, an increase in vessel wall permeability may be the primary damaging event *in vivo*, leading to further rise of the already elevated tumour interstitial pressure. A rapid increase in tumour vessel permeability has been demonstrated using the isolated P22 carcinosarcoma tumour model. Using an admixture of ^{125}I-albumin and ^{86}RbCl, an uptake index for the labelled albumin can be calculated, normalising the tumour to blood ratios of labelled albumin to the tumour to blood ratios of ^{86}RbCl. In this model system, tumour vascular permeability to albumin was increased by 80-100% within minutes of systemic administration of CA4P (Kanthou *et al.*, 2001). Studies using a physiologic model (Milosevic *et al.*, 1999) suggest that a rise in interstitial pressure could lead to a reduction in tumour blood flow. Griffon-Etienne et al (Griffon-Etienne *et al.*, 1999) suggest that chronic blood flow reduction in tumours is caused by increased density of neoplastic cells causing blood vessel compression rather than elevated interstitial pressure. However the reduction in cell density which led to tumour blood vessel dilation in the latter study was also accompanied by a drop in interstitial pressure. As the vascular shutdown caused by CA4P occurs over a much shorter time course, it is not inconsistent that an acute rise in interstitial pressure could lead to a drop in tumour blood flow. Increased vascular permeability could also increase blood viscosity, and this would contribute to blood flow reduction. As blood flow slows, red blood cell rouleaux formation has been observed in window chamber experiments (Dr G Tozer, personal communication), which will further increase blood viscosity. Exposure of basement membrane produced by endothelial cell rounding will also promote activation of the coagulation cascade, producing intravascular coagulation, which may prolong the vascular shutdown.

No significant change in form factor is seen for confluent cells at this time, although there is a smaller reduction in cell area measurable by 20 minutes and longer. Nevertheless, this is sufficient to produce an increase in permeability of dextran across confluent HUVEC monolayers (Watts *et al.*, 1997; Kanthou *et al.*, 2001). A transient increase in vessel permeability in normal tissues may not produce such disastrous consequences as in tumours as a result of much lower interstitial pressure in normal tissues compared with tumours (Jain,

1988). There is a large difference in concentration at which shape change occurs in proliferating versus confluent cells. The reduction in cell area is significant at 10 nM for proliferating cells but only becomes significant for confluent cells at 100 nM. This increased sensitivity of proliferating endothelium to the action of CA4P could also contribute to the wide therapeutic window seen for this drug in pre-clinical studies (Dark *et al.*, 1997), since endothelial cells lining tumour vessels are proliferating between 20 and 2000 times as rapidly as normal endothelium (Denekamp & Hobson, 1982).

There are several possible reasons for the sensitivity of proliferating HUVECs to the action of CA4P. There is evidence that the presence of microtubule associated proteins (MAPs) reduces microtubule dynamic instability and sensitivity to depolymerisation by colchicine and other colchicine analogues (Billger *et al.*, 1991; Drechsel *et al.*, 1992; Maccioni & Cambiazo, 1995; Billger *et al.*, 1996). Rapidly dividing cells have fewer post-translational modifications of their tubulin (Tint *et al.*, 1991), and fewer MAPs (Mandelkow & Mandelkow, 1995). In addition, dividing cells may have a different spectrum of tubulin isotypes than more differentiated cells, with a consequent differential sensitivity to depolymerisation (Gundersen *et al.*, 1989; Falconer *et al.*, 1992; Dumontet *et al.*, 1996). The interaction of microtubules with other cytoskeletal filaments, particularly actin microfilaments, is important in the maintenance of cell shape (Tint *et al.*, 1991; Malek & Izumo, 1996; van Deurs *et al.*, 1996). In more mature confluent endothelial cells the actin microfilaments are organised into a dense peripheral band as shown in Figure 2.15. Before formation of a mature actin microfilament network the cell may be reliant on the microtubule network for maintenance of extended cell shape, but once the actin network is established, disruption of the microtubules has less effect on cell shape (Ingber *et al.*, 1995; Mooney *et al.*, 1995). The observation that there is a smaller reduction in cell area in confluent cells even when the microtubules are depolymerised supports this hypothesis. Thus it may not be just a lower proliferation rate in confluent cell cultures which decreases sensitivity to shape change, but an increase in differentiation, associated with a change in tubulin isotype spectrum or the presence of a more mature actin cytoskeleton. There was no difference in the drug availability in confluent and proliferating cell cultures as the drug concentration was the same at the end of 30 minutes drug exposure for both confluent cultures and in cell free dishes.

At CA4P doses below 10 μM, despite marked cell shape changes with treatment, cells are able to recover their original morphology after a 4-hour recovery period. Nevertheless, there are still anti-proliferative effects at doses of 0.5 μM and above. This may be explained by the

loss of some small, fully rounded cells at these doses. Many fully rounded cells exhibit a membrane blebbing phenotype, and there is evidence that suggests that these cells may proceed to apoptosis (Mills *et al.*, 1998), (Dr C Kanthou, personal communication). Cell morphology has a critical role in mediating responses dependent on extracellular matrix (ECM)–integrin interactions. Ingber et al demonstrated that, despite maintaining similar ECM and integrin concentrations, cells could be directed to either proliferate or undergo apoptosis by altering cell shape alone (Chen *et al.*, 1997a). Some loss of cells will overestimate the extent of recovery seen, but the images of recovering cells (Figures 2.10 and 2.12) clearly demonstrate the initial depolymerisation of the microtubule network at doses ≥ 10 nM, with reformation of this network after 4 hours at doses <10 μM. Thus loss of cells does not fully account for the effects observed. In the *in vivo* studies with CA4P the maximal tumour blood flow reduction was seen between 1 and 6 hours after treatment (Horsman *et al.*, 1998; Grosios *et al.*, 1999; Tozer *et al.*, 1999). Although the initial endothelial cell rounding, vessel permeability increase and vascular shutdown all have a similar time-course, the physiological consequences of endothelial cell shape change are likely to last longer than the shape change itself. Recovery of endothelial cell morphology by 4 hours after treatment is therefore compatible with the time-course of vascular shutdown seen *in vivo*.

The results of the cell shape experiments in human smooth muscle cells and fibroblasts show that proliferating endothelial cells are particularly sensitive to the effects of CA4P. Even at 100 μM, not all the microtubules in the HMSCs were fully depolymerised, suggesting that they have a proportion of more stable microtubules, which may have a higher proportion of stable tubulin isotypes, more associations with MAPs or be stabilised by connections to other elements of the cytoskeleton. Similarly, although some shape change did occur in fibroblasts at 1 μM, this was less than in HUVECs and tubulin depolymerisation was not seen in these cells at lower doses. An increased formation of actin stress fibres was observed in both the HSMCs and HUVECs following treatment with CA4P, consistent with an increase in the ratio of polymerised to depolymerised actin measured by immunoblotting (Dr C Kanthou, personal communication). In addition many of the fully rounded cells which exhibit the membrane blebbing phenomenon, have peripheral condensation of the actin cytoskeleton. The formation of stress fibres occurs in response to signals generated by the activation of the GTP-binding protein Rho, which leads to phosphorylation of the myosin light chain. This produces interactions between myosin and actin, increased contractility of actin stress fibres, and cell rounding (Kanthou & Tozer, 2000). In the HSMCs, the incomplete depolymerisation

of the microtubule network may allow the remaining microtubules to continue to oppose the increased contraction produced by stress fibre formation, preventing significant cell shape change.

2.5 Summary

The results presented in this chapter indicate that CA4P induces rapid cell shape changes in HUVECs, at lower doses than those that have anti-proliferative effects. Unlike the anti-proliferative and apoptotic effects of CA4P on endothelial cells, which are manifest after some hours or days, the rapid time course of HUVEC shape change is consistent with that of the *in vivo* vascular shutdown. Proliferating HUVECs are more sensitive to this action of CA4P than confluent cells. HUVECs treated at $\leq$ 1 μM CA4P fully recover their original morphology after 4 hours. HUVECs are much more sensitive to shape change after CA4P treatment than human smooth muscle cells or human fibroblasts. Changes in the microtubule cytoskeleton produced by CA4P induce an increase in actin stress fibre formation, which may be involved in the induction of cell shape change.

CHAPTER 3 - COMPARATIVE EFFECTS OF OTHER TUBULIN-BINDING AND CYTOTOXIC AGENTS

3.1 Introduction

This chapter includes experiments comparing the anti-proliferative and shape change effects seen in HUVECs after CA4P treatment with those produced by other tubulin-binding agents, and by doxorubicin. The rate and extent of recovery from the shape change effects with a range of tubulin-binding agents is described, and related to their vascular targeting effects seen *in vivo*. The tubulin-binding agents chosen were colchicine, vinblastine, paclitaxel and N-acetyl colchinol phosphate. The latter compound has now been licensed by Astra-Zeneca plc., as ZD6126, and is in Phase I clinical trial in the U.S. It has a similar chemical structure to CA4P and colchicine (Figure 3.1), and like CA4P is converted to its active parent drug N-acetyl colchinol (Davis *et al.*, 2000) by non-specific endogenous phosphatases present in plasma and on endothelial cells. Pre-clinical studies have shown that it has selective tumour vascular targeting activity at well-tolerated doses (Davis *et al.*, 2000). The MTD of ZD6126 in CBA mice is around 750 mg/kg. Vascular volume in CaNT breast adenocarcinoma tumours in these mice was reduced by 80% 6 hours after treatment with ZD6126 at 25 mg/kg and by >90% at 125 mg/kg. At this dose extensive haemorrhagic necrosis was seen 24 hours after treatment, with sparing of the tumour rim. Despite this, a single dose of 125-200 mg/kg produces minimal growth delay (Blakey *et al.*, 2000; Davis *et al.*, 2000). Thus the pre-clinical studies with this drug demonstrate a similar pattern of activity to CA4P, and both drugs appear to have a wide therapeutic window for tumour vascular targeting activity.

3.2 Methods and materials

Cell culture, the neutral red assay and the cell shape change assay methods are all described in Chapter 2. A 30 minute drug exposure was used for these assays.

3.2.1 Drug preparation

Colchicine and doxorubicin were supplied by Sigma, paclitaxel (Taxol) by Bristol-Myers Squibb, UK, and vinblastine by David Bull Laboratories, Warwick, UK. N-acetyl colchinol phosphate was supplied by Angiogene Pharmaceuticals. All drugs were dissolved in PBS to a concentration of 10 mM then diluted in HUVEC medium to the desired concentration.

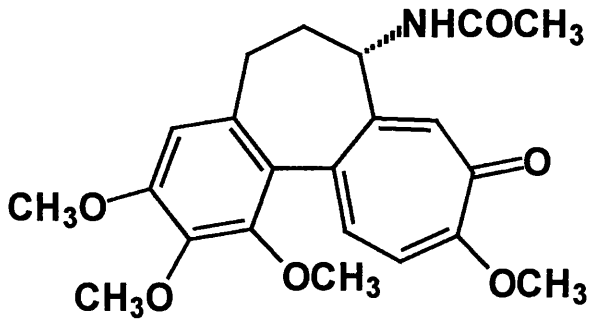

Colchicine

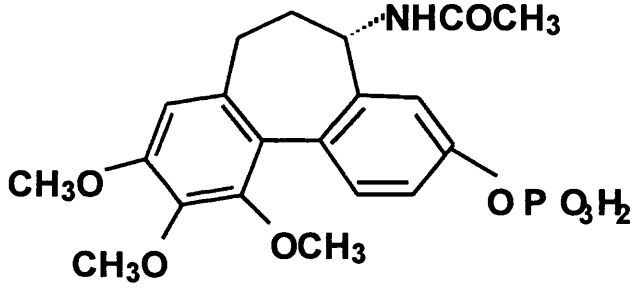

N-acetyl colchinol phosphate

Figure 3.1 Chemical structure of Colchicine and ZD6126 (N-acetyl colchinol phosphate)

3.3 Results

3.3.1 Anti-Proliferative Activity on HUVECs

The results of the neutral red assay for cytotoxic/anti-proliferative effect are shown in Figure 3.2. Paclitaxel has antiproliferative activity on HUVECs at lower doses (0.01 μM) than the other agents. Significant anti-proliferative activity was seen at 0.1 μM with vinblastine and at 0.5 μM with colchicine and CA4P. At higher doses, colchicine had increased anti-proliferative activity compared with CA4P. At 50 μM and above, doxorubicin treated wells had near 100% loss of absorbance, and phase contrast microscopy of these wells 48 hours after treatment revealed no visible adherent cells. ZD6126 had no significant anti-proliferative effect at doses below 50 μM.

3.3.2 Cell Shape Change Assay

Neither 10 μM paclitaxel nor 50 μM doxorubicin had any significant effect on HUVEC area or form factor measured immediately after a 30 minute drug exposure. Median cell area (+/- interquartile ranges) and mean form factor (+/- SE) for control and treated cells are shown in Figure 3.3. Corresponding images are illustrated in Figure 3.4. In the paclitaxel treated cells the microtubule density appears to be increased particularly in the peripheral areas of the cells compared with controls. There is no apparent effect of doxorubicin on the microtubule network at this time point.

Dose response curves at 30 minute drug exposure times for colchicine, vinblastine, and ZD6126 on HUVEC area are compared with CA4P in Figure 3.5, and comparative effects of these agents on form factor are shown in Figure 3.6. All 4 of these tubulin depolymerising agents induce significant reduction in HUVEC area and form factor in proliferating cell cultures, with a smaller effect on confluent cell area and no significant decrease in confluent cell form factor The doses at which endothelial cell shape change begins varies however. CA4P causes a significant reduction in form factor at 0.01 μM, vinblastine at 0.01 μM, ZD6126 at 0.1 μM and colchicine at 1 μM. In comparison with the data for anti-proliferative effects of these drugs (Figure 3.2), colchicine only has cell shape change effects at the same dose as anti-proliferative effects. Vinblastine has some effect on cell shape at one-tenth of its anti-proliferative dose, but CA4P and ZD6126 have significant effects on cell shape at doses one-fiftieth and five-hundredth respectively of those that have anti-proliferative activity. Appearances of the cells and their microtubule network after treatment with these drugs are illustrated in Figure 3.7. As with CA4P, depolymerisation of the microtubule network is

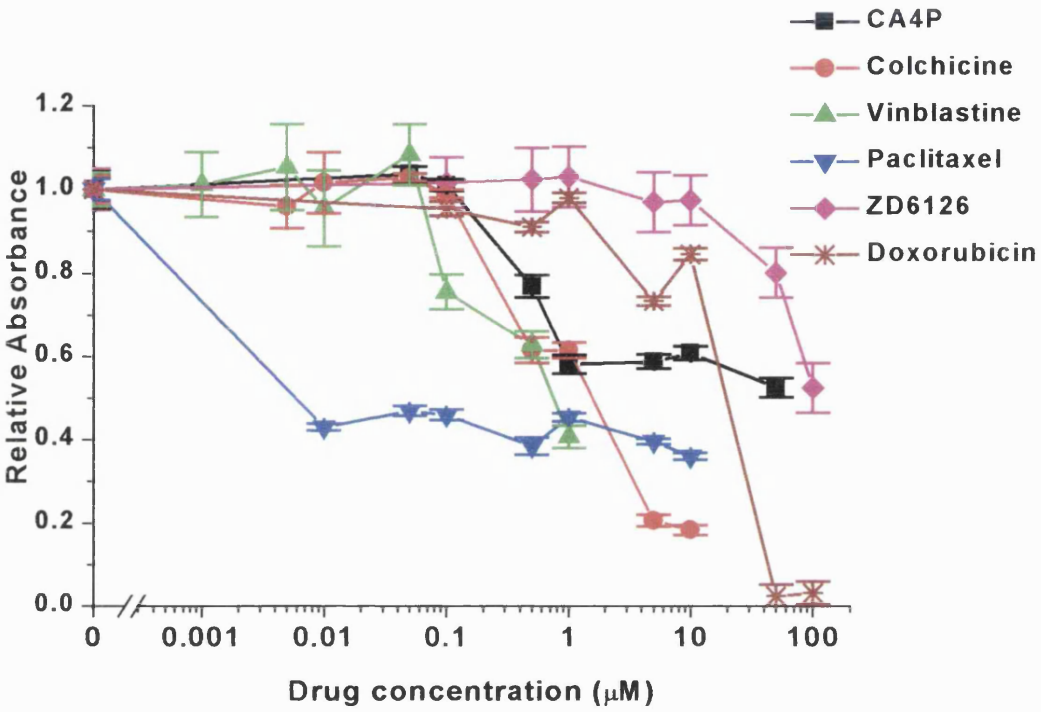

Figure 3.2 Neutral red assay for anti-proliferative/cytotoxic effects of a range of tubulin binding agents and doxorubicin on HUVECs. Relative absorbance of HUVECs stained with neutral red plotted against drug concentration. HUVECs were exposed to drug for 30 minutes, then washed x3 and fresh medium replaced. Assay performed once control wells reached confluence (5 days). Results plotted as mean +/- SE for 6 replicate wells.

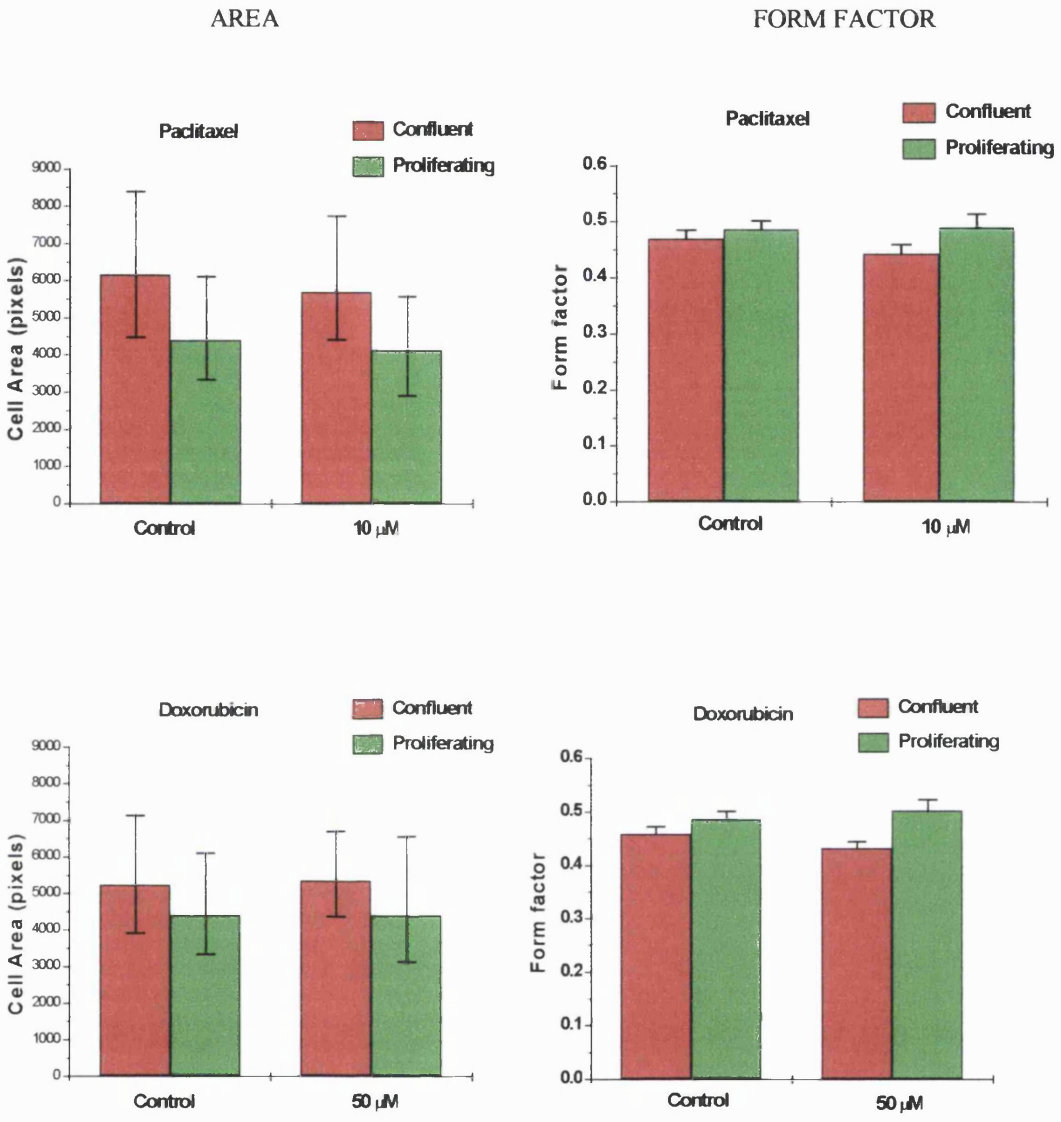

Figure 3.3 Effect of paclitaxel 10 µM (top) and doxorubicin 50 µM (bottom) on HUVEC area (left) and form factor (right), after 30 minutes drug exposure in confluent and proliferating cell cultures

Figure 3.4 Effect of paclitaxel and doxorubicin on HUVEC tubulin cytoskeleton.
HUVECs fixed and stained with primary mouse monoclonal anti-β tubulin antibody and secondary FITC-linked anti-mouse antibody. Left – confluent cell cultures. Right – Proliferating cultures. Top – treated with doxorubicin 50 μM. Middle – treated with paclitaxel 10 μM. Bottom – untreated controls. Bar = 50 μm

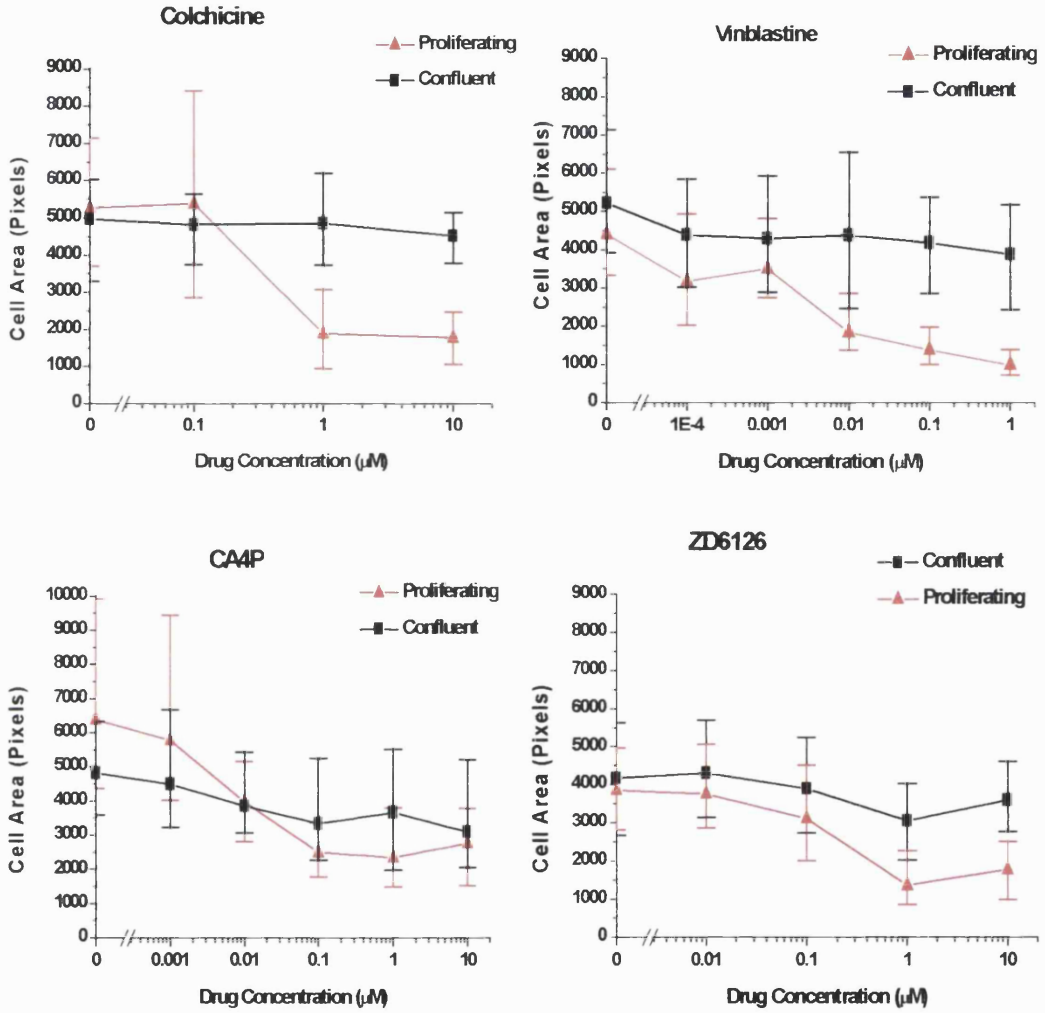

Figure 3.5 Effects of colchicine, vinblastine, CA4P and ZD6126 on HUVECs area for confluent and proliferating cell cultures, after 30 minutes drug exposure

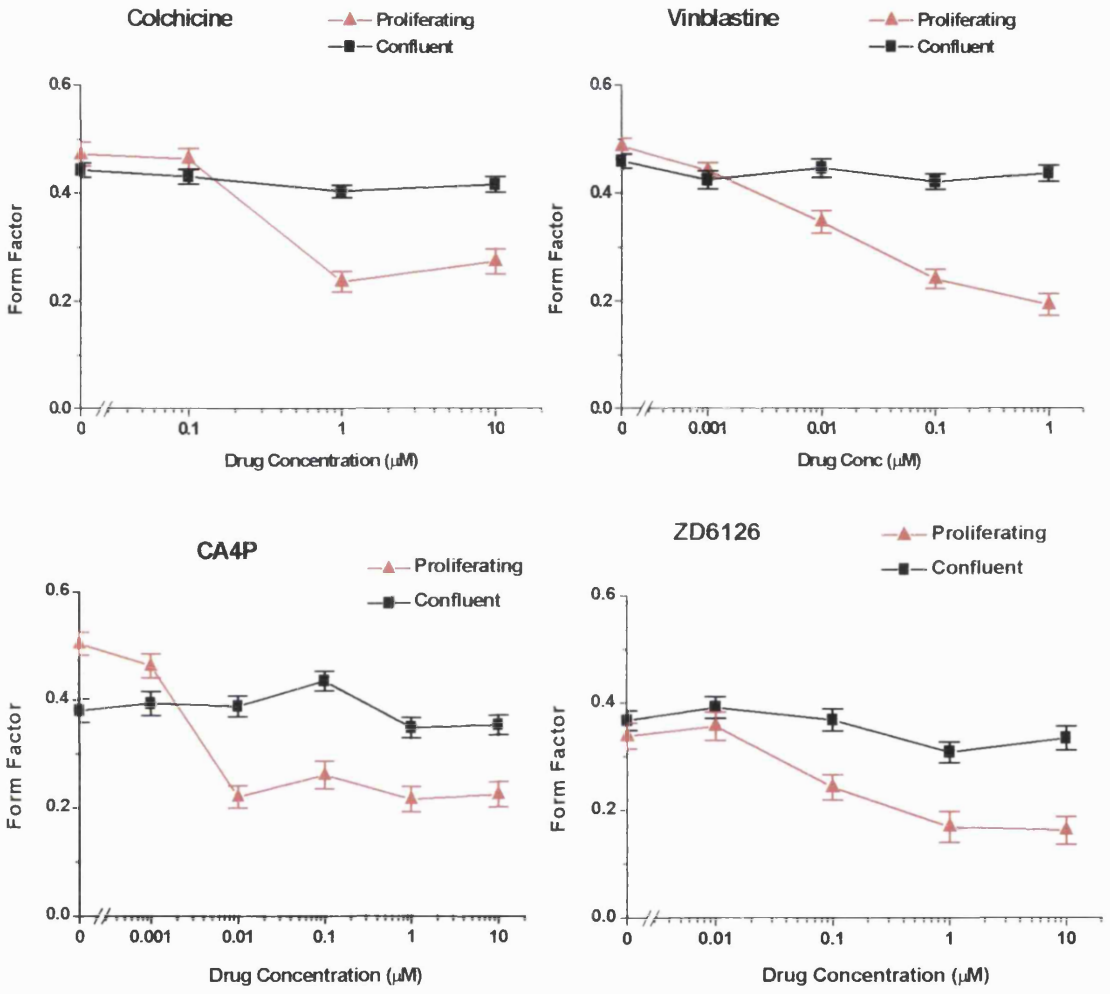

Figure 3.6 Effects of colchicine, vinblastine ZD6126 and CA4P on HUVECs form factor for confluent and proliferating cell cultures, after 30 minutes drug exposure

visible in both confluent and proliferating cell cultures, with more marked cell shape change occurring in the proliferating cultures. Some cells display the membrane blebbing phenotype described in Chapter 2.

3.3.3 Recovery of Cell Shape

Figure 3.8 shows the recovery of cell form factor after a 24-hour recovery period following a 30-minute exposure to the four drugs that produced an initial significant change in shape. At the highest concentration in the range tested for initial cell shape change (10 μM), cells treated with ZD6126 recover completely. At this concentration of CA4P there is some recovery of form factor to 86% of controls as described in Chapter 2. After recovery, the form factor is still significantly lower than for controls ($p = 0.03$, z test). However, there was complete recovery at lower concentrations (see Figure 2.9). At 1 μM colchicine, the lowest concentration at which initial reduction in form factor was seen (Figure 3.6), there is no recovery of form factor by 24 hours. This concentration of colchicine also produces anti-proliferative effects (Figure 3.2). At 0.1 μM vinblastine there is no recovery of form factor by 24 hours. At the lowest dose of vinblastine that produces significant shape change (0.01 μM) there is recovery of form factor by 24 hours, but not by 4 hours, as shown in Figure 3.9. Anti-proliferative effects of vinblastine were seen at 0.1 μM and above. Figure 3.9 also illustrates the time course of recovery after ZD6126, which like CA4P produces changes in HUVEC morphology that recover completely by 4 hours.

3.4 Discussion

Previous studies suggested that the wide therapeutic window seen for CA4P *in vivo* was related to the relative sensitivity of proliferating endothelial cells to anti-proliferative effects of this drug (Dark *et al.*, 1997; Iyer *et al.*, 1998). As discussed in Chapter 2, however, the time course of cell shape changes suggests this effect may be an early event in vascular shutdown and therefore a more relevant *in vitro* assay when considering vascular targeting activity. In addition to the endothelial cell shape change seen in this study for a range of tubulin depolymerising agents, other modalities of vascular targeting also affect endothelial cell morphology. Photodynamic therapy has been shown to produce microtubular disruption at sub-lethal doses 5-15 min post treatment (Sporn & Foster, 1992), and changes in endothelial cell morphology have been noted after TNF treatment (Sato *et al.*, 1986), and after treatment with flavone acetic acid (Watts & Woodcock, 1992), resulting in increased permeability. There may be a common mechanism for production of tumour vascular shutdown via

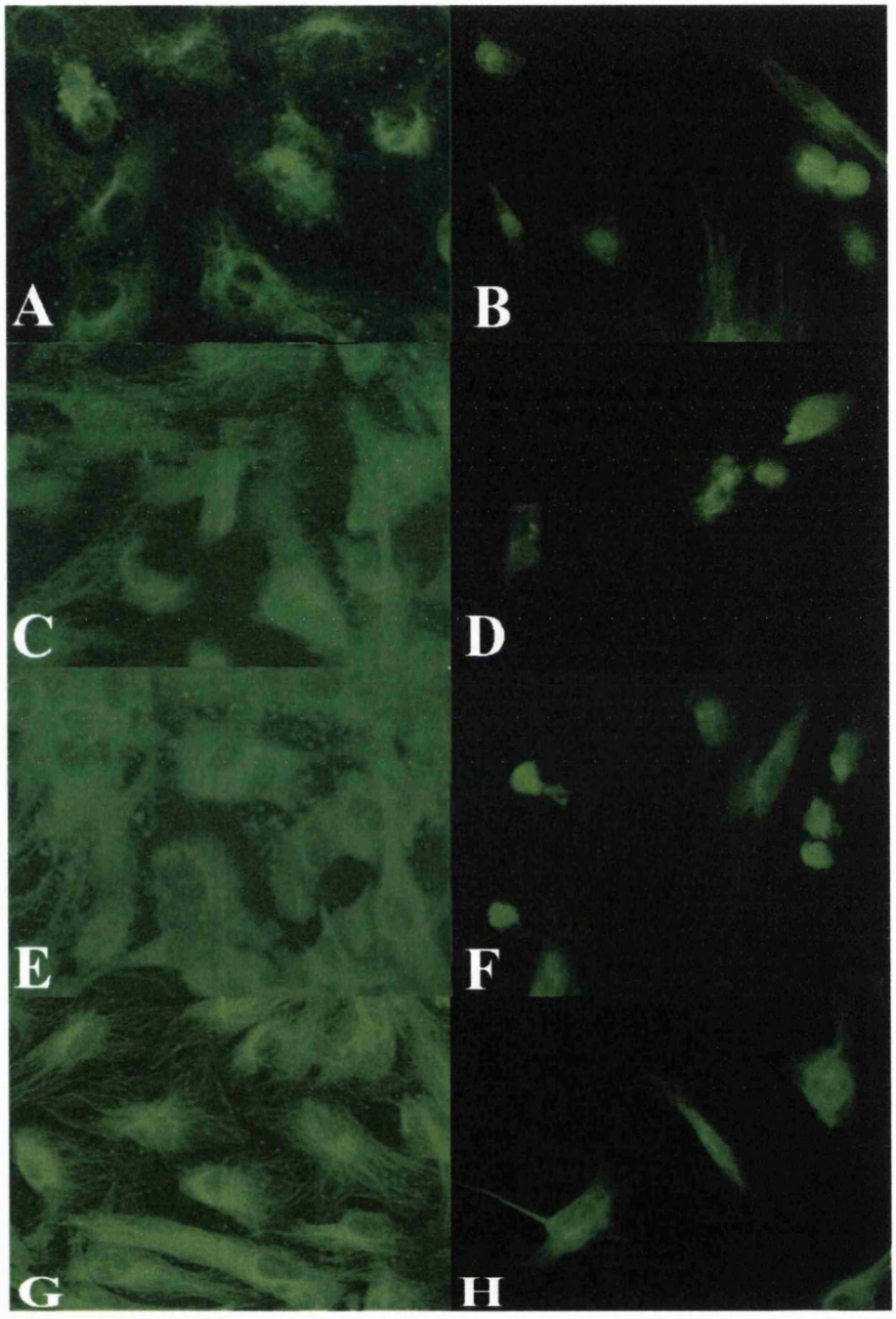

Figure 3.7 Changes in HUVEC tubulin cytoskeleton after treatment with tubulin-binding agents.
Effects of 30 minute exposure with colchicine 10 μM (A confluent and B proliferating), vinblastine 1 μM (C confluent and D proliferating), ZD6126 10 μM (E confluent and F proliferating) and untreated cells (G confluent and H proliferating).
Cells fixed after treatment and stained with primary mouse monoclonal anti-β tubulin antibody and secondary FITC-linked anti-mouse antibody.

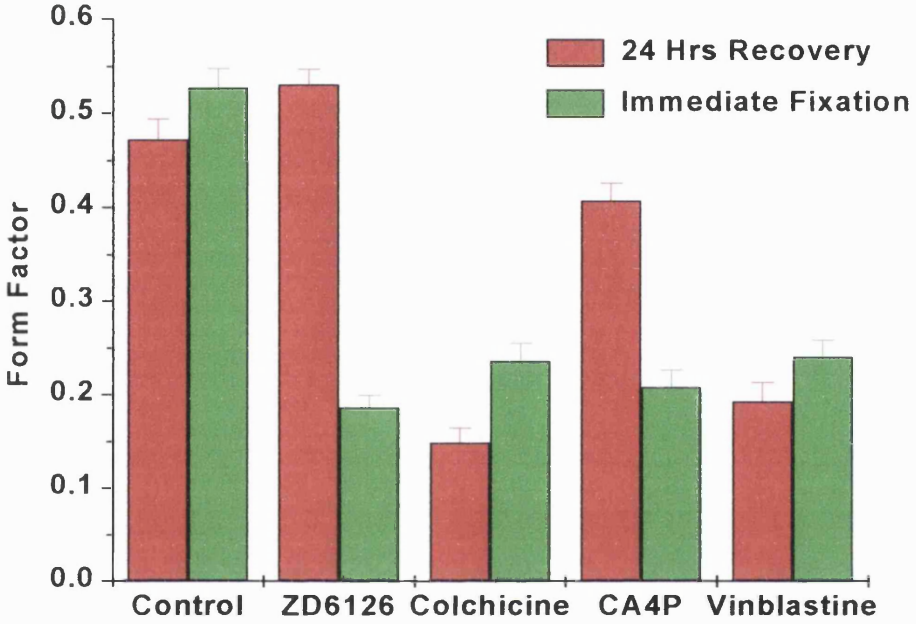

Figure 3.8 Comparison of recovery of HUVEC shape change after a 30 minute exposure to 10 μM ZD6126, 1 μM Colchicine, 10 μM CA4P and 0.1 μM vinblastine

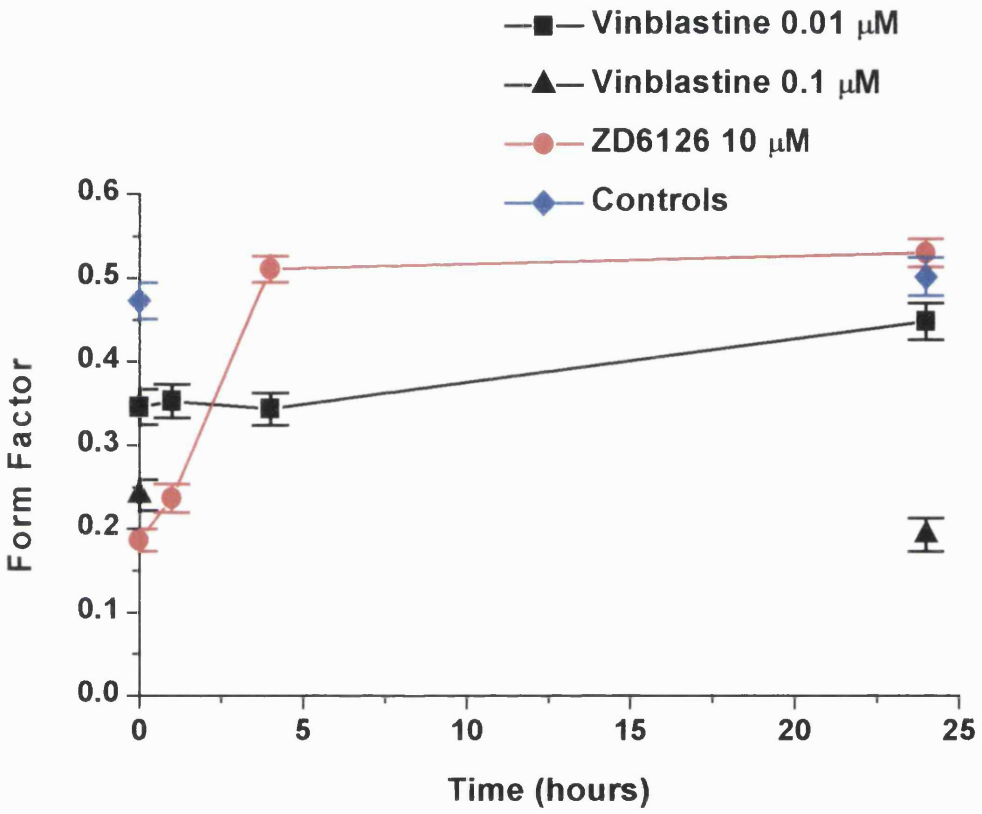

Figure 3.9 Time course of recovery of form factor for 0.01 and 0.1 μM vinblastine and for 10 μM ZD6126

damage to endothelial cells, affecting the integrity of the endothelium, and acutely increasing vessel permeability

Both doxorubicin and paclitaxel caused greater anti-proliferative effects on HUVECs than CA4P in the neutral red assay yet neither produced any significant change in cell morphology after the same exposure time. Doxorubicin is a cytotoxic agent that acts via intercalation of the drug between DNA strands, and induction of topoisomerase-DNA complexes, causing inhibition of DNA synthesis and repair (Smith & Soues, 1994). It causes cell death by apoptosis (Han *et al.*, 1997), a process that takes some hours. At a concentration that produces a marked anti-proliferative effect, there was no effect on cell shape after 30 minutes treatment. The concentrations where anti-proliferative activity was seen are much higher than those reported in other studies, which may be due to the much longer (> 24 hours) exposure times used, compared with 30 minutes exposure in this study (Ling *et al.*, 1993; Han *et al.*, 1997; Petak *et al.*, 2000). Doxorubicin has been reported to cause reductions in tumour blood flow within 2-3 minutes in animal models measured using laser Doppler, recovering by 60 minutes (Durand & Le, 1994; Durand & Le, 1997). However, no changes were seen with laser Doppler flowmetry in breast cancers in patients treated with anthracyclines (Dr K. Goodchild, personal communication).

Paclitaxel is a tubulin-binding agent, binding to a different site than colchicine or the vinca alkaloids, as discussed in Chapter 1. Unlike the other tubulin-binding agents tested, it stabilises microtubules, producing an increased density of microtubules as seen in Figure 3.4. The concentrations at which anti-proliferative activity was seen are consistent with literature reports after 3 hours exposure (Au *et al.*, 1998). As the microtubular cytoskeleton is stabilised rather than depolymerised, rapid changes in cell shape would not be expected after treatment, and were not seen. Paclitaxel has no vascular targeting activity *in vivo* (Dr S. Hill, personal communication).

In addition to their increased sensitivity to anti-proliferative effects, proliferating endothelial cells also show greater sensitivity to changes in morphology after CA4P treatment than confluent cells. However, this is also true for two drugs that have a narrow therapeutic window for tumour vascular targeting activity, colchicine and vinblastine. The increased sensitivity of proliferating endothelial cells cannot therefore fully explain the size of the therapeutic window. The difference in cell shape change effects between the two drugs that have a narrow therapeutic window for vascular targeting activity, and the two that have a

wide therapeutic window lies in the recovery of cell shape after 4 to 24 hours. HUVECs treated with colchicine do not recover their shape and there is only recovery by 24 hours after treatment with 0.01 μM vinblastine. At higher doses there is no recovery. These data are consistent with a study of permeability changes in HUVEC monolayers following treatment with vinblastine, combretastatin A1 (CA1) and other cytotoxics (Watts *et al.*, 1997). Permeability increases recovered by 2 hours after treatment with CA1, but not with vinblastine 0.1 to 0.4 μM. The lack of recovery in the cell shape assay with colchicine and vinblastine indicates that the recovery seen with CA4P and ZD6126 is not merely due to loss of fully rounded cells from the slide, as discussed in Chapter 2, but does reflect actual recovery of cell shape. The kinetics of binding to tubulin of colchicine and CA4 are very different. CA4 binds more rapidly and has a much shorter dissociation half-life than colchicine (Lin *et al.*, 1989); 3.6 minutes compared with 405 minutes. Binding is associated with a conformational change in the tubulin-colchicine complex (Andreu & Timasheff, 1982). This difference in tubulin-binding kinetics is reflected in the *in vivo* pharmacokinetics. Colchicine has a plasma distribution half-life of 1.8 hours, a very high volume of distribution (700 l), and a long elimination half-life (20 hours) (Sabouraud *et al.*, 1992), as the drug binds to tubulin in many different tissues, and is slowly released. Similarly, vinblastine has a large volume of distribution (1400-2500l), indicating extensive tissue binding, and a terminal half life of 20-35 hours in man (van Tellingen *et al.*, 1992). In patients treated with 7-10 mg/m^2 vinblastine plasma levels at 4 hours were 0.01 μM (Nelson, 1982). In the mouse, 5 hours after treatment with 3 mg/kg, plasma levels were 0.1 μM, and the terminal half-life was 7-9 hours (van Tellingen *et al.*, 1992). This dose is the lowest dose at which vascular volume reduction was seen in a murine tumour (Hill *et al.*, 1993). The plasma concentrations achieved in man at clinically useable doses are therefore lower than those needed in mice to produce vascular targeting activity. For both vinblastine and colchicine, the exposure times used in the cell shape assay underestimate the duration of exposure of endothelial cells *in vivo*.

Like CA4P, ZD6126 has a much shorter half-life than either colchicine or vinblastine. In CBA mice given 200 mg/kg i.p., the half-life for dephosphorylation of ZD6126 to the parent drug N-acetyl colchinol was 13 minutes, and the half-life of N-acetyl colchinol was 22 minutes, with peak plasma concentrations of 100 μM and 200 μM respectively (Dr M.R.L. Stratford, personal communication). The effects of both ZD6126 and CA4P on cell shape are both of short duration, and this may be important in determining the ability to induce marked effects in tumour vasculature, whilst producing less effects in normal tissue vessels.

However, the duration of endothelial shape change *in vivo* might differ from that observed in this *in vitro* assay due to the differing microenvironment, and the presence in some areas of underlying basement membrane. As discussed in Chapter 2, although the effects on cell shape are less for confluent HUVECs, sufficient changes are produced in confluent cultures to produce permeability changes at concentration levels equivalent to those seen in murine plasma after treatment with an effective dose of CA4P. If such changes are of short duration, it is possible that the well-organised microcirculation in normal tissues may cope with the insult without permanent damage. Prolonged induction of increased microvessel permeability in normal tissues, however could be more damaging. In tumours, due to the already chaotic microvasculature described in Chapter 1, a short term insult might produce a cascade of other events, leading to a greater initial reduction in blood flow rate, and a longer recovery period than for normal tissues. Therefore, agents which produced a more prolonged change in endothelial shape, and consequently more prolonged change in permeability might actually have a poorer therapeutic index. Alternatively, the lack of recovery of cell shape after treatment with these agents may just reflect the slower kinetics of dissociation from tubulin, which also affects the pharmacokinetcs *in vivo* (Nelson, 1982; Himes, 1991). Prolonged exposure to the drugs induces side effects by affecting cells other than endothelial cells, producing neutropaenia, neurotoxicity and gut toxicity, which occur at similar doses to those that cause endothelial cell shape change, and vascular targeting effects.

Both CA4P and ZD6126 have a similar time course of tumour vascular shutdown *in vivo*, maximal between 1 to 6 hours after treatment, which is compatible with the duration of cell shape change effects seen *in vitro* for both agents. There are no reports of the time course of normal tissue or tumour blood flow rate or vascular volume changes after treatment with colchicine. It was noted to induce complete tumour necrosis at doses $\geq$ 3.5 mg/kg in mice (Baguley *et al.*, 1991), and reduced tumour vascular volume by 40%, 24 hours after treatment with 2.5 mg/kg (Dr S. Hill, personal communication). At this dose the mice appeared unwell however, demonstrating the narrow therapeutic window for this drug. Reductions in tumour blood flow rate 6 hours after treatment in murine colon adenocarcinoma were only seen at lethal doses for both vinblastine (40 mg/kg) and colchicine (4 mg/kg) (Nihei *et al.*, 1999). However, the method used for measurement of perfusion in this study, Evans blue extraction may underestimate reduction in perfusion as it is also affected by vessel permeability. Vinblastine at the MTD of 10 mg/kg in mice reduced tumour blood flow rate by 90% after 2 hours, and by >80% at 24 hours (Hill *et al.*, 1993). Even at the lowest dose at which tumour blood flow rate reduction was seen (3 mg/kg), it was reduced by >40% at 24

hours. There was some tumour selectivity, with smaller reductions in blood flow rate in normal tissues, which recovered by 6 hours. The longer half-life in man may further reduce the therapeutic window for vascular targeting effects with this drug.

3.5 Summary

Doxorubicin and paclitaxel did not cause any shape change in HUVECs, even at concentrations where anti-proliferative activity was seen. All the tubulin depolymerising agents tested produced greater shape change in proliferating versus confluent cells. HUVEC morphology recovered by 4 hours after treatment over a >100 fold concentration range with ZD6126 and CA4P. Both these agents exhibit HUVEC morphology changes at concentrations well below those that have anti-proliferative effects. Colchicine and vinblastine had shape change effects and anti-proliferative effects at similar concentrations, with no recovery at the concentrations seen in plasma *in vivo*. These results suggest that the use of this *in vitro* assay for cell shape change, and recovery might be useful in the assessment of novel vascular targeting agents, although correlation of therapeutic index *in vivo* with assay results for more agents would be required for further validation. A method for determining endothelial cell shape *in vivo* would also be useful in supporting or refuting this hypothesis.

CHAPTER 4 - MRI METHODS

4.1 Overview of MRI principles

Water molecules make up 60-70% of the constituents of body tissues. The protons that are contained in water molecules have a positive charge and are constantly spinning. As they do so the moving charge produces an electric current and an associated magnetic field. When placed in an external magnetic field, such as in an MRI machine, the protons align themselves either parallel or anti-parallel to this field. More protons are aligned parallel to the external magnetic field, producing a longitudinal magnetic moment in this direction. They continue to spin, like a spinning top, a motion known as precession, and the precession frequency, ω_0 (Lamor frequency) is determined by the magnetic field strength, B_0:

$$\omega_0 = \gamma B_0$$

where γ is the gyromagnetic ratio. By the use of radiofrequency (RF) wave pulses, the proton alignment can be temporarily altered, changing the longitudinal magnetisation, and the protons precess in phase, producing a magnetic moment in a transverse plane. Once the pulse stops, the protons relax back to their original position, and gradually precess out of phase due to interactions with locally fluctuating magnetic fields. As they relax, they emit a RF signal that can be detected in a receiver coil, in which an electrical current is induced. The RF signal intensity depends on the type of RF pulse sequence used and the structure and water content of the tissues. The relaxivity of a tissue can be described in terms of spin-lattice, or longitudinal relaxation time (T1), which reflects the rate that the spinning protons are able to transfer energy to the surrounding lattice, and spin-spin or transverse relaxation time (T2), which is affected by local magnetic field inhomogeneities.

The used of magnetic field gradients in orthogonal planes allows encoding of spatial information and construction of 2D or 3D images of signal intensity. The RF pulses and field gradients can be adjusted in multiple ways to give different signal intensities for a single tissue - for example on a T1 weighted image fat appears bright, but intermediate on a T2 weighted image. This gives MRI an advantage over CT scanning of excellent soft tissue contrast, without the use of ionising radiation, and the ability to image in any plane.

It is possible to use intrinsic contrast within tissues to image microvascular blood flow, using pulse sequences that are sensitive to either the motion of water in the vessels, or to distortion of magnetic field homogeneity caused by the presence of deoxyhaemoglobin, which acts as an intrinsic, oxygen sensitive paramagnetic marker. BOLD (Blood Oxygen Level Dependent) and FLOOD (Flow and Oxygen Dependent) sequences are examples (Robinson *et al.*, 1995). These sequences are sensitive to both microvascular blood flow as well as oxygen level. However, these techniques are limited by lower signal to noise compared to those that use extrinsic paramagnetic contrast agents.

4.2 Properties of Gadopentetate dimeglumine (Gd-DTPA)

Gadopentetate dimeglumine (Gd-DTPA), a lanthanide chelate, is an extracellular contrast agent, which has been licensed for clinical use since 1988 and has an excellent safety record. In a study of over 5000 patients, an adverse reaction rate of 2.2% was reported (Nelson *et al.*, 1995). The commonest event was flushing, and the rate of anaphylaxis currently estimated is 1 in 200,000 (Runge, 2000). This compound contains unpaired electrons, which produce a dipole-dipole interaction with proton nuclear spins, enhancing their relaxation. In most tissues it has a dominant effect on T1 relaxation time, which is decreased, which results in an increase in signal intensity on T1 weighted images. It is excreted renally, with a plasma half-life of 90 minutes (Magnevist product information, Schering AG).

4.3 Theory of dynamic contrast enhanced MRI

The theory underlying the use of dynamic contrast enhanced MRI (DCE-MRI) to measure physiologic parameters such as tissue blood flow and permeability is based on the Kety equation described in Chapter 1 for a freely diffusible tracer.

$$C_t(T) = EF \int_0^T C_a e^{\frac{-EF}{\lambda}(T-t)} dt \qquad (1)$$

where E is the extraction fraction, F is blood flow rate (ml whole blood per g of tissue per minute), λ is the tissue-blood partition coefficient of the substance, C_a is the arterial blood concentration and C_t is the tissue concentration. This can be adapted for intravenous bolus injection of an extracellular tracer such as Gd-DTPA (Tofts *et al.*, 1999):

$$C_t(T) = K^{trans} \int_0^T C_p(t) e^{-k_{ep}(T-t)} dt \qquad (2)$$

where C_p is arterial plasma concentration of Gd-DTPA, K^{trans} is the volume constant for the transfer of Gd-DTPA from the vessel into the extracellular extravascular space (EES), and k_{ep} is the rate constant for the transfer of Gd-DTPA from the EES back into the plasma. From the above two equations,

$$K^{trans} = EF\rho(1-Hct) \qquad (3)$$

where ρ is tissue density (g/ml) and Hct is haematocrit. K^{trans} has several physiologic interpretations depending on the balance between capillary permeability to Gd-DTPA and blood flow rate in the tissue of interest. In tissues with highly permeable vessels, where flux across the endothelium is flow limited, E is close to 1 so K^{trans} is equal to the blood plasma flow rate per unit volume of tissue (ml plasma per ml tissue per minute):

$$K^{trans} = F\rho(1-Hct) \qquad (4)$$

Adapting Renkin's equation (Renkin, 1959) for extraction fraction for a freely diffusible tracer to an extracellular tracer,

$$E = 1 - e^{-\frac{PS}{F(1-Hct)}} \qquad (5)$$

where PS is the permeability (P) vessel surface area (S) product. Therefore, when PS<<F, as in tissues such as brain with low vessel permeability, flux across the endothelium is permeability limited,

$$E = \frac{PS}{F(1-Hct)} \qquad (6)$$

and K^{trans} is equal to the permeability surface area product per unit volume of tissue:

$$K^{trans} = PS\rho \qquad (7)$$

In tumours there will be heterogeneity of vessel permeability, and K^{trans} will be determined by a combination of flow, permeability and vessel surface area. The ratio of K^{trans} to k_{ep} gives the volume of EES per unit volume of tissue, v_e, otherwise known as the Gd-DTPA leakage space:

$$v_e = \frac{K^{trans}}{k_{ep}} \qquad (8)$$

This model assumes an instantaneous bolus, instant mixing of Gd-DTPA within the blood and within the leakage space after transfer from the vessel, and ignores the contribution of intravascular tracer to the tissue concentration.

In order to use equation 2 to derive the parameters K^{trans}, K_{ep} and v_e, tissue concentration of Gd-DTPA has to be derived from the MRI signal intensity information. It has been assumed by some groups that for the range of concentrations of Gd-DTPA used in clinical studies, there is a linear relationship between 1/T1 and tissue concentration of Gd-DTPA (Belfi *et al.*, 1992). This has been confirmed by measuring tissue concentration and relaxation rate (Strich *et al.*, 1985). However, it is also dependent on the initial T1 of the tissue: (Tweedle *et al.*, 1991)

$$\frac{1}{T1_{(t)}} - \frac{1}{T1_{(0)}} = \beta.C_a(t) \qquad (9)$$

and signal intensity on a T1 weighted image is not linearly related to 1/T1, as it also depends on aspects of the RF pulse sequence used and the tissue proton density (Evelhoch, 1999). However the T1 of the tissue can be calculated by obtaining a proton density weighted image prior to contrast injection. Providing the machine scaling factors are not altered during the sequence of T1 weighted images, only one proton density image is required, as signal from this image should not vary with contrast agent concentration. Using a calibration curve generated from measurements on a variety of phantoms with known T1 levels, the ratio of the T1 weighted images to the proton density image can allow T1 values to be calculated (Parker *et al.*, 1997), and the concentration of Gd-DTPA can be obtained.

The technique of dynamic contrast enhanced MRI (DCE-MRI) is becoming increasingly widespread, both for improving diagnostic imaging (Hittmair *et al.*, 1995; Ostergaard *et al.*, 1998; Postema *et al.*, 1998) but also in research into aspects of tissue microcirculation (Hawighorst *et al.*, 1997; Daldrup-Link *et al.*, 2000; Padhani *et al.*, 2000; Wen *et al.*, 2000) and assessment of changes in microcirculation following a treatment intervention (Kennedy *et al.*, 1994; Reddick *et al.*, 1995; Baba *et al.*, 1997; Beauregard *et al.*, 1998; Galbraith *et al.*, 2000). The development of novel therapeutic agents in the field of cancer medicine, such as those that act on the tumour vasculature, has increased the importance of standardising this powerful tool so that accurate assessment of a drug's activity can be made early in its

clinical development (Eckhardt & Pluda, 1997). Tofts et al have recently set out a consensus of opinion about the standard quantities and symbols that should be adopted when using this technique to obtain fully quantitative parameters which relate to tissue perfusion, vessel permeability and surface area (Tofts *et al.*, 1999). However many groups still use semi-quantitative parameters, such as the initial gradient of the signal enhancement derived from the signal intensity time curves, which are simpler to obtain. In the absence of absolute T1 measurements, or the use of a proton density image to derive T1, the relative change in signal intensity (S), divided by the initial signal (S_0), has been used. This is called the enhancement (E):

$$E = \frac{S_t - S_0}{S_0} \tag{10}$$

The gradient (G) is calculated from the rate of change of enhancement:

$$G = \frac{dE}{dT} \tag{11}$$

The maximum enhancement and maximum or initial gradient are usually used. Relative changes in such semi-quantitative parameters can be examined, which may be indirectly related to changes in the physiological end-point of interest such as blood flow rate (Bonnerot *et al.*, 1992; Mayr *et al.*, 1996; Beauregard *et al.*, 1998; Ostergaard *et al.*, 1998; Hawighorst *et al.*, 1999). If there is no correction for initial T1 relaxation time, then variations in this value will affect enhancement to some degree, as illustrated in Figure 4.1, which shows the signal intensity time curves for regions of interest (ROIs) in fat and muscle from the same patient. Fat has a high initial T1 and enhances 4 times as much as muscle. The calculated gradient is also 3.8 times as great in fat than muscle. After correction for the initial T1 level, using the method described above, the resultant Gd-DTPA concentration time curves demonstrate that there is now little difference between fat and muscle, in fact the gradient, and the calculated K^{trans} in fat is now greater than muscle. Semi-quantitative parameters, which are not corrected for initial T1, could not therefore be used to compare relative levels of blood flow in different tissues or patients, although they could be used to compare changes within the same tissue after an intervention.

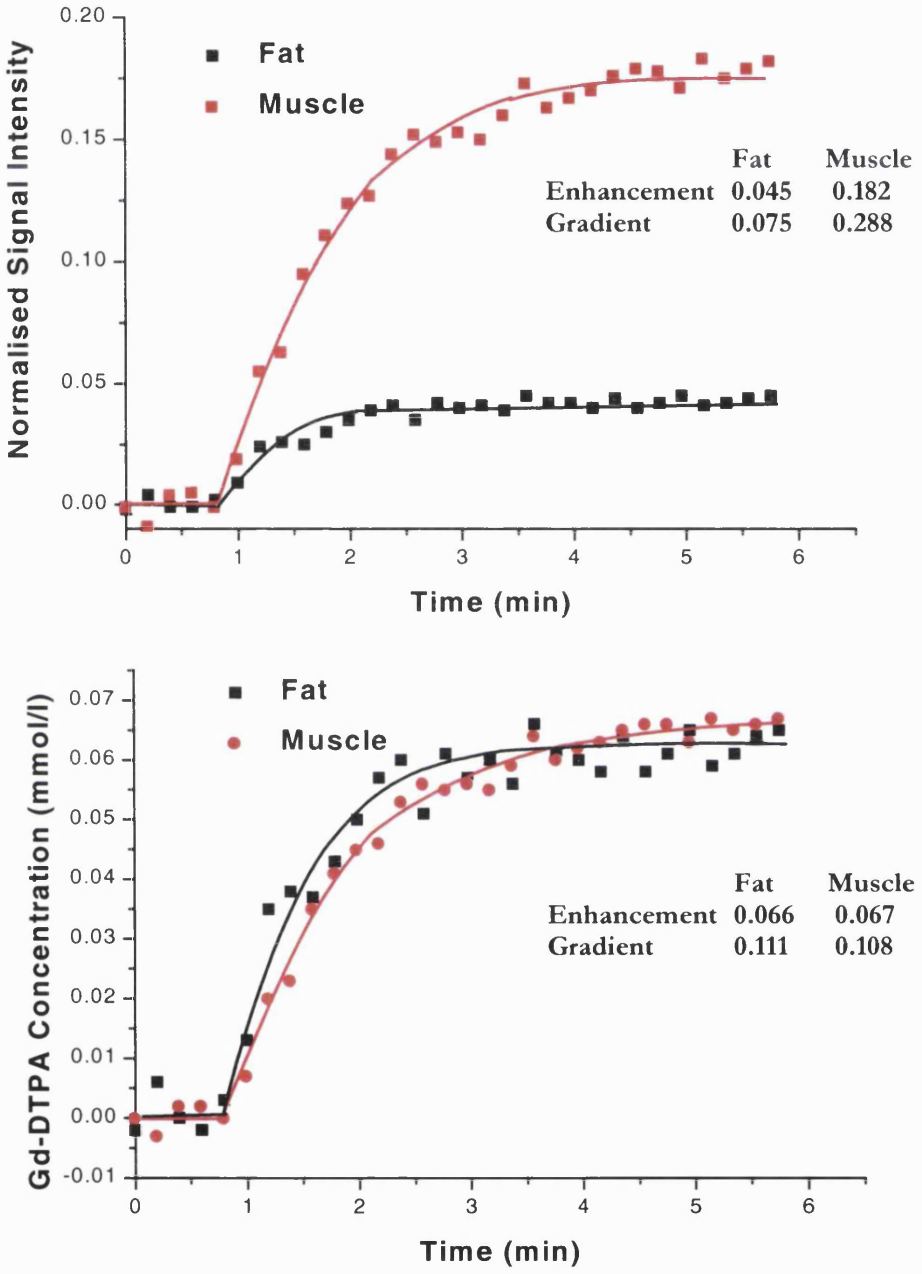

Figure 4.1 Illustration of the influence of initial T1 level on signal enhancement and gradient.

Top – Normalised signal intensity plotted against time for fat which has a high T1, and muscle which has a lower T1. The enhancement and gradient in muscle is ~4 times greater than that in fat.

Bottom - This data is corrected for initial T1 level to calculate Gd-DTPA concentration, which is plotted against time. The gradient in fat is now greater than that in muscle, and the enhancement is only slightly greater in muscle than fat.

4.4 Standardisation of data collection for DCE-MRI

In order to obtain fully quantitative data from DCE-MRI, the following recommendations have been made (Evelhoch, 1999; Brasch *et al.*, 2000):

- Correlate dynamic series images with high resolution T1 and T2 weighted anatomic images in same plane
- Obtain T1 image map prior to contrast injection
- Use a power injector where possible for contrast injection of 0.1-0.2mmol/kg body weight Gd-DTPA to minimise variations in timing and rate of injection.
- Obtain arterial input function with temporal resolution of 1 second
- Acquire multislice, serial images of tumour with temporal resolution of < 12 seconds, for a total of 6-10 minutes
- Use maximal spatial resolution possible with above constraints

Where it is not possible to obtain an arterial input function, Evelhoch recommends using the uptake integral (the area under the concentration time curve over the first 90 seconds after the onset time, AUC), and normalising to a normal tissue such as muscle (Evelhoch, 1999), as this minimises errors due to variations in the arterial input. Like the parameters obtained from semi-quantitative analysis, however, the AUC will be related to, but not a direct measurement of the physiological parameters of interest

Evelhoch also suggests obtaining an arterial input function from a major artery at the same scanning session as the dynamic series by first using a bolus of Gd-DTPA of the same volume, but one-tenth dilution as for the dynamic series. The data can then be obtained with high temporal resolution (1 second). There are other technical difficulties with obtaining an arterial input function using such a technique. In order to eliminate signal intensity changes due to inflow of blood from outside the imaged slice, a 'saturation slab' has to be applied to the body proximal to the imaged slice. For wider areas of the body such as the thorax or abdomen, this creates a problem with the total energy deposition in the body. Work is proceeding to try and use a suitable sequence to image the femoral artery to avoid this problem. For the studies described in this thesis, these technical difficulties meant that an assumed rather than a measured arterial function had to be used. In addition, a mechanical injector was not available, so injections were performed manually using a standardised technique.

4.5 MRI protocol used at Mount Vernon Hospital

The MRI studies were performed on a 1.5 T System, Magnetom Symphony (Siemens Medical Systems, Erlangen, Germany) using a body coil. At each scanning session, diagnostic images required for disease assessment were first obtained. A marker lesion (>2cm in size) was chosen for the DCE-MRI. Care was taken when positioning the patient to be in exactly the same position on subsequent visits in order to obtain the same anatomical slice location. Between 3 to 5 slices were chosen up to 8 cm apart with one slice through the centre of the marker lesion, and muscle. Proton density weighted spoiled gradient echo FLASH (Fast Low Angle SHot) images (TR = 350 ms, TE = 9.8 ms, flip angle 20°) were then acquired at the same slice positions to enable the calculation of tissue Gd-DTPA concentration (Parker *et al.*, 1997). A dynamic series of 30 T1 weighted FLASH images was acquired for the same slice positions, with 3 images prior to a manual bolus intravenous injection of 0.1 mmol/kg Gd-DTPA, given over 10-12 seconds using a standardised injection protocol. Images were acquired consecutively with no time gaps. Each set of images took 11.9 seconds to acquire, and the whole sequence took 6 minutes. The imaging parameters for the T1 weighted FLASH sequence were TE 9-10 ms, TR 80 ms, 70° flip angle and 10 mm slice width. System gain factors were maintained between acquisition of the proton density and T1 weighted dynamic series of images.

4.5.1 Data analysis

Images were transferred to a Sun workstation (Sparc 10, Sun Microsystems, Mountain View, CA), and analysed using Analyze™ software (Mayo Foundation, Rochester, MN). Using information from anatomic T1 or T2 weighted images and post contrast T1 images, ROIs were carefully drawn around the tumours, including the whole tumour where possible, but excluding pulsatility artefacts from blood vessels, and susceptibility artefacts from adjacent bowel. ROIs were also drawn for areas of skeletal muscle (usually paraspinal muscle). Identical ROIs were used for each pre-treatment examination and for post treatment examinations at 4 and 24 hours after the first dose of CA4P. For examinations at later times in a patient's treatment, tumour progression or shrinkage meant that new ROIs had to be drawn to encompass the entire tumour. ROIs in normal tissue were unchanged.

The dynamic image data were analysed using both quantitative and semi-quantitative approaches. Semi-quantitative analysis was performed directly with the T1-weighted images but quantitative analysis required conversion of the MR signal intensities to Gd-DTPA concentrations (Parker *et al.*, 1997). This was performed by converting signal intensities to T1

relaxation time values using the proton density images in conjunction with data from a calibration experiment that involved samples with known T1 relaxation time values (done by Dr J Taylor and Dr M Lodge). Gadolinium concentration $C_t(t)$ was then inferred from the tissue T1 using the equation,

$$C_t(t) = (1/T1(t) - 1/T1_0) / R_1 \qquad (12)$$

where $T1_0$ is the tissue T1 without contrast and R_1 is the longitudinal relaxivity of protons *in vivo* due to Gd-DTPA (taken to be 4.5 $ls^{-1}mmol^{-1}$).

The ROIs were subsequently applied to the dynamic image data in two ways. In the first method (*ROI* analysis), the mean of the image data within the ROI was calculated for each of the dynamic images, resulting in a single time-intensity data set. In the second method (*pixel* analysis), time-intensity data were obtained for each pixel within the ROI. Each individual time-intensity data set was separately analysed as described below and the results were presented as parametric images. Although the tumour tissue response was frequently heterogeneous, a single global value for the entire region was obtained by taking the mean of all the individual pixel parameters. In normal tissues analysis was only done on a whole ROI basis.

Using equation (2) above the arterial input function $C_p(t)$ was approximated by a bi-exponential function that was scaled according to the administered dose of Gd-DTPA, D (mmol/kg body weight) (Tofts & Kermode, 1991; Tofts *et al.*, 1999):

$$C_p(t) = D\{a_1 \exp(-m_1 t) + a_2 \exp(-m_2 t)\} \qquad (13)$$

Where $a_1 = 3.99$ kg/l, $a_2 = 4.78$ kg/l, $m_1 = 0.144$ min^{-1} and $m_2 = 0.0111$ min^{-1}.

This model was fitted to the dynamic MR Gd-DTPA concentration data using non-linear least squares estimation to obtain values for the two free parameters K^{trans} and k_{ep}, and v_e was obtained by dividing K^{trans} by k_{ep}. The time between the start of data acquisition and the arrival of the bolus at the region of interest was estimated from the whole ROI time-intensity data and fixed for each of the individual pixel fits. Pixels that resulted in poor fits were excluded from subsequent analysis. The criteria for acceptance were:

1. the mean absolute difference between the measured data and the fitted curve, as a fraction of the curve itself, was less than 0.5
2. $0.0 < K^{trans} < 5.0$ and
3. $0.0 < v_e < 1.0$.

Those pixels that both failed criterion (1) and did not enhance were assigned values of 0 for K^{trans}, k_{ep} and v_e.

In addition to these quantitative parameters, the maximum gradient, G of the signal intensity time curve and the enhancement E were calculated:

$$E = \left[\frac{S_t - S_0}{S_0}\right]_{max} \quad (14), \qquad \text{and } G = \left[\frac{d((S_t - S_0)/S_0)}{dt}\right]_{max} \quad (15)$$

where S_t is the signal intensity at time t, S_0 is the baseline signal intensity and t is time. The initial AUC was calculated as the area under the Gd-DTPA concentration time data for the first 90 seconds after bolus arrival, t_0.

4.6 Comparison of DCE-MRI with a radiotracer method in rat tumours

As discussed above, the MRI protocol has some limitations due to the characteristics of Gd-DTPA, and the lack of a directly measured arterial input function. The validity of this technique in measuring tumour blood flow was therefore tested in rat tumours by comparison with radiolabelled iodoantipyrine (IAP) an established method for obtaining reliable and fully quantitative blood flow measurements (Tozer & Morris, 1990; Tozer & Shaffi, 1993). This work was carried out by Dr Ross Maxwell, Ian Wilson, Vivien Prise and Dr Gill Tozer, but is briefly described here because of its relevance to the interpretation of the clinical studies.

4.6.1 Tumour Model

P22 carcinosarcoma tumours were grown subcutaneously in the flank of male BD9 rats. Animals were treated with saline, 10mg/kg or 100mg/kg CA4P by intraperitoneal injection and underwent MRI or IAP studies at time 0, 1 hour, 6 hours or 24 hours post treatment. Three to six animals were studied in each group.

4.6.2 MRI protocol

The MRI protocol used the same sequence as the clinical studies, but with 2mm slice thickness, and a smaller field of view. Anaesthesia was achieved using Hypnorm (fentanyl-

fluanisone) and midazolam, and one tail vein was cannulated. 0.1mmol/kg Gd-DTPA, in a volume of 1ml/kg was injected over 5 seconds after 3 initial scans. Each scan took 11.9 seconds. The total dynamic scan time was 6.5 minutes. The assumed arterial input function was one previously described for Gd-DTPA in rats (Rozijn *et al.*, 1998). A T1 measurement was obtained prior to the dynamic sequence to allow calculation of the tissue Gd-DTPA concentration in the dynamic series.

4.6.3 IAP methods

Full details of these methods have been published (Tozer & Shaffi, 1993). ^{125}I labelled IAP was used (Institute of Cancer Research, Sutton). Animals were anaesthetised as above and two tail veins and one tail artery were cannulated. At the appropriate measurement time, 0.3MBq of ^{125}I-IAP was infused into a tail vein for 30 s at a rate of 1.6 ml/min. During this period, arterial free flowing blood was collected at 1 s intervals into pre-weighed vials. The rat was then killed by i.v. injection of Euthatal and the tumour and normal tissues were excised. Blood and tissue samples containing ^{125}I-IAP were counted using a well counter. Blood flow was calculated using equation 1, from the tissue counts, the partition coefficient for IAP in the tissue and the arterial input function derived from the arterial blood counts.

4.6.4 Analysis

The mean value for blood flow for each group of rats was plotted against the mean value for K^{trans}, gradient and AUC for each corresponding group of rats undergoing the MR protocol. Linear regression was performed to derive the correlation coefficient, and intercept and slope estimates of the IAP versus DCE-MRI data.

4.6.5 Results

The time course of blood flow reduction is shown in Figure 4.2 for each method. At 6 hours after 100mg/kg CA4P blood flow measured by IAP was reduced to 1% and K^{trans} to 7% of controls. 6 hours after 10mg/kg blood flow was reduced to 14% and K^{trans} to 16% of controls, but by 24hrs recovered to 91%, and 99% respectively. Figure 4.3 illustrates the correlation between K^{trans} measurements using DCE-MRI and absolute blood flow measurements with ^{125}I-IAP. The correlation coefficient R was 0.99 ($p<0.0001$) on this relatively small number of data points. A fuller range of blood flow and DCE-MRI blood flow parameters would be required to fully test this correlation

When the gradient from the signal intensity time curve was used as a measure of flow, the correlation with IAP measurements remained good ($R=0.97$ $p=0.002$), Figure 4.3. However,

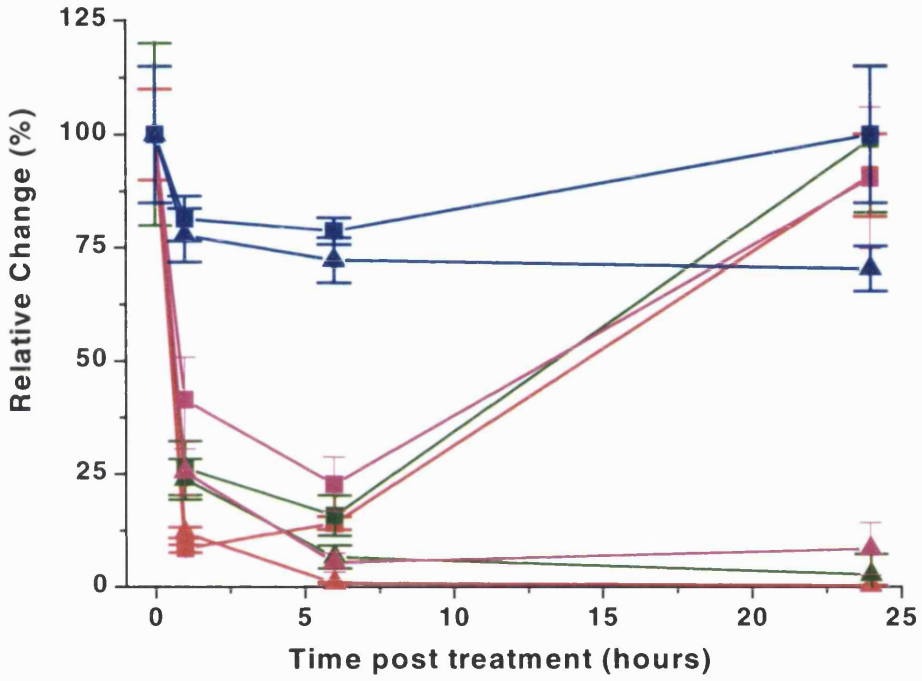

Figure 4.2 Time course of relative change in IAP measured blood flow in P22 carcinosarcomas in BD9 rats after 10 mg/kg (■) or 100mg/kg (▲), and relative change in K^{trans} (■ 10mg/kg, ▲ 100mg/kg) and gradient (■ 10mg/kg, ▲ 100mg/kg) and AUC (■ 10 mg/kg, ▲ 100 mg/kg)

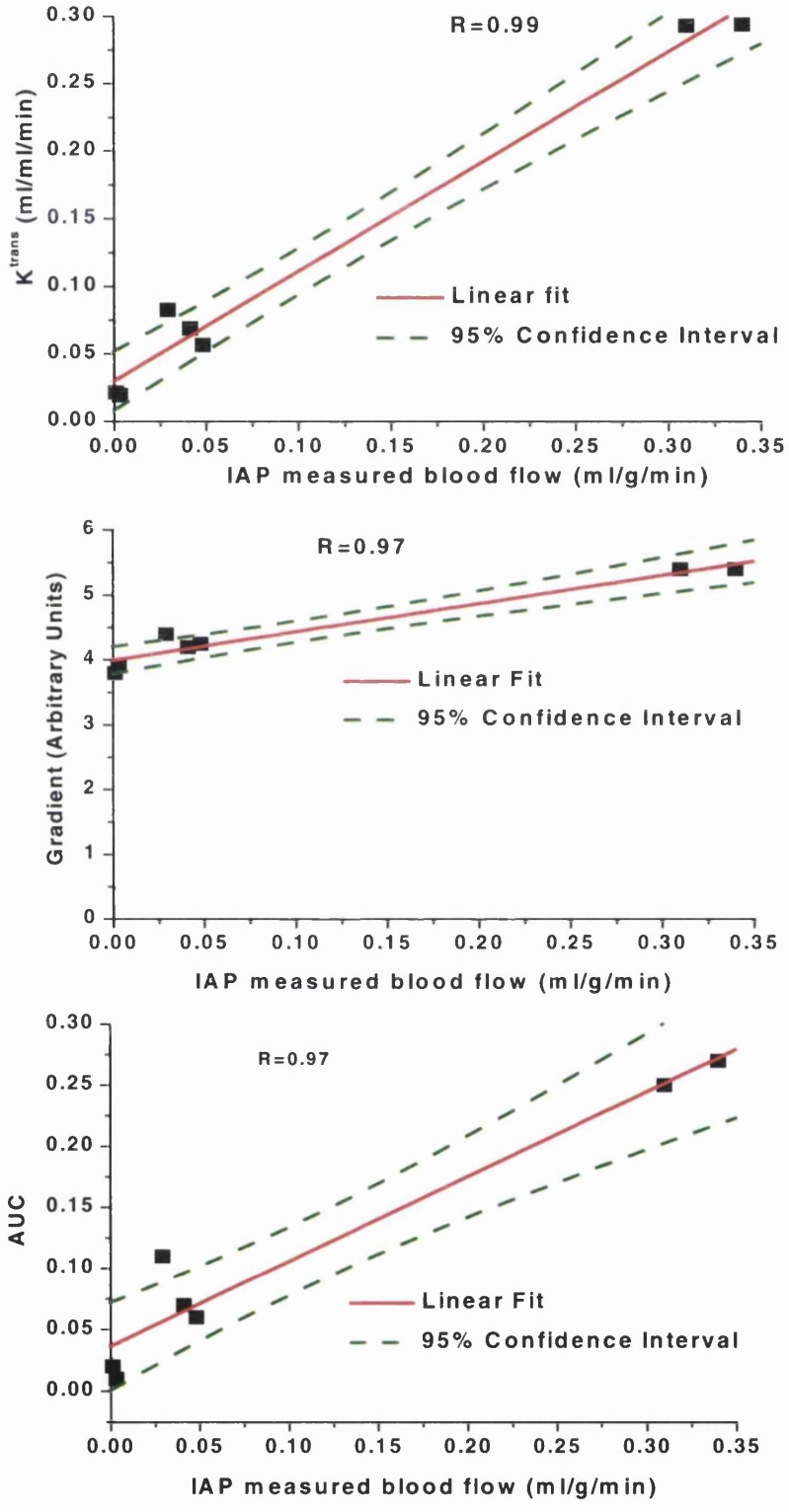

Figure 4.3 Top - Linear regression plot of mean K^{trans} values versus mean blood flow values measured by IAP for groups of P22 carcinosarcomas in BD9 rats treated with 0, 10 or 100 mg/kg CA4P at 1, 6 and 24 hours post treatment. Middle – Linear regression plot of mean gradient values versus mean blood flow measured by IAP for the same groups of rats Bottom – Linear regression plot of mean AUC values versus mean blood flow measured by IAP for the same group of rats

the maximum reduction in gradient was only 30% after 100mg/kg at 6 and 24 hours, Figure 4.2. This difference in the magnitude of the measured treatment effect is reflected in the value of the intercept for the linear fit, which was 4.00 +/- 0.08 for gradient, and 0.03 +/- 0.01 for K^{trans}. AUC was also well correlated with IAP measurements ($R=0.97$, $p<0.001$). The reduction in AUC was 95% 6 hours after 100 mg/kg and 77% 6 hour after 10 mg/kg (Figure 4.2). The intercept for the linear fit for AUC versus IAP blood flow measurement was 0.04 +/-0.01.

4.6.6 Discussion

These results show that K^{trans} changes accurately reflect true changes in tumour blood flow in this animal model after treatment with CA4P, thus justifying its use in human experiments with this agent. However, similar comparisons across a range of tissues and different tumour types would not necessarily confirm that K^{trans} accurately reflects differences in blood flow in general. As discussed above, blood flow, vessel permeability and surface area all contribute to K^{trans} values and the relative contribution of each of these will vary in different tissues. There is evidence that tumour blood vessel permeability increases early after CA4P treatment in an isolated tumour model, using radiolabelled albumin and correcting for blood flow changes with ^{86}RbCl (Kanthou *et al*, 2001). At the same time both blood flow and vessel surface area decrease. The above data demonstrate that in this tumour model these latter two effects predominate, and the resultant K^{trans} values reflect blood flow changes.

Whilst gradient values also correlated well with IAP blood flow changes, these changes were less reliable at low flow values. This may be due to a better signal to noise ratio for K^{trans} than for gradient at low flow levels. As the gradient is calculated as the maximum gradient seen over the whole dynamic series, random noise will still produce values of gradient greater than zero even when there is no blood flow at all. This is demonstrated in the large positive value for the intercept of gradient versus IAP linear fit. The calculation of K^{trans} however employs a fitting routine where all 30 time points are considered. As a result, the value for the intercept of K^{trans} versus IAP linear fit is close to zero. The parameter AUC also underestimated the size of CA4P effect on blood flow, but much less than gradient. This suggests that whilst the semi-quantitative gradient method can be used as a relative measure of blood flow, with a treatment producing a blood flow reduction, the gradient change is likely to underestimate the true size of the treatment effect. AUC provides a better estimate of treatment effect than gradient, but K^{trans} gives the most accurate estimate of actual blood flow reduction of these parameters.

CHAPTER 5 -REPRODUCIBILITY OF CLINICAL MRI METHODOLOGY

5.1 Introduction

To date there has been very little published on the reproducibility of DCE-MRI between scanning sessions on different days (Li *et al.*, 2000b). This is clearly an important aspect particularly when assessing the size of effects seen following treatment. This chapter describes the reproducibility of this technique in 21 patients who had 2 scans within a week with no intervention in between. Semi-quantitative parameters, gradient, AUC (area under the signal intensity time curve for the first 90 s) and enhancement were compared with the quantitative parameters K^{trans}, k_{ep} and v_e. In addition, the results obtained by calculating these parameters on a whole ROI or individual pixel analysis were compared in tumour.

5.2 Methods

Patients participating in the Cancer Research Campaign Phase I trials of DMXAA and Combretastatin A4 Phosphate (CA4P) had serial DCE-MRI scans, including 2 pre-treatment scans performed within 1 week of each other. All patients participating in this study gave written informed consent and the local ethics committee approved the trial protocols. The MRI methodology was as described in Chapter 4.

5.2.1 Statistical analysis

For each patient, the difference between the measurements of a parameter at each scan, d was calculated. The distribution of d was tested for normality using the Shapiro-Wilk test. To establish if the size of d was dependent on the parameter value, Kendall's tau for correlation of the absolute value of d against the mean value for the 2 scans of each parameter was calculated. Values of p obtained from the above statistical tests were adjusted for multiple comparisons using Bonferroni's method (Bland & Altman, 1995). If Kendall's tau indicated a significant correlation of the absolute value with the mean then the data were logarithmically transformed (base 10). The Shapiro-Wilk test and Kendall's tau were recalculated on the transformed data to retest for normality, and dependence of the difference on the mean. Wilcoxon's signed ranks test was used to compare distributions of ordinal data between the paired examinations. The following statistical measures of reproducibility were then obtained

from a one way analysis of variance (ANOVA) on the original ordinal data or transformed data as appropriate:

1. The mean squared difference dSD was calculated from:

$$dSD = \sqrt{\frac{\sum d^2}{n}}$$

This can be used to calculate the 95% confidence interval for change which might occur in a group of n patients from:

$$\text{CI} = \pm\frac{1.96 \times dSD}{\sqrt{n}}$$

Any change in a group of n greater than this value would be significant at the 5% level. For transformed data this confidence interval can be expressed as a percentage of the mean by:

$$\%CI = \frac{100 \times anti\log(\log_{10} mean \pm CI)}{mean}$$

This will produce a confidence interval that is not symmetric about the mean

2. the within patient standard deviation (wSD) was obtained by taking the square root of the within patient mean square value in the ANOVA table. This can also be derived from the dSD as

$$wSD = \frac{dSD}{\sqrt{2}}$$

3. the within patient coefficient of variation (wCV) was derived by dividing the wSD by the overall mean for each parameter. For transformed data the wCV was obtained by:

$$\text{wCV=antilog (wSD)-1}$$

When this value is large (>0.5) then the estimation of wCV is unreliable (Bland & Altman, 1996b).

4. the repeatability of a parameter, r, was calculated as 2.77 multiplied by wSD (Bland & Altman, 1996a). The difference between 2 measurements for the same subject will be less than this figure for 95% of pairs of observations. This can be expressed as both an absolute value on the original scale, appropriate for parameters where there is no correlation of d with individual means and on the log scale for parameters with such a correlation. For transformed data it can be expressed as a percentage of the mean by:

$$\%r = \frac{100 \times anti\log(\log_{10} mean \pm r)}{mean}$$

This will again give an asymmetric 95% confidence interval around the mean

5. The ratio of the between patient variance to the within patient variance was derived for each parameter and each method of analysis, and tested for a significant difference in these variances. A parameter with a large variance in the patient population tested, but a small variance within individual patients would have a high value of this ratio.

Statistical analysis was performed using JMP statistics software package (SAS Institute Inc. U.S.A.).

5.3 Results

The patient characteristics, tumour type and size are given in Table 5.1. The range of tumour types was typical for patients in Phase I trials. Twenty-one patients had 2 pre-treatment examinations within a week. Slice repositioning between the 2 examinations was inadequate for 1 patient. Three patients had unreliable injections of contrast agent on one of the 2 examinations due to fracturing of glass syringe containing Gd-DTPA during injection (1 patient) or leakage of Gd-DTPA from injection site (2 patients). One further patient was excluded because of a large number of pixels in the tumour ROI were classed as modelling failures (20%). The shape of the Gd-DTPA concentration time curve for these pixels suggested a significant vascular contribution. The estimation of parameters was therefore inaccurate, as the model used assumes no contribution of intravascular contrast. Thus, 16 patients formed the study cohort.

Figure 5.1 illustrates the mean values of tumour and muscle parameters from the 2 examinations for the individual patients, calculated using pixel analysis in tumour and ROI

Age	Sex	Tumour type	Tumour site	Tumour size (cm)
55	M	Renal cell carcinoma	Liver	14 x 12
61	M	Renal cell carcinoma	Kidney	12 x 10
44	F	Renal cell carcinoma	Renal bed	5 x 5
60	F	Renal cell carcinoma	Kidney	13 x 13
42	M	Renal cell carcinoma	Para-aortic lymph node	4.5 x 3
70	F	Ovarian serous cystadenocarcinoma	Para-aortic node	6 x 9
57	F	Ovarian serous cystadenocarcinoma	Inguinal lymph node	6 x 5.5
50	F	Ovarian serous cystadenocarcinoma	Pelvis	13 x 11
41	F	Peritoneal carcinoma	Pelvis	6 x 6
58	F	Peritoneal carcinoma	Pelvis	3 x 2
56	F	Leiomyosarcoma	Adrenal	8 x 8.5
59	F	Leiomyosarcoma	Para-aortic lymph node	8 x 7
68	M	Leiomyosarcoma	Abdomen	21 x 18
63	F	Leiomyosarcoma	Pelvis	17 x 9
48	M	Leiomyosarcoma	Chest	18 x 16
69	F	Leiomyosarcoma	Pelvis	17 x 14
62	F	Leiomyosarcoma	Chest	17 x 19
54	F	Neuroendocrine thymic carcinoma	Anterior chest wall	11 x 6
48	F	Adrenocortical carcinoma	Liver	5 x 3.5
56	F	Colonic adenocarcinoma	Liver	8 x 5
46	F	Breast adenocarcinoma	Pelvis	9 x 7

Table 5.1 Patient characteristics- reproducibility cohort

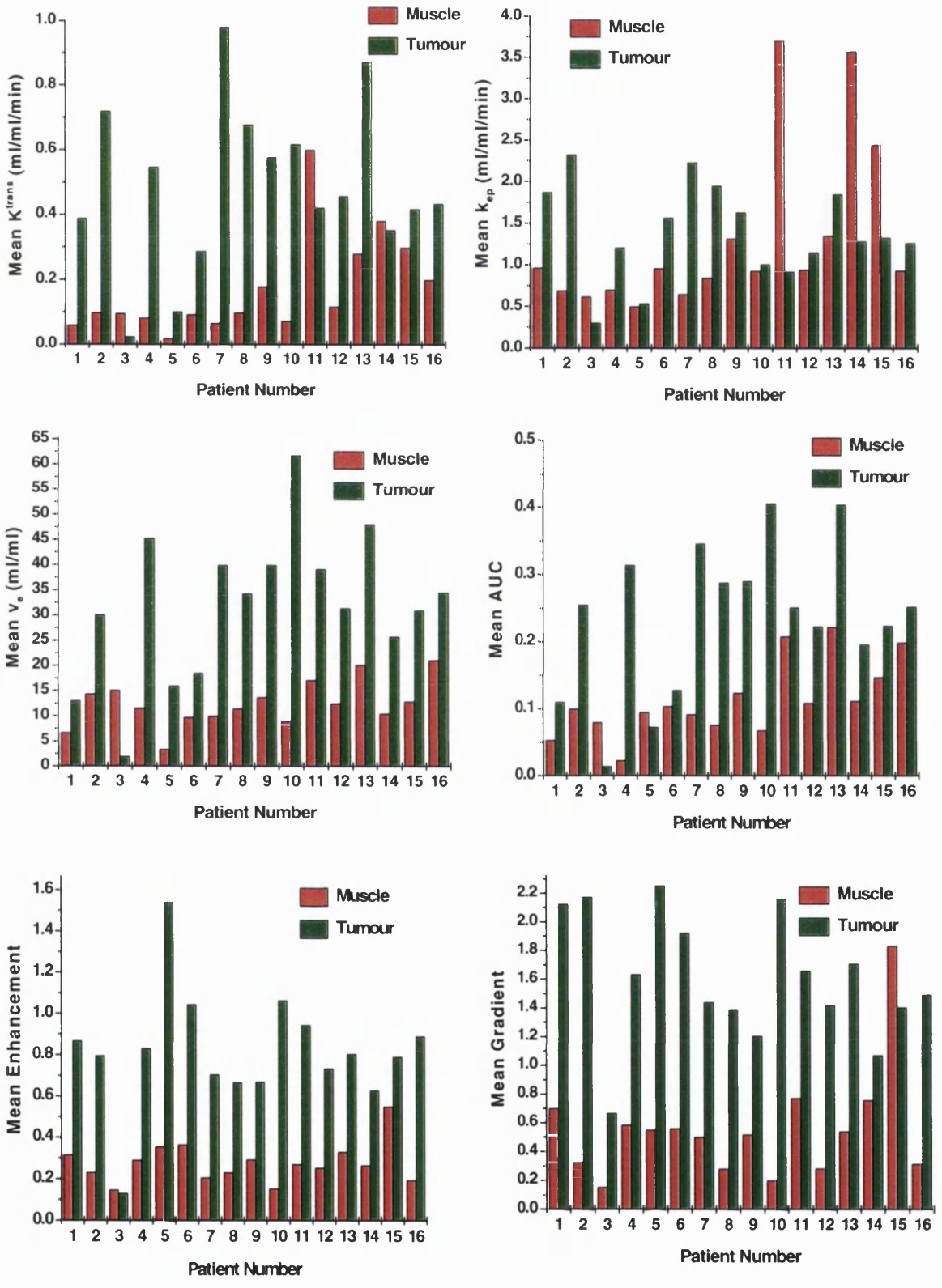

Figure 5.1 Mean DCE-MRI parameter values for tumour and muscle for each patient

analysis in muscle. The mean value of tumour K^{trans} for all patients calculated from the Gd-DTPA time curve was 0.50 ml/ml/min (range, 0.02 to 0.98). This is comparable with literature values for human tumours (Hunter *et al.*, 1998; Padhani *et al.*, 2000). The mean tumour k_{ep} was 1.40 ml/ml/min (range, 0.54 to 2.33). The mean v_e was 31.9 ml/ml expressed as % (range, 1.9 to 61.8%). These values are also in the published range for human tumours.

In Figure 5.2 the absolute value of the difference between the scans (d) is plotted against the mean value for the 2 scans for each parameter using the pixel analysis in tumour for each patient. The mean difference and the 95% confidence intervals for the mean difference are also shown, which ranged from +/- 8% for v_e to 17% for gradient. No parameter had a mean difference significantly different from zero. The distribution of d for each parameter was not significantly different from normal, and only K^{trans} had a significant dependence of d on the mean value (Kendall's tau, p=0.004). After logarithmic transformation of K^{trans} values, there was no longer a significant dependence of d on the mean and Kendall's tau was not significant (p=0.59). The repeatability limits are also shown. The mean value for each parameter, the wSD, wCV and ratio of between patient variance to within patient variance calculated in tumours by pixel analysis are listed in Table 5.2a, and the same results for the tumour ROI analysis are given in Table 5.2b. All parameters had significantly smaller within patient variance than between patient variance, and the value of this ratio, together with the wCV, enables comparison of the reproducibility of each parameter. V_e was the most reproducible parameter, and had the highest variance ratios, indicating relatively small variability within individual patients compared with the large variability in these parameters across the 16 patients in the cohort. When calculated either on a pixel by pixel or whole ROI basis, the wCVs were 9% and 8% for enhancement and v_e in tumours. For K^{trans}, k_{ep} and gradient the results are more variable, with wCVs of 23% to 24%. AUC has intermediate reproducibility, with a wCV of 16%. As there is no significant correlation of d with the initial parameter value except for K^{trans}, the percentage variation will be less for tumours with higher initial parameter values and more for those with a low value. In these cases the statistical terms expressed as absolute values are more useful determinants of measurement variability, such as wSD or repeatability (Bland & Altman, 1996b). In an individual patient changes greater than the repeatability value would be significant. For example, a change in v_e greater than 6.9 ml/ml in an individual tumour would be statistically significant (Figure 5.2a). For K^{trans} the repeatability 0.24 on the logarithmic scale can be expressed as a percentage of the mean (-44% to +79%). Any reduction in an individual greater than 44% or increase greater than 79% would be statistically significant.

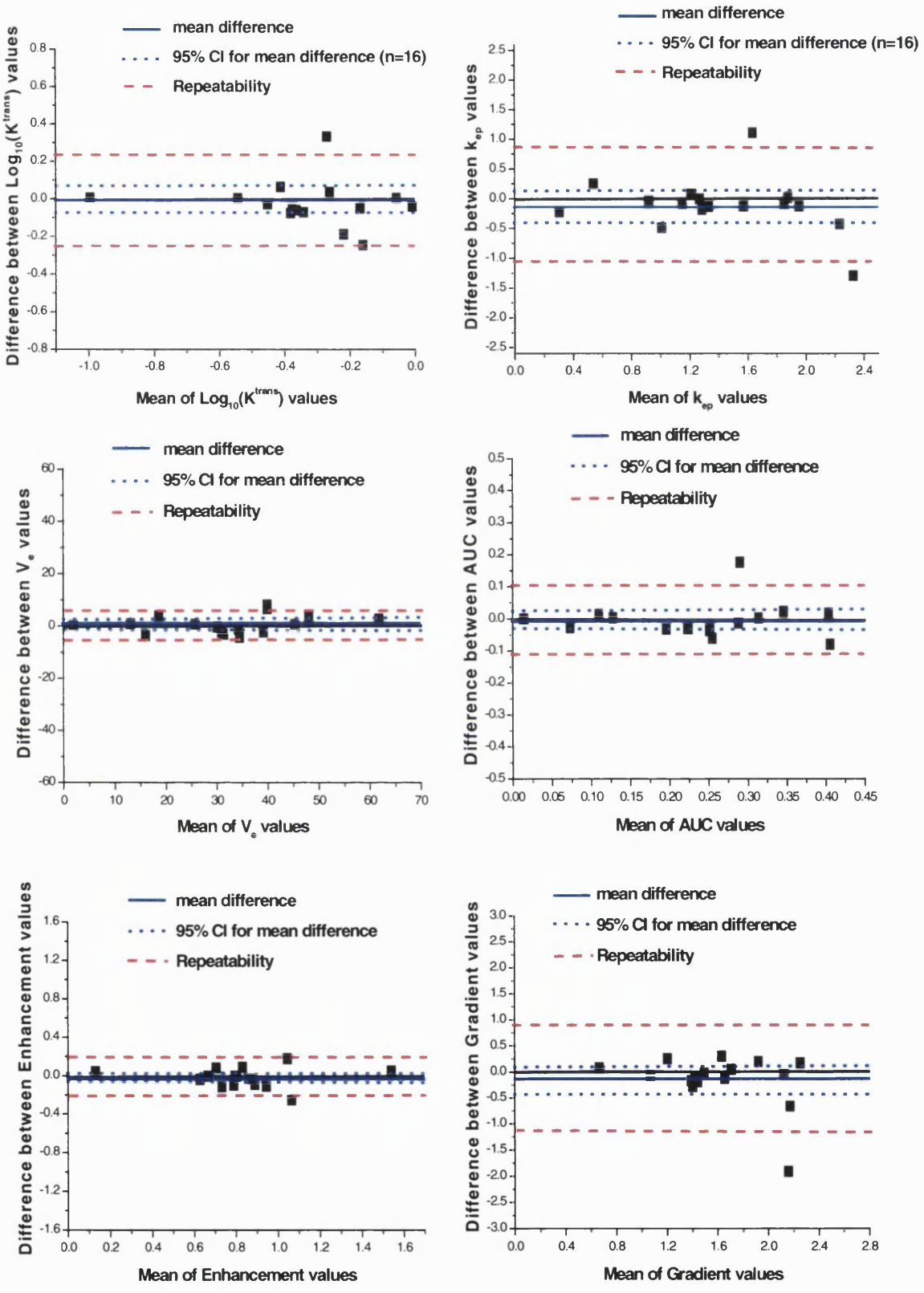

Figure 5. 2 Difference between parameters plotted against mean of parameters for tumour in each patient (pixel analysis). Log_{10} transformed data is shown for K^{trans}. To enable comparison across parameters, the y axis scale was determined as +/- twice the overall mean parameter value (Table 5.2a). The mean difference between scans is shown with the 95% confidence interval (CI). The repeatability (2.77 x wSD (within patient standard deviation)) is also shown and represents the level of change that would be significant in an individual.

Parameter	Mean	Mean difference	95% CI for mean difference	wSD	wCV	Repeatability	Variance ratio
K^{trans}	0.50	-0.04	-0.07 to +0.08^{+} (-14% to +16%)	0.09^{+}	24%	0.24^{+} (-44% to +79%)	40*
K_{ep}	1.40	-0.11	+/- 0.23 (16%)	0.33	24%	0.92	6*
V_e	31.9	0.62	+/- 1.7 (5%)	2.50	8%	6.9	69*
AUC	0.24	-0.006	+/- 0.03 (11%)	0.04	16%	0.10	18*
Gradient	1.63	-0.16	+/- 0.26 (16%)	0.38	23%	1.04	2.8*
Enhancement	0.82	-0.009	+/- 0.05 (6%)	0.07	9%	0.20	33*

Table 5.2a Calculated DCE-MRI kinetic parameters and their reproducibility for tumour: pixel analysis. CI = confidence interval, wSD = within patient Standard Deviation, wCV= within patient Coefficient of Variation (wSD / mean), Repeatability = 2.77 x wSD and is the value of the 95% tolerance limit for the difference between 2 measurements on an individual, Variance ratio = ratio of between patient variance to within patient variance, $^{+}$= $\log_{10}$ transformed data, * = $p<0.05$

Parameter	Mean	Mean difference	95% CI for mean difference	wSD	wCV	Repeatability	Variance ratio
K^{trans}	0.42	-0.03	- 0.07 to 0.08^{+} (-16% to +19%)	0.11^{+}	29%	0.32^{+} (-50% to +100%)	31*
K_{ep}	1.39	-0.16	+/- 0.23 (16%)	0.33	24%	0.91	5*
V_e	30.1	-0.02	+/- 1.91 (6%)	2.75	9%	7.62	53*
AUC	0.30	-0.004	+/- 0.03 (10%)	0.04	14%	0.12	22*
Gradient	1.25	-0.02	+/- 0.21 (17%)	0.31	25%	0.85	3.5*
Enhancement	0.71	-0.01	+/- 0.04 (6%)	0.06	9%	0.17	47*

Table 5.2b Calculated DCE-MRI kinetic parameters and their reproducibility for tumour: whole ROI analysis CI = confidence interval, wSD = within patient Standard Deviation, wCV= within patient Coefficient of Variation (wSD / mean), Repeatability = 2.77 x wSD and is the value of the 95% tolerance limit for the difference between 2 measurements on an individual, Variance ratio = ratio of between patient variance to within patient variance, $^{+}$ = $\log_{10}$ transformed data, * = $p<0.05$

The results were similar for pixel and for whole ROI analysis. Figure 5.3 shows parametric maps for K^{trans}, k_{ep} and v_e overlaid on an anatomical MRI image of the same resolution in a patient with a large pelvic leiomyosarcoma. Visual assessment of the paired images in Figure 5.3 reveals a close spatial reproduction of parameter values, despite the marked intratumour heterogeneity.

Table 5.3 shows the reproducibility analysis for muscle ROIs. The mean values of all parameters are lower for muscle than for tumours, although 3 patients had a higher K^{trans} value in muscle than in tumour. For all parameters, the wCVs were higher for muscle than for tumour, although the wSDs were lower. In this tissue, the semi-quantitative parameters had lower wCVs than the fully quantitative parameters. The estimate of wCV for muscle Ktrans was unreliable. Again, enhancement was the most reproducible of the semi-quantitative parameters, and v_e was the most reproducible of the quantitative parameters.

5.4 Discussion

There are several statistical terms that can be used to quantitate measurement reproducibility, and to determine measurement error for individuals or groups. A desirable parameter is one which is sensitive to wide variations in the characteristic to be studied where such variability exists in a population (large between patient variance), but has a small variation in results obtained on different occasions in the same individual (small within patient variance). It will therefore have a large variance ratio. As shown in Figure 5.1, the population of patients in this study did have a wide variation in initial DCE-MRI parameter values. The variance ratio is therefore useful for comparing reproducibility of different parameters. In this study v_e and enhancement had the highest variance ratios in tumour, and K^{trans} had the highest variance ratio in muscle. Gradient had the lowest variance ratio in both tissues. Other statistical terms are useful for describing the magnitude of spontaneous changes in a parameter. In this study v_e and enhancement had the highest variance ratios in tumour and muscle. Gradient had the lowest variance ratio in both tissues. Other statistical terms are useful for describing the magnitude of spontaneous changes in a parameter. The 95% confidence interval for the mean difference in Tables 5.2 and 5.3 gives a measure of the spontaneous change to be expected in groups of a similar size to this cohort. The formula in the statistical methods section allows calculation of such an interval for groups of different sizes. In individuals, the repeatability derived from the wSD represents the 95% confidence limit of the spontaneous change that might occur. If the absolute difference between examinations is greater for patients with larger parameter values, as for K^{trans} (determined by a significant value for

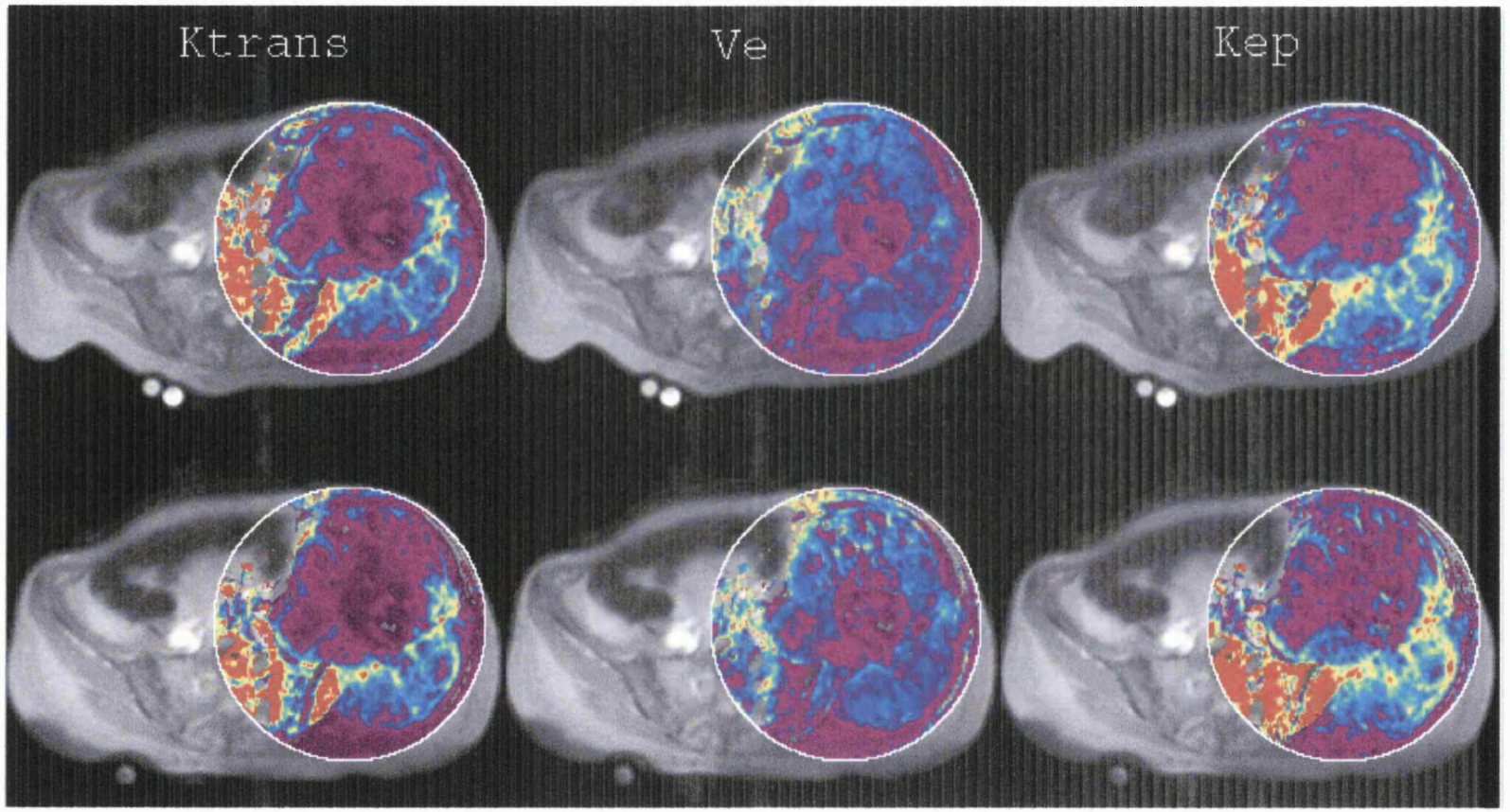

Figure 5.3 Paired pre-treatment MR images with parametric maps from patient 15. These axial images through the pelvic area demonstrate a large leiomyosarcoma metastatic to the left iliac bone. A circular ROI is shown within which parameter maps are displayed. The colour scale is displayed on the right in ml/ml/min. These images demonstrate excellent spatial reproducibility within the tumour and surrounding normal tissues

Parameter	Mean	Mean difference	95% CI for mean difference	wSD	wCV	Repeatability	Variance ratio
K^{trans}	0.15	0.07	-0.04 to 0.06^{+} (-30% to +44%)	0.04^{+}	NA	0.12^{+} (-75% to +308%)	5.7*
K_{ep}	1.05	0.57	+/- 0.81 (61%)	0.46	49%	1.28	5.6*
V_e	12.7	-0.33	+/- 1.67 (13%)	2.1	16%	5.71	10.6*
AUC	0.11	-0.009	+/- 0.02 (18%)	0.03	26%	0.08	7.2*
Gradient	0.44	0.02	+/- 0.09 (20%)	0.13	28%	0.35	4.2*
Enhancement	0.26	0.02	+/- 0.02 (8%)	0.03	12%	0.08	8.8*

Table 5.3 Calculated DCE-MRI kinetic parameters and their reproducibility for muscle: whole ROI analysis. CI = confidence interval, wSD = within patient Standard Deviation, wCV= within patient Coefficient of Variation, Repeatability = 2.77 x wSD and is the value of the 95% limit for the difference between 2 measurements on an individual, Variance ratio = ratio of between patient variance to within patient variance. . $^{+}$= $\log_{10}$ transformed data, * = $p<0.05$, NA - estimate of wCV from transformed data was unreliable

Kendall's tau), then the repeatability is calculated on the logarithmic scale, or can be expressed as a percentage of the overall mean to give 95% limits for the relative change in an individual. For example, the parameter K^{trans} needs to decrease by more than 44% or increase more than 79% to be confident that this is due to treatment effect rather than spontaneous change or measurement error (Table 5.2a). Alternatively, K^{trans} could be used in a group of 16 patients to detect mean reductions greater than 14% or increases greater than 16% and in practice, changes of smaller magnitude than this are unlikely to be of clinical significance. The leakage space v_e, or the volume of the extracellular extravascular space into which Gd-DTPA diffuses, is a much more reproducible parameter, and can be used in individuals to detect changes greater than 6.9 ml/ml.

The semi-quantitative parameters, enhancement and initial AUC are reasonably reproducible, and can be used in individual patients to detect changes above 0.2 (24%) and 0.1 (42%) respectively, or mean changes greater than 6% and 11% respectively in a group of this size. The gradient, like K^{trans} is a more variable parameter, but in a group can be used to detect changes of more than 17%. The greater variability of gradient and K^{trans} may be because they are more sensitive to changes in the arterial input function, which will have day to day variation, and be affected by changes in cardiac output. Thus, using a complex pharmacokinetic model to produce fully quantitative parameters does not significantly alter the reproducibility of the technique. Where measurement of relative changes in an individual or group of patients is required, the simpler semi-quantitative techniques are as reproducible. Nevertheless, the parameters from the pharmacokinetic model are more easily related to the physiological events in the tumour, and allow comparisons between reports from different institutions, and as shown in Chapter 4, gradient measurements more severely underestimate the true size of treatment effects after CA4P than K^{trans}. This is reflected in the variance ratios for these parameters. Although the wCVs are similar (23% and 24%), the variance ratio is greater for K^{trans} than for gradient (40 versus 2.8), indicating a larger spread of K^{trans} values in this cohort of patients. AUC gave a better estimate of treatment effect than gradient, although not as accurate as K^{trans}, but has better reproducibility than either K^{trans} or gradient so may be the best semi-quantitative parameter to use.

Analysing these parameters for each pixel rather than over the whole ROI does not affect the reproducibility. However, tumours are characteristically heterogeneous and averaging the MRI kinetic parameters over the whole tumour removes valuable information about this heterogeneity. Pixel analysis enables tumour heterogeneity to be displayed as a parameter

image, thus retaining the information about tumour heterogeneity without loss of reproducibility. These results also demonstrate that the reproducibility is slightly worse for muscle than for tumours. The lower mean values of parameters in muscle explains this to some degree. Changes in individuals greater than 75% and 79% for K^{trans} and gradient, 27% and 32% for v_e and enhancement would be significant. This tissue therefore provides a useful comparison with tumour for treatment effects, but there would need to be larger changes in MRI parameters in muscle before a significant change is observed.

Standardisation of the Gd-DTPA injection by using a MR-compatible power injector and calculation of individual arterial input functions would be expected to significantly improve the reproducibility of these parameters in both tumour and muscle. Some variability will remain, due to actual changes in tissue blood flow, variations in magnet fields, temperature and positioning of the patient. The fact that 4 patients' data were rejected due to problems with injection or slice positioning illustrates the learning curve associated with using dynamic MRI techniques.

Weber *et al* published a similar assessment of reproducibility of metabolic measurements using FDG-PET (Weber *et al.*, 1999). In their paper, the 95% limits of agreement for an individual represented around 20% change in the parameters studied in tumours, which were mainly in the thorax. In the thorax, compared with regions such as the brain, the low background activity allows more accurate definition of tumour ROIs and therefore more reproducible results. The reproducibility of v_e and enhancement is similar to the PET parameters, whilst the K^{trans} and gradient are more variable. Studies assessing the variability of tumour volume determinations by CT have shown a mean coefficient of variation (CV) of 11% in repeat measurements of the volume of liver metastases (Van Hoe *et al.*, 1997), and CVs between 16.5% and 113% for laryngeal tumours (Hermans *et al.*, 1998). In brain tumours imaged by CT a change in volume of more than 20% was needed to be statistically significant (Mahaley *et al.*, 1990). These studies demonstrate that the reproducibility of DCE-MRI parameters compares reasonably with that of simple volume measurements.

In conclusion, these results show that the DCE-MRI parameters v_e and enhancement have good reproducibility within individuals, and could be used to measure changes following treatment intervention. The parameters K^{trans}, k_{ep} and gradient are more variable but nevertheless can detect changes in tumours in a group of patients of more than −14% to +16%, ±16% and ±16% respectively.

CHAPTER 6 - EFFECT OF CA4P TREATMENT ON HUMAN TUMOUR MICROVASCULAR FUNCTION MEASURED BY DCE-MRI

6.1 Introduction

This chapter and the next describe the results of DCE-MRI scans performed on patients participating in the Phase I trial of CA4P. The traditional Phase I trial is designed to obtain the maximum tolerated dose of a drug, toxicities associated with treatment and the pharmacokinetic parameters that describe the drug's rate of distribution in and elimination from the body. Clinical tumour response rates are not primary endpoints until Phase II, when a drug is used in a specific tumour type. If responses are seen in Phase I however, this information may be used to guide tumour type selection in Phase II studies. Although this model has worked well in the early development of classical cytotoxic drugs, it may not be appropriate for the evaluation of newer drugs, such as anti-angiogenics, vascular targeting agents and biological therapies, which are unlikely to produce responses when used alone. They are also expected to have a specific mechanism of action, so assessment at an early stage in development of whether the expected mechanisms are produced at tolerable doses is vital if active drugs are not to be discarded due to low response rates when used alone. In addition, the maximum tolerated dose is not necessarily the optimum dose to take forward into Phase II if biological efficacy can be demonstrated at lower, less toxic doses. These drugs are expected to have wider therapeutic windows than traditional cytotoxics, so this is an important issue.

The Cancer Research Campaign Phase I trial was therefore designed to incorporate assessment of tumour and normal tissue blood flow changes in addition to the usual endpoints, using PET scanning at the Hammersmith Hospital site, and DCE-MRI at Mount Vernon Hospital.

6.2 Trial protocol

6.2.1 Eligibility criteria

The local ethics committee approved the protocol and all patients gave written informed consent. The eligibility criteria for trial entry are given in Table 6.1.

6.2.2 Dose escalation

The starting dose was 5 mg/m^2, which was one third of the lowest toxic dose in dogs in the pre-clinical toxicology studies performed by Ilex Oncology Inc. The dose escalation schedule

- Histologically confirmed cancer, not amenable to standard curative therapy or refractory to conventional therapy
- No previous irradiation to the tumour to be imaged by MRI/PET or used for assessing response
- WHO performance status 0-2
- Life expectancy ≥ 4 months
- Age ≥ 18 years
- Tumour suitable for PET or MRI examination
- Haematological and biochemical indices:
    a) White Blood Count 4.0 x 10^9/l
    b) Haemoglobin ≥ 10.0g/dl
    c) Platelets 100 x 10^9/l
    d) Bilirubin < 20 μM
    e) Alanine Transaminase and alkaline phosphatase < x2 upper limit of normal unless liver or bone metastases documented
    f) Creatinine < 130 μmol/l
- On no other anti-cancer therapy for 4 weeks
- No active concurrent malignancies except cone biopsied in situ carcinoma of cervix, or adequately treated basal or squamous carcinoma of skin
- No other serious medical condition, ischamic heart disease, open surgery or serious infection in previous 28 days
- Not pregnant / lactating. Taking contraception if of child bearing age for 4 weeks before, during and for 4 weeks after the study
- No active brain metastasis
- Patients taking heparin or warfarin are excluded. Patients on steroids or non-steroidal anti-inflammatory agents (except naproxen) are eligible.
- Patients with auto-immune disorders, inflammatory bowel disease and diabetes are excluded
- Written informed consent obtained

Table 6.1 Patient eligibility criteria for The Cancer Research Campaign CA4P Phase I trial

followed an accelerated titration design with the aim of treating fewer patients at doses below the biologically active level, needing fewer patients overall to complete the trial, whilst maintaining adequate safety precautions (Simon *et al.*, 1997). Initially intra-patient dose escalation was allowed with dose doubling until ≥ grade II toxicity was seen. Subsequent patients were treated at the same dose level, with x 1.3 dose escalation between cohorts. At least 1 patient from each cohort of 3 was required to undergo DCE-MRI scanning. Dose limiting toxicity (DLT) was defined as drug related toxicity ≥ grade II neurotoxicity, grade III or IV other non-haematological toxicity, or grade IV haematological toxicity lasting > 4 days or associated with ≥ grade II fever, infection or bleeding. If 1 patient in a cohort had a DLT, this cohort had to be expanded to 6 patients. If 2 or more patients experienced DLTs then the dose had to be reduced. The maximum tolerated dose (MTD) was defined as a dose below that at which 30% or more of the patient population (≥ 2 of 6 patients) would suffer dose limiting toxicity due to the drug. The trial allowed further expansion of cohorts below the MTD to assess blood flow effects.

6.2.3 Drug administration and dose schedule

CA4P was made up to 100mls in Normal saline, and delivered intravenously over 10 minutes via an infusion pump once a week for 3 weeks, followed by a 14 day interval (one cycle) as shown in Figure 6.1. During the intra-patient dose escalation period, patients received a maximum of 3 cycles. Once intra-patient dose escalation ceased, patients could have further cycles of treatment if they had had a significant reduction in tumour blood flow as assessed by MRI or PET imaging, stable or responding disease and ≤ grade II drug related toxicity that recovered within 2 weeks.

6.2.4 Investigations schedule

DCE-MRI examinations were performed pre-treatment and at 24 hours after the first treatment at each dose level for the initial intra-patient escalation phase (Figure 6.1). At the same time that intra-patient dose escalation was completed, the protocol was modified to allow 2 pre-treatment MRI examinations with further examinations 4-6 hours and 24 hours after the first dose of each cycle of 3 doses, and 13 days after the third dose. Blood pressure and pulse were monitored every 30 minutes for the first 4 hours. ECGs were performed pre treatment and hourly for the first 8 hours. The last 5 patients in the trial also had a 24-hour ECG tape taken on the first dose.

The DCE-MRI protocol used at each MRI examination was as described in Chapter 4.

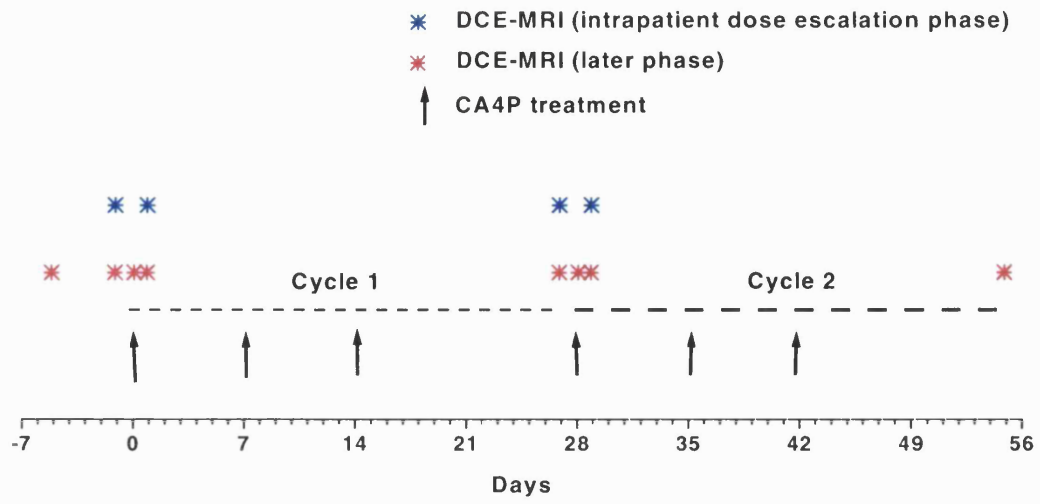

Figure 6.1 Schedule of CA4P treatment and DCE-MRI examinations.

Age	Sex	Trial Number	Tumour type	Tumour site	Tumour size (cm)
50	F	1	Ovarian serous cystadenocarcinoma	Pelvis	13 x 11
64	F	3	Ovarian serous cystadenocarcinoma	Pelvic mass	7 x7
45	M	4	Non small cell lung cancer	Axilla	5 x 4
60	F	8	Renal spindle cell carcinoma	Renal bed	13.5 x 10.5
61	M	9	Melanoma	Groin node	9 x 6.5
59	F	12	Leiomyosarcoma	Para-aortic lymph node	8 x 8
70	F	14	Ovarian serous cystadenocarcinoma	Para-aortic node	9 x 6
62	F	16	Leiomyosarcoma	Chest	19 x 17
57	F	17	Ovarian serous cystadenocarcinoma	Inguinal lymph node	6 x 5.5
45	F	19	Renal cell carcinoma	Renal bed	5 x 5
60	F	20	Renal cell carcinoma	Kidney	13 x 13
59	M	21	Renal cell carcinoma	Para-aortic node	4.5 x 3
48	F	23	Adrenocortical carcinoma	Liver	5 x 3.5
56	F	25	Colonic adenocarcinoma	Spleen	8 x 5
41	F	27	Peritoneal carcinoma	Pelvis	6.5 x 5.5
46	F	28	Breast adenocarcinoma	Pelvis	9 x 7
63	F	29	Leiomyosarcoma	Pelvis	17 x 9
48	M	30	Leiomyosarcoma	Chest	18 x 16
69	F	31	Leiomyosarcoma	Pelvis	17 x 14
58	F	32	Peritoneal carcinoma	Pelvis	3 x 2
62	M	33	Spindle cell sarcoma	Supra-renal mass	15 x 13

Table 6.2 Patient characteristics – CA4P trial, Mount Vernon patients

Where patients had 2 pre-treatment MR examinations the mean value of each parameter was taken as the pre-treatment value. The absolute difference and relative change in parameter values from this pre-treatment value was calculated for all subsequent MR examinations. The mean difference in parameter values was compared with the 95% confidence interval of change for groups established in Chapter 5, including all patients treated at or above 52mg/m2 and also for the group of patients treated at 52 and 68 mg/m2. Parameter maps for K^{trans}, k_{ep} and v_e were obtained for each ROI at each examination.

6.2.5 Pharmacokinetics, Toxicity and Response

Blood samples in 5ml EDTA coated tubes were taken pre-treatment, 1 minute prior to the end of infusion, then every 15 minutes for the first hour, every 30 minutes for the next 2 hours, and at 4, 8, 12 and 24 hours after the infusion. Samples were immediately placed on ice and protected from light. After centrifugation, plasma was pipetted off and transferred to a -70°C freezer. Concentrations of CA4P, CA4 and the principal metabolite, CA4 glucuronide, were measured by Dr M.R.L. Stratford using HPLC (Stratford & Dennis, 1999)

Any adverse event occurring whilst a patient was on trial was recorded, and graded using the NCI Common Toxicity Criteria version 2.0. The relationship of the adverse event to the drug treatment was scored as almost certainly, probably, possibly, unlikely or unrelated. All assessable sites of disease were measured pre treatment, on completion of each cycle of 3 infusions, and at the end of the study. World Health Organisation (WHO) response criteria were used to assess best response.

6.3 Results

6.3.1 Patient details

34 patients were recruited to the trial, 13 at the Hammersmith Hospital and 21 at Mount Vernon Hospital. A total of 21 patients underwent DCE-MRI examinations whilst on the trial. The first 2 patients were examined using a protocol whose spatial resolution and signal to noise ratio was too poor to be useable, and their data were rejected. The subsequent 19 patients were examined using the protocol described in Chapter 4. Table 6.2 lists the patient characteristics. Eleven of these patients form part of the reproducibility dataset described in Chapter 5. One patient (#4) had DCE-MRI examinations at 20 and 40mg/m2, and another (#9) at 52, 68 and 88 mg/m2. The remaining 17 patients had DCE-MRI examinations at one dose level only. Of these, 5 had a second cycle of 3 infusions (#12, 21, 23, 30, 32) and 1 patient (#23) had a series of 8 cycles (24 infusions).

6.3.2 *Pharmacokinetics*

CA4 area under the concentration-time curve (AUC) and peak concentration (Cmax) increased from 0.189 μmol.h/L and 0.41 μM at 5 mg/m^2 to 3.29 μmol.h/L and 4.46 μM at 114 mg/m^2 (Figure 6.2) (Stratford *et al.*, 2000). Mean CA4 AUC and Cmax in 10 patients at 68 mg/m2 were 2.07 μmol.h/L and 2.14 μM respectively, compared to 5.8 μmol.h/L and 9.8 μM in CBA mice bearing CaNT tumours at an active dose of 25 mg/kg. At this dose >40% vascular volume reduction is seen in this responsive tumour model (Dr S. Hill, personal communication).

CA4P was rapidly dephosphorylated to CA4, with a half-life of 2.5 minutes at 68 mg/m^2 (Figure 6.3). CA4 was converted to the principal metabolite, the glucuronide, with a half-life of 27 minutes.

6.3.3 *Toxicity and Response*

Table 6.3 gives the toxicities graded as ≥ grade II which were possibly, probably or almost certainly drug related. The most frequent of these was tumour site pain, seen in 11 patients over a wide range of doses, with 7 more patients having grade I pain. This had a typical temporal pattern, with onset around 30 minutes to 1 hour after treatment, lasting from a few minutes to some hours. This pattern was generally repeated after each dose a patient received. Many patients also experienced a varying degree of fatigue, typically between 1 and 4 days after treatment. One DLT (vasovagal syncope 4 hours after treatment) was seen at 88 mg/m^2 during dose escalation. Five other patients treated at this dose level had no DLTs, although 1 patient had a haemorrhage into a large leiomyosarcoma in the chest, causing increased dyspnoea. A further escalation to 114mg/m^2 was therefore performed. Transient ataxia, a DLT, was seen in 2 of 6 patients at this dose level. One of these patients elected to have a second dose the following week at 88 mg/m^2, and developed recurrent ataxia as well as transient lower limb weakness (grade III neurological toxicity), making a total of 2 DLTs in 7 patients treated at this dose. Further recruitment therefore continued at 68 and 52 mg/m^2 to enable more patients to have DCE-MRI and PET examinations. A total of 10 patients were treated at 68 mg/m^2, of whom 2 had a drug related grade II toxicity. One patient had transient hypotension 4 to 7 hours after treatment, requiring brief intravenous fluid replacement, another patient developed diarrhoea after 12 doses, but had no grade II toxicities on previous cycles. The maximum tolerated dose was therefore 68 mg/m^2. Eight patients were treated at 52 mg/m^2. One of these (#29) had been treated 17 years previously

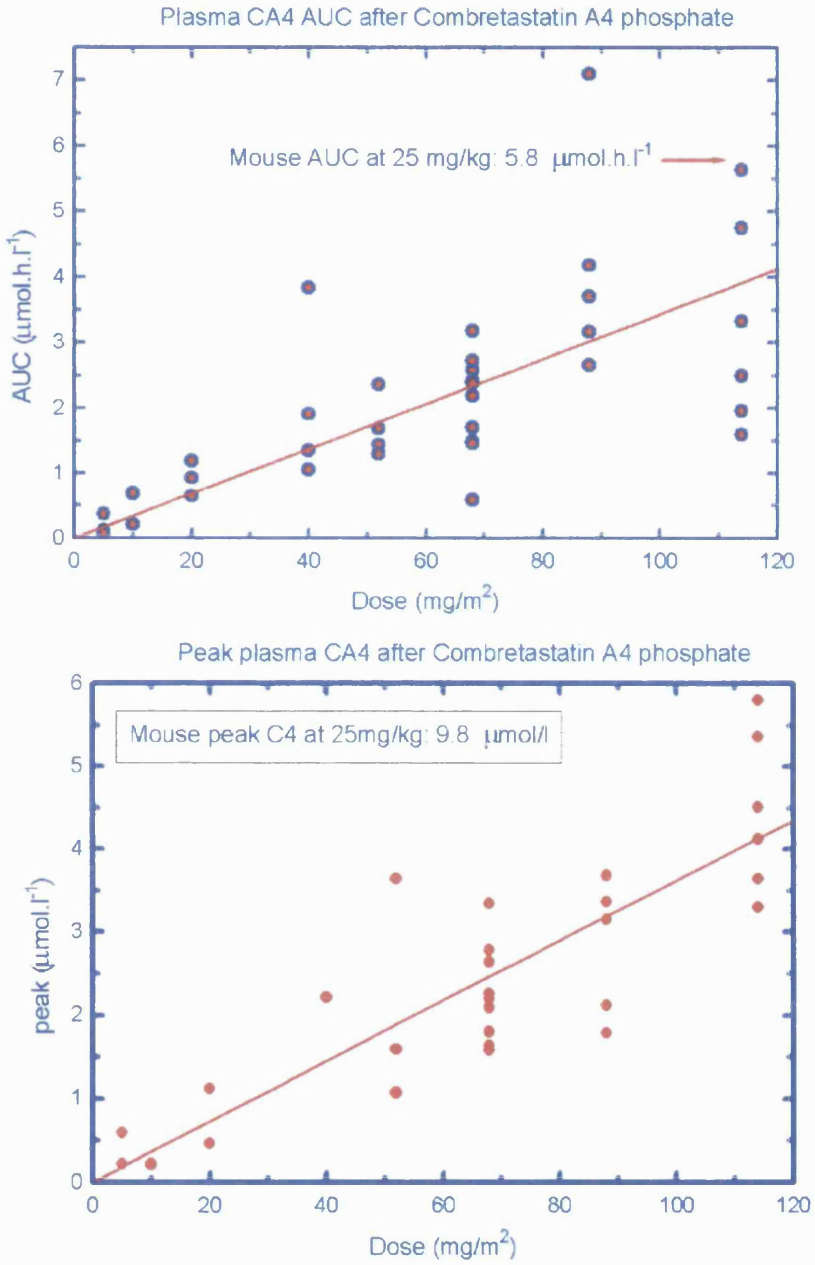

Figure 6.2 CA4 concentration AUC (top) and peak plasma concentration (Cmax) (bottom) versus dose for patients in the CRC Phase I trial of CA4P. (Data kindly supplied by Dr M.R.L. Stratford)

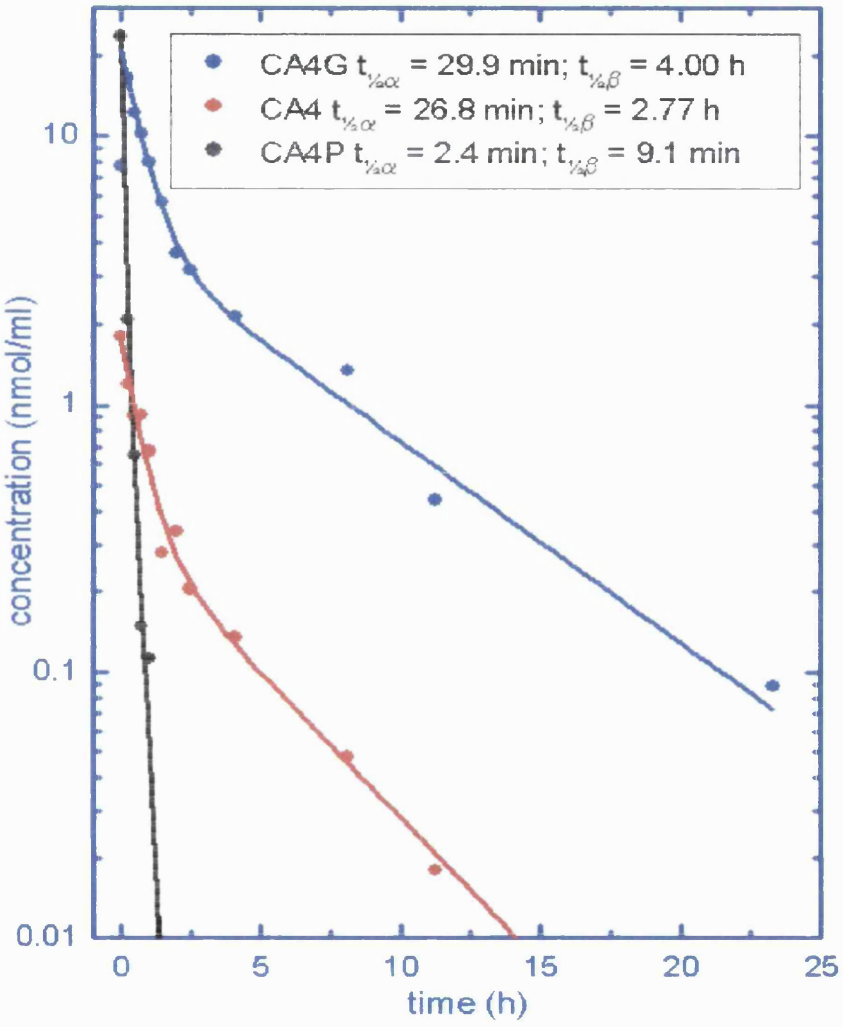

Figure 6.3 Plasma concentrations of CA4P, CA4 and CA4 glucuronide (CA4G) after 68 mg/m² CA4P infused over 10 min

Toxicity	Max. Grade (NCI CTC v.2.0)	Dose mg/m^2	No. of patients
Tumour pain	3	40-114	11
Fatigue	3	52-114	4
Abdominal pain	3	52-88	3
Vomiting	2	52-88	3
Diarrhoea	2	52-114	3
Visual	3	88-114	3
Hypertension	2	88	3
Ataxia (reversible)	4 (DLT)	114*	2
Hypotension (within 12 hrs of treatment)	2	68-88	2
Neuromotor – transient lower limb weakness	3 (DLT)	88	1
Nausea	2	114	1
Vasovagal syncope	3 (DLT)	88	1
Small bowel ischaemia	4 (DLT)	52	1
Dyspnoea	4#	88-114	2
Dehydration**	3	52	1

Table 6.3 Drug-related toxicities $\geq$ grade 2 seen after CA4P treatment in the CRC Phase I trial
***recurred at reduced dose 88 mg/m^2 in patient 22**
****associated with episode of small bowel ischaemia in patient 29, who also had hypotension during this episode, but not within 12 hours of treatment**
 # associated with haemorrhage into large tumour in chest in patient 16

with radical whole pelvic radiotherapy (50 Gy in 25 # over 5 weeks) and had a recurrent leiomyosarcoma involving small bowel loops in the pelvis. 3 days after her second CA4P infusion, she developed an overwhelming sepsis, and died. Post mortem findings revealed ischaemic small bowel in the region involved with tumour. She also had signs of long-standing radiation colitis, but the rest of the bowel appeared normal.

Less severe toxicities which were typically seen in patients treated above 40 mg/m^2 included mild nausea, generally controlled with standard anti-emetic drugs, lethargy, hypertension (usually between 1-3 hours post treatment), hypotension (usually 6-12 hours post treatment). These mild toxicities, like the tumour site pain, had a typical temporal pattern of onset after treatment, which was repeated within an individual patient with each infusion.

Figure 6.4 illustrates the mean change in vital signs seen in 8 patients treated at 5 to 40 mg/m^2, and in 22 patients treated at 52 to 114 mg/m^2. There were no significant changes in the group at 5 to 40 mg/m^2. At the higher dose levels, blood pressure was significantly increased by a mean 11 mmHg systolic (8%) and 8 mmHg diastolic (10%) 30 minutes to 1 hour after treatment ($p<0.001$, paired t-test), associated with a 15% decrease in heart rate ($p<0.001$). Four hours after treatment systolic and diastolic blood pressure were significantly decreased by a mean 8 and 6 mmHg (6% and 7%) respectively ($p=0.07$ and 0.02), and heart rate was increased by 15% ($p<0.001$) to 98 beats per minute. After 24 hours there was no significant difference in heart rate or blood pressure compared with pre-treatment.

One patient with liver metastases from adrenocortical carcinoma (#23) had a partial response after 3 cycles of treatment, but this was not maintained. Her pre treatment and post fourth cycle T2 weighted MR images are shown in Figure 6.5. The reduction in tumour size was associated with a reduction in the levels of adrenal androgens and corticosteroids measured on 24-hour urine collection, as shown in Table 6.4. Her next 4 cycles were given over a prolonged period, and she had documented progression of disease 9 months after beginning treatment, when a new lesion was noted, at which time her adrenal hormone levels had increased. Four patients had stable disease after 2 cycles of 3 infusions, but all of these had progressed after 3 or 4 cycles.

6.3.4 DCE-MRI Results

Figure 6.6 illustrates the absolute pre-treatment values of K^{trans}, v_e and k_{ep} for the tumour ROIs in the cohort of 19 patients. Initial tumour K^{trans} values ranged from 0.10 to 2.34

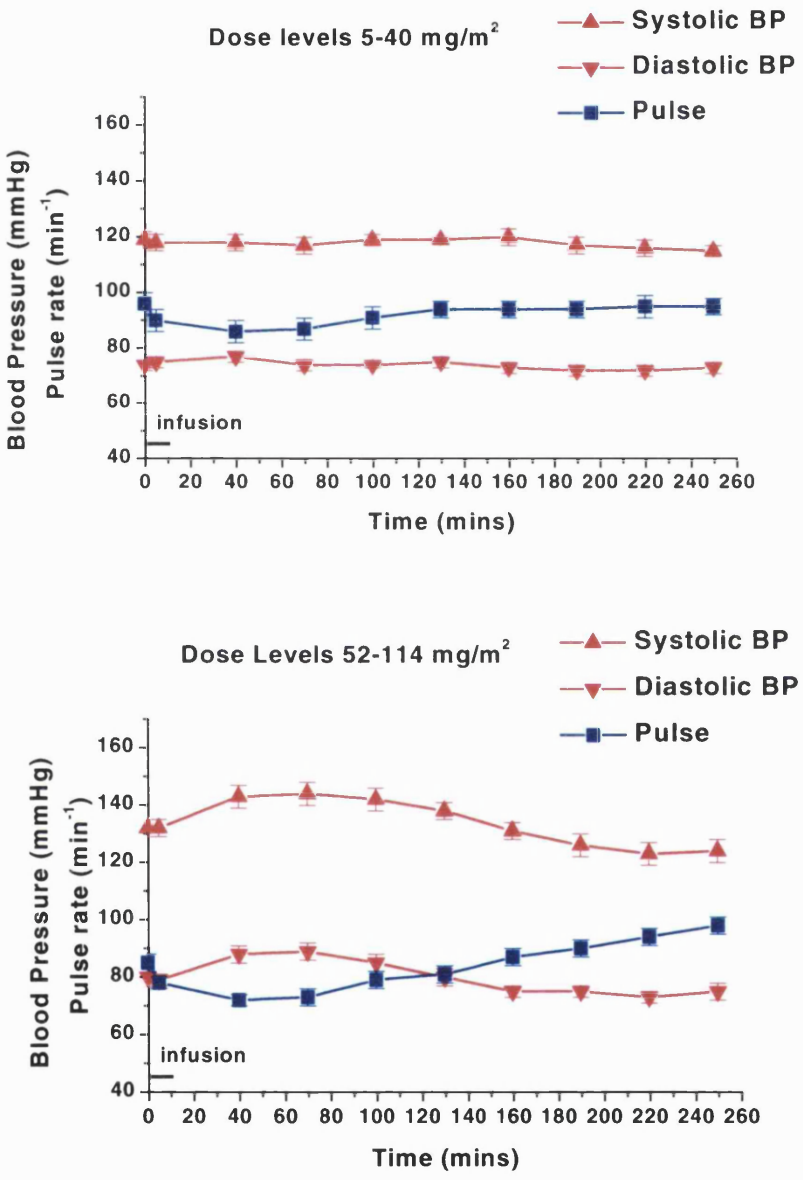

Figure 6.4 Changes in Blood Pressure and Pulse after CA4P

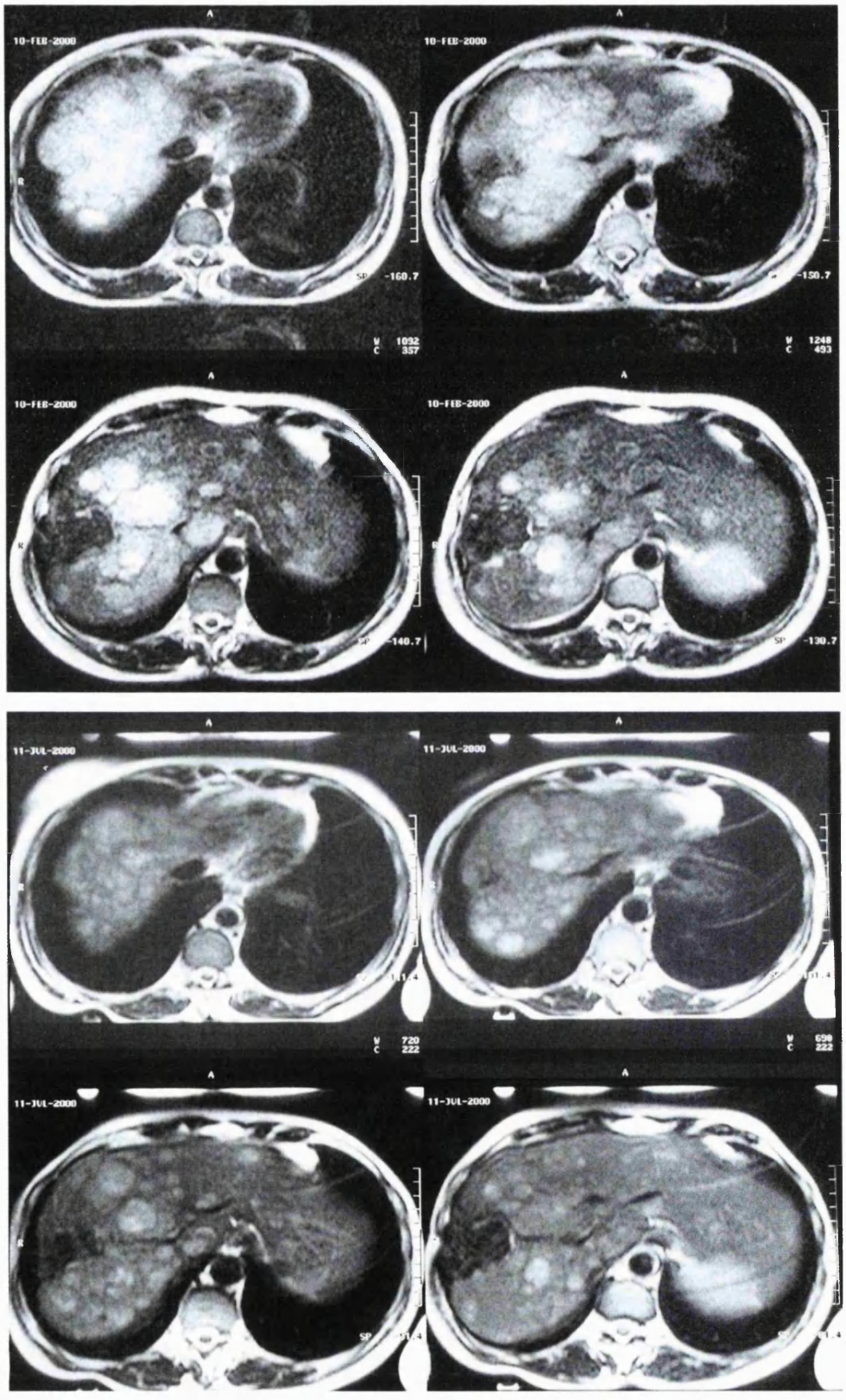

Figure 6.5 Patient #23 T2 weighted axial images through the liver – 4 contiguous 1 cm slices demonstrating multiple metastases from adrenocortical carcinoma. Top - pre-treatment. Bottom - post 4 cycles of CA4P

Steroid	Pre-treatment	Post 4 cycles	Post 7 cycles	Normal range
ADRENAL ANDROGENS				
Andosterone (5α)	430	40	600	260-1270
Aetiocholanolone (5β)	6680	1580	5040	270-1390
Dehydroepiandrosterone	7020	2350	4730	<50-970
16α-hydroxy-DHA	4080	1490	4810	<50-510
Androstenetriol	4950	3440	10170	100-350
CORTISOL METABOLITES				
11β-hydroxyandrosterone	2500	1120	1480	130-680
11β-hydroxyaetiocholanolone	2650	230	670	<50-200
Tetrahydrocortisone	3060	1450	2340	980-3240
Tetrahydrocortisol (THF)(5β)	5430	2600	2880	440-1610
Allo-THF (5α)	230	130		160-640
α-cortolone	1850	1050	1920	310-1330
β-cortolone +β-cortol	3060	1800		350-1110

Table 6.4 Change in steroid hormone production in patient #23 with CA4P treatment

ml/ml/min (mean 0.68), mean v_e was 31.8 ml/ml (range 8.0 to 57.9 ml/ml), and mean k_{ep} was 1.89 ml/ml/min (range 0.54 to 4.96). The absolute and relative change in each parameter, 4 hours and 24 hours after the first dose of CA4P is shown in Figures 6.7 and 6.8. In these Figures 2 patients treated at >1 dose level (#4 and 9) have changes at 4 and 24 hours after the first dose at each level shown. One patient treated at 52 mg/m^2 was excluded (#27). She had an ovarian carcinoma, with abdominal ascites. This required drainage between the pre-treatment examinations and twice during the first cycle of treatment. The accumulation and drainage of fluid caused changes in the appearance of the tumour such that adequate registration of post treatment images with pre-treatment images was impossible.

There is evidence from Figures 6.7 and 6.8 of a dose effect. The 2 patients treated at 40 mg/m^2 had an increase in K^{trans} at 24 hours, whereas all of the 16 patients treated at 52 mg/m^2 and above had reductions in K^{trans} at either 4 or 24 hours. Five patients treated ≥52 mg/m^2 had a decrease in v_e greater than the repeatability value of 6.9 ml/ml. Six patients (1 at 52 mg/m^2, 3 at 68 mg/m^2 and 2 at 88 mg/m^2) had a reduction in $Log_{10}K^{trans}$ greater than the repeatability value of 0.24 ml/ml/min. Most patients had the greatest reduction at 4 hours, but 4 patients had a greater reduction in K^{trans} or v_e at 24 hours rather than 4 hours. At the DCE-MRI examinations 24 hours after the first dose or 13 days after the last dose of CA4P, 5 of 8 patients treated at ≥88 mg/m^2 had significant decreases in v_e greater than 6.9 ml/ml. Of these, 4 had an associated increase in the number of completely non-enhancing pixels. This is shown for patient #12 in Figure 6.9 where there is a marked increase in black (non-enhancing) pixels after treatment from 20% pre-treatment to 64% at the end of treatment. The fifth patient had a tumour with a high value of K^{trans} (1.13 ml/ml/min) pre-treatment. This increase in non-enhancing pixels was not an artefact induced by setting the non-enhancing pixels to have a value of 0 for v_e, as all 5 patients also had a significant decrease in v_e of similar magnitude when calculated for the whole region of interest rather than using pixel analysis. Maintained reductions in v_e were not seen at 52 and 68 mg/m^2.

Parameter maps for K^{trans} and v_e pre treatment, and at 4 and 24 hours after treatment for patients #32 and 12 treated at 52 and 88 mg/m^2 are shown in Figure 6.9. The tumour is outlined and also seen in the corresponding anatomical image. The heterogeneity within the tumour is seen on the pre-treatment maps. Following treatment there is a marked reduction in K^{trans} and v_e values particularly in the centre of the tumours, with sparing of the tumour rim. This pattern is very reminiscent of the pattern of post CA4P changes seen in animal tumours.

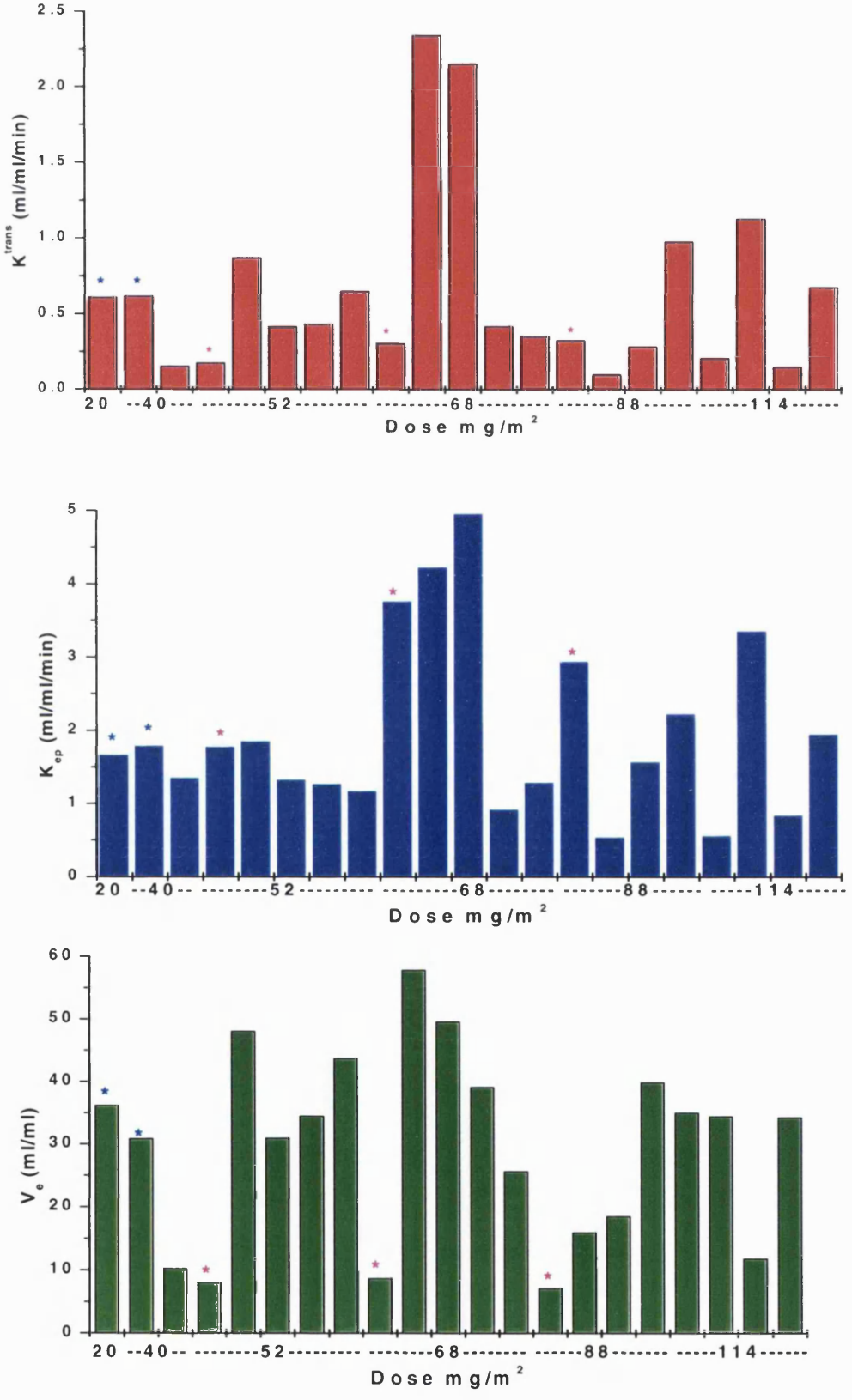

Figure 6.6 Pre-treatment median values for K^{trans} (top), k_{ep} (middle), and v_e (bottom) in tumour ROIs
* indicates patients treated at more than one dose level

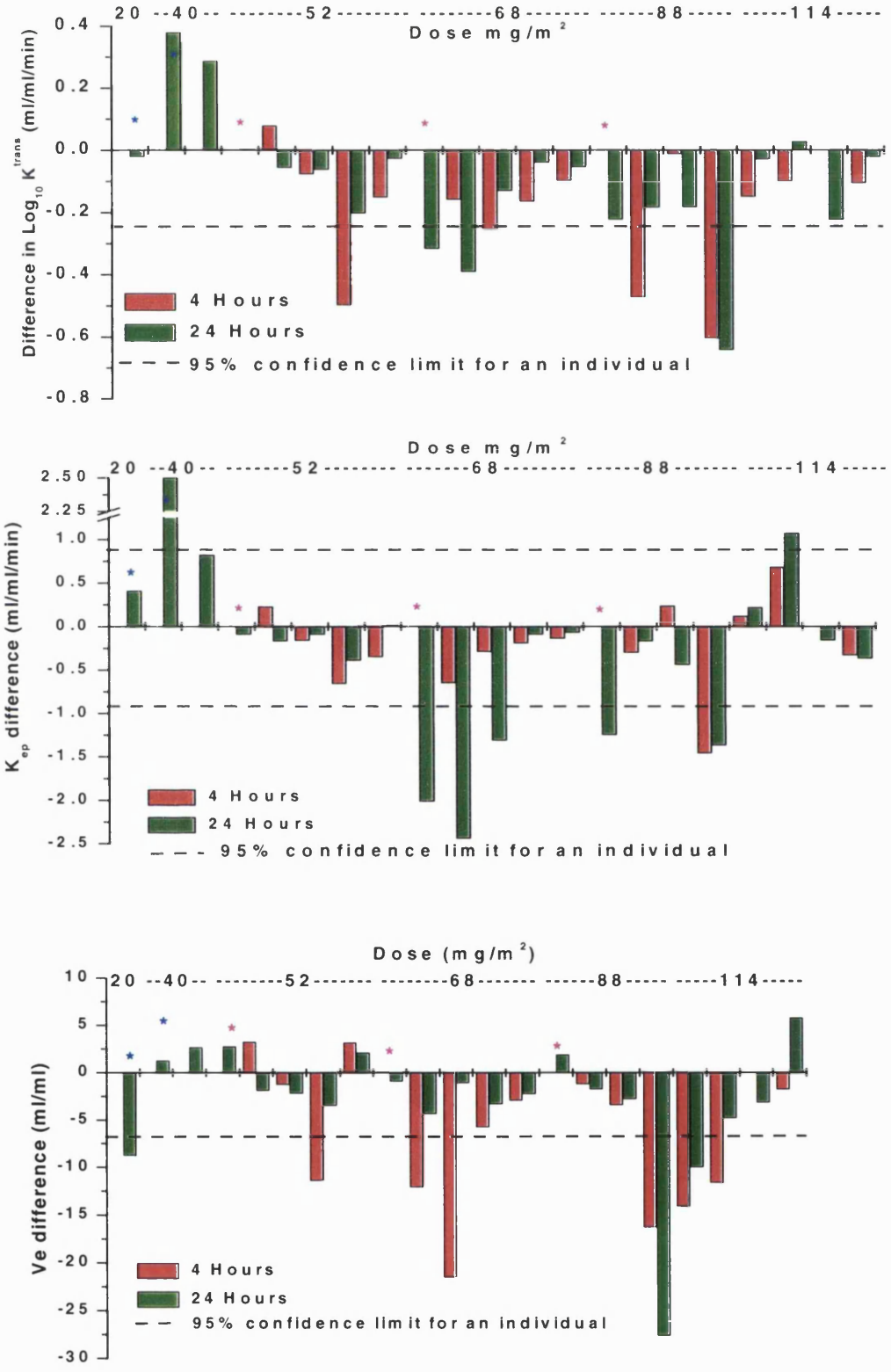

Figure 6.7 Absolute change in $Log_{10} K^{trans}$ (top), k_{ep} (middle) and v_e (bottom) 4 hours and 24 hours after the first dose of CA4P
* indicates patients treated at more than one dose level

Figure 6.8 Relative changes in DCE-MRI parameters at 4 hours and 24 hours after the first dose of CA4P
***indicates patients treated at more than one dose level**

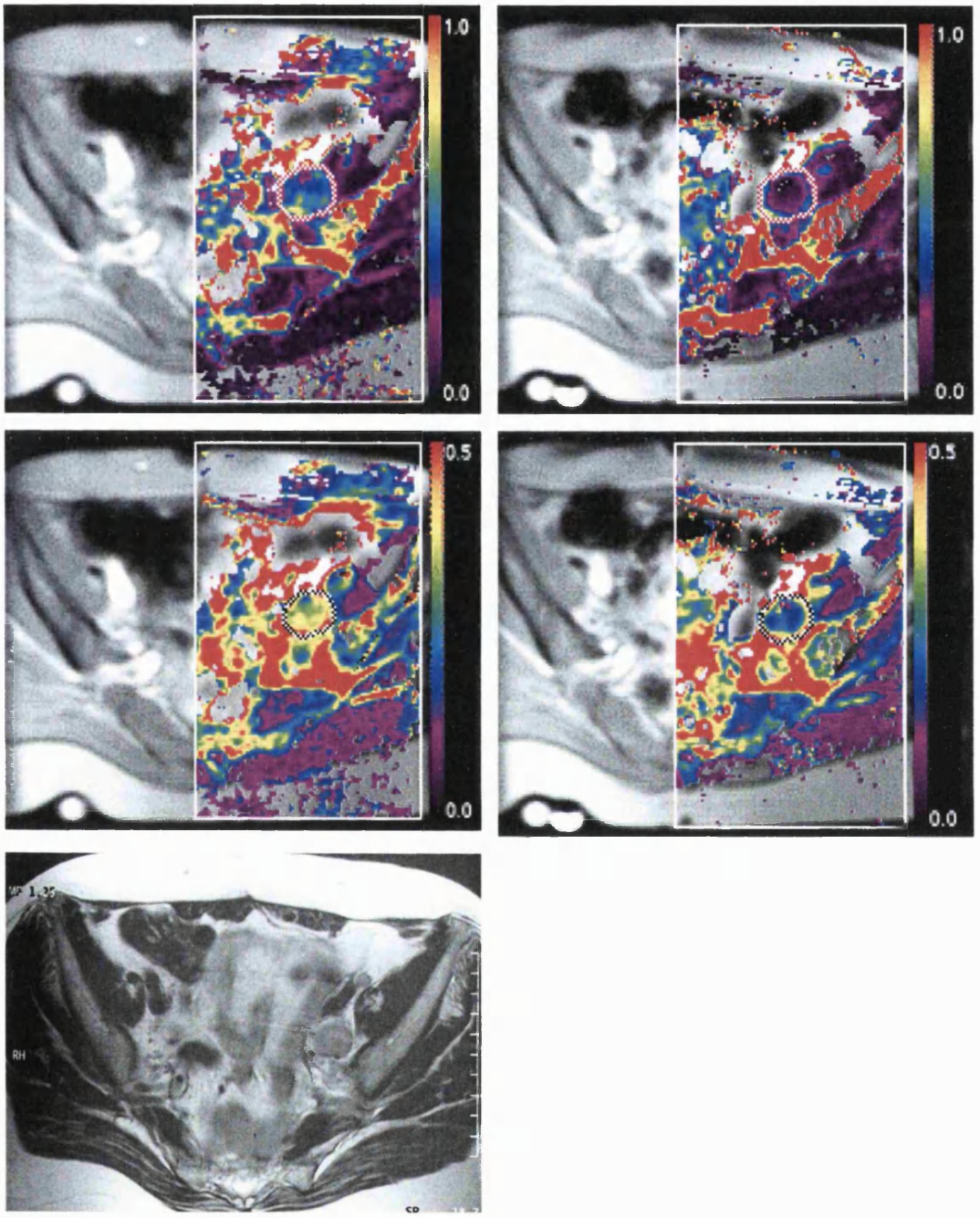

Figure 6.9 Parametric maps overlain on T1 weighted images for patient #32 treated at 52 mg/m^2. Top – K^{trans} map, Bottom – v_e map. Left – pre-treatment, Right – 4 hours post first dose of CA4P

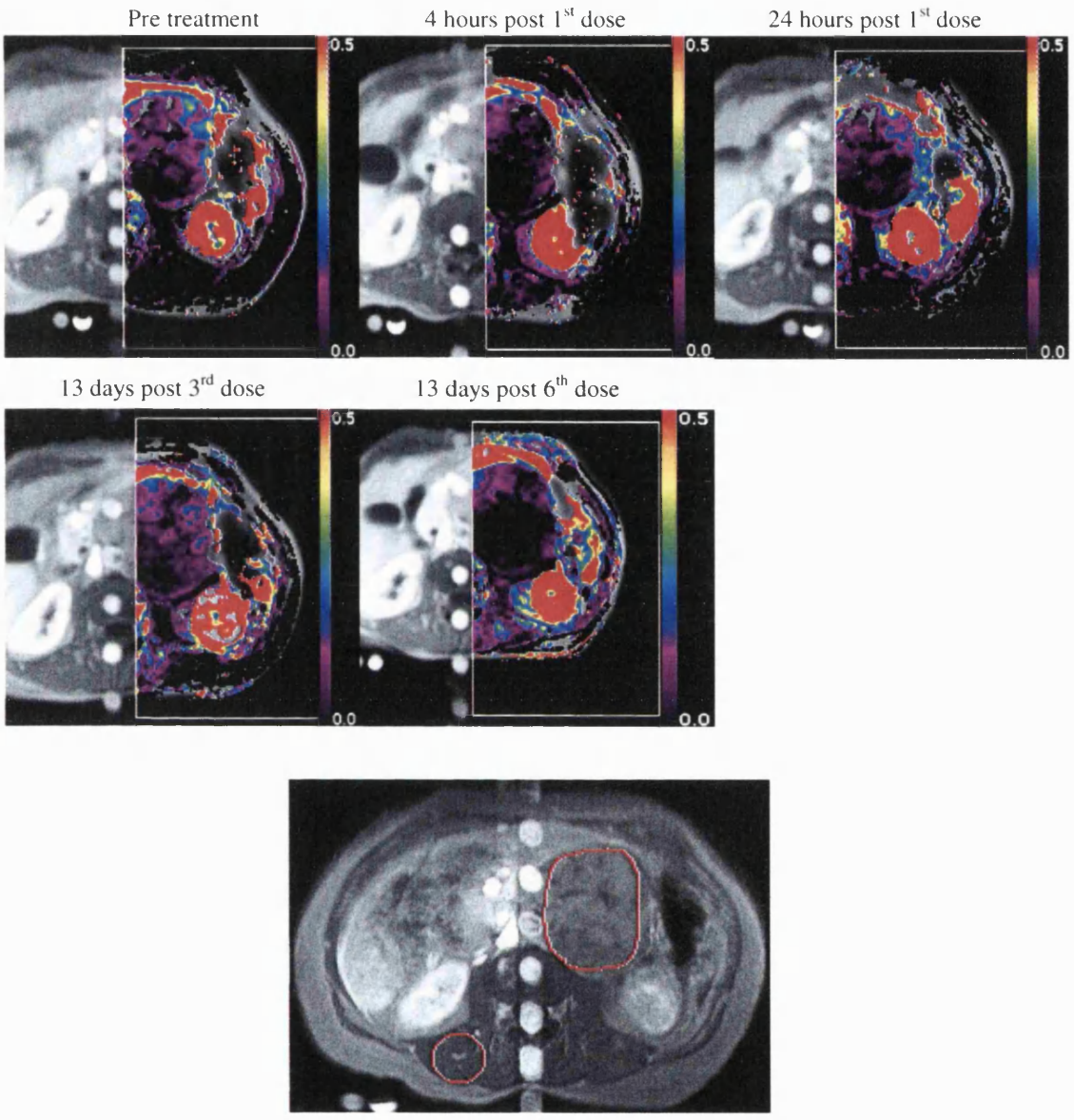

Figure 6.9b Serial parametric maps overlain on T1 weighted images for patient #12 treated at 88 mg/m^2. Bottom – corresponding anatomical image with tumour and muscle ROIs shown.

As there was no evidence of consistent reductions in DCE-MRI parameters at ≤40 mg/m^2, mean changes after treatment were calculated for all 16 patients treated at or above 52 mg/m^2. Since DLTs were seen at 88 and 114 mg/m^2, mean reductions in the 9 patients treated at 52 and 68 mg/m^2 who had DCE-MRI examinations were also calculated.

The mean reduction in K^{trans} v_e and k_{ep} in tumour ROIs for all patients treated at ≥52 mg/m^2, 4 hours and 24 hours after the first dose of CA4P, and 13 days after the third dose are shown in Figure 6.10. Mean $Log_{10}K^{trans}$ was reduced by 0.20 ml/ml/min (37%) at 4 hours and by 0.15 (29%) at 24 hours after the first dose. Both these reductions are statistically significant, being greater than the 95% confidence limits determined from the reproducibility dataset 0.068 and 0.064 ml/ml/min calculated for a group of 14 and 16 respectively. At the end of cycle examination, 13 days after the third dose, there was also a significant reduction of 0.10 ml/ml/min (20%) compared to pre-treatment. V_e was also significantly reduced at 4 and 24 hours, 7.0 ml/ml (21%) at 4 hours, and 3.7 ml/ml (11%) at 24 hours but at the end of the cycle there was no significant difference from pre-treatment. These reductions are also greater than the 95% confidence limits, 1.85 and 1.73 ml/ml for groups of 14 and 16 respectively. The mean reduction in k_{ep} was significant at 24 hours, -0.43 ml/ml/min (22%), but not at 4 hours, –0.23 ml/ml/min (12%) or 13 days post treatment. Again, the reduction at 24 hours was greater than that expected spontaneously (0.23 ml/ml/min, for a group of 16).

If the patients treated at dose levels above the MTD are excluded from this analysis (thus including the 9 patients treated at 52 and 68 mg/m^2), the mean reduction in $Log_{10}K^{trans}$ was 0.17 (32%) and 0.13 (25%) ml/ml/min at 4 and 24 hours respectively, as shown in Figure 6.11. These reductions are still greater than the 95% confidence limits of change, 0.090 and 0.085 for groups of 8 and 9 subjects respectively. The mean reduction in v_e for this group was 6.1 ml/ml (16%) and 1.8 ml/ml (5%) at 4 and 24 hours respectively, which was statistically significant at 4 hours but not at 24 hours, the 95% limits being 2.45 and 2.31 respectively. The mean reduction in k_{ep} was 0.28 (13%) and 0.62 (28%) at 4 and 24 hours, significant at 24 hours but not 4 hours, the 95% limits being 0.33 and 0.31 at 4 and 24 hours respectively.

There was a significant negative correlation ($R = -0.48$, $p = 0.03$) between the concentration of CA4 AUC with maximum relative change in K^{trans} at either 4 hours or 24 hours, as shown in Figure 6.12. The correlation was also significant when calculated for relative change at 24

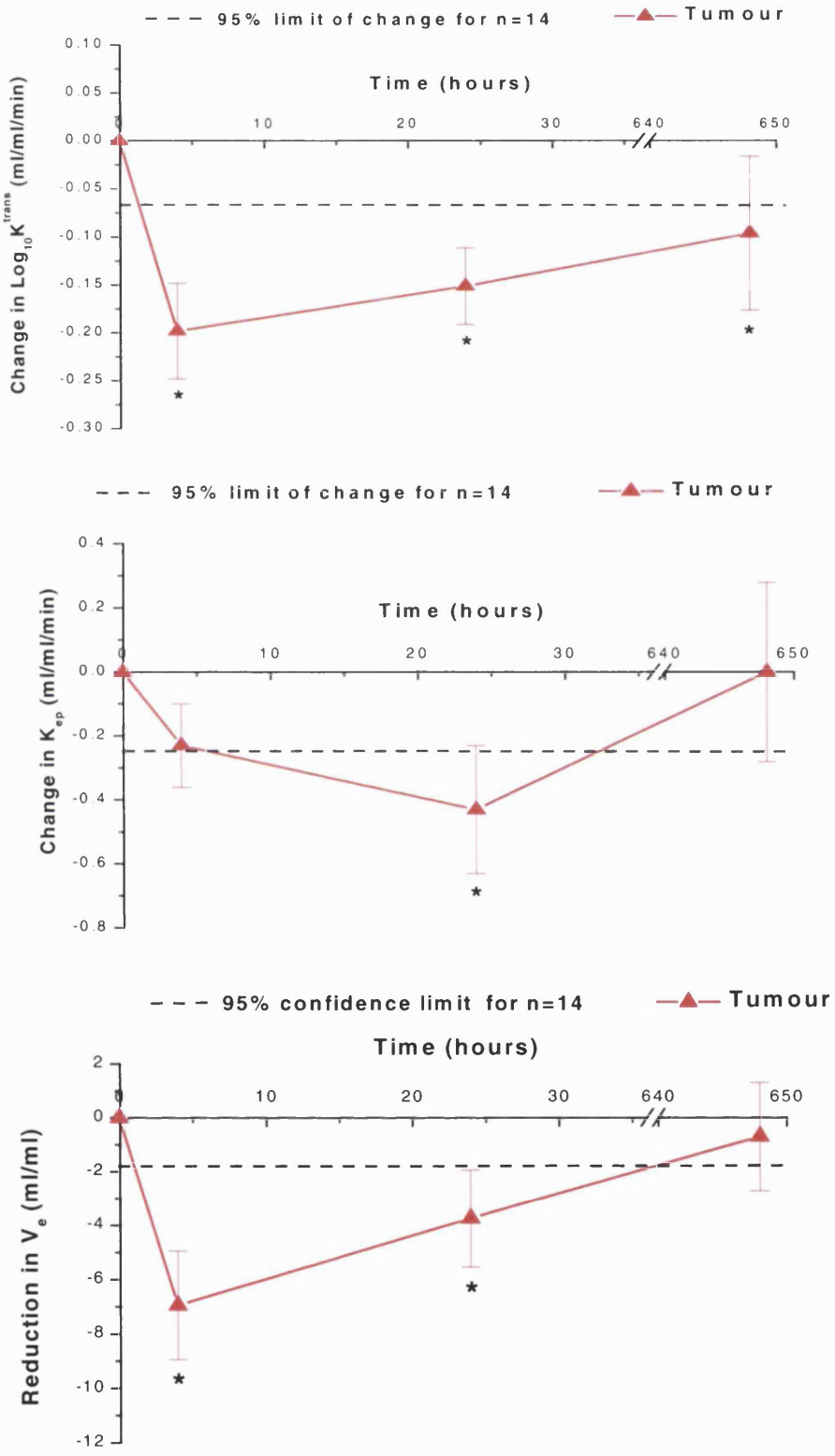

Figure 6.10 Mean changes in DCE-MRI parameters at 4 hours and 24 hours after the first dose of CA4P and 13 days after the third dose for all patients treated at ≥52 mg/m². * = significant change ($p<0.05$)

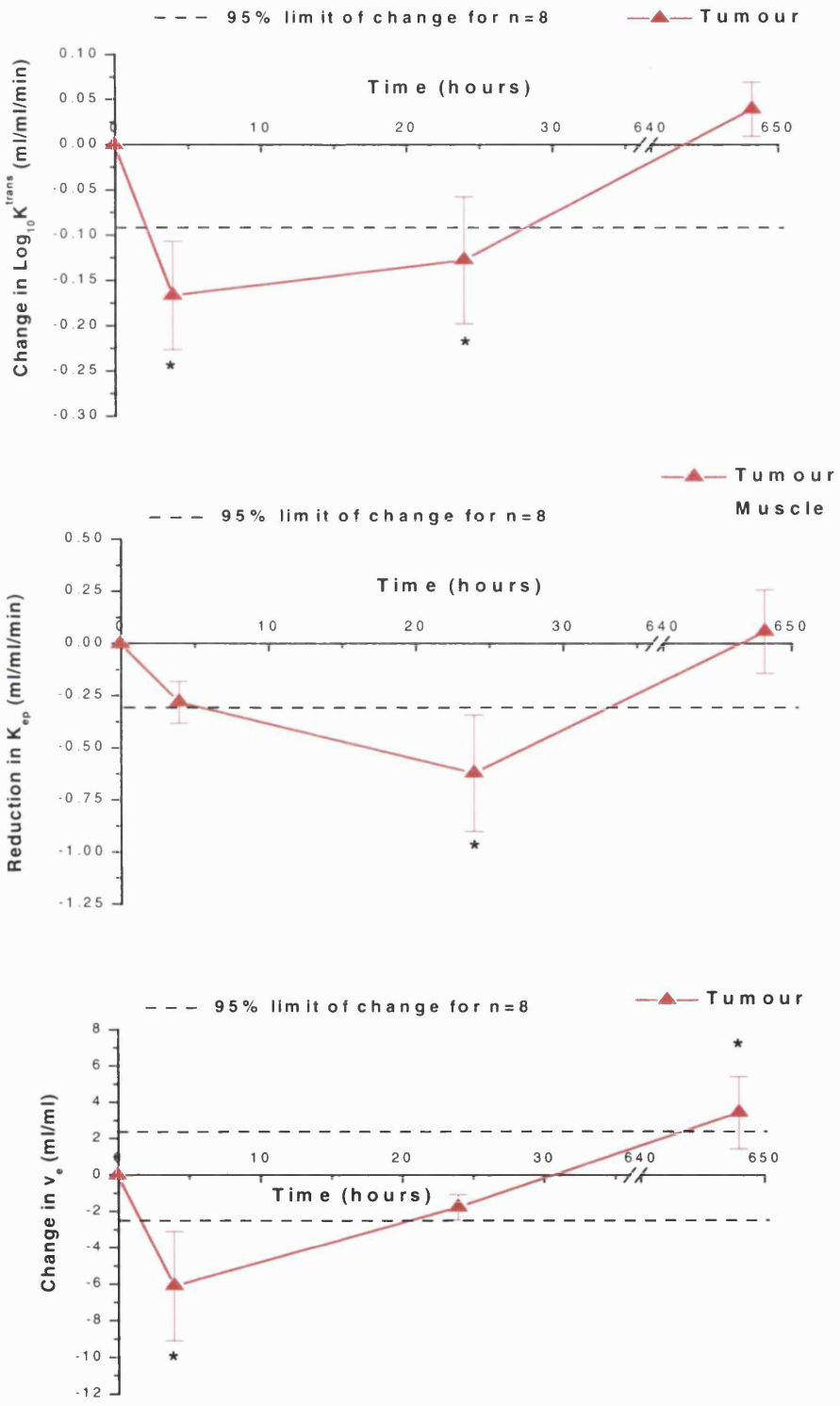

Figure 6.11 Mean changes in DCE-MRI parameters at 4 hours and 24 hours after the first dose of CA4P, and 13 days after the third dose in patients treated at 52 to 68 mg/m². *= significant change ($p<0.05$)

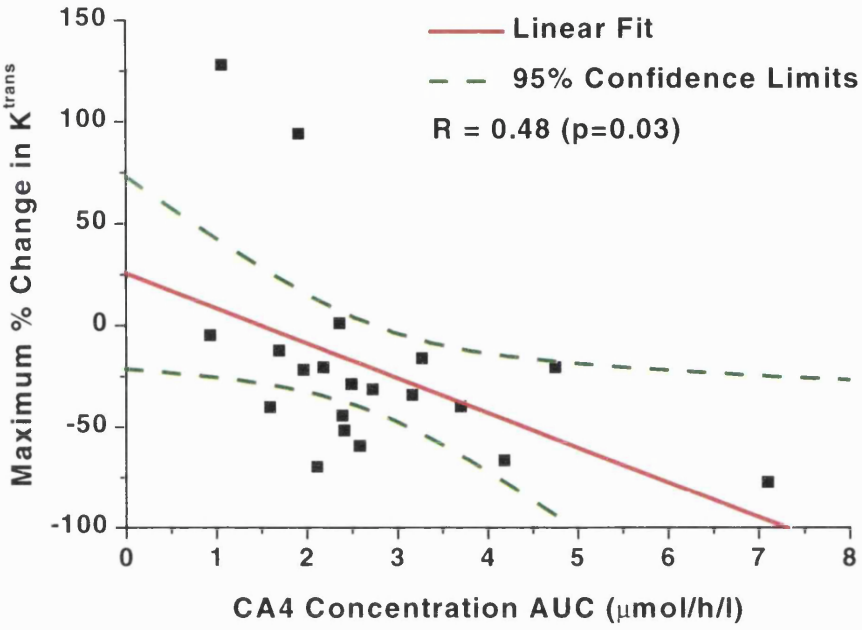

Figure 6.12 Linear regression of maximum percentage change in K^{trans} with CA4 concentration AUC for the patients in the CA4P Phase I trial treated at Mount Vernon

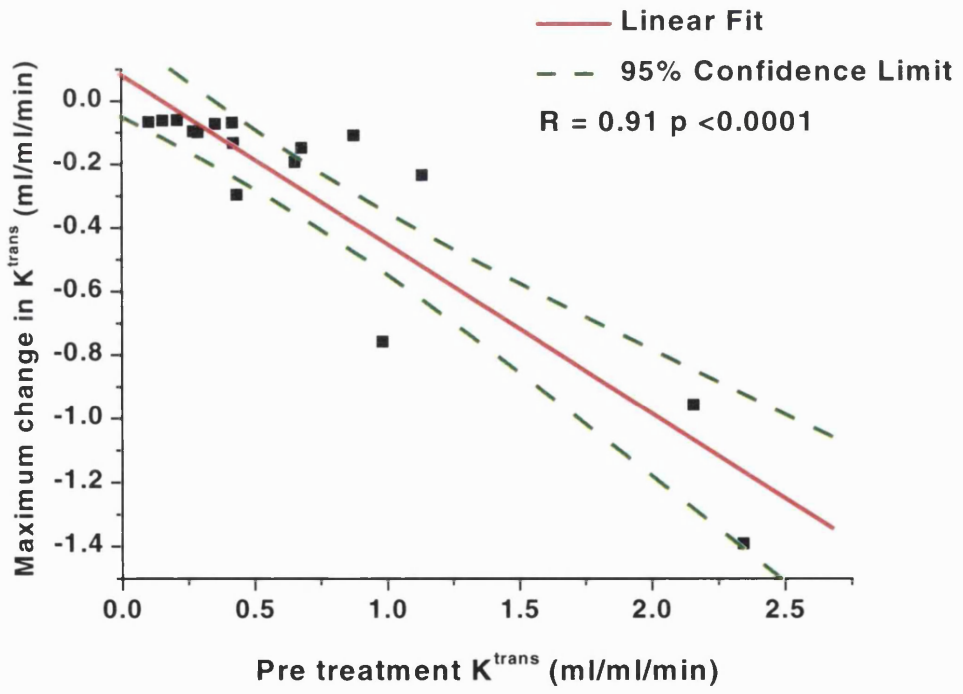

Figure 6.13 Linear regression of change in K^{trans} versus pre-treatment K^{trans} values

hours. There was no correlation with the peak concentration of CA4, C_{max}. In Figure 6.13 pre-treatment K^{trans} value for each patient treated at ≥52 mg/m^2 is plotted against the difference in K^{trans} at 24 hours. There is a highly significant negative correlation, R =-0.91, $p<0.0001$. There was no significant correlation between pre-treatment K^{trans} and relative change in K^{trans} at any time.

Five patients had 2 or more cycles of treatment at the same dose level, 1 at 52 mg/m^2, 2 at 68 mg/m^2 1 at 88 mg/m^2 and 1 at 114 mg/m^2. The DCE-MRI parameter values for these patients are plotted against time in Figure 6.14. The temporal pattern of change seen after the first dose of CA4P is repeated after the first dose of the second cycle in 4 of these patients, although the magnitude of the change seen is less than after the first dose. Three patients had a maintained reduction in K^{trans} 13 days after the sixth dose of CA4P (#12, 21 and 30). All 3 of these patients had leiomyosarcomas with progressive disease at this time. One patient (#23) had 8 cycles of treatment (total of 24 infusions), with prolonged gaps in treatment between cycles 4, 5 and 6. She had a partial response after 4 cycles, which was not maintained after several weeks off treatment. Her serial parameters are plotted in Figure 6.15. The reductions in K^{trans} after the first dose of the third, fourth and eighth cycles are less than those after the first two cycles. Over the course of the cycles when tumour regression was occurring, there was no pattern of maintained reduction in K^{trans} .

6.4 Discussion

These results establish proof of principle that CA4P significantly reduces DCE-MRI kinetic parameters related to tumour blood flow in humans. Significant reductions in v_e and increases in numbers of non-enhancing pixels within tumours suggest local vascular shutdown within the tissue as the mechanism of action, rather than global reduction in blood flow. Visual inspection of parametric images demonstrating the heterogeneity of change in K^{trans} and v_e across the tumours provide further evidence for this. A global reduction in blood flow to the tumour due to an extrinsic effect, such as reduction in cardiac output, would be expected to reduce the MR parameters more evenly across the tumour. In addition, as discussed in Chapter 4 it would not be expected to reduce the Gd-DTPA leakage space in the tissue, but only transfer constant (K^{trans}) values.

Mean reductions in K^{trans} and v_e in the patients treated at and above 52 mg/m^2 follow a similar temporal pattern to that seen in rat and murine tumours, with maximal reduction at 4 hours and some recovery by 24 hours. However, individual patients do not all follow this

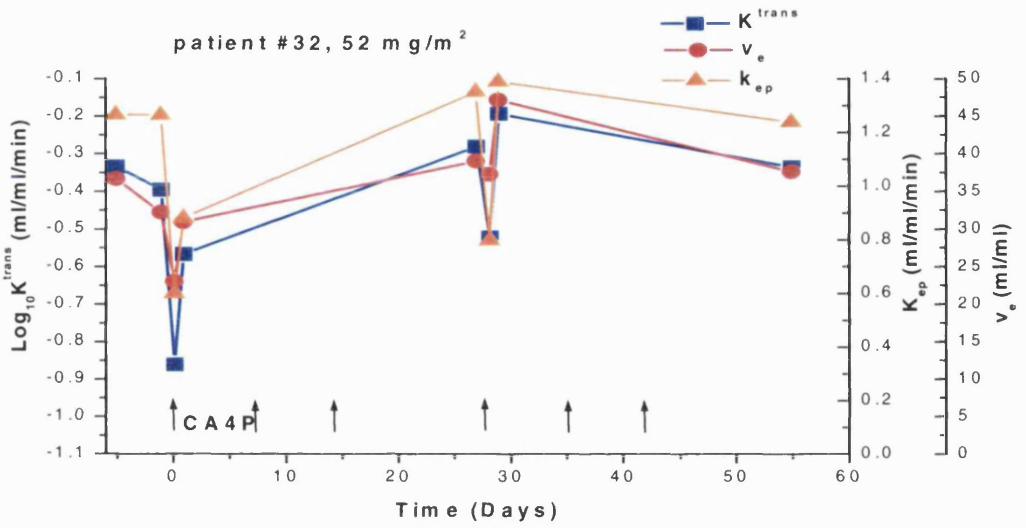
patient #32, 52 mg/m²
K trans
v e
k ep
Log10K trans (ml/ml/min)
Kep (ml/ml/min)
ve (ml/ml)
CA4P
Time (Days)

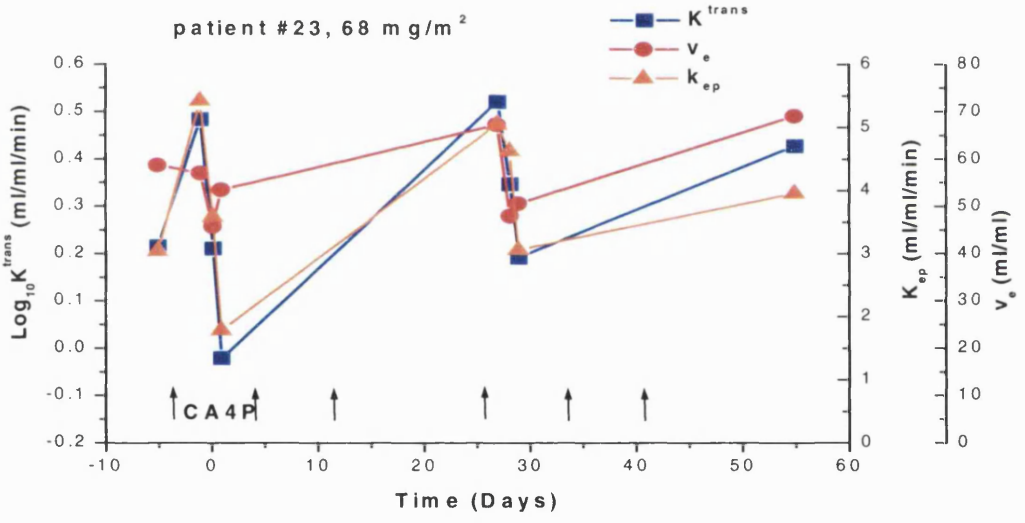
patient #23, 68 mg/m²
K trans
v e
k ep
Log10K trans (ml/ml/min)
Kep (ml/ml/min)
ve (ml/ml)
CA4P
Time (Days)

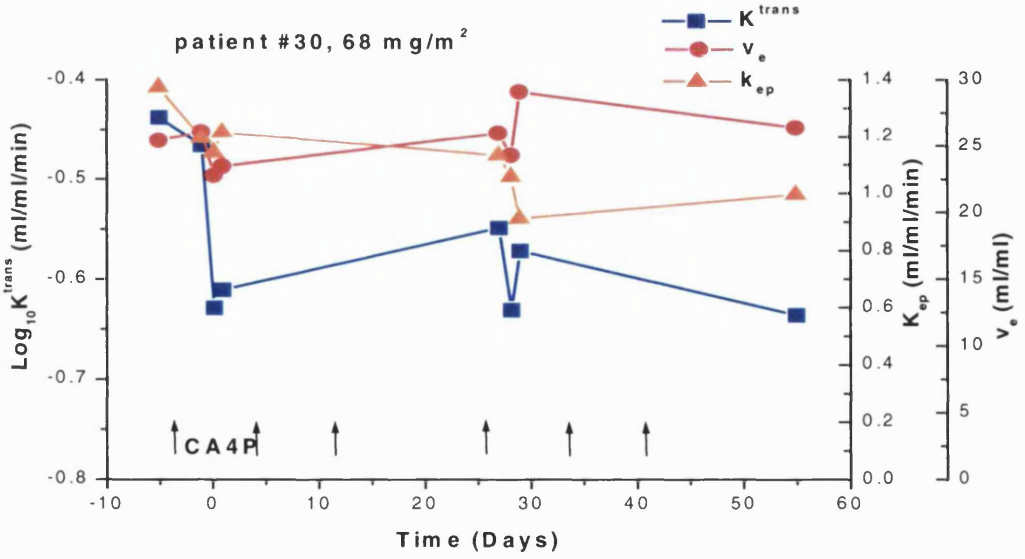
patient #30, 68 mg/m²
K trans
v e
k ep
Log10K trans (ml/ml/min)
Kep (ml/ml/min)
ve (ml/ml)
CA4P
Time (Days)

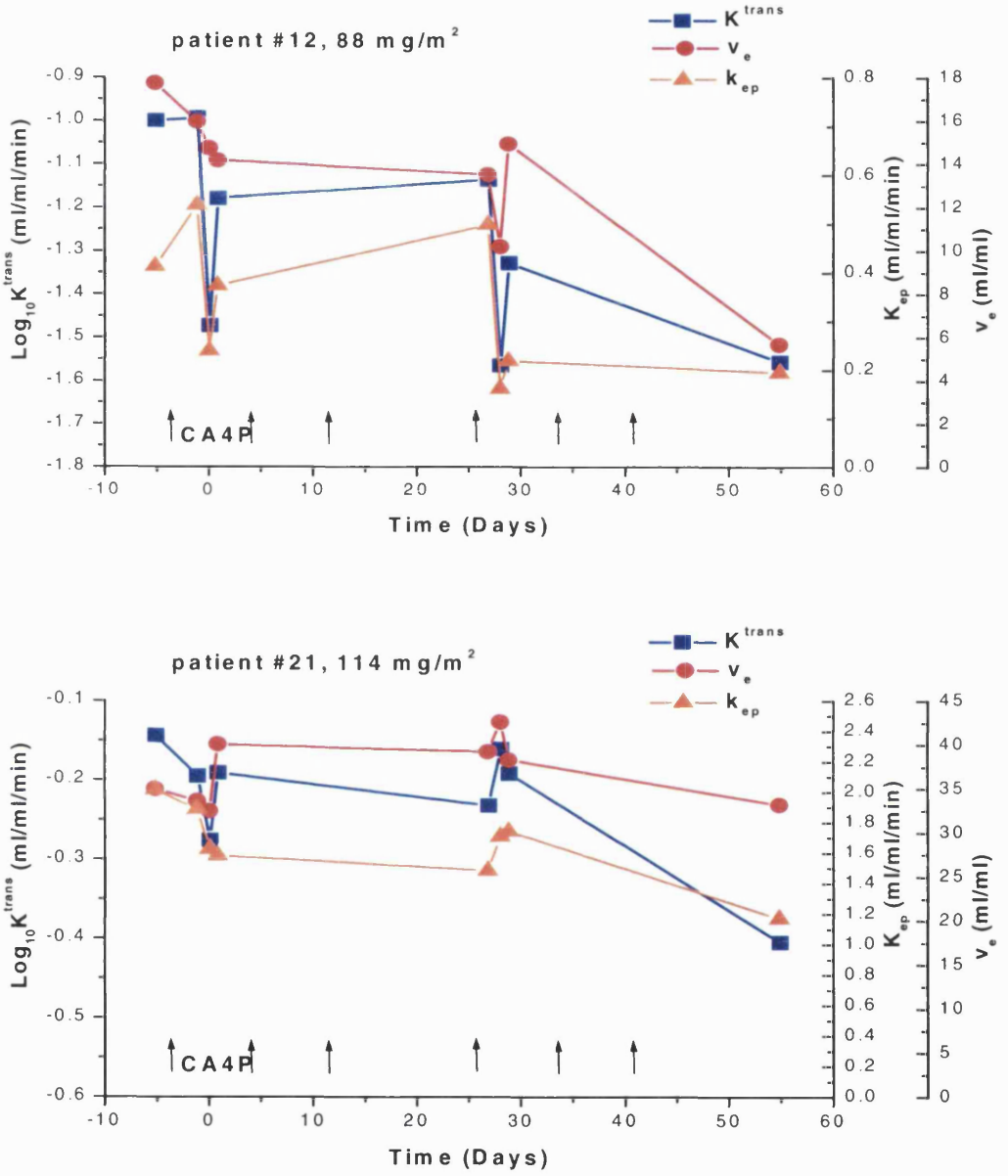

Figure 6.14 Serial changes in K^{trans}, k_{ep} and v_e in 5 patients who completed 2 cycles (6 infusions) of CA4P

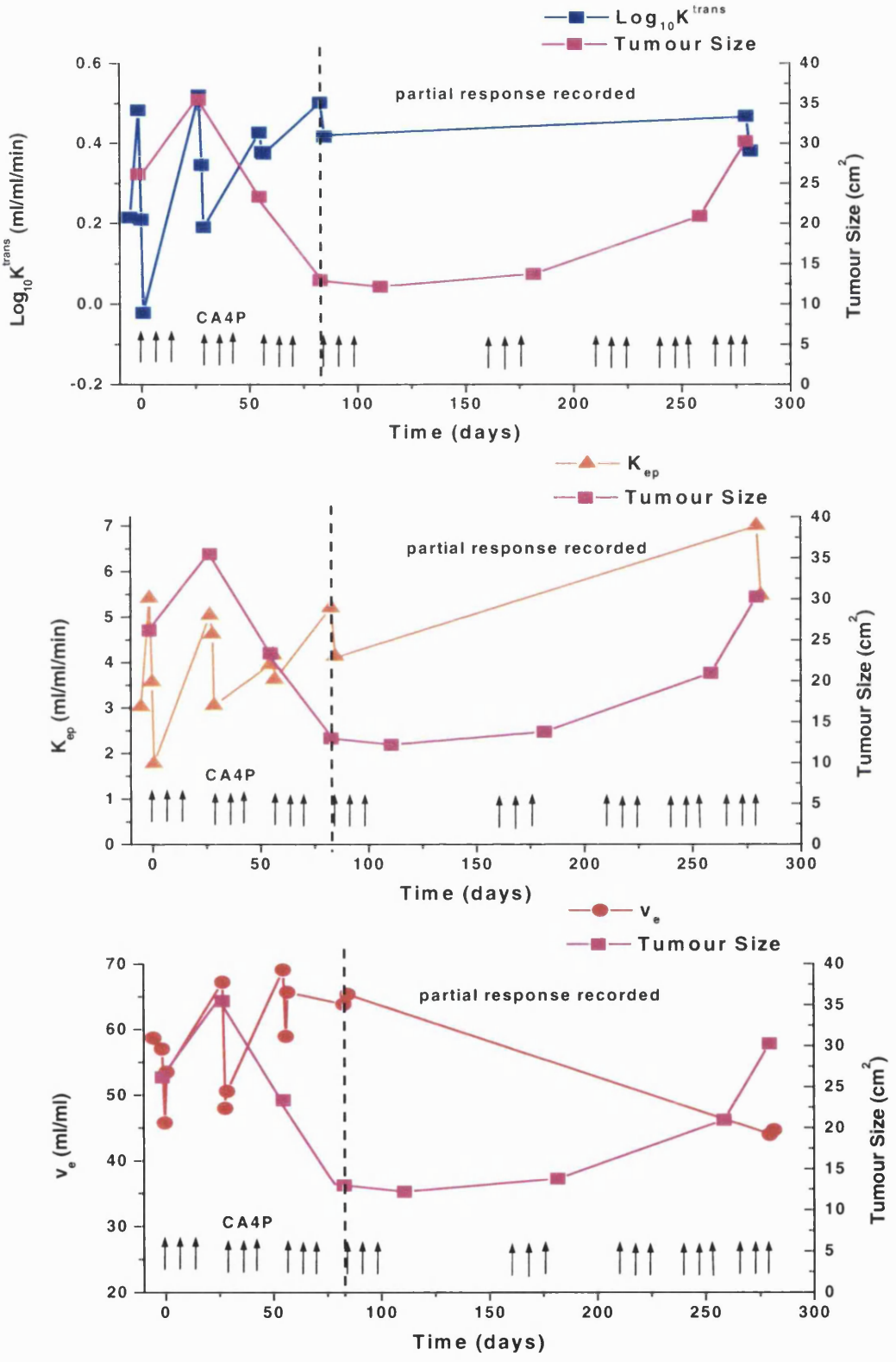

Figure 6.15 Serial changes in DCE-MRI parameters in patient #23 who received a total of 8 cycles of CA4P (24 infusions). DCE-MRI investigations were not performed with every cycle. This patient had >50% reduction in tumour size (calculated as the sum of the products of orthogonal diameters for 4 marker lesions) after the third cycle, although one lesion increased in size by the fourth cycle. At the time of the final DCE-MRI examination, a new lesion was seen.

pattern with 4 patients having a greater reduction at 24 hours than at 4 hours. A more prolonged reduction in blood flow might be expected to cause increased tumour cell death (Denekamp *et al.*, 1983), although reperfusion injuries after shorter duration ischaemia (Parkins *et al.*, 1995) and neutrophil infiltration (Parkins *et al.*, 2000) also influence tumour cell kill. This cohort of patients is too small to correlate temporal pattern of blood flow response with clinical effect.

The mean reduction in K^{trans} (37%) in patients treated $\geq$ 52 mg/m^2 is similar to the 40% reduction in tumour vascular volume seen after a dose of 25mg/kg in mice (Dr S. Hill, personal communication). This dose is insufficient to cause significant growth delay in this murine tumour model after a single dose. Repeat dosing twice daily for 10 days does produce some growth delay, but no tumour regression (Hill *et al.*, 1999). The achievement of 1 partial response after 4 cycles of treatment was therefore unexpected. This patient treated at 68 mg/m^2 had a greater reduction in K^{trans} and v_e after 24 hours rather than 4 hours, and a larger than average relative reduction in K^{trans} (60%), which might explain the increased effect on tumour growth in her case.

Those patients with initial high values of K^{trans} had a greater absolute reduction in this parameter after treatment. Given that the spontaneous variation in K^{trans} is also dependent on the initial value as shown in Chapter 5, this is not unexpected. When relative reductions in K^{trans} were considered there was no correlation with pre-treatment values. This is in contrast to pre-clinical data which suggests that tumour types with a high permeability assessed using dynamic MRI and high molecular weight contrast agents, were more likely to respond to CA4P treatment (Beauregard *et al.*, 2000). It has been suggested that this might be due to the tumours producing more VEGF, and therefore inducing a higher proliferation rate in the endothelium, thus making the endothelial cells more susceptible to shape change as shown in Chapter 2. Alternatively, tumours with more permeable microvasculature might have more abnormally increased interstitial fluid pressure, making them more susceptible to vascular shutdown following a further rapid increase in permeability after CA4P treatment. A third possibility is that such tumours have an increased ratio of immature to mature blood vessels, and the response to CA4P occurs to a greater degree in the immature vessels. Tumour types with a relatively poor response to CA4P, also have a higher proportion of mature vessels, assessed by actin staining of vessels to determine those which have a smooth muscle coat (Dr S. Hill, personal communication).

There may be several reasons for the discrepancy between these pre-clinical data and the clinical results. Firstly, the pre-clinical data measured vessel permeability to a high molecular weight contrast agent, which is a different parameter than K^{trans} calculated using Gd-DTPA. As discussed in Chapter 4, changes in K^{trans} accurately reflected tumour blood flow changes, even though CA4P has been shown to increase vessel permeability. Secondly, the pre-clinical data were obtained from groups of tumours of a small number of different types, but within each type the tumour size, position and pre-treatment permeability were relatively similar. In contrast the clinical data were obtained in a heterogeneous group of tumour types, sizes and sites treated over a range of dose levels. Other factors may be more important in determining tumour vessel response to CA4P than just permeability, even if this aspect of the tumour vasculature were being measured directly. For example, there is a significant correlation between CA4 concentration AUC and K^{trans} relative changes.

Thirteen patients in the trial were treated at the Hammersmith Hospital, and underwent PET imaging with $H_2{}^{15}O$ to measure absolute blood flow, and ^{14}CO to measure blood volume. The arterial input function was measured directly via arterial samples collected through a cannula inserted in the radial artery. The first post treatment examination was done at a different time than the DCE-MRI examinations (30 minutes to 1 hour post treatment rather than 4 hours) and there was also an examination at 24 hours. The pre-treatment examination was performed just prior to drug infusion, so the patient remained in the same position for the first two examinations. Despite these differences, the size of changes seen in relative blood flow with PET were similar in magnitude to those seen in K^{trans} with DCE-MRI. In the dose range 52-88 mg/m^2, a 30-60% reduction in tumour perfusion was seen in 4 of 5 patients at 30 minutes to 1 hour (Anderson *et al.*, 2000). One of these patients had a maintained reduction at 24 hours. The arterial input function was significantly altered at the 30 minute to 1 hour time point, which was interpreted as being due to a reduction in cardiac output of 7% to 24% at doses ≥52 mg/m2 at this time. The mean reduction in cardiac output in 3 patients treated at 52 and 68 mg/m2 was 9%, with the larger reductions seen at 88 and 114 mg/m2. There were no significant changes in arterial input function at 24 hours, at which time no significant mean difference in tumour perfusion was seen compared to pre-treatment values. The 30 minute to 1 hour time point for PET imaging coincided with the peak of rise in blood pressure and fall in heart rate, whereas at the time of the 4 hour MRI examination blood pressure was reduced and heart rate increased. The effects on cardiac output at these times may therefore be different. Any reduction in cardiac output would lead to an overestimation of treatment effect with DCE-MRI, as an assumed arterial input function was

used. However, 1 patient had DCE-MRI examinations one cycle, and PET around the first dose of the next, showing similar levels of treatment effect (58% reduction in K^{trans} and 60% reduction in perfusion), and a similar pattern of recovery at 24 hours. The discrepancy in results seen at 24 hours with these two techniques may be due to differences in tumour types. The Hammersmith cohort had 6 patients with metastatic bowel tumours in liver, and only 1 sarcoma, whereas the Mount Vernon cohort had 6 patients with sarcomas and only 1 with a colon tumour. Four of 5 patients with leiomyosarcoma had a similar percentage reduction in K^{trans} at 4 and 24 hours or a greater reduction at 24 hours than at 4 hours. As mentioned above, there is heterogeneity within the MRI dataset, with some patients recovering by 24 hours and others having a greater change at 24 hours. It is possible that the 9 patients treated at Hammersmith Hospital at ≥52 mg/m2 might have a different pattern of change than the cohort at Mount Vernon.

The changes observed in blood pressure and heart rate follow a similar pattern to those seen in rats bearing P22 carcinosarcomas, although the period of hypertension was more prolonged in rats, and the percentage increase in blood pressure was greater than in patients (Tozer *et al.*, 1999). In the latter study the mean arterial blood pressure 1 hour after treatment with 100 mg/kg was increased by 24 mmHg (30%), associated with a relative bradycardia. Blood pressure was returning to baseline by 6 hours, at which time there was a 25% increase in heart rate.

Changes in tumour blood flow in rats have been seen with hypertensive agents such as angiotensin II (Tozer & Shaffi, 1993). However angiotensin II produced only a 20% reduction in tumour blood flow at doses that caused much larger changes in BP and HR than observed in either this study or after CA4P treatment in rats (Tozer *et al.*, 1999). Larger reductions were seen in normal tissue blood flow. Other studies have shown an increase in tumour blood flow with angiotensin II *relative* to that in normal tissues (Suzuki *et al.*, 1981; Burton *et al.*, 1985). The relative lack of tumour blood vessels with smooth muscle responsive to systemic vasoconstrictors may explain why the doses of angiotensin that induce tumour vasoconstriction tend to have a greater constrictive effect on the normal tissue vessels. Reductions in tumour blood flow have also been observed in experimental models, after treatment with the vasodilator hydralazine (Voorhees & Babbs, 1982; Horsman *et al.*, 1992). Low doses of this agent produced up to 30% increases in tumour blood flow, and higher doses produced >80% reduction of tumour blood flow, but at these doses blood pressure was reduced by 50%. When hydralazine was used in patients with lung tumours, tumour

blood flow measured using ^{99m}Tc-HMPAO increased by 38%, at doses that induced 10% reduction in BP (Rowell *et al.*, 1990).

The changes in blood pressure seen in the CA4P trial are therefore much smaller than the changes needed to produce significant reductions in tumour blood flow in the above studies. These data provide further evidence suggesting that the changes seen in patients treated with CA4P are due to a direct effect on local tumour vasculature rather than solely due to a systemic effect such as a change in blood pressure or cardiac output. The blood pressure and cardiac output changes are more likely to be a reflection of increased vascular resistance to a variable degree in a range of tissues including tumour.

6.5 Summary

The DCE-MRI data demonstrate significant reductions in parameters that reflect tumour blood flow changes in patients treated with CA4P at 4 and 24 hours in the well-tolerated dose range of 52 to 68 mg/m^2. In some patients there were maintained reductions in these parameters after repeated doses. One patient treated at 68 mg/m^2 had a transient partial response even though there was no maintained reduction in tumour DCE-MRI parameters. Relative change in K^{trans} was significantly correlated with the AUC for the concentration of CA4. The marked heterogeneity of change within tumours together with significant reductions in v_e and increases in non-enhancing pixels suggest that local vascular shutdown within the tumour is the mechanism of action of tumour blood flow reduction after CA4P treatment.

CHAPTER 7 EFFECTS OF CA4P ON NORMAL TISSUE DCE-MRI PARAMETERS

7.1 Introduction

This chapter describes the changes seen on DCE-MRI examination in a range of normal tissues for the patients treated in the Phase I trial of CA4P. Technical difficulties associated with the use of DCE-MRI for this purpose are discussed. The reproducibility of the semi-quantitative parameters in kidney, liver and spleen, and the temporal patterns of change seen following CA4P in these tissues and in skeletal muscle are described.

7.2 Measurement of normal tissue blood flow with DCE-MRI

Measurement of CA4P effects on the microcirculation in a range of normal tissues is important to determine whether the changes described in Chapter 6 are tumour specific in patients, and whether the changes seen follow a similar pattern to that seen in pre-clinical models (Tozer *et al*, 1999). When other groups have evaluated response to other treatment modalities using DCE-MRI, normal tissue has often been sampled in order to evaluate the effect of the therapy on these tissues (Mayr *et al*, 1996; Su *et al*, 1996; Kovar *et al, 1998;* Padhani *et al*; 2000). Fat, skeletal muscle and bone marrow are frequently chosen as the normal tissues because of their wide body distribution and the intrinsic homogeneity in their anatomic structure. It has also been suggested that tumour kinetic DCE-MRI parameters normalised to reference normal tissues can be used to compensate for variations in physiological factors (e.g., cardiac output, blood pressure) that can alter kinetic parameter estimates (Evelhoch, 1999). This assumes that normal tissues have narrow ranges of intrinsic variability of kinetic parameter estimates, and that the treatment being monitored does not affect the reference tissue directly. In BD9 rats there were significant changes in skeletal muscle 6 hours after 100 mg/kg CA4P (Tozer *et al.*, 1999), so it was not felt appropriate to use this as a reference tissue for the clinical studies. The tissues chosen for analysis were kidney, liver, spleen and skeletal muscle.

There are several problems involved in the use of DCE-MRI to monitor changes in perfusion and permeability in normal tissues. The discussion below outlines these difficulties, and the reasons why a semi-quantitative parameter, initial AUC was chosen to monitor changes caused by CA4P in kidney, liver and spleen ROIs.

Firstly, as Gd-DTPA is concentrated and excreted by the kidneys, the compartmental model described in Chapter 4 cannot be used to measure kidney blood flow. After a few minutes there is concentration of Gd-DTPA in the collecting system, leading to a reduction in signal intensity due to an increase in local inhomogeneities in the magnetic field (T2* effects). This is illustrated in a time series of images in Figure 7.1, where signal loss in the renal medulla is seen after image 18, or about 3 minutes after contrast injection. Even if a ROI is drawn to just include renal cortex, avoiding the medulla and collecting region, the shape of the Gd-DTPA concentration-time curve has a large initial peak as shown in Figure 7.2, suggesting a large vascular volume fraction. If an arterial input function had been obtained it would be possible to estimate the size of this fraction, v_p as another parameter calculated from the model:

$$C_t(T) = K^{trans} \int_0^T C_p(t) e^{-k_{ep}(T-t)} dt + v_p C_p(t)$$

In the absence of a directly measured arterial input function use of such a term would merely increase the uncertainty and variability in the other parameters calculated from the model. The simpler semi-quantitative parameters, gradient and initial AUC do not make the assumptions of the model, and as they only take into account the first 90 seconds after bolus injection, the problem of signal loss at later times is avoided. Similarly the peak signal intensity in kidney was typically seen at around 60 seconds, so the initial AUC parameter should not be affected by the T2* effect.

The dual blood supply in liver, from the hepatic artery and the portal vein again presents problems for quantitative modelling of Gd-DTPA kinetics, and this tissue also has a higher vascular volume fraction than is assumed in the model. The values of initial AUC obtained from analysis of the Gd-DTPA concentration time curve for this tissue may well be different than other tissues with a similar blood flow due to this dual supply. Furthermore the variation of blood flow in the portal vein will affect the reproducibility of this parameter.

In the spleen the high vascular volume fraction again prevents use of the quantitative parameters. In addition, kidney, liver and spleen all move with respiration, causing problems due to motion artefact It was not feasible to use a breath hold technique with the sequence used for the dynamic scans, due to the duration of the dynamic series (6.5 minutes). The maximum signal enhancement after a bolus Gd-DTPA injection has been used by Su et al (Su *et al.*, 1996) in a study comparing the effects of angiotensin II, hydralazine and histamine on blood flow in kidney, liver, muscle and tumour

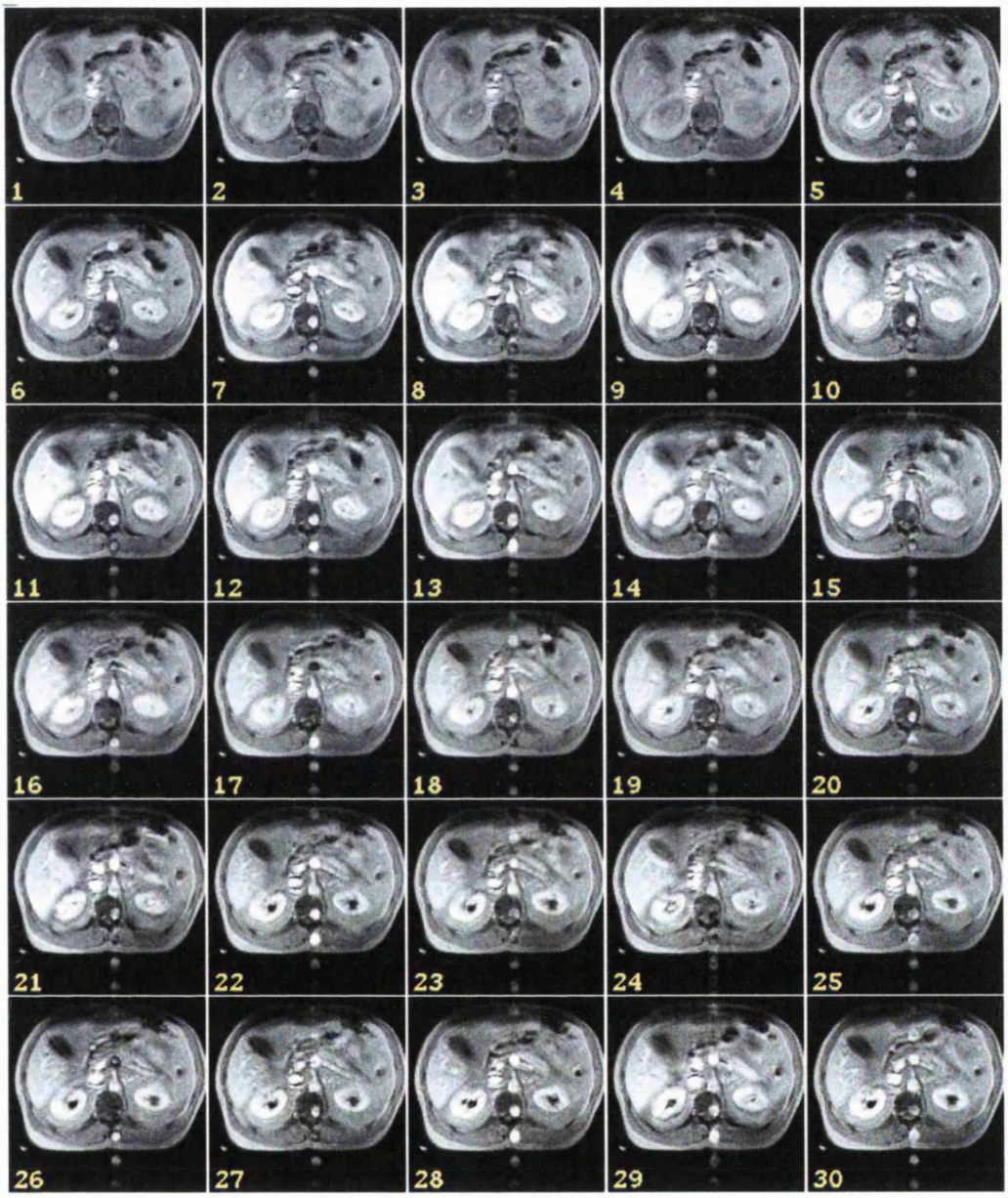

Figure 7.1 Dynamic series of T1 weighted axial images through kidney demonstrating loss of signal in the pelvicalyceal systems due high concentrations of Gd-DTPA producing T2* effects

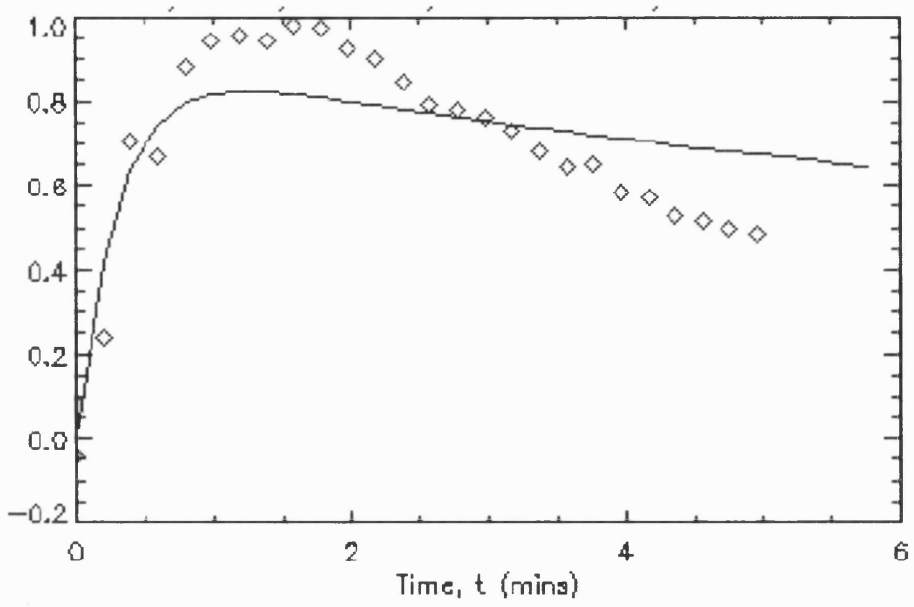

Figure 7.2 Gd-DTPA concentration time data (↓) for a kidney ROI, and estimated fitted curve using pharmacokinetic model described in Chapter 4. There is a poor fit of the observed data, probably due to a high vascular volume in this tissue

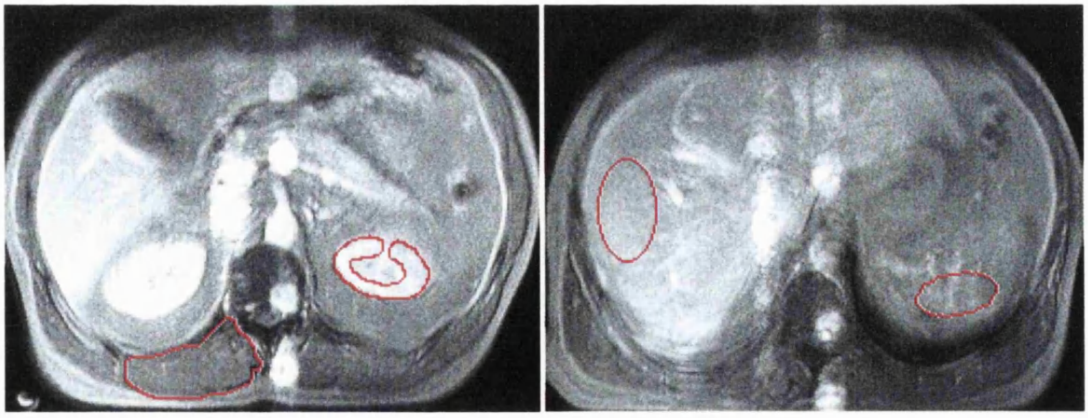

Figure 7.3 ROIs drawn in kidney, skeletal muscle (left), liver and spleen (right) for patient #30

in rats. They used a spin-echo sequence without cardiac or respiratory gating. Nevertheless, in 24 rats the standard deviation for maximum enhancement expressed as a percentage was 12%, 10%, 15% and 24% in kidney, liver, muscle and tumour respectively. This was a measure of the inter-animal variation, rather than the reproducibility of the parameter in the same animal, so the high variability in tumours is consistent with their known heterogeneity. Normalised signal enhancement after Gd-DTPA injection has also been used with an ECG gated turbo FLASH sequence as a measure of renal perfusion before and after dipyridamole stress (Tello *et al.*, 1996), with 3 second temporal resolution. Alternative methods for measuring kidney perfusion with MRI include arterial spin labelling sequences (Chen *et al.*, 1997b; Karger *et al.*, 2000). Some of these are liable to magnetic susceptibility artefacts in regions at the boundary between materials of different susceptibility such as air or bone-soft tissue interfaces. (Schenck, 1996).

Although it was not possible to use the quantitative model for kidney, liver or spleen for the reasons given above, the parameter initial AUC calculated from the Gd-DTPA concentration time curve data was chosen to assess normal tissue changes after CA4P treatment in liver, kidney and spleen. As discussed in Chapter 4 this parameter gives almost the same estimate of size of treatment effect in tumours after CA4P as K^{trans}. By using AUC from the Gd-DTPA concentration time curve rather than from the signal intensity time curve, the problem of dependence of signal enhancement on tissue T1 levels is avoided. The larger vascular contribution to the tissue Gd-DTPA concentration time curve in liver spleen and kidney, means that the initial AUC parameter in these tissues has a greater contribution from blood volume than in muscle or tumour. Thus the same DCE-MRI parameter in these different tissues reflects a different combination of blood flow, vessel permeability to Gd-DTPA and blood volume.

In skeletal muscle, resting blood flow is generally lower than that in tumours, therefore there will be a lower signal to noise ratio in this tissue, and greater variability in DCE-MRI parameters. However the vascular volume is low, avoiding the problems discussed above for kidney, liver and spleen. Analysis using the Tofts' pharmacokinetic model and the fully quantitative parameters was therefore still appropriate. Despite the lower signal to noise ratio, the reproducibility studies described in Chapter 5 indicate that reductions in muscle K^{trans} greater than 30% in a group of 16 patients or 50% in an individual would be statistically significant. Muscle ROIs were analysed using the quantitative kinetic parameters K^{trans}, k_{ep} and

v_e, as for tumour, but tumour AUC values were also obtained for the purposes of comparison with the other normal tissues.

7.3 Methods

The MRI protocol is described in Chapter 4. Not all of the above normal tissues were imaged in every patient, as a maximum of 5 slices was imaged, with slice positioning optimised for the tumour. ROIs in kidney were outlined around the perimeter of the cortex, to form a horse-shoe shape, thus excluding the medulla and the renal hilar vessels, and including at least 150 pixels, as illustrated in Figure 7.3. In liver an elliptical ROI was selected, avoiding obvious vascular structures and including at least 150 pixels. A similar sized ellipse was chosen in spleen, for those patients where this organ was imaged. Muscle ROIs were usually placed in paraspinal muscle as described in Chapter 4. All normal tissues were analysed on a whole ROI basis to improve the signal to noise ratio. Reproducibility analysis was performed as described in Chapter 5.

7.4 Results

7.4.1 Reproducibility studies

14 patients had paired pre-treatment examinations with kidney ROIs, 14 with liver ROIs and 5 with spleen ROIs. Two of the patients in the liver and kidney groups had a problem with contrast injection on one of the pre-treatment scans, and were excluded from the reproducibility analysis. Mean values for AUC pre-treatment for kidney, liver and spleen were 0.66, 0.61 and 0.83 respectively (compared with 0.27 for tumour). The results of the reproducibility analysis for these tissues are given in Table 7.1. As for tumour and muscle, there was no dependence of initial AUC on the mean parameter value, so analysis on the original scale was appropriate. The variability in kidney was greater than that in either liver or spleen, with wCVs of 19%, 15% and 10% respectively for AUC (compared with 16% and 26% for tumour and muscle). Changes in AUC in kidney of >0.09 (15%) in a group of 12, and 0.32 (52%) in individuals would be statistically significant. In liver, changes in AUC > 0.08 (12%) in a group of 12, or 0.28 (42%) in an individual would be significant. In spleen changes in AUC >0.10 (12%) in a group of 5, or 0.22 (27%) in an individual would be significant.

7.4.2 Effects of CA4P in normal tissues

The absolute and relative changes in AUC for kidney, liver and spleen 4 hours and 24 hours after the first dose of CA4P are shown in Figures 7.4 to 7.6. For the purposes of comparison

Tissue	Mean	Mean difference	95% CI for mean difference	wSD	wCV	Repeatability	Variance ratio
Liver	0.66	-0.02	+/-0.08 (12%)	0.10	15%	0.28	15*
Kidney	0.61	0.01	+/- 0.09 (15%)	0.12	19%	0.32	1.3
Spleen	0.83	0.10	+/- 0.10 (12%)	0.08	10%	0.22	6*

Table 7.1 Reproducibility of initial AUC calculated from Gd-DTPA concentration time curve for liver kidney and spleen: whole ROI analysis. CI = confidence interval, wSD = within patient Standard Deviation, wCV= within patient Coefficient of Variation, Repeatability = 2.77 x wSD and is the value of the 95% limit for the difference between 2 measurements on an individual, Variance ratio = ratio of between patient variance to within patient variance. ., * = $p<0.05$.

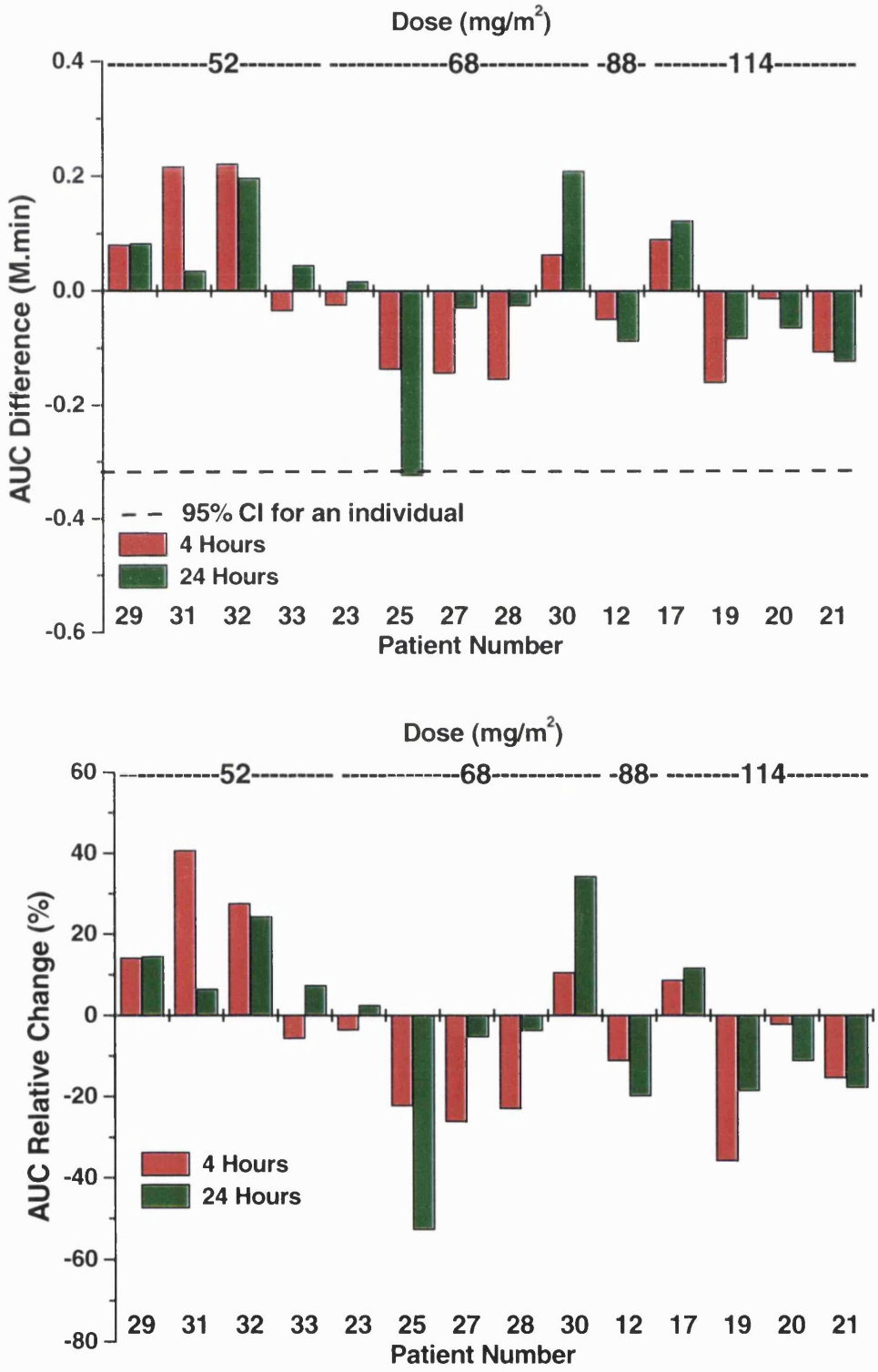

Figure 7.4 Absolute (top) and relative (bottom) change in AUC in kidney ROIs 4 and 24 hours after the first dose of CA4P.

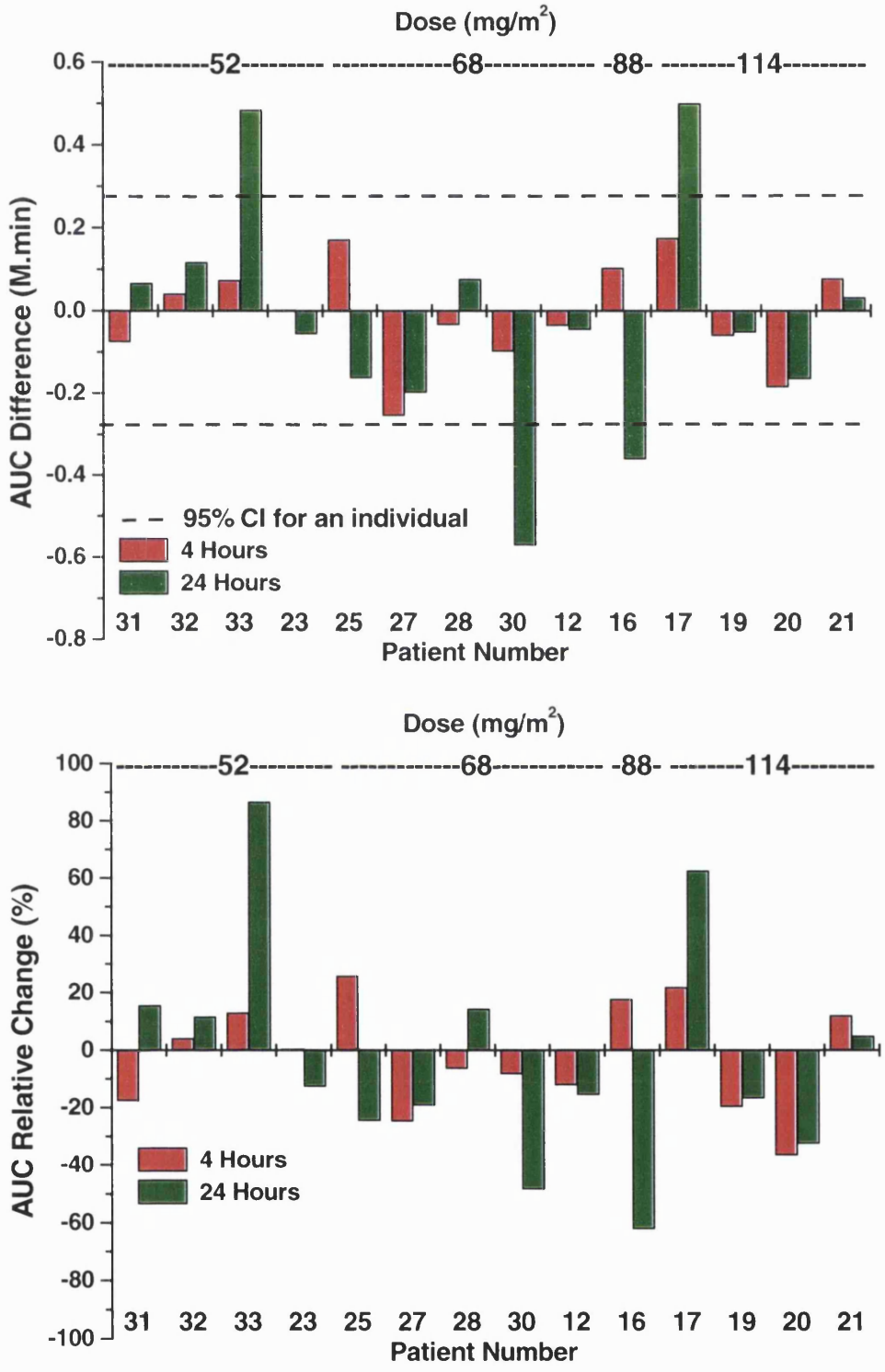

Figure 7.5 Absolute (top) and relative (bottom) change in AUC in liver ROIs 4 and 24 hours after the first dose of CA4P

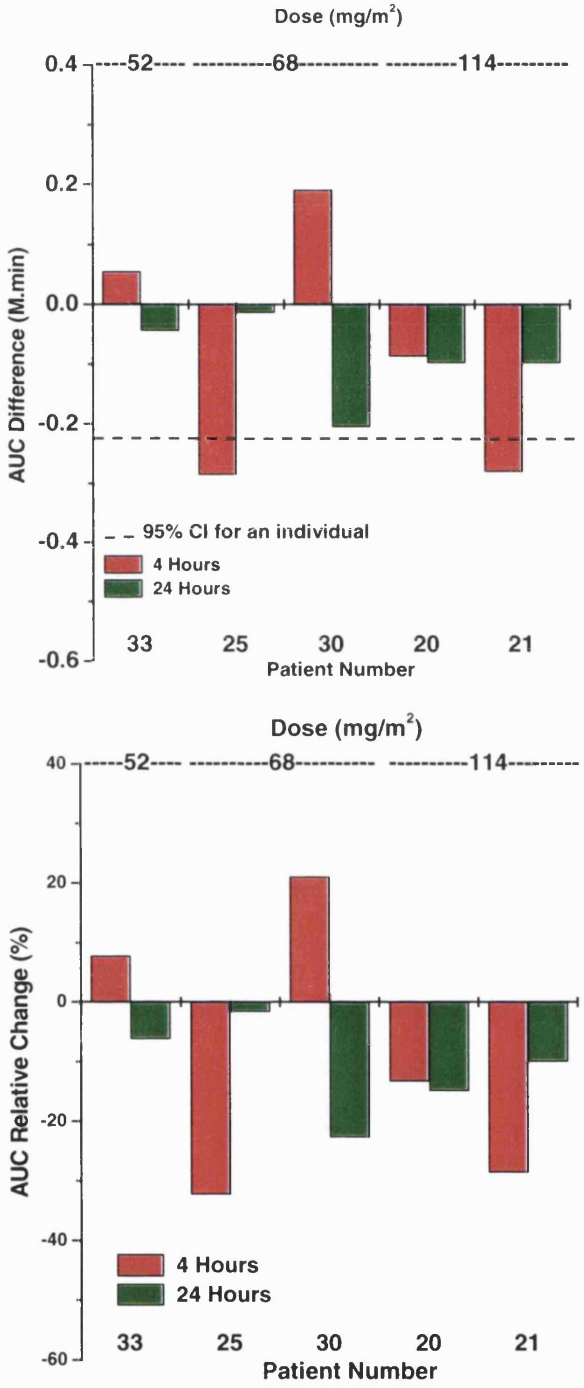

Figure 7.6 Absolute (top) and relative (bottom) change in AUC in spleen ROIs 4 and 24 hours after the first dose of CA4P.

changes in this parameter for the tumour ROIs are shown in Figure 7.7. As anticipated from the animal MRI study described in Chapter 4, the relative changes in AUC in tumour were generally smaller than those seen for K^{trans} described in Chapter 6. One patient (#25) treated at 68 mg/m^2 had a significant reduction in AUC of 0.32 (53%) at 24 hours in kidney, which was no longer significant 13 days after the third dose of CA4P, and was not associated with a rise in serum urea or creatinine. Two patients (#17 and 33) had significant increases in AUC in liver 24 hours after the first dose of CA4P, and 2 others (#16 and 30) had significant reductions at this time, one of whom (#30) had a maintained reduction 13 days after the third dose of CA4P. No associated changes in liver function tests were seen. Two patients (#21 and 25) had significant reductions in spleen AUC 4 hours after the first dose of CA4P, which were no longer significant at 24 hours.

Mean changes in AUC for kidney, liver and spleen for all the patients treated at ≥52 mg/m^2 are shown in Figure 7.8. There were no significant reductions in kidney, liver or spleen AUC at 4 or 24 hours after the first dose of CA4P, or 13 days after the third dose, and the maximal mean change in each tissue was around 10%. Even when patients treated at 68 to 114 or 88 to114 mg/m^2 were grouped together, there were still no significant mean changes in AUC in these tissues (data not shown).

Serial changes in AUC in tumour and normal tissue ROIs are shown in Figure 7.9 for the 5 patients who had 6 or more doses of CA4P. The patient with a maintained reduction in liver AUC after 3 doses (#30) had recovery of liver AUC to pre-treatment levels by 13 days after the sixth dose of CA4P. He also had a reduction in spleen AUC 24 hours after each dose, with later recovery, but no change in kidney AUC. None of the other patients in this group had maintained significant reductions in normal tissue ROIs. Patient #23 had a total of 24 doses of CA4P, without any significant reduction in kidney or liver AUC at the end of treatment.

Absolute and relative changes in K^{trans}, k_{ep} and v_e in muscle are shown in Figure 7.10 and 7.11. In contrast to the changes seen in tumour ROIs, there were no individuals with significant reductions in K^{trans} in muscle, although 1 had a significant increase (#31). One patient (#28) had a significant decrease in k_{ep}, and 2 had a significant increase (#25 and 31). Three patients had a significant decrease in v_e and 4 had significant increases. Thus there was no clear pattern of changes or obvious dose response as seen for tumour ROIs. The mean change in muscle parameters for all patients treated at ≥52mg/m^2 are shown in Figure 7.12. There was

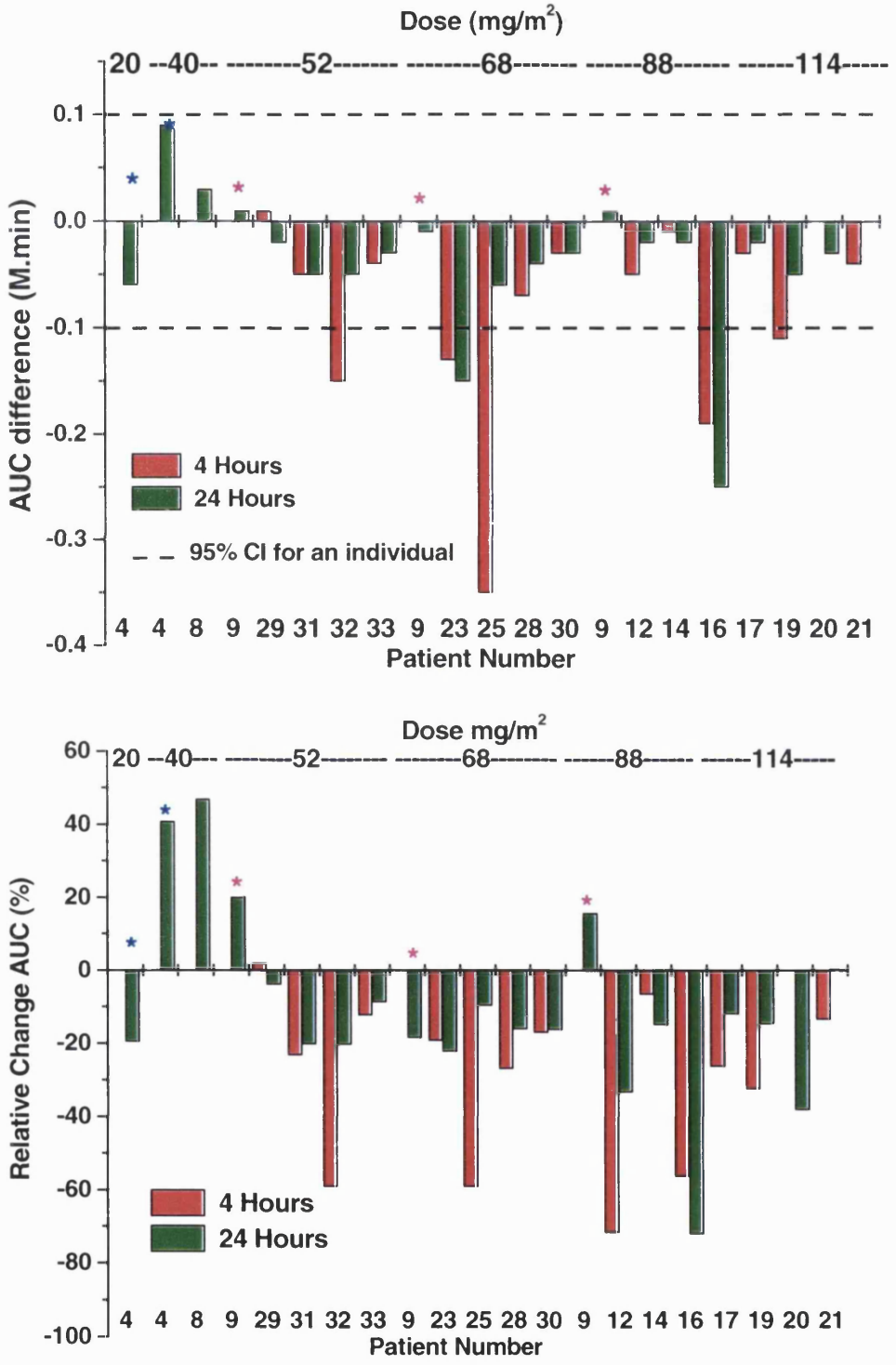

Figure 7.7 Absolute (top) and relative (bottom) change in AUC in tumour ROIs 4 hours and 24 hours after the first dose of CA4P. * indicates patients treated at more than one dose level

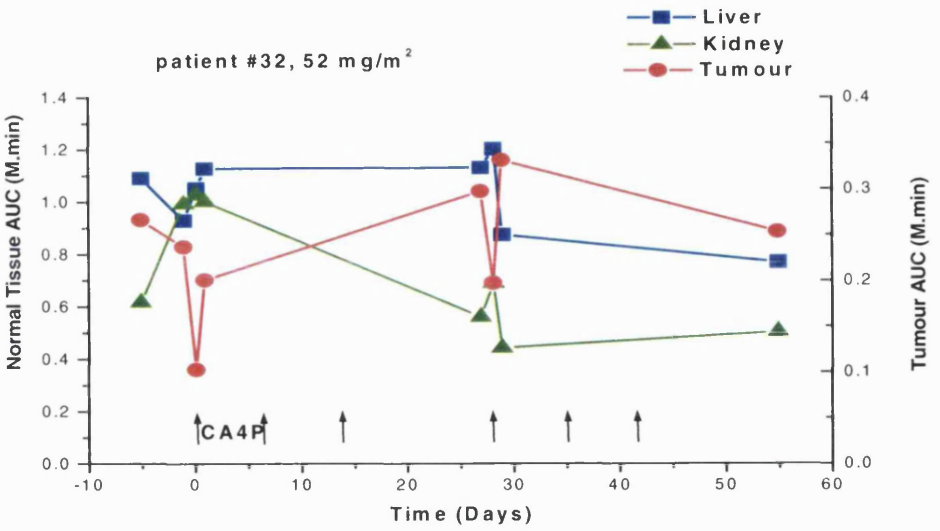
patient #32, 52 mg/m²
Liver
Kidney
Tumour
Normal Tissue AUC (M.min)
Tumour AUC (M.min)
CA4P
Time (Days)

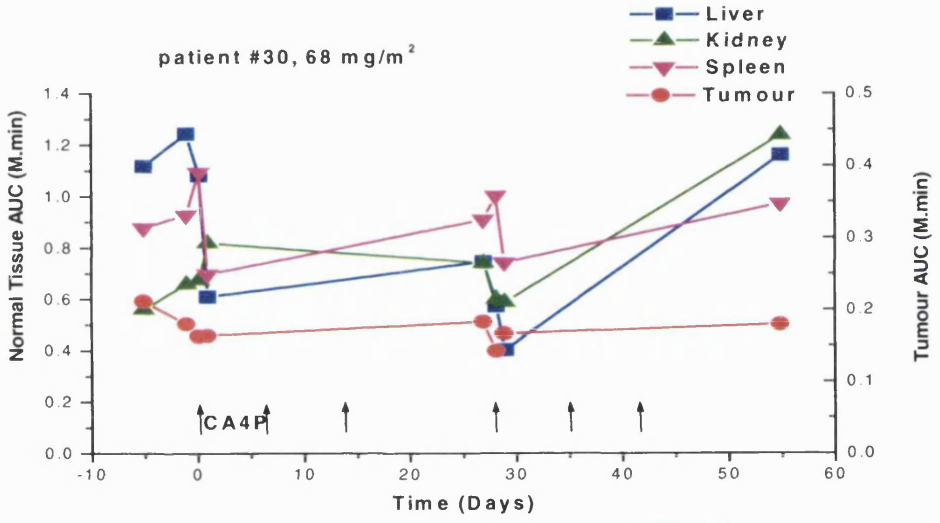
patient #30, 68 mg/m²
Liver
Kidney
Spleen
Tumour
Normal Tissue AUC (M.min)
Tumour AUC (M.min)
CA4P
Time (Days)

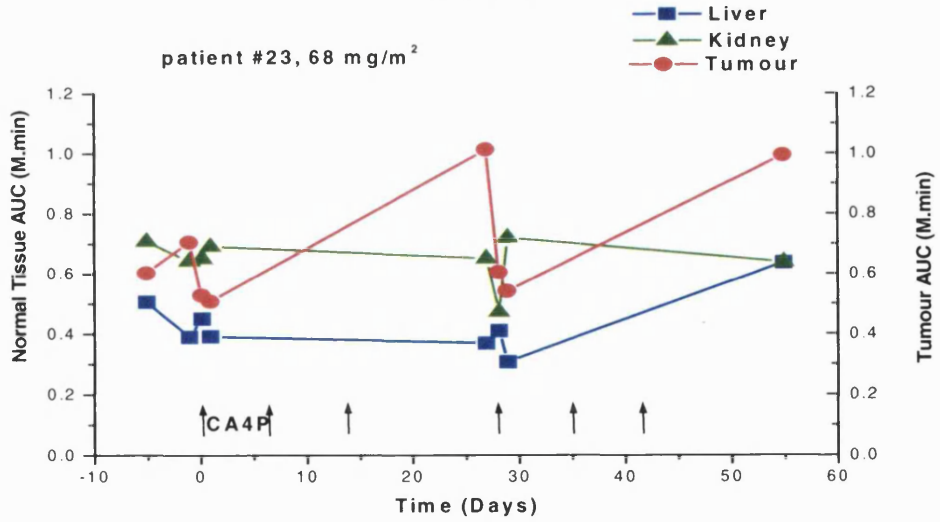
patient #23, 68 mg/m²
Liver
Kidney
Tumour
Normal Tissue AUC (M.min)
Tumour AUC (M.min)
CA4P
Time (Days)

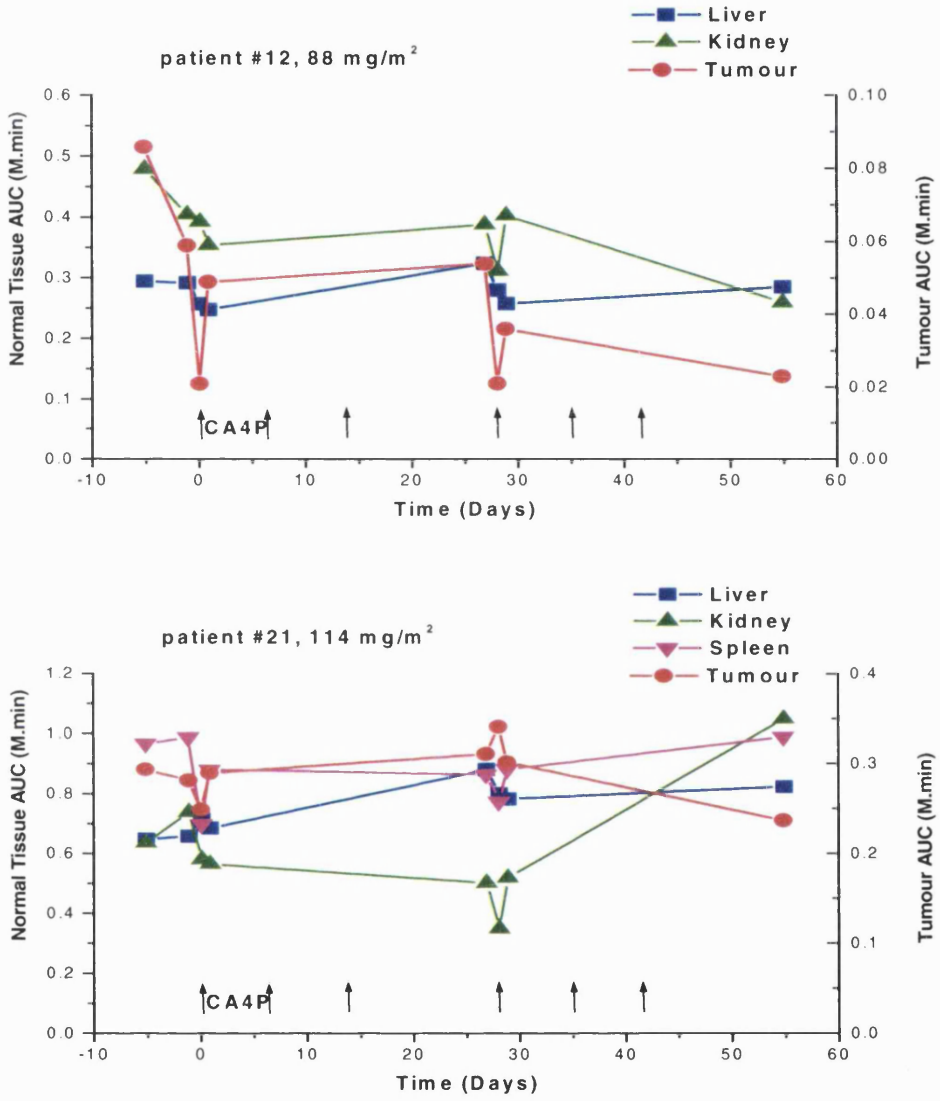

Figure 7.8 Serial changes in AUC for tumour and normal tissue ROIs in 5 patients who completed 2 cycles (6 infusions) of CA4P

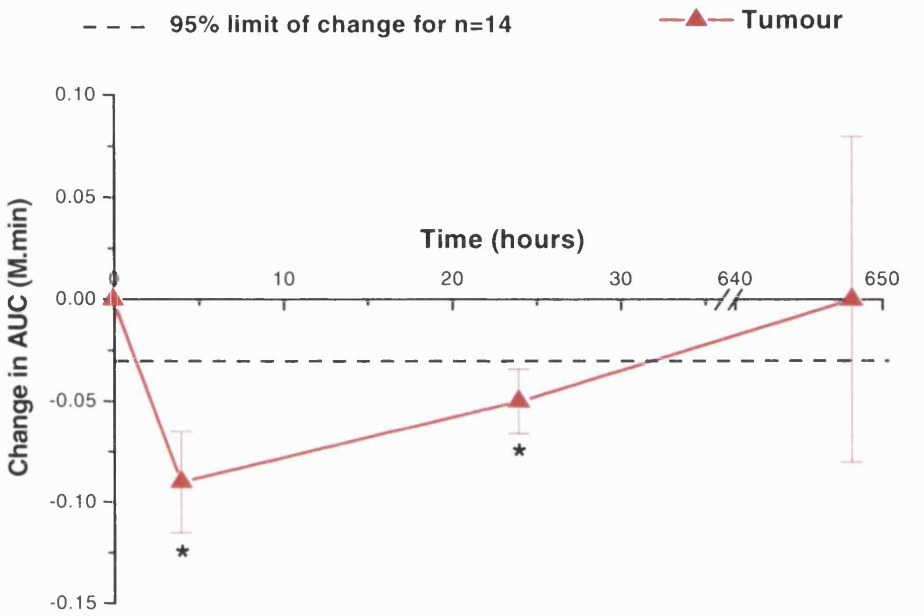
95% limit of change for n=14
Tumour
Change in AUC (M.min)
0.10
0.05
0.00
-0.05
-0.10
-0.15
Time (hours)
0
10
20
30
640
650
*
*

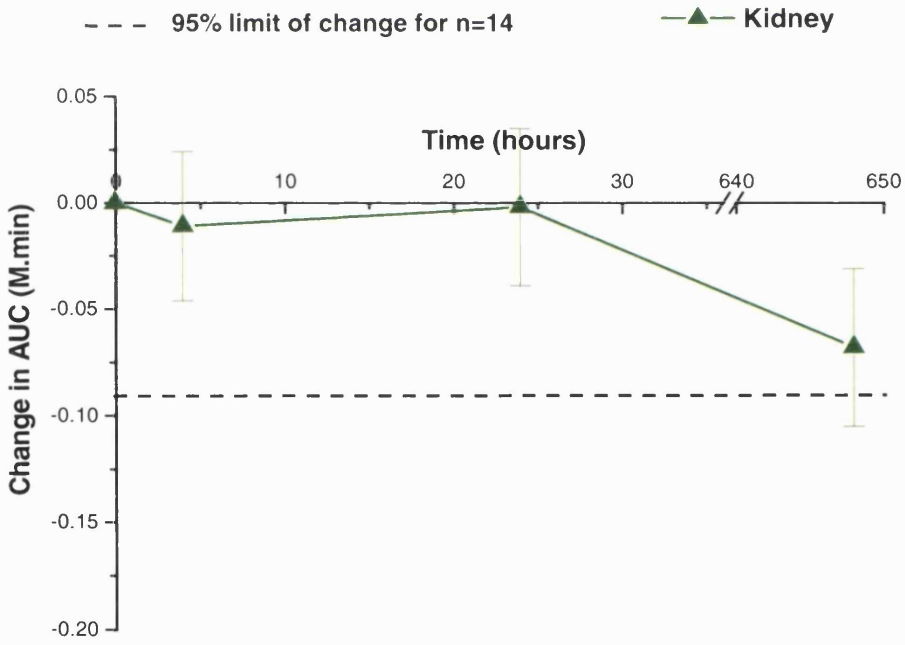
95% limit of change for n=14
Kidney
Change in AUC (M.min)
0.05
0.00
-0.05
-0.10
-0.15
-0.20
Time (hours)
0
10
20
30
640
650

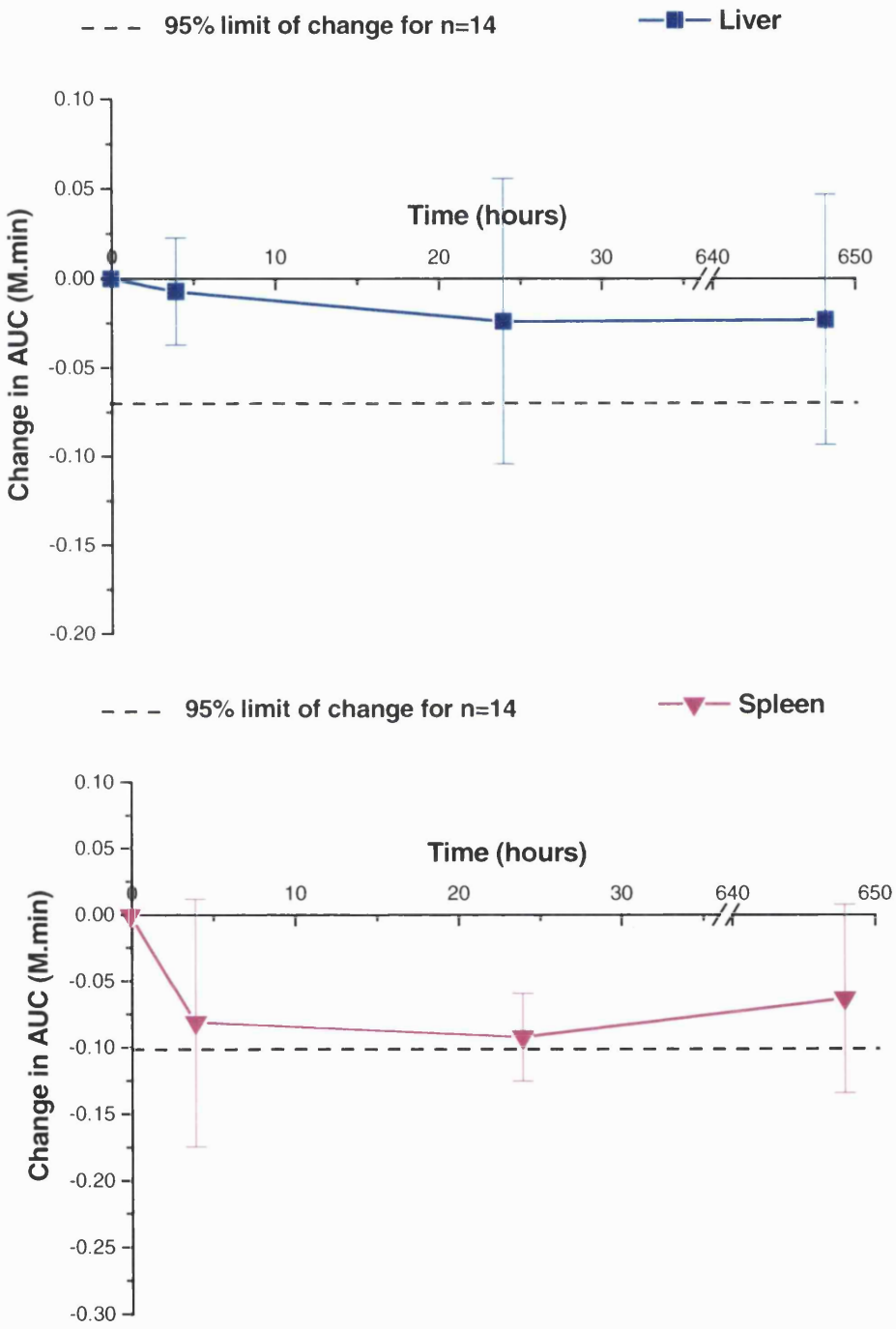

Figure 7.9 Mean changes in AUC for patients treated ≥52 mg/m².
*= significant change, p<0.05

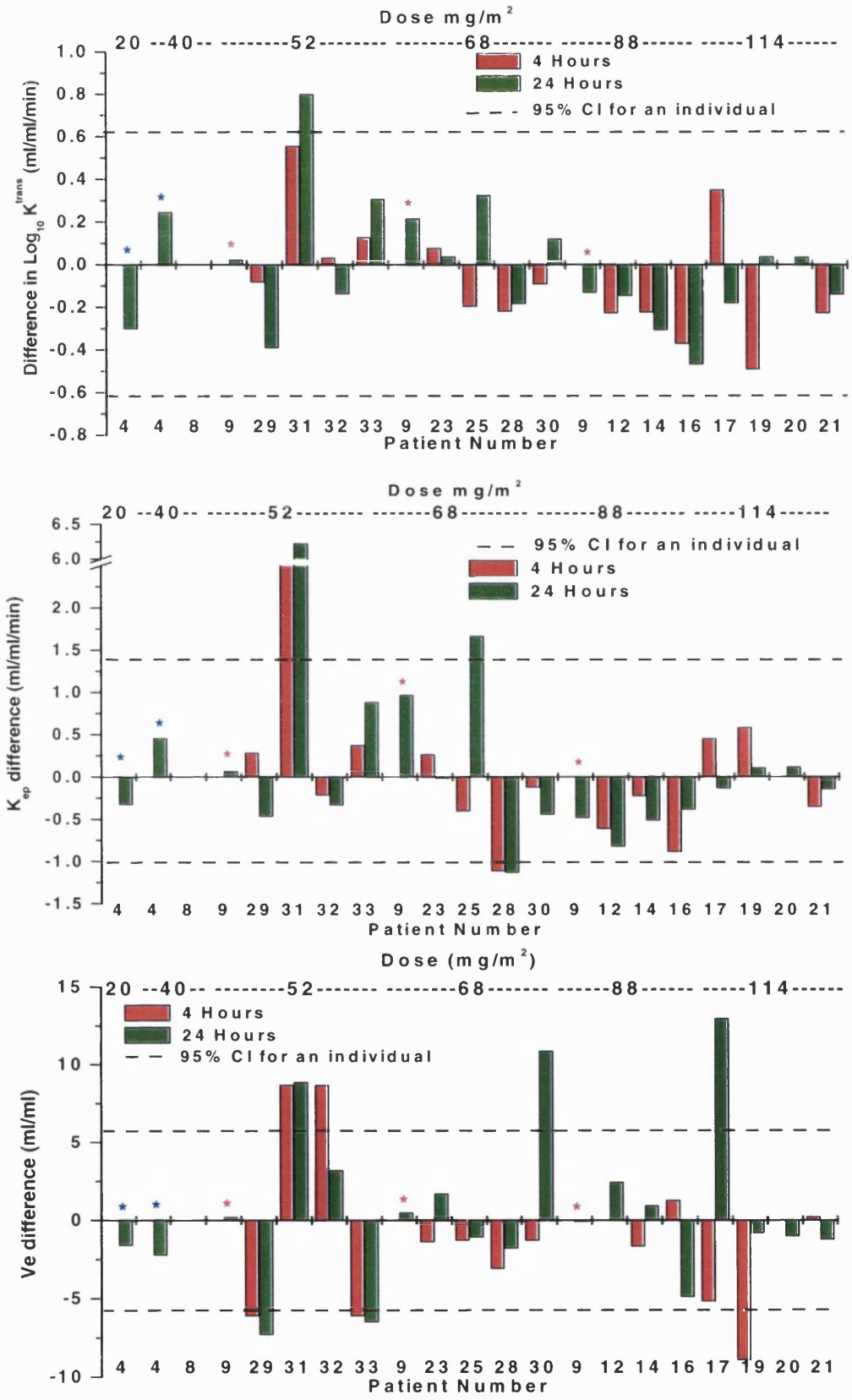

Figure 7.10 Absolute change in $Log_{10} K^{trans}$ (top), k_{ep} (middle) and v_e (bottom) 4 hours and 24 hours after the first dose of CA4P for muscle ROIs. CI = confidence interval. * indicates patients treated at more than one dose level

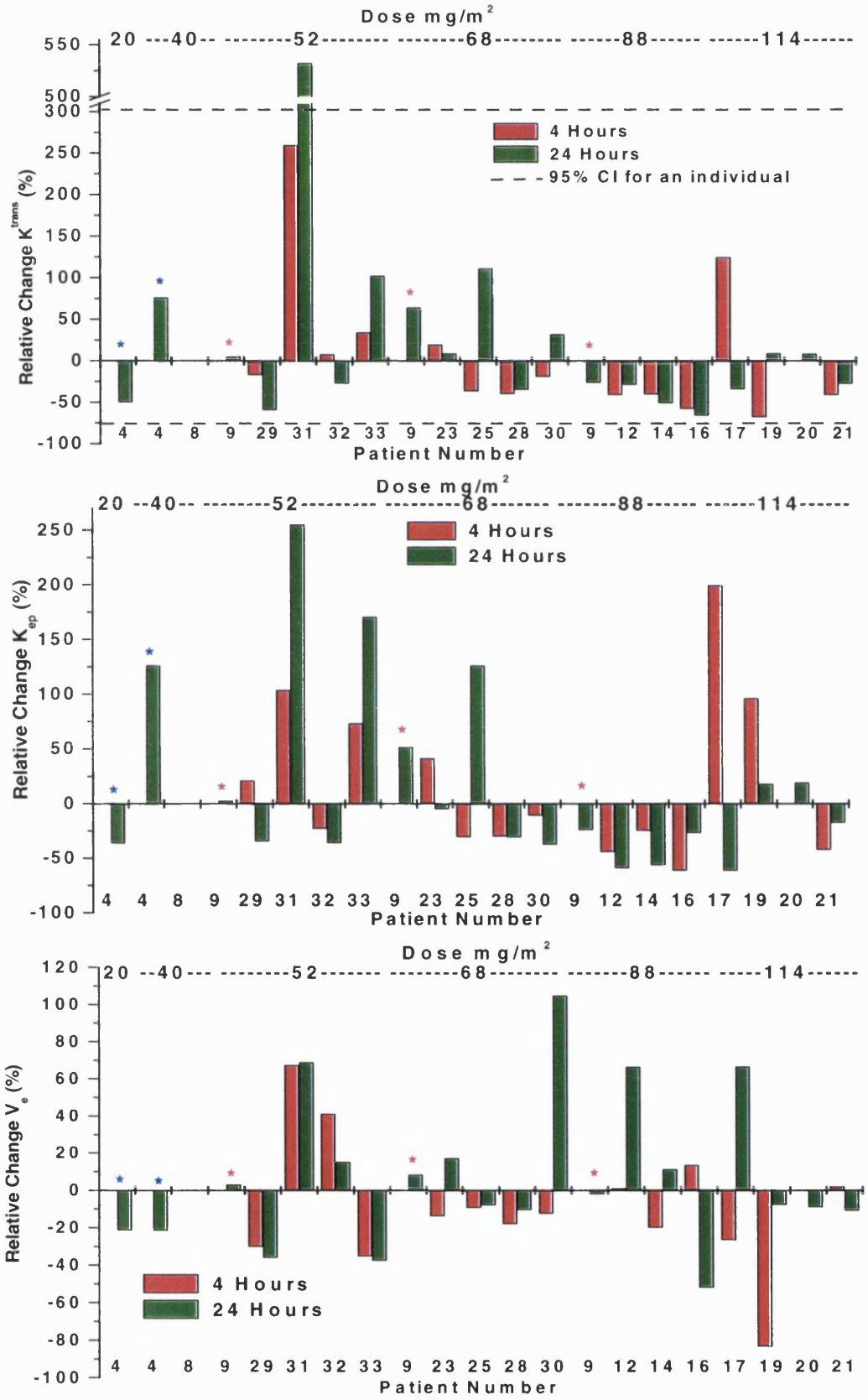

Figure 7.11 Relative changes in DCE-MRI parameters at 4 hours and 24 hours after the first dose of CA4P for muscle ROIs

*indicates patients treated at more than one dose level

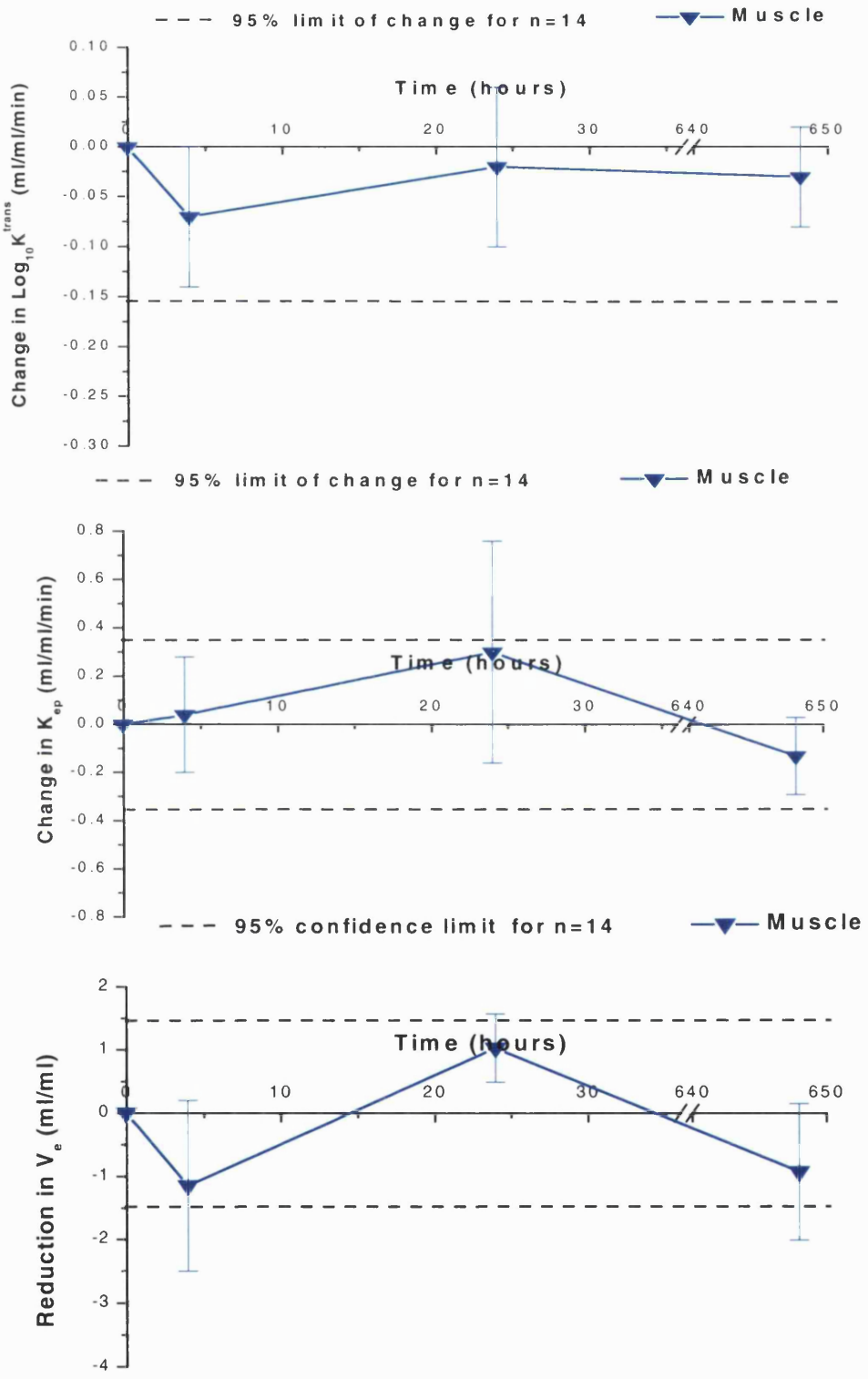

Figure 7.12 Mean changes in DCE-MRI parameters at 4 hours and 24 hours after the first dose of CA4P and 13 days after the third dose for all patients treated at ≥52 mg/m².

no significant change in any parameter at any time point for muscle ROIs. Even when the group of patients at 88 and 114 mg/m^2 was considered separately, there was no significant change in any parameter (data not shown).

7.5 Discussion

These results show that consistently significant reductions in DCE-MRI parameters were not seen in kidney, liver, spleen or resting skeletal muscle at doses of CA4P from 52 to 114 mg/m^2, in contrast to the significant reductions seen in tumour ROIs. This provides evidence that the vascular shutdown produced by CA4P is relatively selective for tumour vasculature in humans, and is consistent with the tumour selective action seen in animal models (Tozer *et al.*, 1999). Nevertheless, there was some evidence for variable reduction in DCE-MRI parameters in normal tissues. A small proportion of patients had significant transient reductions in AUC in kidney and liver (1 of 14 and 2 of 14 respectively). The group of patients for whom measurements in spleen were obtained was small and 2 of these 5 patients had significant changes at 4 hours after CA4P treatment Only 1 patient had a maintained reduction in liver AUC, with no associated clinical consequences. Blood flow assessments were not made in brain, the tissue associated with dose-limiting toxicity.

In BD9 rats bearing P22 carcinosarcomas there were significant but small reductions in blood flow in spleen, skin, skeletal muscle and brain 6 hours after CA4P 100 mg/kg (Tozer *et al.*, 1999), with the largest changes (6-fold) seen in spleen. No changes were seen in kidney or heart at this dose and time. At 10 mg/kg however, >90% blood flow reduction was still seen in tumour and 40% reduction in spleen at 6 hours, but there were no longer significant reductions in blood flow in brain or skeletal muscle (personal communication, Dr G. Tozer). The changes seen in patients therefore correspond to the lower end of the dose range tested in animal models. Blood flow in skeletal muscle was still reduced at the earlier time of 1 hour, with an associated increase in its vascular resistance. The time course of increase in vascular resistance in skeletal muscle corresponded to that for the rise in blood pressure. As the skeletal muscle is the major determinant of peripheral vascular resistance, this may therefore explain the blood pressure rise.

The patients treated at the Hammersmith Hospital who had PET imaging, also had measurable effects on kidney and spleen blood flow. At doses of 40 mg/m2 and above significant changes in perfusion were observed in spleen ranging from 2% to -58% and in kidney ranging from -2% to 63% at 30 minutes to 1 hour after the first dose of CA4P, but

were not maintained at 24 hours (Anderson, 2000). At this early time point there were also significant reductions in kidney and spleen blood volume. Not all patients treated had reductions in normal tissue blood flow, in agreement with the DCE-MRI results. The discrepancy between the results from the Hammersmith patients and the DCE-MRI data may be related to the earlier observation point in the PET experiments. It is possible that a higher proportion of patients may have had significant reductions in normal tissue blood flow at the early time points, which recovered by 4-6 hours after treatment. The lack of changes seen at 24 hours is consistent with the MRI results at this time.

Despite the theoretical problems with modelling DCE-MRI parameters in these tissues, the semi-quantitative parameter AUC gives reasonably reproducible results in kidney, liver and spleen for small groups of patients. Mean changes in AUC greater than 10-15% would be significant in the size of groups studied. However, it is possible that changes in AUC underestimate the actual changes in normal tissue blood flow, due to the contribution of vessel permeability and vascular volume to this parameter.

Although the mean reductions in AUC were not significant in normal tissues, a few patients had large (50-60%) relative reductions in kidney or liver AUC at some time points. The consequences of such reductions in blood flow in these tissues may well be different from similar sized reductions in tumour. As discussed in Chapter 1, many areas of tumour are hypoxic before treatment, whereas this is unusual in normal tissues, especially those with relatively high blood flow such as kidney, liver and spleen. A 30 to 40% reduction in tumour blood flow, even if it were even across the tumour might well induce hypoxic areas to become necrotic. Further injury to tumour tissue will occur on reperfusion (Parkins *et al.*, 1995), and neutrophil infiltration may also contribute to tumour cell death (Parkins *et al.*, 2000). In contrast >50% reduction in kidney blood flow has been observed at the end of a period of vigorous exercise, which illustrates that the changes observed in this study and with PET imaging, are within the physiological range of the kidney. Even with this level of reduction, kidney blood flow still far exceeds that of most tumours, and as it is more homogeneously distributed across the kidney, tissue damage due to ischaemia would not be expected. Providing that such changes are not maintained over a prolonged period, sustained effects on renal function would not be anticipated either, and there was no evidence for such effects even in the patient who had a 53% reduction in renal AUC 24 hours after the first dose of CA4P.

7.6 Summary

There is evidence from these DCE-MRI studies of tumour specificity for the action of CA4P. A small proportion of patients had significant reductions in some normal tissues, which were not associated with any adverse clinical events.

CHAPTER 8 CONCLUDING DISCUSSION

The results presented in this thesis demonstrate that

- The assay of endothelial cell shape change after CA4P treatment shows a time course that is more relevant to the *in vivo* vascular shutdown in tumours than assays of anti-proliferative activity, and endothelial cells are more sensitive to this action than smooth muscle cells or fibroblasts

- The rate of recovery from these changes in cell shape allows discrimination between tubulin-binding drugs with a wide or narrow therapeutic window for vascular targeting activity. Differential sensitivity of proliferating and confluent endothelial cells is seen with all the microtubule depolymerising agents tested

- Tumour K^{trans} changes after CA4P accurately estimate the level of blood flow reduction produced in tumour in a rat model

- DCE-MRI parameters are reasonably reproducible within patients, so that changes of clinical significance can be detected in individuals or in groups of patients. The limits of reproducibility in a range of tissues have been determined

- CA4P produces significant decreases in K^{trans} in tumours at well tolerated doses at 4 and 24 hours after the first dose. The decreases are maintained in some patients after repeated doses. Reductions in v_e in tumours support the hypothesis that CA4P causes local vascular shutdown in tumours

- There were no mean reductions in DCE-MRI parameters in kidney, liver, spleen or skeletal muscle. A small proportion of patients had significant reductions in DCE-MRI parameters in these tissues. The reductions were generally not maintained and had no adverse clinical consequences

One of the aims of the Phase I trial – to see if significant reductions in tumour blood flow after CA4P could be detected at tolerable doses has therefore been achieved. Despite the lack

of tumour regression in pre-clinical studies when CA4P is used alone, there are several demonstrating enhanced efficacy when the drug is used in combination with chemotherapy and radiotherapy (Chaplin *et al.*, 1999; Grosios *et al.*, 2000; Horsman *et al.*, 2000; Li *et al.*, 1998). The challenge is now to determine the anti-tumour efficacy of this drug when incorporated with conventional anti-cancer therapy in patients, and to optimise the scheduling of the combinations. These pre-clinical studies have shown no detrimental effect of CA4P induced blood flow reduction on the efficacy of subsequent radiotherapy. This may be because the dose of CA4P used in the animal models were sufficient to cause >95% blood flow reduction, and extensive necrosis in the central regions of the tumours. The previously hypoxic areas of the tumour, which would be relatively insensitive to radiation treatment, have therefore been killed by vascular shutdown. The concern in human tumours would be that such an extensive reduction in blood flow was not seen in all patients at tolerable doses, so some areas of the tumour may be made hypoxic rather than necrotic after CA4P, and therefore more radioresistant. One strategy to overcome this might be to incorporate the CA4P on the last day of radiotherapy in each week, giving the weekend to recover blood flow in those areas where necrosis was not induced. Such strategies should be tested in pre-clinical models, perhaps using lower doses of CA4P to mimic the level of blood flow reduction seen in the clinical studies, or in tumour models such as the HT29, which are relatively resistant to the action of CA4P.

The optimal scheduling of the combination of CA4P with chemotherapy also presents challenges. Pre-clinical studies have shown no difference in effect whether chemotherapy was given before or after CA4P, which may again relate to the dose at which such studies were performed. Doses which produce smaller changes in tumour blood flow, might show a timing effect in combination, possibly due to increased trapping of the chemotherapy agent in the tumour tissue if CA4P is given after the chemotherapy agent, or due to hypoxic areas in tumour affecting the drug's activity. In a murine colorectal xenograft model combining DMXAA with radioimmunotherapy (RIT) there was a clear effect of timing, with RIT treatment given 48 hours before DMXAA proving optimal for improved trapping of the radioisotope in the tumour (Pedley *et al.*, 1996). This combination produced complete tumour cures in 5 of 6 mice. Similar efficacy has been seen after combination with CA4P (Pedley *et al.*, 2000).

DCE-MRI could be used in the further clinical development of CA4P, in the monitoring of effects of combination therapy on tumour physiology, and also for the selection of patients

who might gain greater benefit from combination therapy. For example, patients could have a single dose of CA4P, with monitoring of effect on blood flow, and only those with a >45% reduction in K^{trans} would proceed to combination treatment the following week. This would inevitably affect the rate of patient accrual, but would also reduce the number of patients suffering side effects of the combination for no added benefit.

Improvements in the reproducibility of DCE-MRI technique might be achieved by use of a mechanical power injector, which has now been purchased, and the development of a sequence to allow non-invasive acquisition of an individual arterial input function for each MRI examination. Work on this sequence is in progress. Further reproducibility studies will be required once these changes have been implemented, which are likely to enhance the sensitivity of the technique in detecting individual patients with significant changes in tumour blood flow. Such studies have been planned as part of a protocol designed to examine whether acute changes in tumour blood flow are detectable at 4 or 24 hours after conventional chemotherapy agents such as doxorubicin.

In addition, high molecular weight MR contrast agents will be clinically available in the next 12 months, which act as blood pool agents, enabling determination of blood volume and permeability. It will then be possible to perform dual contrast agent studies, with Gd-DTPA given initially during a dynamic examination with high temporal resolution, followed by a further dynamic series using the blood pool agent at a later time. If arterial input functions are obtained, the residual Gd-DTPA from the first study can be accounted for in the latter (Su *et al.*, 1998). The ability to more clearly separate the measurements of microvessel permeability, perfusion and blood volume will also be useful in determining the effects of vascular targeting agents on these different physiological aspects in human tumours, as has been done in pre-clinical models (Kanthou *et al.*, 2001).

Other methods for examining the mechanism of action of CA4P *in vivo* would be useful, such as methods for determining whether endothelial call shape change is measurable *in vivo*, perhaps using electron microscopy. Determination of interstitial fluid pressure (IFP) changes within tumours treated with CA4P would also help to confirm whether an acute increase in IFP is indeed involved in the process of vascular shutdown.

The cell shape change assay, and determination of recovery rate look promising for providing an *in vitro* assay for novel vascular targeting agents. The lack of such an assay has been a barrier to the rapid expansion of this area of drug development. Further evaluation with a

range of drugs with varying *in vivo* therapeutic windows would be required to validate this suggestion. The assay would be more practically useful if the process of cell outlining could be automated, and work on this has been done by Dr Paul Barber of the Advanced Technology Group in the Gray Laboratory. If the recovery rate is determined by the kinetics of binding and dissociation from tubulin, it might be possible to establish 'optimal' kinetics for vascular targeting drugs, allowing more rapid screening of novel compounds. However, comparison of relative toxicities of vinca alkaloids suggests that lipophilicity might also affect elimination half-life, due to drug retention in membranes (Donoso *et al.*, 1977; Ferguson & Cass, 1985), so a tubulin-binding assay may not give all the information required to evaluate a drug's potential.

Further elucidation of the process of endothelial cell shape change induced by tubulin-binding agents and the cell signalling processes involved might identify novel targets for vascular targeting drugs, or strategies for further improving the therapeutic window for these agents. For example, the GTP-binding protein Rho kinase mediates phosphorylation of myosin light chain, and it has already been shown that inhibition of this enzyme reduces HUVEC contraction and permeability changes after CA4P treatment (Kanthou *et al.*, 2001). There is also evidence that nitric oxide influences tyrosination of tubulin, which may affect the sensitivity to tubulin-binding agents. Nitric oxide levels in tumours have already been shown to have an important influence on the effects of CA4P, with the addition of nitric oxide synthase (NOS) inhibitors demonstrated to improve the therapeutic window *in vivo* (Tozer *et al.*, 1999). The role of nitric oxide on CA4P responses *in vitro*, and its influence on tubulin depolymerisation is the subject of further work within the Tumour Microcirculation Group.

The above discussion illustrates the need for further work on the development of vascular targeting agents, studies to more closely examine their effects on tumour and normal tissue vascular physiology, and further improvements in non-invasive techniques to monitor their effects in patients. Results from such work might allow more informed decisions about the optimal way to integrate them into the conventional anti-cancer armoury. This need for integration of work *in vitro*, *in vivo* and in the clinic has made this project an extremely interesting one on which to work.

REFERENCES

Abdulrauf, S., Edvardsen, K., Ho, K., Yang, X., Rock, J. & Rosenblum, M. (1998). Vascular endothelial growth factor expression and vascular density as prognostic markers of survival in patients with low-grade astrocytoma. *J Neurosurg*, **88,** 513-20.

Abramovitch, R., Dafni, H., Smouha, E., Benjamin, L. & Neeman, M. (1999). In vivo prediction of vascular susceptibility to vascular susceptibility endothelial growth factor withdrawal: magnetic resonance imaging of C6 rat glioma in nude mice. *Cancer Res*, **59,** 5012-6.

Acker, J.C., Dewhirst, M.W., Honore, G.M., Samulski, T.V., Tucker, J.A. & Oleson, J.R. (1990). Blood perfusion measurements in human tumours: evaluation of laser Doppler methods. *Int J Hyperthem*, **6,** 287-304.

Albrecht, T., Blomley, M.J., Cosgrove, D.O., Taylor-Robinson, S.D., Jayaram, V., Eckersley, R., Urbank, A., Butler-Barnes, J. & Patel, N. (1999). Non-invasive diagnosis of hepatic cirrhosis by transit-time analysis of an ultrasound contrast agent. *Lancet*, **353,** 1579-83.

Alberts, B, Bray, D, Lewis, J, Raff, M, Roberts, K, Watson, JD (1994) *Molecular biology of the cell.* Third Ed. Chapter 16 The Cytoskeleton. Garland Publishing Inc. New York

Algire, G., Legallis, F. & Anderson, B. (1954). Vascular reactions of normal and malignant tissues in vivo: VI The role of hypotension in the actions of components of podophyllotoxin on transplanted sarcomas. *J Natl Cancer Inst*, **14,** 879.

Amos, L. & Amos, W. (1991). *Molecules of the cytoskeleton.* Guilford Press: New York.

Andersen, A. (1989). 99mTc-D,L-hexamethylene-propyleneamine oxime (99mTc-HMPAO): basic kinetic studies of a tracer of cerebral blood flow. *Cerebrovasc Brain Metab Rev*, **1,** 288-318.

Anderson, H., Jap, J. & Price, P. (2000). Measurement of tumour and normal tissue perfusion by positron emission tomography in the evaluation of antivascular therapy: results in the Phase I trial of combretastatin A4 phosphate. *Proc Am Soc Clin Oncol.*

Andreu, J.M. & Timasheff, S.N. (1982). Conformational states of tubulin liganded to colchicine, tropolone methyl ether, and podophyllotoxin. *Biochemistry*, **21,** 6465-76.

Arap, W., Pasqualini, R. & Ruoslahti, E. (1998). Cancer treatment by targeted drug delivery to tumour vasculature in a mouse model. *Science*, **279,** 377-380.

Au, J., Li, D., Gan, Y., Gao, X., Johnson, A., Johnston, J., Millenbaugh, N., Jang, S., Kuh, H., Chen, C. & Wientjes, M. (1998). Pharmacodynamics of immediate and delayed effects of paclitaxel: role of slow apoptosis and intracellular drug retention. *Cancer Res*, **58,** 2141-8.

Avila, J. (1992). Microtubule functions. *Life Sci*, **50,** 327-34.

Baba, Y., Furusawa, M., Murakami, R., Yokoyama, T., Sakamoto, Y., Nishimura, R., Yamashita, Y., Takahashi, M. & Ishikawa, T. (1997). Role of dynamic MRI in the evaluation of head and neck cancers treated with radiation therapy. *Int J Radiat Oncol Biol Phys*, **37,** 783-7.

Baguley, B.C., Holdaway, K.H., Thomsen, L.L., Zhuang, L. & Zwi, L. (1991). Inhibition of growth of colon 38 adenocarcinoma by vinblastine and colchicine: evidence for a vascular mechanism. *Eur J Cancer*, **27,** 482-487.

Baguley, B.C., Zhuang, L. & Kestell, P. (1997). Increased plasma serotonin following treatment with flavone-8-acetic acid, 5,6-dimethylxanthenone-4-acetic acid, vinblastine, and colchicine: relation to vascular effects. *Oncol Res*, **9,** 55-60.

Banerjee, A. & Luduena, R.F. (1992). Kinetics of colchicine binding to purified beta-tubulin isotypes from bovine brain. *J Biol Chem*, **267,** 13335-9.

Barbee, K.A. (1995). Changes in surface topography in endothelial monolayers with time at confluence: influence on subcellular shear stress distribution due to flow. *Biochem Cell Biol*, **73,** 501-5.

Baxter, L.T. & Jain, R.K. (1989). Transport of fluid and macromolecules in tumors. I. Role of interstitial pressure and convection. *Microvasc Res*, **37,** 77-104.

Baxter, L.T. & Jain, R.K. (1990). Transport of fluid and macromolecules in tumors. II. Role of heterogeneous perfusion and lymphatics. *Microvasc Res*, **40,** 246-63.

Bayssas, M., Gouveia, J., de Vassal, F., Misset, J.L., Schwarzenberg, L., Ribaud, P., Musset, M., Jasmin, C., Hayat, M. & Mathe, G. (1980). Vindesine: a new vinca alkaloid. *Rec Res Cancer Res*, **74,** 91-7.

Beaney, R.P., Lammertsma, A.A., Jones, T., McKenzie, C.G. & Halnan, K.E. (1984). Positron emission tomography for in-vivo measurement of regional blood flow, oxygen utilisation, and blood volume in patients with breast carcinoma. *Lancet*, **1,** 131-4.

Beauregard, D., Hill, S., Chaplin, D. & Brindle, K. (2000). Vascular permeability is correlated with susceptibility to

combretastatin A4 phosphate in four tumor models. *Proc Int Soc Magn Res Med*, 11, Sydney.

Beauregard, D.A., Thelwall, P.E., Chaplin, D.J., Hill, S.A., Adams, G.E. & Brindle, K.M. (1998). Magnetic resonance imaging and spectroscopy of combretastatin A4 prodrug-induced disruption of tumour perfusion and energetic status. *Br J Cancer*, **77**, 1761-7.

Beavon, I. (1999). Regulation of E-cadherin: does hypoxia initiate the metastatic cascade? *Mol Pathol*, **52**, 179-88.

Beck, I., Ramirez, S., Weinmann, R. & Caro, J. (1991). Enhancer element at the 3'-flanking region controls transcriptional response to hypoxia in the human erythropoietin gene. *J Biol Chem*, **266**, 15563-6.

Belfi, C.A., Ting, L.L., Hassenbusch, S.J., Tefft, M. & Ngo, F.Q. (1992). Determination of changes in tumor blood perfusion after hydralazine treatment by dynamic paramagnetic-enhanced magnetic resonance imaging. *Int J Radiat Oncol Biol Phys*, **22**, 477-82.

Benjamin, L., Golijanin, D., Itin, A., Pode, D. & Keshet, E. (1999). Selective ablation of immature blood vessels in established human tumors follows vascular endothelial growth factor withdrawal [see comments]. *J Clin Invest*, **103**, 159-65.

Bernsen, H.J., Rijken, P.F., Oostendorp, T. & van der Kogel, A.J. (1995). Vascularity and perfusion of human gliomas xenografted in the athymic nude mouse. *Br J Cancer*, **71**, 721-6.

Bershadsky, A. & Vasiliev, J. (1988). *Cytoskeleton*. Plenum Press: New York.

Bibby, M.C., Double, J.A., Phillips, R.M., Loadman, P.M. & Gummer, J.A. (1988). Experimental anti-tumor effects of flavone acetic acid (LM975). *Prog Clin Biol Res*, **280**, 243-6.

Billger, M., Str¨omberg, E. & Wallin, M. (1991). Microtubule-associated proteins-dependent colchicine stability of acetylated cold-labile brain microtubules from the Atlantic cod, Gadus morhua. *J Cell Biol*, **113**, 331-8.

Billger, M.A., Bhatacharjee, G. & Williams, R.C., Jr. (1996). Dynamic instability of microtubules assembled from microtubule-associated protein-free tubulin: neither variability of growth and shortening rates nor "rescue" requires microtubule-associated proteins. *Biochemistry*, **35**, 13656-63.

Black, M.M., Aletta, J.M. & Greene, L.A. (1986). Regulation of microtubule composition and stability during nerve growth factor-promoted neurite outgrowth. *J Cell Biol*, **103**, 545-57.

Blagosklonny, M.V., Giannakakou, P., el-Deiry, W.S., Kingston, D.G., Higgs, P.I., Neckers, L. & Fojo, T. (1997). Raf-1/bcl-2 phosphorylation: a step from microtubule damage to cell death. *Cancer Res*, **57**, 130-5.

Blakey, D., Ashton, S., Douglas, S., Westwood, F. & Curry, B. (2000). Anti-tumour activity of the novel vascular targeting agent ZD6126 in a human lung tumour xenograft. *Clin Cancer Res*, **6 (Suppl)**, 4522s.

Bland, J. & Altman, D. (1996a). Measurement error . *Br Med J*, **313**, 744.

Bland, J. & Altman, D. (1996b). Measurement error proportional to the mean. *Br Med J*,**313**, 106.

Bland, J.M. & Altman, D.G. (1995). Multiple significance tests: the Bonferroni method. *Br Med J*, **310**, 170.

Blomley, M.J., Coulden, R., Bufkin, C., Lipton, M.J. & Dawson, P. (1993). Contrast bolus dynamic computed tomography for the measurement of solid organ perfusion. *Invest Radiol*, **28 Suppl 5**, S72-7; discussion S78.

Bochner, B., Cote, R., Weidner, N., Groshen, S., Chen, S., Skinner, D. & Nichols, P. (1995). Angiogenesis in bladder cancer: relationship between microvessel density and tumor prognosis. *J Natl Cancer Inst*, **87**, 1603-12.

Boggio, K., Nicoletti, G., Di Carlo, E., Cavallo, F., Landuzzi, L., Melani, C., Giovarelli, M., Rossi, I., Nanni, P., De Giovanni, C., Bouchard, P., Wolf, S., Modesti, A., Musiani, P., Lollini, P.L., Colombo, M.P. & Forni, G. (1998). Interleukin 12-mediated prevention of spontaneous mammary adenocarcinomas in two lines of Her-2/neu transgenic mice. *J Exp Med*, **188**, 589-96.

Bond, J.F., Fridovich-Keil, J.L., Pillus, L., Mulligan, R.C. & Solomon, F. (1986). A chicken-yeast chimeric beta-tubulin protein is incorporated into mouse microtubules in vivo. *Cell*, **44**, 461-8.

Bonnerot, V., Charpentier, A., Frouin, F., Kalifa, C., Vanel, D. & Di Paola, R. (1992). Factor analysis of dynamic magnetic resonance imaging in predicting the response of osteosarcoma to chemotherapy. *Invest Radiol*, **27**, 847-55.

Borisy, G. & Taylor, E. (1967). The mechanism of action of colchicine. Colchicine binding to sea urchin eggs and the mitotic apparatus. *J Cell Biol*, **34**, 535-48.

Boucher, Y., Baxter, L.T. & Jain, R.K. (1990). Interstitial pressure gradients in tissue-isolated and subcutaneous tumors: implications for therapy. *Cancer Res*, **50**, 4478-84.

Boucher, Y. & Jain, R.K. (1992). Microvascular pressure is the principal driving force for interstitial hypertension in solid tumors: implications for vascular collapse. *Cancer Res*, **52**, 5110-4.

Brasch, R., Li, Husband, J., Keogan, M., Neeman, M., Padhani, A., Shames, D. & Turetschek, K. (2000). MRI for the evaluation of tumour angiogenesis. *Acad Radiol*, **Submitted**.

Bremer, G., Tiebosch, A., van, d.P.H., Schouten, H., de, H.J. & Arends, J. (1996). Tumor angiogenesis: an independent prognostic parameter in cervical cancer. *Am J Obstet Gynecol*, **174**, 126-31.

Brizel, D., Scully, S., Harrelson, J., Layfield, L., Bean, J., Prosnitz, L. & Dewhirst, M. (1996). Tumor oxygenation predicts for the likelihood of distant metastases in human soft tissue sarcoma. *Cancer Res*, **56**, 941-3.

Brizel, D., Sibley, G., Prosnitz, L., Scher, R. & Dewhirst, M. (1997). Tumor hypoxia adversely affects the prognosis of carcinoma of the head and neck. *Int J Radiat Oncol Biol Phys*, **38**, 285-9.

Brogi, E., Schatteman, G., Wu, T., Kim, E., Varticovski, L., Keyt, B. & Isner, J. (1996). Hypoxia-induced paracrine regulation of vascular endothelial growth factor receptor expression. *J Clin Invest*, **97**, 469-76.

Brooks, P., Montgomery, A., Rosenfeld, M., Reisfeld, R., Hu, T., Klier, G. & Cheresh, D. (1994). Integrin alpha v beta 3 antagonists promote tumor regression by inducing apoptosis of angiogenic blood vessels. *Cell*, **79**, 1157-64.

Brown, R.A., Talas, G., Porter, R.A., McGrouther, D.A. & Eastwood, M. (1996). Balanced mechanical forces and microtubule contribution to fibroblast contraction.J *Cell Physiol*, **169**, 439-47.

Budman, D. (1997). Vinorelbine (Navelbine): a third-generation vinca alkaloid. *Cancer Invest*, **15**, 475-90.

Bugajski, A., Nowogrodzka-Zagorska, M., Lenko, J. & Miodonski, A.J. (1989). Angiomorphology of the human renal clear cell carcinoma. A light and scanning electron microscopic study. *Virchows Archiv. A Pathol Anat Histopathol*, **415**, 103-13.

Bulinski, J.C. & Gundersen, G.G. (1991). Stabilization of post-translational modification of microtubules during cellular morphogenesis. *Bioessays*, **13**, 285-93.

Burton, M.A., Gray, B.N., Self, G.W., Heggie, J.C. & Townsend, P.S. (1985). Manipulation of experimental rat and rabbit liver tumor blood flow with angiotensin II. *Cancer Res*, **45**, 5390-3.

Butler, T.P., Grantham, F.H. & Gullino, P.M. (1975). Bulk transfer of fluid in the interstitial compartment of mammary tumors. *Cancer Res*, **35**, 3084-8.

Cao, Z., Joseph, W.R., Browne, W.L., Mountjoy, K.G., Palmer, B.D., Baguley, B.C. & Ching, L.M. (1999). Thalidomide increases both intra-tumoural tumour necrosis factor-alpha production and anti-tumour activity in response to 5,6-dimethylxanthenone-4-acetic acid. *Br J Cancer*, **80**, 716-23.

Carmeliet, P. (2000). Mechanisms of angiogenesis and arteriogenesis. *Nat Med*, **6**, 389-95.

Carmeliet, P., Dor, Y., Herbert, J., Fukumura, D., Brusselmans, K., Dewerchin, M., Neeman, M., Bono, F., Abramovitch, R., Maxwell, P., Koch, C., Ratcliffe, P., Moons, L., Jain, R., Collen, D., Keshert, E. & Keshet, E.c.t.K.E. (1998). Role of HIF-1alpha in hypoxia-mediated apoptosis, cell proliferation and tumour angiogenesis [published erratum appears in Nature 1998 Oct 1; 395(6701):525]. *Nature*, **394**, 485-90.

Carswell, E.A., Old, L.J., Kassel, R.L., Green, S., Fiore, N. & Williamson, B. (1975). An endotoxin-induced serum factor that causes necrosis of tumors. *Proc Natl Acad Sci USA*, **72**, 3666-70.

Cassimeris, L. (1999). Accessory protein regulation of microtubule dynamics throughout the cell cycle. *Curr Opin Cell Biol*, **11**, 134-41.

Chaplin, D. & Dougherty, G. (1999). Tumour vasculature as a target for cancer therapy. *Br J Cancer*, **80 Suppl 1**, 57-64.

Chaplin, D.J. & Hill, S.A. (1995). Temporal heterogeneity in microregional erythrocyte flux in experimental solid tumours. *Br J Cancer*, **71**, 1210-3.

Chaplin, D.J., Pettit, G.R. & Hill, S.A. (1999). Anti-vascular approaches to solid tumour therapy: evaluation of combretastatin A4 phosphate. *Anticancer Res*, **19**, 189-95.

Chaplin, D.J., Pettit, G.R., Parkins, C.S. & Hill, S.A. (1996). Antivascular approaches to solid tumour therapy: evaluation of tubulin binding agents. *Br J Cancer*, **74**, S86-S88.

Chen, C.S., Mrksich, M., Huang, S., Whitesides, G.M. & Ingber, D.E. (1997a). Geometric control of cell life and death. *Science*, **276**, 1425-8.

Chen, Q., Siewert, B., Bly, B.M., Warach, S. & Edelman, R.R. (1997b). STAR-HASTE: perfusion imaging without magnetic susceptibility artifact. *Magn Reson Med*, **38**, 404-8.

Ching, L.M. & Baguley, B.C. (1987). Induction of natural killer cell activity by the antitumour compound flavone acetic acid (NSC 347 512). *Eur J Cancer Clin Oncol*, **23**, 1047-50.

Ching, L.M., Browne, W.L., Tchernegovski, R., Gregory, T., Baguley, B.C. & Palmer, B.D. (1998). Interaction of thalidomide, phthalimide analogues of thalidomide and pentoxifylline with the anti-tumour agent 5,6-dimethylxanthenone-4-acetic acid: concomitant reduction of serum tumour necrosis factor-α and enhancement of anti-tumour activity *Br J Cancer*, **78**, 336-43.

Ching, L.M., Joseph, W.R. & Baguley, B.C. (1992). Stimulation of macrophage tumouricidal activity by 5,6-dimethyl-xanthenone-4-acetic acid, a potent analogue of the antitumour agent flavone-8-acetic acid. *Biochem Pharmacol*, **44**, 192-5.

Ching, L.M., Joseph, W.R., Crosier, K.E. & Baguley, B.C. (1994). Induction of TNF-α messenger RNA in human and murine cells by the flavone acetic acid analogue 5,6-dimethylxanthenone-4-acetic acid (NSC 640488). *Cancer Res*, **54**, 870-2.

Ching, L.M., Xu, Z.F., Gummer, B.H., Palmer, B.D., Joseph, W.R. & Baguley, B.C. (1995). Effect of thalidomide TNF production and anti-tumour activity induced by 5,6-dimethylxanthenone-4-acetic acid. *Br J Cancer*, **72**, 339-43.

Chretien, D., Fuller, S.D. & Karsenti, E. (1995). Structure of growing microtubule ends: two-dimensional sheets close into tubes at variable rates.J *Cell Biol*, **129**, 1311-28.

Cliffe, S., Taylor, M.L., Rutland, M., Baguley, B.C., Hill, R.P. & Wilson, W.R. (1994). Combining bioreductive drugs (SR 4233 or SN 23862) with the vasoactive agents flavone acetic acid or 5,6-dimethylxanthenone acetic acid. *Int J Radiat Oncol Biol Phys*, **29**, 373-7.

Compagni, A. & Christofori, G. (2000). Recent advances in research on multistage tumorigenesis. *Br J Cancer*, **83**, 1-5.

Cooke, S., Boxer, G., Spencer, D., Lawrence, L., Pedley, R., Chester, K. & Begent, R. (2000). Tumour vascular targeting using a novel anti-vascular endothelial cell growth factor (VEGF) scFv antibody. *Br J Cancer*, **83 Suppl 1**, 11.

Crew, J., O'Brien, T., Bradburn, M., Fuggle, S., Bicknell, R., Cranston, D. & Harris, A. (1997). Vascular endothelial growth factor is a predictor of relapse and stage progression in superficial bladder cancer. *Cancer Res*, **57**, 5281-5.

Dachs, G. & Chaplin, D. (1998). Microenvironmental control of gene expression: implications for tumor angiogenesis, progression, and metastasis. *Semin Radiat Oncol*, **8**, 208-16.

Dachs, G., Patterson, A., Firth, J., Ratcliffe, P., Townsend, K., Stratford, I. & Harris, A. (1997). Targeting gene expression to hypoxic tumor cells. *Nat Med*, **3**, 515-20.

Daldrup-Link, H.E., Link, T.M., Rummeny, E.J., August, C., Konemann, S., Jurgens, H. & Heindel, W. (2000). Assessing permeability alterations of the blood-bone marrow barrier due to total body irradiation: in vivo quantification with contrast enhanced magnetic resonance imaging. *Bone Marrow Transplant*, **25**, 71-8.

Dark, G.G., Hill, S.A., Prise, V.E., Tozer, G.M., Pettit, G.R. & Chaplin, D.J. (1997). Combretastatin A-4, an agent that displays potent and selective toxicity toward tumour vasculature. *Cancer Research*, **57**, 1829-1834.

Davis, P., Hill, S., Galbraith, S., Chaplin, D., Naylor, M., Nolan, J. & Dougherty, G. (2000). ZD6126: A new agent causing selective damage of tumour vasculature. *Br J Cancer*, **83 (Suppl 1)**, 31.

de Waal, R., van, A.M., Erhard, H., Weidle, U., Nooijen, P. & Ruiter, D. (1997). Lack of lymphangiogenesis in human primary cutaneous melanoma. Consequences for the mechanism of lymphatic dissemination. *Am J Pathol*, **150**, 1951-7.

Del, M.L., Gennari, A. & Donati, S. (1999). Chemotherapy of non-small-cell lung cancer: role of erythropoietin in the management of anemia. *Ann Oncol*, **10 Suppl 5**, S91-4.

Denekamp, J. (1982). Endothelial cell proliferation as a novel approach to targeting tumour therapy. *Br J Cancer*, **45**, 136-9.

Denekamp, J. (1991). The current status of targeting tumour vasculature as a means of cancer therapy: an overview. *Int J Radiat Biol*, **60**, 401-8.

Denekamp, J., Hill, S.A. & Hobson, B. (1983). Vascular occlusion and tumour cell death. *Eur J Cancer Clin Oncol*, **19**, 271-5.

Denekamp, J. & Hobson, B. (1982). Endothelial-cell proliferation in experimental tumours. *Br J Cancer*, **46**, 711-20.

Dewhirst, M.W., Tso, C.Y., Oliver, R., Gustafson, C.S., Secomb, T.W. & Gross, J.F. (1989). Morphologic and hemodynamic comparison of tumor and healing normal tissue microvasculature. *Int J Radiat Oncol Biol Phys*, **17**, 91-9.

Dintenfass, L. (1981). The clinical impact of the newer research in blood rheology: an overview. *Angiology*, **32**, 217-29.

Doll, D.C., Ringenberg, Q.S. & Yarbro, J.W. (1986). Vascular toxicity associated with antineoplastic agents. *J Clin Oncol*, **4**, 1405-17.

Donoso, J., Green, L., Heller-Bettinger, I. & Samson, F. (1977). Action of the vinca alkaloids vincristine, vinblastine, and desacetyl vinblastine amide on axonal fibrillar organelles in vitro. *Cancer Res*, **37**, 1401-7.

Drechsel, D.N., Hyman, A.A., Cobb, M.H. & Kirschner, M.W. (1992). Modulation of the dynamic instability of tubulin assembly by the microtubule-associated protein tau. *Mol Biol Cell*, **3**, 1141-54.

Dumontet, C., DurÍan, G.E., Steger, K.A., Murphy, G.L., Sussman, H.H. & Sikic, B.I. (1996). Differential expression of tubulin isotypes during the cell cycle. *Cell Motil Cytoskeleton*, **36**, 49-58.

Durand, R. & Le, P.N. (1994). Modulation of tumor hypoxia by conventional chemotherapeutic agents. *Int J Radiat Oncol Biol Phys*, **29**, 481-6.

Durand, R. & Le, P.N. (1997). Tumour blood flow influences combined radiation and doxorubicin treatments. *Radiother Oncol*, **42**, 171-9.

Dvorak, H.F. & Gresser, I. (1989). Microvascular injury in pathogenesis of interferon-induced necrosis of subcutaneous tumors in mice. *J Natl Cancer Inst*, **81**, 497-502.

Eckhardt, S. & Pluda, J. (1997). Development of angiogenesis inhibitors for cancer therapy. *Invest New Drugs*, **15**, 1-3.

Eddy, H.A. (1980). Alterations in tumor microvasculature during hyperthermia. *Radiology*, **137**, 515-21.

Eggermont, A.M., Schraffordt Koops, H., Klausner, J.M., Lienard, D., Kroon, B.B., Schlag, P.M., Ben-Ari, G. & Lejeune, F.J. (1997). Isolation limb perfusion with tumor necrosis factor alpha and chemotherapy for advanced extremity soft tissue sarcomas. *Sem Oncol*, **24**, 547-55.

Endrich, B., Schosser, R. & Messmer, K. (1981). Blood flow measurements by means of radioactive microspheres. A useful technique in malignant tumours? *Eur J Cancer Clin Oncol*, **17**, 1349-51.

Eriksson, R., Persson, H.W., Dymling, S.O. & Lindstrom, K. (1991). Evaluation of Doppler ultrasound for blood perfusion measurements. *Ultrasound Med Biol*, **17**, 445-52.

Evelhoch, J.L. (1999). Key factors in the acquisition of contrast kinetic data for oncology. *J Magn Reson Imaging*, **10**, 254-9.

Fajardo, L.F., Schreiber, A.B., Kelly, N.I. & Hahn, G.M. (1985). Thermal sensitivity of endothelial cells. *Radiat Res*, **103**, 276-85.

Falconer, M.M., Echeverri, C.J. & Brown, D.L. (1992). Differential sorting of beta tubulin isotypes into colchicine-stable microtubules during neuronal and muscle differentiation of embryonal carcinoma cells. *Cell Motil Cytoskeleton*, **21**, 313-25.

Feldmann, H.J., Molls, M., Hoederath, A., Krumpelmann, S. & Sack, H. (1992). Blood flow and steady state temperatures in deep-seated tumors and normal tissues. *Intl J Radiat Oncol Biol Phys*, **23**, 1003-8.

Feldmann, H.J., Sievers, K., Füller, J., Molls, M. & Löhr, E. (1993). Evaluation of tumor blood perfusion by dynamic MRI and CT in patients undergoing thermoradiotherapy. *Eur J Radiol*, **16**, 224-9.

Ferguson, P. & Cass, C. (1985). Differential cellular retention of vincristine and vinblastine by cultured human promyelocytic leukemia HL-60/Cl cells: the basis of differential toxicity. *Cancer Res*, **45**, 5480-8.

Fingar, V., Kik, P., Haydon, P., Cerrito, P., Tseng, M., Abang, E. & Wieman, T. (1999). Analysis of acute vascular damage after photodynamic therapy using benzoporphyrin derivative (BPD). *Br J Cancer*, **79**, 1702-8.

Folkman, J. (1971). Tumor angiogenesis: therapeutic implications. *New Engl J Med*, **285**, 1182-6.

Folkman, J. (1995). Angiogenesis in cancer, vascular, rheumatoid and other disease. *Nature Med*, **1**, 27-31.

Folkman, J. & Hanahan, D. (1991). Switch to the angiogenic phenotype during tumorigenesis. *Princess Takamatsu Symp*, **22**, 339-47.

Folkman, J., Long, D.M. & Becker, F.F. (1963). Growth and metastasis of tumour in organ culture. *Cancer*, **16**, 453-467.

Folkman, J. & Moscona, A. (1978). Role of cell shape in growth control. *Nature*, **273**, 345-9.

Forsythe, J.A., Jiang, B.H., Iyer, N.V., Agani, F., Leung, S.W., Koos, R.D. & Semenza, G.L. (1996). Activation of vascular endothelial growth factor gene transcription by hypoxia-inducible factor 1. *Mol Cell Biol*, **16**, 4604-13.

Fox, S., Gatter, K., Bicknell, R., Going, J., Stanton, P., Cooke, T. & Harris, A. (1993). Relationship of endothelial cell proliferation to tumor vascularity in human breast cancer. *Cancer Res*, **53**, 4161-3.

Fox, S., Leek, R., Bliss, J., Mansi, J., Gusterson, B., Gatter, K. & Harris, A. (1997). Association of tumor angiogenesis with bone marrow micrometastases in breast cancer patients. *J Natl Cancer Inst*, **89**, 1044-9.

Fuchs, E. & Weber, K. (1994). Intermediate filaments: structure, dynamics, function, and disease. *Ann Rev Biochem*, **63**, 345-82.

Fuchs, E. & Yang, Y. (1999). Crossroads on cytoskeletal highways. *Cell*, **98**, 547-50.

Fukumura, D., Yuan, F., Monsky, W., Chen, Y. & Jain, R. (1997). Effect of host microenvironment on the microcirculation of human colon adenocarcinoma. *Am J Pathol*, **151**, 679-88.

Furman-Haran, E., Margalit, R., Grobgeld, D. & Degani, H. (1998). High resolution MRI of MCF7 human breast tumors: complemented use of iron oxide microspheres and Gd-DTPA. *J Magn Reson Imaging*, **8**, 634-41.

Galbraith, S.M., Chaplin, D., Lee, F., Stratford, M.R.L., Locke, R., Vojnovic, B. & Tozer, G.M. (2001). Effects of combretastatin A4 phosphate on endothelial cell shape in vitro and relation to vascular targeting effects in vivo. *Anticancer Res*, **2**.

Galbraith, S.M., Taylor, N.J., Maxwell, R.J., Lodge, M., Tozer, G.M., Baddeley, H., Wilson, I., Prise, V.E. & Rustin, G.J.S. (2000). Combretastatin A4 Phosphate (CA4P) targets vasculature in animal and human tumours. *Br J Cancer*, **83 Suppl 1**, 12.

Gallo, O., Masini, E., Morbidelli, L., Franchi, A., Fini-Storchi, I., Vergari, W. & Ziche, M. (1998). Role of nitric oxide in angiogenesis and tumor progression in head and neck cancer [see comments]. *J Natl Cancer Inst*, **90**, 587-96.

Gelfand, V.I. & Bershadsky, A.D. (1991). Microtubule dynamics: mechanism, regulation, and function. *Ann Rev Cell Biol*, **7**, 93-116.

Gerlowski, L.E. & Jain, R.K. (1986). Microvascular permeability of normal and neoplastic tissues. *Microvasc Res*, **31**, 288-305.

Gerweck, L. & Seetharaman, K. (1996). Cellular pH gradient in tumor versus normal tissue: potential exploitation for the treatment of cancer. *Cancer Res*, **56**, 1194-8.

Gillies, R., Schornack, P., Secomb, T. & Raghunand, N. (1999). Causes and effects of heterogeneous perfusion in tumors. [In Process Citation]. *Neoplasia*, **1**, 197-207.

Graeber, T., Osmanian, C., Jacks, T., Housman, D., Koch, C., Lowe, S. & Giaccia, A. (1996). Hypoxia-mediated selection of

cells with diminished apoptotic potential in solid tumours [see comments]. *Nature*, **379**, 88-91.

Gray, L., Coger, A. & Ebert, M. (1953). The concentration of oxygen dissolved in tissues at the time of irradiation as a factor in radiotherapy. *Br J Radiol*, **26**, 638.

Griffiths, J.R. (1991). Are cancer cells acidic? [editorial]. *Br J Cancer*, **64**, 425-7.

Griffon-Etienne, G., Boucher, Y., Brekken, C., Suit, H.D. & Jain, R.K. (1999). Taxane-induced apoptosis decompresses blood vessels and lowers interstitial fluid pressure in solid tumors: clinical implications. *Cancer Res*, **59**, 3776-82.

Groopman, J. & Itri, L. (1999). Chemotherapy-induced anemia in adults: incidence and treatment. *J Natl Cancer Inst*, **91**, 1616-34.

Grosios, K., Holwell, S.E., McGown, A.T., Pettit, G.R. & Bibby, M.C. (1999). In vivo and in vitro evaluation of combretastatin A-4 and its sodium phosphate prodrug. *British Journal of Cancer*, **81**, 1318-27.

Grosios, K., Loadman, P.M., Swaine, D.J., Pettit, G.R. & Bibby, M.C. (2000). Combination chemotherapy with combretastatin A-4 phosphate and 5-fluorouracil in an experimental murine colon adenocarcinoma. *Anticancer Research*, **20**, 229-33.

Grunstein, J., Roberts, W., Mathieu-Costello, O., Hanahan, D. & Johnson, R. (1999). Tumor-derived expression of vascular endothelial growth factor is a critical factor in tumor expansion and vascular function. *Cancer Res*, **59**, 1592-8.

Gullino, P. (1975). Extracellular compartments of solid tumors. In *Cancer*, Becker, F. (ed), Vol. 3. pp. 327-354. Plenum: New York.

Gundersen, G.G. & Cook, T.A. (1999). Microtubules and signal transduction. *Curr Opin Cell Biol*, **11**, 81-94.

Gundersen, G.G., Khawaja, S. & Bulinski, J.C. (1989). Generation of a stable, posttranslationally modified microtubule array is an early event in myogenic differentiation. *J Cell Biol*, **109**, 2275-88 issn: 0021-9525.

Gutheil, J. (1998). Phase I study of Vitaxin an anti-angiogenic humanised monoclonal antibody to vascular integrin αVβ3. In *Proc Am Soc Clin Oncol*.

Gutman, M., Inbar, M., Lev-Shlush, D., Abu-Abid, S., Mozes, M., Chaitchik, S., Meller, I. & Klausner, J. (1997). High dose tumor necrosis factor-alpha and melphalan administered via isolated limb perfusion for advanced limb soft tissue sarcoma results in a >90% response rate and limb preservation. *Cancer*, **79**, 1129-37.

Haldar, S., Basu, A. & Croce, C.M. (1997). Bcl2 is the guardian of microtubule integrity. *Cancer Res*, **57**, 229-33.

Hamel, E. (1992). Natural products which interact with tubulin in the vinca domain: maytansine, rhizoxin, phomopsin A, dolastatins 10 and 15 and halichondrin B. *Pharmacol Ther*, **55**, 31-51.

Hamel, E. & Lin, C.M. (1983). Interactions of combretastatin, a new plant-derived anti-mitotic agent, with tubulin. *Biochem Pharmacol*, **32**, 3864-3867.

Hammersley, P., McCready, V., Babich, J. & Coghlan, G. (1987). 99mTc-HMPAO as a tumour blood flow agent. *Eur J Nucl Med*, **13**, 90-4.

Han, J., Dionne, C., Kedersha, N. & Goldmacher, V. (1997). p53 status affects the rate of the onset but not the overall extent of doxorubicin-induced cell death in rat-1 fibroblasts constitutively expressing c-Myc. *Cancer Res*, **57**, 176-82.

Hanahan, D. & Folkman, J. (1996). Patterns and emerging mechanisms of the angiogenic switch during tumorigenesis. *Cell*, **86**, 353-64.

Hansen-Smith, F., Hudlicka, O. & Egginton, S. (1996). In vivo angiogenesis in adult rat skeletal muscle: early changes in capillary network architecture and ultrastructure. *Cell Tissue Res*, **286**, 123-36.

Hartmann, A., Kunz, M., Kostlin, S., Gillitzer, R., Toksoy, A., Brocker, E. & Klein, C. (1999). Hypoxia-induced up-regulation of angiogenin in human malignant melanoma. *Cancer Res*, **59**, 1578-83.

Hastie, S. (1991). Interactions of colchicine with tubulin. *Pharmacol Ther*, **51**, 377-401.

Havlin, K.A., Kuhn, J.G., Craig, J.B., Boldt, D.H., Weiss, G.R., Koeller, J., Harman, G., Schwartz, R., Clark, G.N. & Von Hoff, D.D. (1991). Phase I clinical and pharmacokinetic trial of flavone acetic acid. *J Natl Cancer Inst*, **83**, 124-8.

Hawighorst, H., Knapstein, P.G., Weikel, W., Knopp, M.V., Zuna, I., Knof, A., Brix, G., Schaeffer, U., Wilkens, C., Schoenberg, S.O., Essig, M., Vaupel, P. & van Kaick, G. (1997). Angiogenesis of uterine cervical carcinoma: characterization by pharmacokinetic magnetic resonance parameters and histological microvessel density with correlation to lymphatic involvement. *Cancer Res*, **57**, 4777-86.

Hawighorst, H., Libicher, M., Knopp, M.V., Moehler, T., Kauffmann, G.W. & Gv, K. (1999). Evaluation of angiogenesis and perfusion of bone marrow lesions: role of semiquantitative and quantitative dynamic MRI. J Magn Reson Imaging, **10**, 286-94.

Helmlinger, G., Yuan, F., Dellian, M. & Jain, R.K. (1997). Interstitial pH and pO2 gradients in solid tumors in vivo: high-resolution measurements reveal a lack of correlation. *Nature Med*, **3**, 177-82.

Hering, E.R., Blekkenhorst, G.H. & Jones, D.T. (1995). Tumor blood flow measurements using coincidence counting on

patients treated with neutrons. *Int J Radiat Oncol Biol Phys*, **32**, 129-35.

Hermans, R., Feron, M., Bellon, E., Dupont, P., Van den Bogaert, W. & Baert, A.L. (1998). Laryngeal tumor volume measurements determined with CT: a study on intra- and interobserver variability. *Int J Radiat Oncol Biol Phys*, **40**, 553-7.

Hermans, R., Lambin, P., Van der Goten, A., Van den Bogaert, W., Verbist, B., Weltens, C. & Delaere, P.R. (1999).Tumoural perfusion as measured by dynamic computed tomography in head and neck carcinoma. *Radiother Oncol*, **53**, 105-11.

Hill, S., Galbraith, S., Tozer, G., Dark, G. & Chaplin, D. (1999). Tumour vasculature as a target for drug therapy: studies with combretastatin A4 phosphate. *Br J Cancer*, **80 (Suppl 2)**, 91.

Hill, S., Heary, T., Flower, M., Cronin, B., McCready, V. & Thomas, J. (1994). Blood flow measurement in extremity soft tissue sarcoma with technetium-99m hexamethyl-propyleneamineoxime and single photon emission computed tomography. *Br J Surg*, **81**, 1609-11.

Hill, S.A., Lonergan, S.J., Denekamp, J. & Chaplin, D.J. (1993). Vinca alkaloids: anti-vascular effects in a murine tumour. *Eur J Cancer*, **29A**, 1320-4.

Hill, S.A., Sampson, L.E. & Chaplin, D.J. (1995). Anti-vascular approaches to solid tumour therapy: evaluation of vinblastine and flavone acetic acid. *Int J Cancer*, **63**, 119-23.

Hill, S.A., Williams, K.B. & Denekamp, J. (1989). Vascular collapse after flavone acetic acid: a possible mechanism of its anti-tumour action. *Eur J Cancer Clin Oncol*, **25**, 1419-24.

Hilmas, D.E. & Gillette, E.L. (1974). Morphometric analyses of the microvasculature of tumors during growth and after x-irradiation. *Cancer*, **33**, 103-10.

Himes, R.H. (1991). Interactions of the catharanthus (Vinca) alkaloids with tubulin and microtubules. *Pharmacol Ther*, **51**, 257-67.

Hittmair, K., Eckersberger, F., Klepetko, W., Helbich, T. & Herold, C.J. (1995). Evaluation of solitary pulmonary nodules with dynamic contrast-enhanced MR imaging–a promising technique. *Magn Reson Imaging*, **13**, 923-33.

Hobson, B. & Denekamp, J. (1984). Endothelial proliferation in tumours and normal tissues: continuous labelling studies. *Br J Cancer*, **49**, 405-13.

Hockel, M., Schlenger, K., Aral, B., Mitze, M., Schaffer, U. & Vaupel, P. (1996). Association between tumor hypoxia and malignant progression in advanced cancer of the uterine cervix. *Cancer Res*, **56**, 4509-15.

Hockel, M., Schlenger, K., Hockel, S. & Vaupel, P. (1999). Hypoxic cervical cancers with low apoptotic index are highly aggressive. *Cancer Res*, **59**, 4525-8.

Holash, J., Maisonpierre, P., Compton, D., Boland, P., Alexander, C., Zagzag, D., Yancopoulos, G. & Wiegand, S. (1999). Vessel cooption, regression, and growth in tumors mediated by angiopoietins and VEGF. *Science*, **284**, 1994-8.

Holm, E., Hagmuller, E., Staedt, U., Schlickeiser, G., Gunther, H.J., Leweling, H., Tokus, M. & Kollmar, H.B. (1995). Substrate balances across colonic carcinomas in humans. *Cancer Res*, **55**, 1373-8.

Horak, E.R., Leek, R., Klenk, N., LeJeune, S., Smith, K., Stuart, N., Greenall, M., Stepniewska, K. & Harris, A.L. (1992). Angiogenesis, assessed by platelet/endothelial cell adhesion molecule antibodies, as indicator of node metastases and survival in breast cancer. *Lancet*, **340**, 1120-4.

Hori, K., Suzuki, M., Tanda, S., Saito, S., Shinozaki, M. & Zhang, Q.H. (1992). Circadian variation of tumor blood flow in rat subcutaneous tumors and its alteration by angiotensin II-induced hypertension. *Cancer Res*, **52**, 912-6.

Hori, K., Zhang, Q., Li, H. & Saito, S. (1995). Variation of growth rate of a rat tumour during a light-dark cycle: correlation with circadian fluctuations in tumour blood flow. *Br J Cancer*, **71**, 1163-8.

Hori, K., Zhang, Q., Saito, S., Tanda, S., Li, H. & Suzuki, M. (1993). Microvascular mechanisms of change in tumor blood flow due to angiotensin II, epinephrine, and methoxamine: a functional morphometric study. *Cancer Res*, **53**, 5528-34.

Horsman, M., Ehrnrooth, E., Ladekarl, M. & Overgaard, J. (1998). The effect of combretastatin A-4 disodium phosphate in a C3H mouse mammary carcinoma and a variety of murine spontaneous tumors. *Int J Radiat Oncol Biol Phys*, **42**, 895-8.

Horsman, M., Murata, R., Breidahl, T., Nielsen, F., Maxwell, R., Stodkiled-Jorgensen, H. & Overgaard, J. (2000). Combretastatins novel vascular targeting drugs for improving anti-cancer therapy. Combretastatins and conventional therapy [In Process Citation]. *Adv Exp Med Biol*, **476**, 311-23 .

Horsman, M.R., Christensen, K.L. & Overgaard, J. (1992). Relationship between the hydralazine-induced changes in murine tumor blood supply and mouse blood pressure. *Int J Radiat Oncol Biol Phys*, **22**, 455-8.

Hu, Z., Sun, Y. & Garen, A. (1999). Targeting tumor vasculature endothelial cells and tumor cells for immunotherapy of human melanoma in a mouse xenograft model. *Proc Natl Acad Sci USA*, **96**, 8161-6.

Huang, X., Molema, G., King, S., Watkins, L., Edgington, T.S. & Thorpe, P.E. (1997). Tumor infarction in mice by antibody-directed targeting of tissue factor to tumor vasculature. *Science*, **275**, 547-50.

Hunter, G.J., Hamberg, L.M., Choi, N., Jain, R.K., McCloud, T. & Fischman, A.J. (1998). Dynamic T1-weighted magnetic resonance imaging and positron emission tomography in patients with lung cancer: correlating vascular physiology with

glucose metabolism. *Clin Cancer Res*, **4**, 949-55.

Inaba, T. (1992). Quantitative measurements of prostatic blood flow and blood volume by positron emission tomography. *J Urol*, **148**, 1457-60.

Ingber, D.E. (1997). Tensegrity: the architectural basis of cellular mechanotransduction. *Ann Rev Physiol*, **59**, 575-99.

Ingber, D.E., Madri, J.A. & Folkman, J. (1987). Endothelial growth factors and extracellular matrix regulate DNA synthesis through modulation of cell and nuclear expansion. *In Vitro Cell Develop Biol*, **23**, 387-94.

Ingber, D.E., Prusty, D., Sun, Z., Betensky, H. & Wang, N. (1995). Cell shape, cytoskeletal mechanics, and cell cycle control in angiogenesis. *J Biomech*, **28**, 1471-84.

Iyer, S., Chaplin, D.J., Rosenthal, D.S., Boulares, A.H., Li, L.Y. & Smulson, M.E. (1998). Induction of apoptosis in proliferating human endothelial cells by the tumor-specific antiangiogenesis agent combretastatin A-4. *Cancer Res*, **58**, 4510-4.

Jaffe, E.A., Nachman, R.L., Becker, C.G. & Minick, C.R. (1973). Culture of human endothelial cells derived from umbilical veins. Identification by morphologic and immunologic criteria. *J Clin Invest*, **52**, 2745-56.

Jain, R.K. (1988). Determinants of tumor blood flow: a review. *Cancer Res*, **48**, 2641-58.

Jain, R.K. (1991). Haemodynamic and transport barriers to the treatment of solid tumours. *Int J Radiat Biol*, **60**, 85-100.

Jirtle, R., Clifton, K.H. & Rankin, J.H. (1978). Measurement of mammary tumor blood flow in unanesthetized rats. *J Natl Cancer Inst*, **60**, 881-6.

Jordan, M.A., Margolis, R.L., Himes, R.H. & Wilson, L. (1986). Identification of a distinct class of vinblastine binding sites on microtubules. *J Mol Biol*, **187**, 61-73.

Jordan, M.A. & Wilson, L. (1998). Microtubules and actin filaments: dynamic targets for cancer chemotherapy. *Curr Opin Cell Biol*, **10**, 123-30.

Joshi, H.C. & Cleveland, D.W. (1989). Differential utilization of beta-tubulin isotypes in differentiating neurites. *J Cell Biol*, **109**, 663-73.

Joshi, H.C., Palacios, M.J., McNamara, L. & Cleveland, D.W. (1992). Gamma-tubulin is a centrosomal protein required for cell cycle-dependent microtubule nucleation. *Nature*, **356**, 80-3.

Kakolyris, S., Fox, S., Koukourakis, M., Giatromanolaki, A., Brown, N., Leek, R., Taylor, M., Leigh, I., Gatter, K. & Harris, A. (2000). Relationship of vascular maturation in breast cancer blood vessels to vascular density and metastasis, assessed by expression of a novel basement membrane component, LH39. *Br J Cancer*, **82**, 844-51.

Kakolyris, S., Giatromanolaki, A., Koukourakis, M., Leigh, I., Georgoulias, V., Kanavaros, P., Sivridis, E., Gatter, K. & Harris, A. (1999). Assessment of vascular maturation in non-small cell lung cancer using a novel basement membrane component, LH39: correlation with p53 and angiogenic factor expression. *Cancer Res*, **59**, 5602-7.

Kallinowski, F., Schaefer, C., Tyler, G. & Vaupel, P. (1989). In vivo targets of recombinant human tumour necrosis factor-alpha: blood flow, oxygen consumption and growth of isotransplanted rat tumours. *Br J Cancer*, **60**, 555-60.

Kanthou, C., Prise, V.E., Milson, J. & Tozer, G.M. (2001). The vascular targeting agent combretastatin A4 phosphate alters the andothelial cell actin cytoskeleton and mediates changes in vascular permeability in vitro and in vivo. In *Proc Am Assoc Cancer Res*, New Orleans.

Kanthou, C. & Tozer, G. (2000). Studies on the mechanism of action of the vascular targeting agent combretastatin A4 phosphate. *Br J Cancer*, **83 (Suppl 1)**, 12.

Karger, N., Biederer, J., Lusse, S., Grimm, J., Steffens, J., Heller, M. & Gluer, C. (2000). Quantitation of renal perfusion using arterial spin labeling with FAIR-UFLARE. *Magn Reson Imaging*, **18**, 641-7.

Katoh, R., Hemmi, A., Komiyama, A. & Kawaoi, A. (1999). Confocal laser scanning microscopic observation of angioarchitectures in human thyroid neoplasms. *Hum Pathol*, **30**, 1226-31.

Kaverina, I., Rottner, K. & Small, J.V. (1998). Targeting, capture, and stabilization of microtubules at early focal adhesions. *J Cell Biol*, **142**, 181-90.

Kaye, S.B., Clavel, M., Dodion, P., Monfardini, S., ten Bokkel-Huinink, W., Wagener, D.T., Gundersen, S., Stoter, G., Smith, J., Renard, J. & al, e. (1990). Phase II trials with flavone acetic acid (NCS. 347512, LM975) in patients with advanced carcinoma of the breast, colon, head and neck and melanoma. *Invest New Drugs*, **8 Suppl 1**, S95-9.

Kedar, R., Cosgrove, D., Smith, I., Mansi, J. & Bamber, J. (1994). Breast carcinoma: measurement of tumor response to primary medical therapy with color Doppler flow imaging. *Radiology*, **190**, 825-30.

Kennedy, S.D., Szczepaniak, L.S., Gibson, S.L., Hilf, R., Foster, T.H. & Bryant, R.G. (1994). Quantitative MRI of Gd-DTPA uptake in tumors: response to photodynamic therapy. *Magn Reson Med*, **31**, 292-301.

Kerr, D.J., Kaye, S.B., Cassidy, J., Bradley, C., Rankin, E.M., Adams, L., Setanoians, A., Young, T., Forrest, G., Soukop, M. & al, e. (1987). Phase I and pharmacokinetic study of flavone acetic acid. *Cancer Res*, **47**, 6776-81.

Kerr, D.J., Maughan, T., Newlands, E., Rustin, G., Bleehen, N.M., Lewis, C. & Kaye, S.B. (1989). Phase II trials of flavone acetic acid in advanced malignant melanoma and colorectal carcinoma. *Br J Cancer*, **60**, 104-6.

Kety, S. (1949). Measurement of regional circulation by the local clearance of radioactive sodium. *Am Heart J*, **38**, 321.

Kety, S. (1960a). Blood-tissue exchange methods. Theory of blood-tissue exchange and its application to measurement of blood flow. *Meth Med Res*, **8**, 223-227.

Kety, S. (1960b). Measurement of local blood flow by the exchange of an inert, diffusible substance.*Meth Med Res*, **8**, 228-236.

Kety, S. & Schmidt, C. (1948). Nitrous oxide method for quantitative determination of cerebral blood flow in man: Theory, procedure and normal values. *J Clin Invest*, **27**, 476.

Kieler, J., Skubis, K., Grzesik, W., Strojny, P., Wisniewski, J. & Dziedzic-Goclawska, A. (1989). Spreading of cells on various substrates evaluated by Fourier analysis of shape. *Histochemistry*, **92**, 141-8.

Kimura, H., Braun, R.D., Ong, E.T., Hsu, R., Secomb, T.W., Papahadjopoulos, D., Hong, K. & Dewhirst, M.W. (1996). Fluctuations in red cell flux in tumor microvessels can lead to transient hypoxia and reoxygenation in tumor parenchyma. *Cancer Res*, **56**, 5522-8.

Kolodney, M.S. & Elson, E.L. (1995). Contraction due to microtubule disruption is associated with increased phosphorylation of myosin regulatory light chain. *Proc Natl Acad Sci USA*, **92**, 10252-6.

Konerding, M., van Ackern, C., Fait, E., Steinberg, F. & Streffer, C. (1998). Morphological aspects of tumor angiogenesis and microcirculation. In *Blood perfusion and microenvironment of human tumors*, Molls, M. & Vaupel, P. (eds) pp. 5-17. Springer-Verlag: Berlin Heidelberg New York.

Konerding, M.A., Malkusch, W., Klapthor, B., van Ackern, C., Fait, E., Hill, S.A., Parkins, C., Chaplin, D.J., Presta, M. & Denekamp, J. (1999). Evidence for characteristic vascular patterns in solid tumours: quantitative studies using corrosion casts. *Br J Cancer*, **80**, 724-32.

Kotasek, D., Vercellotti, G.M., Ochoa, A.C., Bach, F.H., White, J.G. & Jacob, H.S. (1988). Mechanism of cultured endothelial injury induced by lymphokine-activated killer cells. *Cancer Res*, **48**, 5528-32.

Koutcher, J.A., Barnett, D., Kornblith, A.B., Cowburn, D., Brady, T.J. & Gerweck, L.E. (1990). Relationship of changes in pH and energy status to hypoxic cell fraction and hyperthermia sensitivity. *Int J Radiat Oncol Biol Phys*, **18**, 1429-35.

Kovar DA, Lewis M, Karczmar GS. A new method for imaging perfusion and contrast extraction fraction: input functions derived from reference tissues (1998). *J Magn Reson Imag* **8**,1126-34.

Krantz, S. (1994). Pathogenesis and treatment of the anemia of chronic disease. *Am J Med Sci*, **307**, 353-9.

Krol, A., Maresca, J., Dewhirst, M. & Yuan, F. (1999). Available volume fraction of macromolecules in the extravascular space of a fibrosarcoma: implications for drug delivery. *Cancer Res*, **59**, 4136-41.

Kuncl, R., Duncan, G., Watson, D., Alderson, K., Rogawski, M. & Peper, M. (1987). Colchicine myopathy and neuropathy. *N Engl J Med*, **316**, 1562-8.

Kurjak, A., Kupesic, S., Anic, T. & Kosuta, D. (2000). Three-dimensional ultrasound and power doppler improve the diagnosis of ovarian lesions. *Gynecol Oncol*, **76**, 28-32.

Laird, A.D., Vajkoczy, P., Shawver, L.K., Thurnher, A., Liang, C., Mohammadi, M., Schlessinger, J., Ullrich, A., Hubbard, S.R., Blake, R.A., Fong, T.A., Strawn, L.M., Sun, L., Tang, C., Hawtin, R., Tang, F., Shenoy, N., Hirth, K.P., McMahon, G. & Cherrington. (2000). SU6668 is a potent antiangiogenic and antitumor agent that induces regression of established tumors. *Cancer Res*, **60**, 4152-60.

Lammertsma, A.A. & Jones, T. (1992). Low oxygen extraction fraction in tumours measured with the oxygen-15 steady state technique: effect of tissue heterogeneity. *Br J Radiol*, **65**, 697-700.

Lash, C.J., Li, A.E., Rutland, M., Baguley, B.C., Zwi, L.J. & Wilson, W.R. (1998). Enhancement of the anti-tumour effects of the antivascular agent 5,6-dimethylxanthenone-4-acetic acid (DMXAA) by combination with 5-hydroxytryptamine and bioreductive drugs. *Br J Cancer*, **78**, 439-45.

Lavelle, F., Michelson, A.M. & Dimitrijevic, L. (1973). Biological protection by superoxide dismutase. *Biochem Biophys Res Comm*, **55**, 350-7.

Laws, A.L., Matthew, A.M., Double, J.A. & Bibby, M.C. (1995). Preclinical in vitro and in vivo activity of 5,6-dimethylxanthenone-4-acetic acid. *Br J Cancer*, **71**, 1204-9.

Lee, S., Wolf, P., Escudero, R., Deutsch, R., Jamieson, S. & Thistlethwaite, P. (2000). Early expression of angiogenesis factors in acute myocardial ischemia and infarction. *N Engl J Med*, **342**, 626-33.

Lee, S.K., Lee, T., Lee, K.R., Su, Y.G. & Liu, T.J. (1995). Evaluation of breast tumors with color Doppler imaging: a comparison with image-directed Doppler ultrasound. *J Clin Ultrasound*, **23**, 367-73.

Lee, W., Berkey, B., Marcial, V., Fu, K., Cooper, J., Vikram, B., Coia, L., Rotman, M. & Ortiz, H. (1998). Anemia is associated with decreased survival and increased locoregional failure in patients with locally advanced head and neck carcinoma: a secondary analysis of RTOG 85-27. *Int J Radiat Oncol Biol Phys*, **42**, 1069-75.

Leek, R.D., Landers, R.J., Harris, A.L. & Lewis, C.E. (1999). Necrosis correlates with high vascular density and focal macrophage infiltration in invasive carcinoma of the breast. *Br J Cancer*, **79**, 991-5.

Lejeune, F., Ruegg, C. & Lienard, D. (1998). Clinical applications of TNF-alpha in cancer. *Curr Opin Immunol*, **10**, 573-80.

Lev-Chelouche, D., Abu-Abeid, S., Nakache, R., Issakov, J., Kollander, Y., Merimsky, O., Meller, I., Klausner, J. & Gutman, M. (1999). Limb desmoid tumors: a possible role for isolated limb perfusion with tumor necrosis factor-alpha and melphalan. *Surgery*, **126**, 963-7.

Levy, A.P., Levy, N.S., Wegner, S. & Goldberg, M.A. (1995). Transcriptional regulation of the rat vascular endothelial growth factor gene by hypoxia. *J Biol Chem*, **270**, 13333-40.

Li, C., Shan, S., Huang, Q., Braun, R., Lanzen, J., Hu, K., Lin, P. & Dewhirst, M. (2000a). Initial stages of tumor cell-induced angiogenesis: evaluation via skin window chambers in rodent models. *J Natl Cancer Inst*, **92**, 143-7.

Li, K., Zhu, X., Jayson, G., Carrington, B., Jones, A., Lawrance, J., Waterton, J., Checkley, D., Tessier, J. & Jackson, A. (2000b). Quantitative dynamic contrast-enhanced MRI in tumors. A reproducible technique in the head? A reproducible technique in the breast? In *Proc Intl Soc Mag Reson Med*, Vol. 8. pp. 724, Sydney.

Li, L., Rojiani, A. & Siemann, D. (1998). Targeting the tumor vasculature with combretastatin A-4 disodium phosphate: effects on radiation therapy. *Int J Radiat Oncol Biol Phys*, **42**, 899-903.

Lienard, D., Eggermont, A., Koops, H., Kroon, B., Towse, G., Hiemstra, S., Schmitz, P., Clarke, J., Steinmann, G., Rosenkaimer, F. & Lejeune, F. (1999). Isolated limb perfusion with tumour necrosis factor-alpha and melphalan with or without interferon-gamma for the treatment of in-transit melanoma metastases: a multicentre randomized phase II study. *Melanoma Res*, **9**, 491-502.

Lin, C.M., Ho, H.H., Pettit, G.R. & Hamel, E. (1989). Antimitotic natural products combretastatin A-4 and combretastatin A-2: studies on the mechanism of their inhibition of the binding of colchicine to tubulin. *Biochemistry*, **28**, 6984-91.

Ling, Y., Priebe, W. & Perez-Soler, R. (1993). Apoptosis induced by anthracycline antibiotics in P388 parent and multidrug-resistant cells. *Cancer Res*, **53**, 1845-52.

Ludford, R.J. (1945). Cochicine in the experimental treatment of cancer. *J Natl Cancer Inst*, **6**, 89-101.

Ludueña, R.F. (1993). Are tubulin isotypes functionally significant. *Mol Biol Cell*, **36**, 445-57.

Luduena, R.F., Roach, M.C., Jordan, M.A. & Murphy, D.B. (1985). Different reactivities of brain and erythrocyte tubulins toward a sulfhydryl group-directed reagent that inhibits microtubule assembly. *J Biol Chem*, **260**, 1257-64.

Lyng, H., Skretting, A. & Rofstad, E.K. (1992). Blood flow in six human melanoma xenograft lines with different growth characteristics. *Cancer Res*, **52**, 584-92.

Maccioni, R.B. & Cambiazo, V. (1995). Role of microtubule-associated proteins in the control of microtubule assembly. *Physiol Rev*, **75**, 835-64.

Mace, K.F., Hornung, R.L., Wiltrout, R.H. & Young, H.A. (1990). Correlation between in vivo induction of cytokine gene expression by flavone acetic acid and strict dose dependency and therapeutic efficacy against murine renal cancer. *Cancer Res*, **50**, 1742-7.

Mahadevan, V., Malik, S.T., Meager, A., Fiers, W., Lewis, G.P. & Hart, I.R. (1990). Role of tumor necrosis factor in flavone acetic acid-induced tumor vasculature shutdown. *Cancer Res*, **50**, 5537-42.

Mahaley, M.S.J., Gillespie, G.Y. & Hammett, R. (1990). Computerized tomography brain scan tumor volume determinations. Sensitivity as an objective criterion of response to therapy. *J Neurosurg*, **72**, 872-8.

Makimoto, H., Koizumi, K., Tsunoda, S., Wakai, Y., Matsui, J., Tsutsumi, Y., Nakagawa, S., Ohizumi, I., Taniguchi, K., Saito, H., Utoguchi, N., Ohsugi, Y. & Mayumi, T. (1999). Tumor vascular targeting using a tumor-tissue endothelium-specific monoclonal antibody as an effective strategy for cancer chemotherapy. *Biochem Biophys Res Commun*, **260**, 346-50.

Malek, A.M. & Izumo, S. (1996). Mechanism of endothelial cell shape change and cytoskeletal remodeling in response to fluid shear stress. *J Cell Sci*, **109 (Pt 4)**, 713-26.

Malek, A.M., Lee, I.W., Alper, S.L. & Izumo, S. (1997). Regulation of endothelin-1 gene expression by cell shape and the microfilament network in vascular endothelium. *Am Physiol*, **273**, C1764-74.

Mandelkow, E. & Mandelkow, E.M. (1995). Microtubules and microtubule-associated proteins. *Curr Opin Cell Biol*, **7**, 72-81.

Maniotis, A.J., Chen, C.S. & Ingber, D.E. (1997). Demonstration of mechanical connections between integrins, cytoskeletal filaments, and nucleoplasm that stabilize nuclear structure. *Proc Natl Acad Sci USA*, **94**, 849-54.

Mantyla, M., Heikkonen, J. & Perkkio, J. (1988). Regional blood flow in human tumours measured with argon, krypton and xenon. *Br J Radiol*, **61**, 379-82.

Mantyla, M.J. (1979). Regional blood flow in human tumors. *Cancer Res*, **39**, 2304-6.

Marti, H., Bernaudin, M., Bellail, A., Schoch, H., Euler, M., Petit, E. & Risau, W. (2000). Hypoxia-induced vascular endothelial growth factor expression precedes neovascularization after cerebral ischemia. *Am J Pathol*, **156**, 965-76.

Martinoli, C., Pretolesi, F., Crespi, G., Bianchi, S., Gandolfo, N., Valle, M. & Derchi, L.E. (1998). Power Doppler sonography: clinical applications. *Eur J Radiol*, **27 Suppl 2**, S133-40.

Matsuno, F., Haruta, Y., Kondo, M., Tsai, H., Barcos, M. & Seon, B.K. (1999). Induction of lasting complete regression of preformed distinct solid tumors by targeting the tumor vasculature using two new anti-endoglin monoclonal antibodies. *Clin Cancer Res*, **5**, 371-82.

Maxwell, P.H., Dachs, G.U., Gleadle, J.M., Nicholls, L.G., Harris, A.L., Stratford, I.J., Hankinson, O., Pugh, C.W. & Ratcliffe, P.J. (1997). Hypoxia-inducible factor-1 modulates gene expression in solid tumors and influences both angiogenesis and tumor growth. *Proc Natl Acad Sci USA*, **94**, 8104-9.

Mayr, N.A., Yuh, W.T., Magnotta, V.A., Ehrhardt, J.C., Wheeler, J.A., Sorosky, J.I., Davis, C.S., Wen, B.C., Martin, D.D., Pelsang, R.E., Buller, R.E., Oberley, L.W., Mellenberg, D.E. & Hussey, D.H. (1996). Tumor perfusion studies using fast magnetic resonance imaging technique in advanced cervical cancer: a new noninvasive predictive assay. *Int J Radiat Oncol Biol Phys*, **36**, 623-33.

Mazure, N., Chen, E., Yeh, P., Laderoute, K. & Giaccia, A. (1996). Oncogenic transformation and hypoxia synergistically act to modulate vascular endothelial growth factor expression. *Cancer Res*, **56**, 3436-40.

McGown, A.T. & Fox, B.W. (1989). Structural and biochemical comparison of the anti-mitotic agents colchicine, combretastatin A4 and amphethinile. *Anticancer Drug Des*, **3**, 249-54.

Meyer, K.L., Joseph, P.M., Mukherji, B., Livolsi, V.A. & Lin, R. (1993). Measurement of vascular volume in experimental rat tumors by 19F magnetic resonance imaging. *Invest Radiol*, **28**, 710-9.

Millauer, B., Shawver, L., Plate, K., Risau, W. & Ullrich, A. (1994). Glioblastoma growth inhibited in vivo by a dominant-negative Flk-1 mutant. *Nature*, **367**, 576-9.

Miller, B. & Heilmann, L. (1988). Hemorheologic variables in breast cancer patients at the time of diagnosis and during treatment. *Cancer*, **62**, 350-4.

Mills, J., Stone, N., Erhardt, J. & Pittman, R. (1998). Apoptotic membrane blebbing is regulated by myosin light chain phosphorylation. *J Cell Biol*, **140**, 627-36.

Milosevic, M.F., Fyles, A.W. & Hill, R.P. (1999). The relationship between elevated interstitial fluid pressure and blood flow in tumors: a bioengineering analysis. . *Int J Radiat Oncol Biol Phys*, **43**, 1111-23.

Milosevic, M.F., Fyles, A.W., Wong, R., Pintilie, M., Kavanagh, M.C., Levin, W., Manchul, L.A., Keane, T.J. & Hill, R.P. (1998). Interstitial fluid pressure in cervical carcinoma: within tumor heterogeneity, and relation to oxygen tension. *Cancer*, **82**, 2418-26.

Mineura, K., Sasajima, T., Itoh, Y., Sasajima, H., Kowada, M., Tomura, N., Uesaka, Y., Ogawa, T., Hatazawa, J. & Uemura, K. (1995). Blood flow and metabolism of central neurocytoma: a positron emission tomography study. *cancer*, **76**, 1224-32.

Mineura, K., Shioya, H., Kowada, M., Ogawa, T., Hatazawa, J. & Uemura, K. (1999). Blood flow and metabolism of oligodendrogliomas: a positron emission tomography study with kinetic analysis of 18F-fluorodeoxyglucose. *J Neuro-oncology*, **43**, 49-57.

Miodonski, A., Kus, J., Olszewski, E. & Tyrankiewicz, R. (1980). Scanning electron microscopic studies on blood vessels in cancer of the larynx. *Archiv Otolaryngol*, **106**, 321-32.

Mitchell, C. (1992). Multistage carcinogenesis in paediatric and adult cancers. *Eur J Cancer*, **28**, 296-8.

Mitchison, T. & Kirschner, M. (1984). Dynamic instability of microtubule growth. *Nature*, **312**, 237-42.

Mitchison, T.J. (1993). Localization of an exchangeable GTP binding site at the plus end of microtubules. *Science*, **261**, 1044-7.

Mooney, D.J., Langer, R. & Ingber, D.E. (1995). Cytoskeletal filament assembly and the control of cell spreading and function by extracellular matrix. *J Cell Sci*, **108 (Pt 6)**, 2311-20.

Mukhopadhyay, D., Tsiokas, L. & Sukhatme, V. (1995). Wild-type p53 and v-Src exert opposing influences on human vascular endothelial growth factor gene expression. *Cancer Res*, **55**, 6161-5.

Namba, H., Yanagisawa, M., Yui, N., Togawa, T., Kinoshita, F., Iwadate, Y. & Sueyoshi, K. (1996). Quantifying brain tumor blood flow by the microsphere model with N-isopropyl-p-[123I]iodoamphetamine super-early SPECT. *Ann Nucl Med*, **10**, 161-4.

Nelson, K.L., Gifford, L.M., Lauber-Huber, C., Gross, C.A. & Lasser, T.A. (1995). Clinical safety of gadopentetate dimeglumine. *Radiology*, **196**, 439-43.

Nelson, R. (1982). The comparative clinical pharmacology and pharmacokinetics of vindesine, vincristine, and vinblastine in human patients with cancer. *Med Pediatr Oncol*, **10**, 115-27.

Newell, K., Franchi, A., Pouyssegur, J. & Tannock, I. (1993). Studies with glycolysis-deficient cells suggest that production of lactic acid is not the only cause of tumor acidity. *Proc Natl Acad Sci USA*, **90**, 1127-31.

Nihei, Y., Suzuki, M., Okano, A., Tsuji, T., Akiyama, Y., Tsuruo, T., Saito, S., Hori, K. & Sato, Y. (1999). Evaluation of antivascular and antimitotic effects of tubulin binding agents in solid tumor therapy. *Jpn J Cancer Res*, **90**, 1387-95.

Nogales, E., Whittaker, M., Milligan, R. & Downing, K. (1999). High-resolution model of the microtubule. *Cell*, **96**, 79-88.

Nogales, E., Wolf, S.G. & Downing, K.H. (1998). Structure of the alpha beta tubulin dimer by electron crystallography *Nature*, **391**, 199-203.

O Reilly, S., Rustin, G.J., Farmer, K., Burke, M., Hill, S. & Denekamp, J. (1993). Flavone acetic acid (FAA) with recombinant interleukin-2 (rIL-2) in advanced malignant melanoma: I. Clinical and vascular studies. *Br J Cancer*, **67**, 1342-5.

Oberley, L.W., Lindgren, L.A., Baker, S.A. & Stevens, R.H. (1976). Superoxide lon as the cause of the oxygen effect. *Radiat Res*, **68**, 320-8.

Ohizumi, I., Taniguchi, K., Saito, H., Kawata, H., Tsunoda, S., Makimoto, H., Wakai, Y., Tsutsumi, Y., Nakagawa, S., Utoguchi, N., Kaiho, S., Ohsugi, Y. & Mayumi, T. (1999). Suppression of solid tumor growth by a monoclonal antibody against tumor vasculature in rats: involvement of intravascular thrombosis and fibrinogenesis. *Int J Cancer*, **82**, 853-9.

O'Reilly, M.S., Boehm, T., Shing, Y., Fukai, N., Vasios, G., Lane, W.S., Flynn, E., Birkhead, J.R., Olsen, B.R. & Folkman, J. (1997). Endostatin: an endogenous inhibitor of angiogenesis and tumor growth. *Cell*, **88**, 277-85.

Ostergaard, L., Sorensen, A.G., Kwong, K.K., Weisskoff, R.M., Gyldensted, C. & Rosen, B.R. (1996a). High resolution measurement of cerebral blood flow using intravascular tracer bolus passages. Part II: Experimental comparison and preliminary results. *Magn Reson Med*, **36**, 726-36.

Ostergaard, L., Weisskoff, R.M., Chesler, D.A., Gyldensted, C. & Rosen, B.R. (1996b). High resolution measurement of cerebral blood flow using intravascular tracer bolus passages. Part I: Mathematical approach and statistical analysis. *Magn Reson Med*, **36**, 715-25.

Ostergaard, M., Stoltenberg, M., Lovgreen-Nielsen, P., Volck, B., Sonne-Holm, S. & Lorenzen, I. (1998). Quantification of synovistis by MRI: correlation between dynamic and static gadolinium-enhanced magnetic resonance imaging and microscopic and macroscopic signs of synovial inflammation. *Magn Reson Imaging*, **16**, 743-54.

Ozaki, H., Yu, A., Della, N., Ozaki, K., Luna, J., Yamada, H., Hackett, S., Okamoto, N., Zack, D., Semenza, G. & Campochiaro, P. (1999). Hypoxia inducible factor-1alpha is increased in ischemic retina: temporal and spatial correlation with VEGF expression. *Invest Ophthalmol Vis Sci*, **40**, 182-9.

Padhani, A., Gapinski, C., Macvicar, D., Parker, G., Suckling, J., Revell, P., Leach, M., Dearnaley, D. & Husband, J. (2000). Dynamic contrast enhanced MRI of prostate cancer: correlation with morphology and tumour stage, histological grade and PSA. *Clin Radiol*, **55**, 99-109.

Parker, G.J., Suckling, J., Tanner, S.F., Padhani, A.R., Revell, P.B., Husband, J.E. & Leach, M.O. (1997). Probing tumor microvascularity by measurement, analysis and display of contrast agent uptake kinetics. *J Magn Reson Imaging*, **7**, 564-74.

Parkins, C., Holder, A., Hill, S., Chaplin, D. & Tozer, G. (2000). Determinants of anti-vascular action by combretastatin A-4 phosphate: role of nitric oxide. *Br J Cancer*, **83**, 811-816.

Parkins, C.S., Dennis, M.F., Stratford, M.R., Hill, S.A. & Chaplin, D.J. (1995). Ischemia reperfusion injury in tumors: the role of oxygen radicals and nitric oxide. *Cancer Res*, **31**, 6026-9.

Parodi, S. (1992). AACR/EACR first joint conference: concepts and molecular mechanisms of multistage carcinogenesis. *Ann Oncol*, **3**, 357-9.

Pasqualini, R. (1999). Vascular targeting with phage peptide libraries. *Quart J Nucl Med*, **43**, 159-62.

Pass, H.I. (1993). Photodynamic therapy in oncology: mechanisms and clinical use. *J Natl Cancer Inst*, **85**, 443-56.

Pedley, R., Sharma, S., Boxer, G., Flynn, A., Boden, R., Watson, R., Dearling, J., Hill, S., Springer, C. & Begent, R. (2000). Tumour eradication by combined antibody-directed and antivascular therapy. *Br J Cancer*, **83 (Suppl 1)**, 13.

Pedley, R.B., Boden, J.A., Boden, R., Boxer, G.M., Flynn, A.A., Keep, P.A. & Begent, R.H. (1996). Ablation of colorectal xenografts with combined radioimmunotherapy and tumor blood flow-modifying agents. *Cancer Res*, **56**, 3293-300.

Pe'er, J., Shweiki, D., Itin, A., Hemo, I., Gnessin, H. & Keshet, E. (1995). Hypoxia-induced expression of vascular endothelial growth factor by retinal cells is a common factor in neovascularizing ocular diseases [see comments]. *Lab Invest*, **72**, 638-45.

Petak, I., Tillman, D., Harwood, F., Mihalik, R. & Houghton, J. (2000). Fas-dependent and -independent mechanisms of cell death following DNA damage in human colon carcinoma cells. *Cancer Res*, **60**, 2643-50.

Peters, W., Teixeira, M., Intaglietta, M. & Gross, J.F. (1980). Microcirculatory studies in rat mammary carcinoma. I. Transparent chamber method, development of microvasculature, and pressures in tumor vessels. *J Natl Cancer Inst*, **65**, 631-42.

Peters-Engl, C., Medl, M., Mirau, M., Wanner, C., Bilgi, S., Sevelda, P. & Obermair, A. (1998). Color-coded and spectral Doppler flow in breast carcinomas--relationship with the tumor microvasculature. *Breast Cancer Res Treat*, **47**, 83-9.

Pettit, G.R., Cragg, G.M., Herald, D.L., Schmidt, J.M. & Lohavanijaya, P. (1982). Isolation and structure of combretastatin. *Can J Chem*, **60**, 1374-1376.

Pettit, G.R., Singh, S.B., Hamel, E., Lin, C.M., Alberts, D.S. & Garcia-Kendall, D. (1989). Isolation and structure of the strong growth and tubulin inhibitor combretastatin A-4. *Experentia*, **45**, 209-211.

Pettit, G.R., Temple, C., Jr., Narayanan, V.L., Varma, R., Simpson, M.J., Boyd, M.R., Rener, G.A. & Bansal, N. (1995). Antineoplastic agents 322. synthesis of combretastatin A-4 prodrugs. - *Anticancer Drug Des*, **10**, 299-309.

Phillips, G., Whitehead, R. & Knighton, D. (1991). Initiation and pattern of angiogenesis in wound healing in the rat. *Am J Anat*, **192**, 257-62.

Philpott, M., Baguley, B.C. & Ching, L.M. (1995). Induction of tumour necrosis factor-alpha by single and repeated doses of the antitumour agent 5,6-dimethylxanthenone-4-acetic acid. *Cancer Chemother Pharmacol*, **36**, 143-8.

Pigott, K.H., Hill, S.A., Chaplin, D.J. & Saunders, M.I. (1996). Microregional fluctuations in perfusion within human tumours detected using laser Doppler flowmetry. *Radiother Oncol*, **40**, 45-50.

Pirhonen, J.P., Grenman, S.A., Bredbacka, A.B., Bahado-Singh, R.O. & Salmi, T.A. (1995). Effects of external radiotherapy on uterine blood flow in patients with advanced cervical carcinoma assessed by color Doppler ultrasonography. *Cancer*, **76**, 67-71.

Plowman, J., Narayanan, V.L., Dykes, D., Szarvasi, E., Briet, P., Yoder, O.C. & Paull, K.D. (1986). Flavone acetic acid: a novel agent with preclinical antitumor activity against colon adenocarcinoma 38 in mice. *Cancer Treat Rep*, **70**, 631-5.

Poruchynsky, M.S., Wang, E.E., Rudin, C.M., Blagosklonny, M.V. & Fojo, T. (1998). Bcl-xL is phosphorylated in malignant cells following microtubule disruption. *Cancer Res*, **58**, 3331-8.

Postema, S., Pattynama, P.M., Broker, S., van der Geest, R.J., van Rijswijk, C.S. & Baptist Trimbos, J. (1998). Fast dynamic contrast-enhanced colour-coded MRI in uterine cervix carcinoma: useful for tumour staging? *Clin Radiol*, **53**, 729-34.

Pourati, J., Maniotis, A., Spiegel, D., Schaffer, J.L., Butler, J.P., Fredberg, J.J., Ingber, D.E., Stamenovic, D. & Wang, N. (1998). Is cytoskeletal tension a major determinant of cell deformability in adherent endothelial cells? *Am J Physiol*, **274**, C1283-9.

Pruijn, F.B., van Daalen, M., Holford, N.H. & Wilson, W.R.(1997). Mechanisms of enhancement of the antitumour activity of melphalan by the tumour-blood-flow inhibitor 5,6-dimethylxanthenone-4-acetic acid.*Cancer Chemother Pharmacol*,**39**,541-6.

Putterman, C., Ben-Chetrit, E., Caraco, Y. & Levy, M. (1991). Colchicine intoxication: clinical pharmacology, risk factors, features, and management. *Semin Arthritis Rheum*, **21**, 143-55.

Rak, J., Mitsuhashi, Y., Bayko, L., Filmus, J., Shirasawa, S., Sasazuki, T. & Kerbel, R. (1995). Mutant ras oncogenes upregulate VEGF/VPF expression: implications for induction and inhibition of tumor angiogenesis. *Cancer Res*, **55**, 4575-80.

Ran, S., Gao, B., Duffy, S., Watkins, L., Rote, N. & Thorpe, P.E. (1998). Infarction of solid Hodgkin's tumors in mice by antibody-directed targeting of tissue factor to tumor vasculature. *Cancer Res*, **58**, 4646-53.

Ranganathan, S., Benetatos, C.A., Colarusso, P.J., Dexter, D.W. & Hudes, G.R. (1998a). Altered beta-tubulin isotype expression in paclitaxel-resistant human prostate carcinoma cells. *Br J Cancer*, **77**, 562-6.

Ranganathan, S., Dexter, D.W., Benetatos, C.A., Chapman, A.E., Tew, K.D. & Hudes, G.R. (1996). Increase of beta(III)- and beta(IVa)-tubulin isotopes in human prostate carcinoma cells as a result of estramustine resistance. *Cancer Res*, **56**, 2584-9.

Ranganathan, S., Dexter, D.W., Benetatos, C.A. & Hudes, G.R. (1998b). Cloning and sequencing of human betaIII-tubulin cDNA: induction of betaIII isotype in human prostate carcinoma cells by acute exposure to antimicrotubule agents. *Biochim Biophys Act*, **1395**, 237-45.

Rastinejad, F., Polverini, P. & Bouck, N. (1989). Regulation of the activity of a new inhibitor of angiogenesis by a cancer suppressor gene. *Cell*, **56**, 345-55.

Reddick, W., Bhargava, R., Taylor, J., Meyer, W. & Fletcher, B. (1995). Dynamic contrast-enhanced MR imaging evaluation of osteosarcoma response to neoadjuvant chemotherapy. *J Magn Reson Imaging*, **5**, 689-94.

Reinhold, H.S. & Endrich, B. (1986). Tumour microcirculation as a target for hyperthermia. *Int J Hyperthermia*, **2**, 111-37.

Renkin, E. (1959). Transport of ptassium-42 from blood to tissue in isolated mammalian skeletal muscles. *Am J Physiol*, **197**, 1205-1210.

Rewcastle, G.W., Atwell, G.J., Baguley, B.C., Boyd, M., Thomsen, L.L., Zhuang, L. & Denny, W.A. (1991). Potential antitumor agents. 63. Structure-activity relationships for side-chain analogues of the colon 38 active agent 9-oxo-9H-xanthene-4-acetic acid. *J Med Chem*, **34**, 2864-70.

Risau, W. (1997). Mechanisms of angiogenesis. *Nature*, **386**, 671-4.

Robinson, S.P., Howe, F.A. & Griffiths, J.R. (1995). Noninvasive monitoring of carbogen-induced changes in tumor blood flow and oxygenation by functional magnetic resonance imaging. *Int J Radiat Oncol Biol Phys*, **33**, 855-9.

Roemer, R.B. (1990). The local tissue cooling coefficient: a unified approach to thermal washout and steady-state 'perfusion' calculations. Int J *Hyperthermia*, **6**, 421-30.

Roemer, R.B., Fletcher, A.M. & Cetas, T.C. (1985). Obtaining local SAR and blood perfusion data from temperature measurements: steady state and transient techniques compared. *Int J Radiat Oncol Biol Phys*, **11**, 1539-50.

Rofstad, E. (2000). Microenvironment-induced cancer metastasis. *Int J Radiat Biol*, **76**, 589-605.

Rojas, A., Joiner, M.C., Hodgkiss, R.J., Carl, U., Kjellen, E. & Wilson, G.D. (1992). Enhancement of tumor radiosensitivity and reduced hypoxia-dependent binding of a 2-nitroimidazole with normobaric oxygen and carbogen: a therapeutic comparison with skin and kidneys. *Int J Radiat Oncol Biol Phys*, **23**, 361-6.

Rosen, B.R., Belliveau, J.W., Vevea, J.M. & Brady, T.J. (1990). Perfusion imaging with NMR contrast agents. *Magn Reson Med*, **14**, 249-65.

Roth, J. (1995). Molecular events in lung cancer. *Lung Cancer*, **12 Suppl 2**, S3-15.

Rowell, N., Flower, M., Cronin, B. & McCready, V. (1993). Quantitative single-photon emission tomography for tumour blood flow measurement in bronchial carcinoma. *Eur J Nucl Med*, **20**, 591-9.

Rowell, N.P., Flower, M.A., McCready, V.R., Cronin, B. & Horwich, A. (1990). The effects of single dose oral hydralazine on blood flow through human lung tumours. *Radiother Oncol*, **18**, 283-92.

Rowell, N.P., McCready, V.R., Tait, D., Flower, M.A., Cronin, B., Adams, G.E. & Horwich, A. (1989). Technetium-99m HMPAO and SPECT in the assessment of blood flow in human lung tumours. *Br J Cancer*, **59**, 135-41.

Rowinsky, E.K., Donehower, R.C., Jones, R.J. & Tucker, R.W. (1988). Microtubule changes and cytotoxicity in leukemic cell lines treated with taxol. *Cancer Res*, **48**, 4093-100.

Roychowdhury, D., Tseng, A.J., Fu, K., Weinburg, V. & Weidner, N. (1996). New prognostic factors in nasopharyngeal carcinoma. Tumor angiogenesis and C-erbB2 expression. *Cancer*, **77**, 1419-26.

Rozijn, T.H., van der Sanden, B.P., Heerschap, A., Creyghton, J.H. & Bovee, W.M. (1998). Influence of the pharmacokinetic model on the quantification of the Gd-DTPA uptake rate in brain tumours using direct T1 measurements. *Magma*, **6**, 37-43.

Ruegg, C., Yilmaz, A., Bieler, G., Bamat, J., Chaubert, P. & Lejeune, F. (1998). Evidence for the involvement of endothelial cell integrin alphaVbeta3 in the disruption of the tumor vasculature induced by TNF and IFN-gamma. *Nat Med*, **4**, 408-14.

Runge, V. (2000). Safety of approved MR contrast media for intravenous injection. *J Magn Reson Imaging*, **12**, 205-213.

Sabouraud, A., Rochdi, M., Urtizberea, M., Christen, M.O., Achtert, G. & Scherrmann, J.M. (1992). Pharmacokinetics of colchicine: a review of experimental and clinical data. *Z Gastroenterol*, **30 Suppl 1**, 35-9.

Sackett, D.L. (1995). Vinca site agents induce structural changes in tubulin different from and antagonistic to changes induced by colchicine site agents. *Biochemistry*, **34**, 7010-9.

Sadahiro, S., Suzuki, T., Tokunaga, N., Mukai, M., Tajima, T., Makuuchi, H. & Saito, T. (1998). Anemia in patients with colorectal cancer. *J Gastroenterol*, **33**, 488-94.

Sapirstein, L.A. (1958). Regional blood flow by fractional distribution of indicators. *Am J Physiol*, **193**, 161-168.

Sase, S. (1996). Correction method for end-tidal xenon concentration in CBF measurements with xenon-enhanced CT. *J Comp Ass Tomog*, **20**, 688-92.

Sato, N., Goto, T., Haranaka, K., Satomi, N., Nariuchi, H., Mano-Hirano, Y. & Sawasaki, Y. (1986). Actions of tumor necrosis factor on cultured vascular endothelial cells: morphologic modulation, growth inhibition, and cytotoxicity. *J Natl Cancer Inst*, **76**, 1113-21.

Sato, T., Tozawa, Y., Deutsch, U., Wolburg-Buchholz, K., Fujiwara, Y., Gendron-Maguire, M., Gridley, T., Wolburg, H., Risau, W. & Qin, Y. (1995). Distinct roles of the receptor tyrosine kinases Tie-1 and Tie-2 in blood vessel formation. *Nature*, **376**, 70-4.

Schenck, J. F. (1996).The role of magnetic susceptibility in magnetic resonance imaging: MRI magnetic compatibility of the first and second kinds. *Med Phys* **23**, 815-50.

Schliwa, M. & van Blerkom, J. (1981). Structural interaction of cytoskeletal components. *J Cell Biol*, **90**, 222-35.

Schmidt, J., Ryschich, E., Daniel, V., Herzog, L., Werner, J., Herfarth, C., Longnecker, D., Gebhard, M. & Klar, E. (2000). Vascular structure and microcirculation of experimental pancreatic carcinoma in rats. [In Process Citation]. *Eur J Surg*, **166**, 328-335.

Schulze, E., Asai, D.J., Bulinski, J.C. & Kirschner, M. (1987). Posttranslational modification and microtubule stability. *J Cell Biol*, **105**, 2167-77.

Sensky, P., Prise, V., Tozer, G., Shaffi, K. & Hirst, D. (1993). Resistance to flow through tissue-isolated transplanted rat tumours located in two different sites. *Br J Cancer*, **67**, 1337-41.

Seo, Y., Baba, H., Fukuda, T., Takashima, M. & Sugimachi, K. (2000). High expression of vascular endothelial growth factor is associated with liver metastasis and a poor prognosis for patients with ductal pancreatic adenocarcinoma. *Cancer*, **88**, 2239-45.

Seon, B.K., Matsuno, F., Haruta, Y., Kondo, M. & Barcos, M. (1997). Long-lasting complete inhibition of human solid tumors in SCID mice by targeting endothelial cells of tumor vasculature with antihuman endoglin immunotoxin. *Clin Cancer Res*, **3**, 1031-44.

Sevick, E. & Jain, R. (1989a). Geometric resistance to blood flow in solid tumors perfused ex vivo: effects of tumor size and

perfusion pressure. *Cancer Res*, **49**, 3506-12.

Sevick, E. & Jain, R. (1989b). Viscous resistance to blood flow in solid tumors: effect of hematocrit on intratumor blood viscosity. *Cancer Res*, **49**, 3513-9.

Shearwin, K.E. & Timasheff, S.N. (1994). Effect of colchicine analogues on the dissociation of alpha beta tubulin into subunits: the locus of colchicine binding. *Biochemistry*, **33**, 894-901.

Simon, R., Freidlin, B., Rubinstein, L., Arbuck, S.G., Collins, J. & Christian, M.C. (1997). Accelerated titration designs for phase I clinical trials in oncology. *J Natl Cancer Inst*, **89**, 1138-47.

Skinner, S., Frydman, G. & O'Brien, P. (1995). Microvascular structure of benign and malignant tumors of the colon in humans. *Dig Dis Sci*, **40**, 373-84.

Skinner, S., Tutton, P. & O'Brien, P. (1990). Microvascular architecture of experimental colon tumors in the rat. *Cancer Res*, **50**, 2411-7.

Smith, G.P., Calveley, S.B., Smith, M.J. & Baguley, B.C. (1987). Flavone acetic acid (NSC 347512) induces haemorrhagic necrosis of mouse colon 26 and 38 tumours [letter]. *Eur J Cancer Clin Oncol*, **23**, 1209-11.

Smith, K.A., Hill, S.A., Begg, A.C. & Denekamp, J. (1988). Validation of the fluorescent dye Hoechst 33342 as a vascular space marker in tumours. *Br J Cancer*, **57**, 247-53.

Smith, P. & Soues, S. (1994). Multilevel therapeutic targeting by topoisomerase inhibitors. *Br J Cancer*, **23**, S47.

Sohn, C., Beldermann, F. & Bastert, G. (1997). Sonographic blood flow measurements in malignant breast tumors. A potential new prognostic factor. *Surg Endosc*, **11**, 957-60.

Sporn, L. & Foster, T. (1992). Photofrin and light induces microtubule depolymerization in cultured human endothelial cells. *Cancer Res*, **52**, 3443-8.

Star, W., Marijnissen, H., van, d.B.-B.A., Versteeg, J., Franken, K. & Reinhold, H. (1986). Destruction of rat mammary tumor and normal tissue microcirculation by hematoporphyrin derivative photoradiation observed in vivo in sandwich observation chambers. *Cancer Res*, **46**, 2532-40.

Stearns, M.E. & Tew, K.D. (1988). Estramustine binds MAP-2 to inhibit microtubule assembly in vitro. *J Cell Sci*, **89**, 331-42.

Stewart, J. (1894). Researches on the circulation time in organs and on the influences which affect it. Parts I-III. *J Physiol*, **15**, 1.

Stohrer, M., Boucher, Y., Stangassinger, M. & Jain, R. (2000). Oncotic pressure in solid tumors is elevated. [In Process Citation]. *Cancer Res*, **60**, 4251-4255.

Stratford, M.R. & Dennis, M.F. (1999). Determination of combretastatin A-4 and its phosphate ester pro-drug in plasma by high-performance liquid chromatography. *J Chromatogr B Biomed Sci Appl*, **721**, 77-85.

Stratford, M.R.L., Folkes, L., Galbraith, S.M., Price, P., Anderson, H., Robbins, A., Sena, L. & Rustin, G. (2000). Phase I pharmacokinetic and toxicity study of weekly intravenous combretastatin A4 phosphate (CA4P). *Clin Cancer Res*, **6 (Suppl)**, 4522s.

Stratmann, R., Krieg, M., Haas, R. & Plate, K. (1997). Putative control of angiogenesis in hemangioblastomas by the von Hippel-Lindau tumor suppressor gene. *J Neuropathol Exp Neurol*, **56**, 1242-52.

Strich, G., Hagan, P.L., Gerber, K.H. & Slutsky, R.A. (1985). Tissue distribution and magnetic resonance spin lattice relaxation effects of gadolinium-DTPA. *Radiology*, **154**, 723-6.

Strobel, D., Krodel, U., Martus, P., Hahn, E.G. & Becker, D. (2000). Clinical evaluation of contrast-enhanced color Doppler sonography in the differential diagnosis of liver tumors. *J Clin Ultrasound*, **28**, 1-13.

Strum, S., McDermed, J., Scholz, M., Johnson, H. & Tisman, G. (1997). Anaemia associated with androgen deprivation in patients with prostate cancer receiving combined hormone blockade. *Br J Urol*, **79**, 933-41.

Stubbs, M., Veech, R.L. & Griffiths, J.R. (1995). Tumor metabolism: the lessons of magnetic resonance spectroscopy. *Adv Enzyme Regul*, **35**, 101-15.

Su, M.Y., Mühler, A., Lao, X. & Nalcioglu, O. (1998). Tumor characterization with dynamic contrast-enhanced MRI using MR contrast agents of various molecular weights. *Magn Reson Med*, **39**, 259-69.

Su, M.Y., Taylor, J.A., Villarreal, L.P. & Nalcioglu, O. (2000). Prediction of gene therapy-induced tumor size changes by the vascularity changes measured using dynamic contrast-enhanced MRI. *Magn Reson Imaging*, **18**, 311-7.

Su, M.Y., Wang, Z. & Nalcioglu, O. (1999). Investigation of longitudinal vascular changes in control and chemotherapy-treated tumors to serve as therapeutic efficacy predictors. *J Magn Reson Imaging*, **9**, 128-37.

Su, M.Y., Wang, Z., Roth, G.M., Lao, X., Samoszuk, M.K. & Nalcioglu, O. (1996). Pharmacokinetic changes induced by vasomodulators in kidneys, livers, muscles, and implanted tumors in rats as measured by dynamic Gd-DTPA-enhanced MRI. *Magn Reson Med*, **36**, 868-77.

Sullivan, K.F. (1988). Structure and utilization of tubulin isotypes. *Ann Rev Cell Biol*, **4**, 687-716.

Sundqvist, K., Hafstrom, L. & Persson, B. (1978). Measurements of total and regional tumor blood flow and organ blood flow using 99Tcm labelled microspheres. An experimental study in rats. *Eur Surg Res*, **10**, 433-43.

Sutherland, R. (1998). Tumor hypoxia and gene expression–implications for malignant progression and therapy. *Acta Oncol*, **37**, 567-74.

Suzuki, M., Hori, K., Abe, I., Saito, S. & Sato, H. (1981). A new approach to cancer chemotherapy: selective enhancement of tumor blood flow with angiotensin II. *J Natl Cancer Inst*, **67**, 663-9.

Tanigawa, N., Amaya, H., Matsumura, M., Lu, C., Kitaoka, A., Matsuyama, K. & Muraoka, R. (1997). Tumor angiogenesis and mode of metastasis in patients with colorectal cancer. *Cancer Res*, **57**, 1043-6.

Tanigawa, N., Amaya, H., Matsumura, M., Shimomatsuya, T., Horiuchi, T., Muraoka, R. & Iki, M. (1996). Extent of tumor vascularization correlates with prognosis and hematogenous metastasis in gastric carcinomas. *Cancer Res*, **56**, 2671-6.

Tannock, I.F. (1968). The relation between cell proliferation and the vascular system in a transplanted mouse mammary tumour. *Br J Cancer*, **22**, 258-73.

Tannock, I.F. & Steel, G.G. (1969). Quantitative techniques for study of the anatomy and function of small blood vessels in tumors. *J Natl Cancer Inst*, **42**, 771-82.

Teicher, B.A., Lazo, J.S. & Sartorelli, A.C. (1981). Classification of antineoplastic agents by their selective toxicities toward oxygenated and hypoxic tumor cells. *Cancer Res*, **41**, 73-81.

Tello, R., Hartnell, G.G., Hill, T., Volpe, J., Finn, J.P. & Cohen, M. (1996). MR perfusion imaging of the kidney pre- and post-dipyridamole stress. *J Magn Reson Imaging*, **6**, 460-4.

Tew, K.D., Glusker, J.P., Hartley-Asp, B., Hudes, G. & Speicher, L.A. (1992). Preclinical and clinical perspectives on the use of estramustine as an antimitotic drug. *Pharmacol Ther* **56**, 323-39.

Thatcher, N., Dazzi, H., Mellor, M., Ghosh, A., Carrington, B., Johnson, R.J., Loriaux, E.M. & Craig, R.P. (1990). Recombinant interleukin-2 (rIL-2) with flavone acetic acid (FAA) in advanced malignant melanoma: a phase II study. *Br J Cancer*, **61**, 618-21.

Thomlinson, R. & Gray, L. (1955). The histologic structure of some human lung cancers and the possible implications for radiotherapy. *Br J Cancer*, **9**, 537-549.

Tint, I.S., Bershadsky, A.D., Gelfand, I.M. & Vasiliev, J.M. (1991). Post-translational modification of microtubules is a component of synergic alterations of cytoskeleton leading to formation of cytoplasmic processes in fibroblasts. *Proc Natl Acad Sci U S A*, **88**, 6318-22.

Tofts, P., Brix, G., Buckley, D., Evelhoch, J., Henderson, E., Knopp, M., Larsson, H., Lee, T., Mayr, N., Parker, G., Port, R., Taylor, J. & Weisskoff, R. (1999). Estimating kinetic parameters from dynamic contrast-enhanced T(1)-weighted MRI of a diffusable tracer: standardized quantities and symbols. *J Magn Reson Imaging*, **10**, 223-32.

Tofts, P.S. & Kermode, A.G. (1991). Measurement of the blood-brain barrier permeability and leakage space using dynamic MR imaging. 1. Fundamental concepts. *Magn Reson Med*, **17**, 357-67.

Toglia, A., Kittelson, J., Roemer, R., Hodak, J. & Carter, L. (1996). Cerebral bloodflow in and around spontaneous malignant gliomas. *Int J Hyperthermia*, **12**, 461-76.

Tozer, G. & Morris, C. (1990). Blood flow and blood volume in a transplanted rat fibrosarcoma: comparison with various normal tissues. *Radiother Oncol*, **17**, 153-65.

Tozer, G.M., Prise, V.E., Wilson, J., Locke, R.J., Vojnovic, B., Stratford, M.R., Dennis, M.F. & Chaplin, D.J. (1999). Combretastatin A-4 phosphate as a tumor vascular-targeting agent: early effects in tumors and normal tissues. *Cancer Res*, **59**, 1626-34.

Tozer, G.M. & Shaffi, K.M. (1993). Modification of tumour blood flow using the hypertensive agent, angiotensin II. *Br J Cancer*, **67**, 981-8.

Tozer, G.M., Shaffi, K.M., Prise, V.E. & Cunningham, V.J. (1994). Characterisation of tumour blood flow using a 'tissue-isolated' preparation. *Br J Cancer*, **70**, 1040-6.

Tufto, I., Lyng, H. & Rofstad, E. (1996). Interstitial fluid pressure, perfusion rate and oxygen tension in human melanoma xenografts. *Br J Cancer Suppl*, **27**, S252-5.

Tweedle, M., Wedeking, P., Telser, J., Sotak, C., Chang, C., Kumar, K., Wan, X. & Eaton, S. (1991). Dependence of MR signal intensity on Gd tissue concentration over a broad dose range. *Magn Reson Med*, **22**, 191-4; discussion 195-6.

van der Woude, H.J., Bloem, J.L., van Oostayen, J.A., Nooy, M.A., Taminiau, A.H., Hermans, J., Reynierse, M. & Hogendoorn, P.C. (1995). Treatment of high-grade bone sarcomas with neoadjuvant chemotherapy: the utility of sequential color Doppler sonography in predicting histopathologic response.. *Am J Roentgenol*, **165**, 125-33.

van Deurs, B., von B˜ulow, F., Vilhardt, F., Holm, P.K. & Sandvig, K. (1996). Destabilization of plasma membrane structure by prevention of actin polymerization. Microtubule-dependent tubulation of the plasma membrane. *J Cell Sci*, **109**, 1655-65.

Van Hoe, L., Van Cutsem, E., Vergote, I., Baert, A.L., Bellon, E., Dupont, P. & Marchal, G. (1997). Size quantification of

liver metastases in patients undergoing cancer treatment: reproducibility of one-, two-, and three-dimensional measurements determined with spiral CT. *Radiology*, **202**, 671-5.

van Tellingen, O., Sips, J.H., Beijnen, J.H., Bult, A. & Nooijen, W.J. (1992). Pharmacology, bio-analysis and pharmacokinetics of the vinca alkaloids and semi-synthetic derivatives (review). *Anticancer Res*, **12**, 1699-715.

Vaupel, P. (1977). Hypoxia in neoplastic tissue. *Microvasc Res*, **13**, 399-408.

Vaupel, P. (1998). Tumor blood flow. In *Blood perfusion and microenvironment of human tumors*, Molls, M. & Vaupel, P. (eds) pp. 41-45. Springer-Verlag: Berlin Heidelberg New York.

Vaupel, P. & Hockel, M. (1998). Oxygenation of human tumours. In *Blood perfusion and microenvironment of human tumours*, Molls, M. & Vaupel, P. (eds) pp. 63-72. Springer-Verlag: Berlin Heidelberg.

Vaupel, P. & Kallinowski, F. (1987). Hemoconcentration of blood flowing through human tumor xenografts. *Int J Microcirc Clin Exp*, **6**, 72.

Vaupel, P., Kallinowski, F. & Okunieff, P. (1989). Blood flow, oxygen and nutrient supply, and metabolic microenvironment of human tumors: a review. *Cancer Res*, **49**, 6449-65.

Verschueren, H., Houben, B., De Braekeleer, J., De Wit, J., Roggen, D. & De Baetselier, P. (1993). Methods for computer assisted analysis of lymphoid cell shape and motility, including Fourier analysis of cell outlines. *J Immunol Meth*, **163**, 99-113.

Verweij, J., Clavel, M. & Chevalier, B. (1994). Paclitaxel (Taxol) and docetaxel (Taxotere): not simply two of a kind. *Ann Oncol*, **5**, 495-505.

Vile, R. & Hart, I. (1993). In vitro and in vivo targeting of gene expression to melanoma cells. *Cancer Res*, **53**, 962-7.

Vogel, A. (1965). Intratumoral vascular changes with increased size of a mammary adenocarcinoma- new methods and results. *J Natl Cancer Inst*, **30**, 571-578.

Vogelstein, B. & Kinzler, K. (1993). The multistep nature of cancer. *Trends Genet*, **9**, 138-41.

von Oettingen, G., Bergholt, B., Rasmussen, M., Ostergaard, L. & Astrup, J. (2000). Pulmonary function affects the quantification of rCBF by non-invasive xenon methods. *J Neurosci Methods*, **95**, 159-69.

von Tempelhoff, G., Heilmann, L., Hommel, G., Schneider, D., Niemann, F. & Zoller, H. (1998). Hyperviscosity syndrome in patients with ovarian carcinoma. *Cancer*, **82**, 1104-11.

Voorhees, W.D.d. & Babbs, C.F. (1982). Hydralazine-enhanced selective heating of transmissible venereal tumor implants in dogs. *Eur J Cancer Clin Oncol*, **18**, 1027-33.

Wade, R.H. & Hyman, A.A. (1997). Microtubule structure and dynamics. *Curr Opin Cell Biol*, **9**, 12-7.

Walenta, S., Dellian, M., Goetz, A.E., Kuhnle, G.E. & Mueller-Klieser, W. (1992). Pixel-to-pixel correlation between images of absolute ATP concentrations and blood flow in tumours. *Br J Cancer*, **66**, 1099-102.

Wallace, S. (1973). Colchicum: the panacea. *Bull N Y Acad Med*, **49**, 130-5.

Wallace, S. (1974). Colchicine. *Semin Arthritis Rheum*, **3**, 369-81.

Walle, T., Walle, U.K., Kumar, G.N. & Bhalla, K.N. (1995). Taxol metabolism and disposition in cancer patients. *Drug Metab Disp*, **23**, 506-12.

Wang, D., Villasante, A., Lewis, S.A. & Cowan, N.J. (1986). The mammalian beta-tubulin repertoire: hematopoietic expression of a novel, heterologous beta-tubulin isotype. *J Cell Biol*, **103**, 1903-10.

Wang, G.L. & Semenza, G.L. (1993). General involvement of hypoxia-inducible factor 1 in transcriptional response to hypoxia. *Proc Natl Acad Sci USA*, **90**, 4304-8.

Wani, M.C., Taylor, H.L., Wall, M.E., Coggon, P. & McPhail, A.T. (1971). Plant antitumor agents. VI. The isolation and structure of taxol, a novel antileukemic and antitumor agent from Taxus brevifolia. *J Am Chem Soc*, **93**, 2325-7.

Warren, B. (1979). The vascular morphology of tumors. In *Tumor blood circulation: Angiogenesis, vascualr morphology and blood flow of experimental and human tumors*, Peterson, H.-I. (ed). CRC Press Inc.

Watts, M.E. & Woodcock, M. (1992). Flavone acetic acid induced changes in human endothelial permeability: potentiation by tumour-conditioned medium. *Eur J Cancer*, **28A**.

Watts, M.E., Woodcock, M., Arnold, S. & Chaplin, D.J. (1997). Effects of novel and conventional anti-cancer agents on human endothelial permeability: influence of tumour secreted factors. *Anticancer Res*, **72**, 71-5.

Weber, W.A., Ziegler, S.I., Thodtmann, R., Hanauske, A.R. & Schwaiger, M. (1999). Reproducibility of metabolic measurements in malignant tumors using FDG PET. *J Nucl Med*, **40**, 1771-7.

Weidner, N. (1995). Intratumor microvessel density as a prognostic factor in cancer [comment]. *Am J Pathol*, **147**, 9-19.

Weidner, N., Folkman, J., Pozza, F., Bevilacqua, P., Allred, E., Moore, D., Meli, S. & Gasparini, G. (1992). Tumor angiogenesis: a new significant and independent prognostic indicator in early-stage breast carcinoma [see comments]. *J Natl Cancer Inst*, **84**, 1875-87.

Weidner, N., Semple, J., Welch, W. & Folkman, J. (1991). Tumor angiogenesis and metastasis--correlation in invasive breast carcinoma. *N Engl J Med*, **324**, 1-8.

Weisenberg, R., Borisy, G. & Taylor, E. (1968). The colchicine-binding protein of mammalian brain and its relation to microtubules. *Biochemistry*, **7**, 4466-79.

Wen, J.G., Chen, Y., Ringgaard, S., Frokiaer, J., Jorgensen, T.M., Stodkilde-Jorgensen, H. & Djurhuus, J.C. (2000). Evaluation of renal function in normal and hydronephrotic kidneys in rats using gadolinium diethylenetetramine-pentaacetic acid enhanced dynamic magnetic resonance imaging. *J Urol*, **163**, 1264-70.

Wesseling, P., van, d.L.J., de, L.H., Ruiter, D. & Burger, P. (1994). Quantitative immunohistological analysis of the microvasculature in untreated human glioblastoma multiforme. Computer-assisted image analysis of whole-tumor sections. *J Neurosurg*, **81**, 902-9.

Wiemann, B. & Starnes, C. (1994). Coley's toxins, tumor necrosis factor and cancer research: a historical perspective. *Pharmacol Ther*, **64**, 529-64.

Wike-Hooley, J.L., van den Berg, A.P., van der Zee, J. & Reinhold, H.S. (1985). Human tumour pH and its variation. *european J Cancer Clin Oncol*, **21**, 785-91.

Wilson, L. (1975). Microtubules as drug receptors: pharmacological properties of microtubule protein. *Ann New York Acad Sci*, **253**, 213-31.

Wilson, W.R., Li, A.E., Cowan, D.S. & Siim, B.G. (1998). Enhancement of tumor radiation response by the antivascular agent 5,6-dimethylxanthenone-4-acetic acid. *Int J Radiat Oncol Biol Phys*, **42**, 905-8.

Woods, J.A., Hadfield, J.A., Pettit, G.R., Fox, B.W. & McGown, A.T. (1995). The interaction with tubulin of a series of stilbenes based on combretastatin A-4. *Br J Cancer*, **71**, 705-11.

Zheng, Y., Wong, M.L., Alberts, B. & Mitchison, T. (1995). Nucleation of microtubule assembly by a gamma-tubulin-containing ring complex. *Nature*, **378**, 578-83.

Zhu, Z. & Witte, L. (1999). Inhibition of tumor growth and metastasis by targeting tumor-associated angiogenesis with antagonists to the receptors of vascular endothelial growth factor. *Invest New Drugs*, **17**, 195-212.

Zweifach, B. & Lipowsky, H. (1984). Pressure-flow relations in blood and lymph microcirculation. In *Handbook of Physiology*, Renkin, E.a.M., CC (ed), Vol. 4. pp. 251-308. American Physiological Society: Bethesda, MD.

Zwi, L.J., Baguley, B.C., Gavin, J.B. & Wilson, W.R. (1994). Correlation between immune and vascular activities of xanthenone acetic acid antitumor agents. *Oncology Res*, **6**, 79-85.

APPENDIX I - LIST OF PUBLICATIONS

Published

Galbraith, S.M., Chaplin, D., Lee, F., Stratford, M.R.L., Locke, R., Vojnovic, B. & Tozer, G.M. (2001).

Effects of combretastatin A4 phosphate on endothelial cell shape in vitro and relation to vascular targeting effects in vivo. *Anticancer Res*, **2**.

Submitted

Galbraith S.M., Lodge M.A., Taylor N.J., Rustin G.J.S., Bentzen S., Stirling J. J. & Padhani A.R.

Reproducibility of Dynamic Contrast Enhanced MRI in Human Muscle and Tumours - Comparison of Quantitative and Semi-Quantitative Analysis *submitted to NMR in Biomed*

Galbraith S.M., Lodge M.A., Taylor N.J., Jameson, M., Padhani A.R., Stirling J. J., Gumbrell, L., Rustin G.J.S.

Change in Human Tumour Blood Flow assessed by Dynamic Contrast Enhanced MRI in the Phase I trial of DMXAA *submitted to J Clin Oncol*

Galbraith S.M., Lodge M.A., Taylor N.J., Maxwell R., Tozer G.M., Wilson I, Prise VE, Sena L, Robbins A, Padhani A.R., Stirling J.J., Rustin G.J.S.

Combretastatin A4 Phosphate reduces blood flow in animal and human tumours, demonstrated by dynamic contrast enhanced MRI